Loop-mediated isothermal nucleic acid amplification coupled with CRISPR-Cas12b for rapid and sensitive detection of SARS-CoV-2 and Nipah virus

By

Dominic Miguel Simard Kielich

A thesis

Submitted to the Faculty of Graduate Studies of

University of Manitoba

In Partial Fulfillment of the Requirement

For the Degree of

MASTER OF SCIENCE

Department of Medical Microbiology and Infectious Diseases

University of Manitoba

Winnipeg, Manitoba

Canada, R3T 2N2

Copyright © 2024 by Dominic Kielich

Table of Contents

Abstract VII
Acknowledgements VIII
List of Abbreviations IX
List of Tables XII
List of Figures XIII
1. SARS-CoV-2 and Nipah Virus RT-LAMP-Cas12b 1
1.1 SARS-CoV-2 Overview and Disease Epidemiology 1
1.1.1. SARS-CoV-2 Viral Epidemiology and Evolution 5
1.1.2. SARS-CoV-2 Biology 7
1.1.2.1. Genetic Biology 7
1.1.2.1.1. Non-Structural Proteins 8
1.1.2.1.2. Structural Proteins 10
1.1.2.1.3. Accessory Proteins 11
1.1.2.2. Cell Entry 12
1.1.2.3. Transcription and Replication 13
1.1.2.4. Tropism and Hosts 14
1.2. Nipah Virus (NiV) Overview and Disease Epidemiology 15
1.2.1. Nipah virus Viral Epidemiology and Evolution 21
1.2.2. Nipah virus Biology 22
1.2.2.1. Genetic Biology 22
1.2.2.2. Cell Entry 23
1.2.2.3. Transcription and Replication 24
1.2.2.4. Tropism and Hosts 26
1.3. CRISPR-Associated Proteins (Cas Proteins) 27
1.3.1. CRISPR-Associated Proteins 27
1.3.2. Diagnostic Potential of CRISPR-Associated Proteins 29
1.3.2.1. Cas12b, Cas13a, Cas14a and Cas ϕ Overviews 29
1.3.2.2. Cas12b Structure and Function 31
1.4. Diagnostics 33
1.4.1. Routine Molecular Diagnostics 33
1.4.1.1. Quantitative polymerase chain reaction (qPCR) 33
1.4.2. Non-Routine Molecular Diagnostics 34

1.4.2.1. Reverse-Transcriptase Loop-Mediated Isothermal Amplification (RT-LAMP) 34
1.4.2.2. Recombinase Polymerase Amplification (RPA) 38
1.4.2.3. CRISPR-Cas-based molecular detection 41
1.5. Nucleic Acid Extraction Strategies 42
1.5.1. Organic extraction 42
1.5.2. Silica-Membrane Column Extractions 42
1.5.3. Paramagnetic Particle Extractions 43
1.5.3.1. Ceres Magnetic NanoTrap Technology for SARS-CoV 2 Extractions 43
1.6. STOPCovid 44
1.6.1. STOPCovid Protocol Limitations 45
1.6.2. Conservation analysis of the RT-LAMP Primers and AapCas12b target site 49
1.7. Ma *et al.* 2019's Nipah Virus RT-LAMP 50
1.8. Isothermal amplification and CRISPR enhancement strategies 51
1.9. Hypothesis 52
1.10. Rationale 52
1.11. Aim 53
1.12. Objectives and Outcomes 53
2. Materials and methods 54
2.1. Nuclease-Free Workflow 54
2.2. Handling and Removal of Samples from High Containment 55
2.3. Cell Lines, Maintenance, Virus propagation 55
2.4. Viruses and RNA 56
2.5. Plaque Assays 57
2.6. Ultracentrifugation Virus Concentration 58
2.7. Clinical Swab and Mock Clinical Sample Preparation 58
2.8. RNA Extractions 59
2.8.1. QIAamp Viral RNA Mini Kit (Qiagen, Cat No.: 52904) 59
2.8.2. MagMAX™ CORE Nucleic Acid Purification Kit (Applied Biosciences, Cat. No.: A32702) 59
2.8.3. In-house developed SARS-CoV-2 Rapid Extraction using Nanotrap® Magnetic Virus Particles (Ceres Nanosciences, Inc., Cat. No.: 44202) 59
2.9. RNA Quantification 60
2.10. RT-LAMP Cas12b assay 61
2.10.1. RT-LAMP Cas12b Primer and sgRNA Design 62

2.10.2. Optimized One-Pot Reverse-Transcriptase Loop-Mediated Isothermal Amplification-AapCas12b collateral cleavage and fluorescent detection 63
2.10.3. Fluorometers 64
2.11. SARS-CoV-2 RT-qPCR 64
2.12. Statistical Analysis 65
3. Results 65
3.1 Virus propagation 66
3.2. SARS-CoV-2 RT-LAMP Cas12b 66
3.2.1. Iterative Optimization Metrics 66
3.2.1.1. Core Assay Conditions 67
3.2.1.1.1. New England Biolabs AapCas12b-sgRNA Titration and comparison to SignalChem AapCas12b 67
3.2.1.1.2. dNTP Titration 72
3.2.1.1.3. $MgSO_4$ Titration 74
3.2.1.1.4. Temperature Gradient of the SARS-CoV-2 RT-LAMP Cas12b Assay 78
3.2.1.2. RT-LAMP Reaction Buffer 80
3.2.1.2.1. Three Non-Ionic Detergents Within the Reaction Buffer 80
3.2.1.2.2. Published LAMP Buffers 82
3.2.1.2.3. Commercially Available Amplification Buffers 85
3.2.1.2.4. Comparison of Each Optimal Buffer Condition 88
3.2.1.2.5. Optimal Reaction Buffer pH 90
3.2.1.3. Reaction Enzymes 93
3.2.1.3.1. DNA Polymerase Titration and Comparison 93
3.2.1.3.2. Reverse Transcriptase Titration and comparison 96
3.2.1.4. Additional Parameters 98
3.2.1.4.1. Effect of Poly-T Linked FIP and BIP Primer 98
3.2.1.4.2. Use of 4 Primers vs. 6 Primers in RT-LAMP Cas12b 100
3.2.1.4.3. Pre-Incubation of AapCas12b with sgRNA, $MgSO_4$ and Nuclease-Free H_2O and Two-Week Storage of a Pre-Assembled Master Mix 103
3.2.1.4.4. RT-LAMP Cas12b Chemical Enhancers 107
3.2.1.4.4.1. L-Proline, Bovine Serum Albumin and Synergistic Enhancement 107
3.2.1.4.4.2. Dithiothreitol Titration to Reduce Nucleic Acid Secondary Structures 111
3.2.1.4.5. Nuclease-shielded sgRNA 113
3.2.1.4.6. Adding a Helicase to Reduce Nontemplate amplification 115

3.2.1.4.7. Effects of Reporter Fluorophore on SARS-CoV-2 N gene RT-LAMP Cas12b 117
3.2.2. Validation and Performance Characteristics 119
3.2.2.1. Specificity to SARS-CoV-2 Variants 119
3.2.2.2. Cross-Reactivity to Homologous and Pathologically Similar Agents 121
3.2.2.3. SARS-CoV-2 Genome Limit of Detection Without Enrichment Extraction 124
3.2.2.4. Limit of Detection Reproducibility 126
3.2.2.5. Analytical Characteristics (Sensitivity, Specificity & Predictive Values) 128
3.3. Nipah virus RT-LAMP Cas12b 131
3.3.1. P, F, G, M and N Gene Primer and sgRNA Designs 131
3.3.2. Iterative Optimization 132
3.3.2.1. Core Assay Conditions 132
3.3.2.1.1. Primer Selection Based on Temperature Gradient of the NiV RT-LAMP Cas12b Assay 132
3.3.2.1.2. AapCas12b-sgRNA Titration 135
3.3.2.2. Additional Optimization 137
3.3.2.2.1. Three Non-Ionic Detergents Within the Reaction Buffer 137
3.3.2.2.2. Optimal Reaction Buffer pH 140
3.3.2.2.3. Addition of DTT to Reduce NiV Genome Secondary Structures 142
3.3.3. Validation and Performance Characteristics 144
3.3.3.1. Specificity to Nipah Genotypes 144
3.3.3.2. Cross-Reactivity to Homologous and Pathologically Similar Agents 146
3.3.3.3. Nipah virus Genome Limit of Detection 148
3.3.3.4. Limit of Detection Reproducibility 148
3.4. Rapid RNA Extraction protocol 150
3.4.1. Optimization Guided for SARS-CoV-2 RNA Extractions 151
3.4.1.1. Identifying the Optimal Proteinase K Enzyme for RNA Extraction Using a SARS-CoV-2 Recombinase Polymerase Amplification Assay Coupled with Cas13a 151
3.4.1.2. Thermolabile Proteinase K Titration and Incubation Period 152
3.4.1.3. Proteinase K Inhibitor Titration 157
3.4.1.4. Pre-incubation of Thermolabile Proteinase K with the Extraction/Elution buffer 159
3.4.1.5. Magnetic NanoTrap Particle Titration 161
3.4.2. Validation and Performance Characteristics Based on SARS-CoV-2 Extractions 163
3.4.2.1. Bead Binding Capacity to Mixed Virus Samples 163
3.4.3. Use of the Rapid RNA Extraction Protocol on Nipah viruses 165

3.4.3.1. Enrichment Extraction Limit of Detection Using Plaque Forming Units Per Sample 165
4. Discussion 166
4.1. Summary 166
4.2. Key Findings 167
4.2.1. Increased signal maxima in the STOPCovid.v2 is generated with the increase in $MgSO_4$ concentration, the addition of Dithiothreitol, and the substitution of Tween 20 with Brij-35 in the RT-LAMP buffer. 167
4.2.2. The optimized SARS-CoV-2 RT-LAMP Cas12b assay can detect relevant virus variants without cross-reacting to homologous coronaviruses and pathophysiologically relevant pathogens. 180
4.2.3. SARS-CoV-2 N gene RT-LAMP Cas12b detects clinical mink and deer samples at reduced sensitivity and specificity than human clinical samples tested by Joung *et al*. 182
4.2.4. The optimized SARS-CoV-2 N gene RT-LAMP Cas12b assay is directly translated to detect the Nipah virus N gene, generating a novel Nipah virus molecular diagnostic assay. 184
4.2.5. 2000-fold improvement in sensitivity from the colorimetric Nipah virus N gene RT-LAMP assay to a CRISPR-Cas12b assay. 187
4.2.6. SARS-CoV-2 RNA is easily extracted and enriched using inexpensive and accessible commercial reagents at room temperature. 189
4.3. Conclusions and Future Directions 191
5. Appendices 193
5.1. RT-LAMP Cas12b Thermal Profile 193
5.2. Calculation examples 193
5.2.1. RNA Dilution Calculations 193
5.3. Oligonucleotide sequences 194
5.3.1. CDC N2 RT-qPCR 194
5.3.2. Joung *et al.* SARS-CoV-2 RT-LAMP Cas12b oligonucleotides including the poly-thymine FIP and BIP and the ALT-R sgRNA 195
5.3.3. Ma *et al.* Nipah Virus RT-LAMP oligonucleotides and in-house designed NiV N gene sgRNA 196
5.4. SARS-CoV-2 N gene RT-LAMP Cas12b Worksheet 196
5.5. Reagents and solution preparations 196
5. ..... References 198

Abstract

SARS-CoV-2 and Nipah virus are two zoonotic viruses responsible for global and local outbreaks of high consequence, respectively, putting a strain on capacity for rapid testing and diagnostic testing. Developed by Joung *et al.* 2020, STOPCovid.v2 combines chemical RNA extraction with loop-mediated isothermal amplification and Cas12b-mediated detection, capable of detecting SARS-CoV-2 nucleic acid. However, the assay sensitivity is not as good as the gold standard RT-qPCR. Moreover, an assay of this sort does not exist to detect Nipah virus. In this investigation, various RT-LAMP and Cas12b optimization strategies, based on extensive literature reviews, were employed to examine their effects on the assay to potentially improve kinetic and detection performance. It was found that substituting Tween-20 with Brij-35 in the reaction buffer, increasing the $MgSO_4$ concentration, and adding dithiothreitol to the reaction only slightly improved assay characteristics. A rapid enrichment-extraction protocol using minimal commercially available reagents and resources was developed herein. Beyond this, a previously published Nipah virus RT-LAMP primer set combined with an in-house-designed sgRNA was developed and found to detect the Nipah virus N gene, improving the sensitivity 2000-fold compared to the published colorimetric RT-LAMP assay. These findings show that combining previously developed isothermal amplification with CRISPR-based detection can improve pathogen detection, paving the way for developing CRISPR-based point-of-care diagnostics.

Acknowledgements

First and foremost, I would like to thank Dr. Bradley Pickering for his support, starting with my undergraduate degree and continuing throughout graduate school. His guidance and opportunities have led me to work on unique cutting edge and novel work. I would like to sincerely thank him for his empathy, understanding, encouragement and kind words in light of the multiple challenges faced throughout the last few years aside from graduate school. I would also like to thank my committee members, Dr. Jim Strong, Dr. Kevin Coombs and Dr. Darwyn Kobasa for their support and advice throughout the progression of the hurdle that is graduate school. I would also like to formally thank researchers at the Massachusetts Institute of Technology and Broad Institute of MIT and Harvard, notably Dr. Julia Joung, Dr. Feng Zhang, Dr. Jonathan Gootenberg and Dr. Omar Abudayyeh for foundationally developing the STOPCovid assay and providing me a platform by which I was able to learn, develop and excel as a scientist.

As for the many, many colleagues at the NCFAD of which I cannot all thank enough, I would like to select a few notable members: Greg Smith, thank you for being there to support me throughout the entirety of my studies; I do not know where I would be if I did not have anyone to vent to, and to learn from. Peter Marszal, thank you for the technical guidance working in CL3/CL3ag; you were an excellent mentor. Mathieu Pinette, thank you for constantly being there to discuss results, whether good or bad, and to help brain storm the most logical next steps. Dr. Hongzhao Li, thank you for being there, for dealing with my hundreds of questions; for troubleshooting every aspect of this project together, and for being there to discuss anything, anytime however long it took. Moreover, I would like to thank all other members of the Special Pathogens Unit, notably Melissa Goolia, Matthew Suderman and Ji-young Kim, as well as CRISPR-Dx members Dr. Alexander Bello and Dr. Guodong Liu.

Lastly, I cannot thank my friends and family enough for their patience, support and encouragement throughout this challenge. Without your love, motivation and drive, I would not be where I am today. To my wife, Gabrielle; Thank you for being there and supporting me, through thick and thin. To my son, Léon; Love what your heart sees, and be what you want to be!

❤

List of Abbreviations

µL	Microliter
AapCas12b	*Alicyclobacillus acidiphilus* Cas12b
AacCas12b	*Alicyclobacillus acidoterrestris* Cas12b
ACE2	Angiotensin-converting enzyme 2
ATP	Adenosine 5'-triphosphate
BSA	Bovine serum albumin
Cas	CRISPR-associated protein
CD209	Cluster of differentiation 209
cDNA	Complimentary DNA
CL3	Containment Level 3
CL3ag	Containment Level 3-agriculture
CL4	Containment Level 4
CMR	Case mortality rate
COVID-19	2019 Coronavirus disease
cp	Genome copies
cp/µL	Genome copies per microliter
CRISPR	Clustered regularly interspaced short palindromic repeats
crRNA	CRISPR-RNA; also known as a sgRNA
DC-SIGN	Dendritic cell-specific Intercellular adhesion molecule-3-Grabbing Non-integrin 1
ddH_2O	double-distilled water
DMEM	Dulbecco's modified Eagle medium
DNA	Deoxyribonucleic acid
dNTP	deoxyribonucleotide triphosphate
DPBS	Dulbecco's Phosphate-Buffered Saline
dsDNA	Double-stranded DNA
DTT	Dithiothreitol

gRNA	Genomic RNA
HCoV	Human coronavirus
HeV	Hendra virus
IBV	Infectious Bronchitis Virus
JEV	Japanese encephalitis virus
kb	Kilo basepairs
L-SIGN	Liver/Lymph node-specific Intracellular adhesion molecule-3-Grabbing Non-integrin
MERS-CoV	Middle East respiratory syndrome coronavirus
mL	Milliliter
mM	Millimolar
MNP	Nanotrap® Magnetic Particles
mV	Millivolts
NCFAD	National Centre for Foreign Animal Disease
NF-κB	Nuclear factor-kappa B pathway
NiV	Nipah virus
NiV-BD	Nipah virus strain Bangladesh
NiV-I	Nipah virus strain India
NiV-MY	Nipah virus strain Malaysia
nm	Nanometer
nM	Nanomolar
NSP	Non-structural protein
nt	Nucleotide
NTC	No template control
ORF	Open reading frame
PAM	Protospacer adjacent motif
PFU	Plaque forming units
pH	Hydrogen potential
PHAC	Public Health Agency of Canada

PKI	Proteinase K inhibitor solution
Poly-T	Poly-thymine
qPCR	Quantitative polymerase chain reaction
RdRp	RNA-dependent RNA polymerase
RFU	Relative/raw fluorescent unit
RNA	Ribonucleic acid
RNP	Ribonucleoprotein
RTC	Replication and Transcription Complex
RT-LAMP	Reverse-transcriptase loop-mediated isothermal amplification
RT-qPCR	Reverse-transcription quantitative polymerase chain reaction
S	Spike protein
SARS-CoV	Severe acute respiratory syndrome coronavirus
SARS-CoV-2	Severe acute respiratory syndrome coronavirus 2
sgRNA	single-guide RNA
SOPs	Standard Operating Procedures
ssDNA	Single-stranded DNA
TLPK	Thermolabile Proteinase K
TMPRSS2	Transmembrane protease serine 2
U	Unit (defined by the manufacturer, may vary by enzyme)
UTR	Untranslated region
VTM	Viral transport medium
YOA	Years of age
τ	Time to surpass the minimum positive threshold (referred to as the threshold)

List of Tables

Table 1 AacCas12b and AapCas12b single-guide RNA sequences.

Table 2 Reagents used in the SARS-COV-2 rapid enrichment-extraction and N gene RT-LAMP Cas12b assay.

Table 3 List of two published LAMP buffer constituents.

Table 4 Analytical characteristics of the SARS-CoV-2 rapid enrichment-extraction and N gene RT-LAMP Cas12b assay (sensitivity, specificity and predictive values)

Table 5 CDC N2 RT-qPCR primers and probe sequences

Table 6 SARS-CoV-2 N gene RT-LAMP Cas12b oligonucleotides and single-guide RNA sequences

Table 7 Nipah virus RT-LAMP Cas12b oligonucleotides and single-guide RNA sequences

List of Figures

Figure 1 Genome structure of SARS-COV-2.

Figure 2 Genome structure of Nipah virus.

Figure 3 Structure of a single-guide RNA.

Figure 4 sgRNA scaffolds of AacCas12b and AapCas12b.

Figure 5 Schematic representation of the RT-LAMP DNA polymerase amplification mechanism.

Figure 6 Schematic representation of the recombinase polymerase DNA amplification mechanism.

Figure 7 Equimolar titration of the New England Biolabs Inc. AapCas12b and SARS-CoV-2 N gene sgRNA to identify the optimal RNP complex concentration.

Figure 8 Equimolar titration of the SignalChem Lifesciences Corporation AapCas12b and SARS-CoV-2 N gene sgRNA to identify the optimal RNP complex concentration.

Figure 9 Deoxyribonucleotide titration signal maxima, detection times, and times to half of the maximum fluorescence.

Figure 10 Wide range magnesium sulfate signal maxima, detection times, and times to half of the maximum fluorescence.

Figure 11 Narrow range magnesium sulfate signal maxima, detection times, and times to half of the maximum fluorescence.

Figure 12 Temperature gradient effect on the signal maxima, detection times, and times to half of the maximum fluorescence of the SARS-CoV-2 N gene RT-LAMP Ca12b assay.

Figure 13 The effect of different non-ionic detergents within the RT-LAMP reaction buffer in the SARS-CoV-2 N gene RT-LAMP Cas12b assay, on assay kinetics and signal maximum.

Figure 14 The effect of various published RT-LAMP buffers with different chemistries than the STOPCovid buffer on the SARS-CoV-2 N gene RT-LAMP Cas12b assay kinetics and signal maximum.

Figure 15 The effect of various commercially available amplification buffers on the SARS-CoV-2 N gene RT-LAMP Cas12b assay kinetics and signal maximum.

Figure 16 Summary of the effects of the optimal of each of the buffer conditions (non-ionic detergents, published buffers and commercial buffers) on the SARS-CoV-2 N gene RT-LAMP Cas12b assay kinetics and signal maximum.

Figure 17 Titration of the pH of the 2% Brij-35 buffer to identify the optimal pH condition for the SARS-CoV-2 RT-LAMP Cas12b assay.

Figure 18 Titration of five DNA polymerases of varying strand displacement activity to identify the optimal enzyme improving the signal maximum and reaction kinetics of the SARS-CoV-2 N gene RT-LAMP Cas12b assay.

Figure 19 Titration of four reverse-transcriptases with optimal activities near 60°C to identify the optimal enzyme improving the signal maximum and reaction kinetics of the SARS-CoV-2 N gene RT-LAMP Cas12b assay.

Figure 20 The effect of poly-thymine linkers between 1c and 2 regions of forward and backward inner primers on the SARS-CoV-2 N gene RT-LAMP Cas12b assay kinetics and signal maximum when compared to unlinked primers.

Figure 21 Comparison of the effects of utilizing 4 or 6 primers in the SARS-CoV-2 N gene RT-LAMP Cas12b assay on assay kinetics and signal maxima.

Figure 22 Comparison of the effects of pre-incubating and directly adding AapCas12b with $MgSO_4$ and the SARS-CoV-2 N gene sgRNA prior to performing the RT-LAMP Cas12b assay.

Figure 23 Comparison of the effects of freezing and directly using the SARS-CoV-2 N gene RT-LAMP Cas12b buffer when performing the assay.

Figure 24 The effects on signal maxima and kinetics when checkerboard-titrating L-proline and bovine serum albumin into the SARS-CoV-2 N gene RT-LAMP Cas12b assay.

Figure 25 Replicates of the SARS-CoV-2 N gene RT-LAMP Cas12b assay when chemically enhanced with bovine serum albumin at 100 µg/mL in comparison to unenhanced assay replicates.

Figure 26 The effects on signal maxima and assay kinetics when titrating dithiothreitol from 10 mM to 0 mM into the SARS-CoV-2 N gene RT-LAMP Cas12b assay.

Figure 27 The effects on the SARS-CoV-2 N gene RT-LAMP Cas12b signal maximum and assay kinetics when using an ALT-R-modified SARS-CoV-2 N gene sgRNA or a unmodified SARS-CoV-2 N gene sgRNA.

Figure 28 The effects on signal maxima and assay kinetics when adding 0 ng, 10 ng or 20 ng of helicase and 1 mM of ATP into the SARS-CoV-2 N gene RT-LAMP Cas12b assay.

Figure 29 Kinetic profile and signal maxima of the SARS-CoV-2 N gene RT-LAMP Cas12b assay when using FAM or HEX as fluorophore on the DNA reporter.

Figure 30 Detection times of the SARS-CoV-2 N gene RT-LAMP Cas12b assay when testing against the Wuhna-1, Delta and Omicron variants.

Figure 31 Signal maxima of cross-reactivity of the SARS-CoV-2 N gene RT-LAMP Cas12b assay to closely homologous or pathophysiologically similar pathogens.

Figure 32 Signal maximum of the limit of detection of the SARS-CoV-2 N gene RT-LAMP Cas12b assay without performing the viral enrichment RNA extraction protocol.

Figure 33 Signal maxima of the reproducibility of the SARS-CoV-2 N gene RT-LAMP Cas12b assay limit of detection.

Figure 34 Temperature gradient effect on the signal maxima and detection times of the Nipah virus M, N and G gene RT-LAMP Ca12b assays.

Figure 35 Titration of the New England Biolabs Inc. AapCas12b and Nipah virus N gene sgRNA to identify the ideal RNP complex concentration.

Figure 36 The effect of different non-ionic detergents within the RT-LAMP reaction buffer in the Nipah virus N gene RT-LAMP Cas12b assay, on assay detection time and signal maximum.

Figure 37 Titration of the pH of the 1% Brij-35 buffer to identify the optimal pH condition for the Nipah virus RT-LAMP Cas12b assay.

Figure 38 The effects on signal maxima and detection time when titrating dithiothreitol from 0 mM to 12 mM into the Nipah virus N gene RT-LAMP Cas12b assay.

Figure 39 Specificity of the Nipah virus N gene RT-LAMP Cas12b assay.

Figure 40 Signal maxima of cross-reactivity of the Nipah virus N gene RT-LAMP Cas12b assay to closely homologous or pathophysiologically similar pathogens.

Figure 41 Signal maxima of the reproducibility of the Nipah virus N gene RT-LAMP Cas12b assay limit of detection.

Figure 42 Signal maxima generated from the SARS-CoV-2 RT-LAMP Cas12b assay upon titration of the TLPK used in SARS-CoV-2 rapid enrichment-extraction.

Figure 43 The effects of TLPK incubation time during extraction on signal maximum and detection time of the SARS-CoV-2 N gene RT-LAMP Cas12b assay.

Figure 44 Detection time and signal maxima of the SARS-CoV-2 N gene RT-LAMP Cas12b assay when testing a titration series of proteinase K inhibitor added to the extraction-elution buffer prior to being added to the assay.

Figure 45 The effects of pre-incubating TLPK with extraction/elution buffer prior to performing the SARS-CoV-2 N gene RT-LAMP Cas12b assay, on signal maximum and detection time.

Figure 46 Signal maxima and detection times generated from extracting SARS-CoV-2 samples with 100 PFU or 10 PFU using 100 µL of MNP or 10 µL MNP.

Figure 47 Comparison of detection times and signal maxima generated from pooled virus samples to samples only containing SARS-CoV-2.

Figure 48 Nipah virus genotypes India and Bangladesh RT-LAMP Cas12b N gene amplicon sequence alignments.

1. SARS-CoV-2 and Nipah Virus RT-LAMP-Cas12b

1.1 SARS-CoV-2 Overview and Disease Epidemiology

Severe acute respiratory syndrome coronavirus 2 (SARS-CoV-2) is a novel high-consequence zoonotic pathogen of the *Coronaviridae* family. SARS-CoV-2 first emerged at the end of December 2019 when officials reported a cluster of cases of pneumonia of unknown origin in Wuhan city, Hubei Province of China. On March 11, 2020, the World Health Organization (WHO) declared the SARS-CoV-2 outbreak a global pandemic[1]. As of May 17, 2023, over 766 million infections of SARS-CoV-2, which causes coronavirus disease (COVID-19), have been confirmed worldwide, with nearly 7 million reported fatalities[2]. SARS-CoV-2 is known to cause varying disease severity in populations living with certain host factors, including but not limited to comorbidities, sex, genetic predisposition, health status, and age. For instance, after the first epidemic wave in Mexico, the case mortality rate (CMR) was estimated to be nearly 0% in individuals below 30 years of age (YOA). In contrast, the CMR increased to 1% in men from 50 to 59 YOA and women from 60 to 69 YOA. In male and female populations above 80 YOA, the CMR was 5.88% and 6.23%, respectively[3].

Current disease management for severe COVID-19 relies heavily on supplemental oxygen, ventilatory support, and supportive care. Pain management and sedatives, including morphine sulfate, midazolam, and benzodiazepine, may be administered if needed. There was early speculation of hydroxyquinoline or ivermectin as potential therapeutic options, though clinical trials debunked the functionality of these two as treatments[4,5]. Current therapeutic options for SARS-CoV-2 infection and disease are divided into antiviral and monoclonal antibody treatments. The main two antiviral treatments are Pfizer's Paxlovid and Merck's Molnupiravir, although more are available. Currently in Canada, Paxlovid is used typically as an outpatient treatment method.

Paxlovid inhibits the SARS-CoV-2-3CL protease, a protease generated from the self-excised proteolytic activity of polyproteins-pp1a and pp1ab (also known as ORF-1a and ORF-1b), which is more thoroughly described in 1.1.2.1.. Also referred to as the main protease, this enzyme further cleaves the polyproteins into 16 nonstructural proteins (NSP), which are necessary for the assembly of the viral replication transcription complex during viral replication[6]. Molnupiravir interferes with viral replication by introducing mutations into the viral ribonucleic acid (RNA), leading to replication issues with the viral RNA-dependent RNA polymerase (RdRp)[7]. As for monoclonal antibody therapies, several regimens may be suggested depending on the infection's severity or the infected individual's age. Some examples of available monoclonal antibody therapeutics are Bamlanivimab, Etesevimab, Casirivimab, Imdevimab, Sotrobimab, and Tixagevimab. An alternative approach to antibody therapies for the treatment of COVID-19 is convalescent plasma transfusions which leverage antibodies produced by a patient who has recovered from the disease. This approach received FDA EUA (Food and Drug Administration Emergency Use Authorization), whereas the WHO recommends against using this approach in non-severe COVID-19 cases[8].

Mild COVID-19 manifestations are similar to the flu, including; fever, chills, breathing impediment, aches, loss of taste and smell, and nausea. In severe cases, COVID-19 may require intensive care and ventilator support. In some cases, the disease has been reported to cause acute respiratory distress syndrome (ARDS), which can progress into multi-organ failure, systemic cytokine release syndrome, other potential life-threatening manifestations, and death. Symptoms may also amplify in severity with SARS-CoV-2 coinfections[9]. As of 2020, the disease incubation period was suspected to be 5 to 7 days, where the majority of infected individuals present symptoms within 12 days[10,11]. It should be noted however, these studies were likely related to the

less infectious Wuhan (HU-1) virus. When infected with variants enhanced for pathogenicity or transmissibility, shorter incubation periods have been identified. Serial intervals effectively also follow the same trend, with early variants proving a four to five day period between primary and secondary cases, whereas the Omicron BA.1 variant is estimated to be three days[12-14]. The inferred duration of infectivity (infectious period) was estimated at 6.5 to 9.5 days in asymptomatic cases and one to four days in pre-symptomatic cases[15,16].

Reports suggest that one of the latest SARS-CoV-2 variant, Omicron (all lineages), spreads from an infected individual to healthy individuals at an effective reproduction value (R_E) between 1.05-12.70[17-23]. That said, prophylactic and pre-emptive mediation measures for COVID-19 rely heavily on the large-scale public use of COVID-19 vaccines to reduce these transmission numbers. According to the Regulatory Affairs Professional Society COVID-19 vaccine tracker, as of June 10, 2022, 37 authorized/approved COVID-19 vaccines were available in varying global regions[24].

Diagnostic approaches to identify SARS-CoV-2 infections can be divided into molecular-based approaches and antigen-based approaches, each with advantages and limitations. First and foremost, nucleic acid detection of SARS-CoV-2 using reverse-transcriptase quantitative polymerase chain reaction (RT-qPCR) may be used to identify an active infection and is considered the "gold standard" in pathogen detection. RT-qPCR has a high specificity to the target virus and sensitivities detecting 1-100 genome copies (genome copies also referred to as cp) per sample[25]. The polymerase chain reaction amplification system is also robust, produces low mutation rates, and is highly specific and sensitive[26]. Although the pros outweigh the cons, molecular pathogen detection has its drawbacks. The cost of reagents, in addition to the thermocycler used to perform the reaction are expensive. Further, the assay is performed at a centralized laboratory with highly trained individuals requiring a stable power supply. Generally,

due to the requirements for a centralised laboratory, the turn-around-time (TAT) from sampling to patient result may take up to 72 hours or longer[27].

CRISPR-Cas (Clustered Regularly Interspaced Short Palindromic Repeat-associated proteins)-based molecular pathogen detection is a nascent approach to sensitively and specifically detecting pathogens. These methods combine isothermal amplification; usually, loop-mediated isothermal amplification (LAMP) or recombinase polymerase amplification (RPA), to amplify the pathogen genome target, which then leverages RNA-guided non-specific indiscriminate cleavage by a Cas protein to detect the pathogen[28,29]. Although a CRISPR-Cas-based molecular approach is nearly as sensitive as RT-qPCR, it has drawbacks. Unlike PCR-based molecular detection, at low genome copy numbers, Cas-mediated detection is increasingly stochastic and in most formats is not quantifiable, identifying the need to optimize current assays to improve detection ability and consistency[30].

Concerning antigen-based detection methods, identification of SARS-CoV-2 infection relies on detecting viral surface antigens, usually the nucleocapsid or spike proteins, using an enzyme-linked immunosorbent assay or an antibody-based lateral flow strip[31,32]. In contrast to PCR-based detection, a rapid antigen test (RAT) takes approximately 15-20 minutes to obtain results from start to end. This method of testing is quick and inexpensive to produce and can be accomplished outside of lab setting including at home. However, RATs have lower specificity and sensitivity than PCR-based testing; therefore, this testing method may produce false-positive or false-negative results[33]. Albeit less common, false positives occur due to the non-specific binding of the anti-SARS-CoV-2 antibody to a foreign antigen, eliciting a false signal identified as a positive result. This specificity is lost when the antibodies have been produced to detect a specific protein phenotype (i.e., that of a particular variant) whereas the pathogen in question may be

another genetic variant, therefore not detecting SARS-CoV-2. When looking at the analytical characteristics of a rapid antigen test (RAT) developed by Roche/SD Biosensor, the sensitivity was determined to be 65.3% (overall) and 44.0% (asymptomatic)[34]. The limit of detection for these commercial rapid antigen tests is variable (>10^6 genome copies/mL), with a limit of detection significantly lower than that of RT-qPCR (1-100 genome copies/µL)[35]. Combined, PCR-based molecular detection of SARS-CoV-2 and rapid antigen testing have their respective limitations outlining a critical gap in global capacity to respond to high-impact infectious disease events.

1.1.1. SARS-CoV-2 Viral Epidemiology and Evolution

The "ground zero" to the first SARS-CoV-2 infections is suspected to originate from the Huanan Seafood Wholesale Market, Jianghan District, Wuhan City, Hubei, China. First reported on December 30, 2019, SARS-CoV-2 was officially isolated from human respiratory epithelial cells and characterized as "2019-nCoV" on January 7, 2020[36,37]. Although SARS-CoV and MERS-CoV are thought to have originated in bats, civets or camel, SARS-CoV-2 transmission is suspected by some, but not confirmed, to be direct from bats to humans obtained through sales in this market[38,39]. The transmission route can only be hypothesized, not knowing if the pathogen was transmitted directly from the primary host or indirectly through intermediate hosts. Considering the variety of potential hosts found at the Huanan Seafood Wholesale Market, identifying the specific primary host and transmission route is made more complex[40]. That said, the market would have served as a super-spreading environment, with biological and environmental samples testing positive for virus throughout the market. Aerosolized respiratory droplets and, less likely, fomites are hypothesized as the primary mode of transmission[41,42].

The most commonly proposed nomenclature approach to classifying SARS-CoV-2 phylogeny, Phylogenetic Attribution of Named Worldwide Epidemic Lineages (Pangolin; referred

to as Pango lineages), uses the maximum likelihood approach to track and understand the global dynamics of SARS-CoV-2[43]. As of August 2022, there are over 2000 Pango-designated lineages elucidating the pathogen's viral evolution and genetic diversity. However, these designations are not conducive to "easy-to-say" labels used by the general public. To surmount this issue, the WHO assigned significant variants (Variants of concern, VOC; Variants formerly of concern, VFOC; Omicron sub-variants under surveillance, OSVUS; Variants of interest, VOI) simple labels following the Greek alphabet[44]. Using to the Greek alphabet lineage designation, the most common SARS-CoV-2 variant globally in infected individuals is the Omicron variant (and descendant lineages)[45].

The *Coronaviridae* family can be subdivided into; alphacoronaviruses, betacoronaviruses, gammacoronaviruses and deltacoronaviruses. Known outbreak-causing coronaviruses like Middle-East Respiratory Syndrome Coronavirus (MERS-CoV) and Severe Acute Respiratory Syndrome Coronaviruses (SARS-CoV) are classified within the betacoronavirus genus, in which SARS-CoV-2 is also classified. Conversely, other common human coronaviruses (HcoV), including HcoV-229E, HcoV-OC43, HCoV-HKU1 and HcoV-NL63, which cause types of seasonal common cold, are classified as Alpha-, Beta- and Alpha-coronaviruses, respectively.

Although classified within the same genus, SARS-CoV-2 has a higher nucleotide homology to related novel and individually characterized bat-coronaviruses than MERS and SARS-CoV, suggesting the 2019 pandemic agent may be a novel agent obtained from an novel source, likely from an environmental bat exposure. The first isolated SARS-CoV-2 virus was designated the type strain Wuhan-1 or HU-1. Subsequent variants were designated the Alpha, Beta, Gamma, Delta, Epsilon, Zeta, Eta, Theta, Iota, Kappa, Lambda, Mu, and Omicron[46]. Key differences within variants are found at the single nucleotide variation level and amino acid

changes, particularly within the spike protein-encoding gene. For instance, notable missense mutations inducing amino acid changes being monitored within the spike protein in Omicron variants are R346K, L452X, and F486V due to the potential of increasing virulence, transmissibility, and consequently, pathogenicity while improving immune evasion mechanisms[47-49].

The earliest documented variant differing from the HU-1 type strain was in May 2020 in South Africa (Beta). Variants following suit were first documented in the fall of 2020, although the most virulent, transmissible, and consequently, prevalent variant, Omicron, became prevalent around November of 2021[50,51]. The SARS-CoV-2 whole genome nucleotide mutation rate is approximately 6.667×10^{-4} nucleotide substitutions per site per year. In contrast, within the spike protein, the nucleotide mutation rate is 8.066×10^{-4} substitutions per site per year within the S gene[52]. Some reports identify SARS-CoV-2 as having a slow mutation rate or average compared to other RNA viruses[52,53]. Although this information provides insight into the molecular evolution of the pathogen, the SARS-CoV-2 pandemic is ongoing. Novel variants with novel mutations will be more rapidly detected due to the increased SARS-CoV-2 genomic surveillance globally.

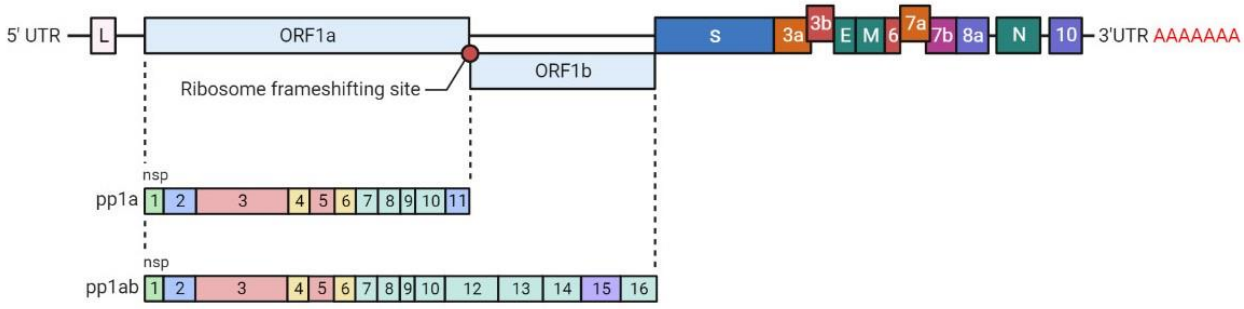
1.1.2. SARS-CoV-2 Biology

1.1.2.1. Genetic Biology

SARS-CoV-2 is a pleomorphic to spherical enveloped virus of approximately 80-120 nanometers (nm) in diameter, encapsulating a positive-sense single-stranded non-segmented RNA genome of roughly 30 kb in length. Within the genome, there are 13-15 open reading frames (ORFs), of which only 12 are known to be functional, encoding 27 to 29 different proteins[36-38,54-56]. From 5' to 3', the SARS-CoV-2 genome specific protein coding regions: a 5' untranslated region (UTR) followed by a replicase and protease encoding ORF (ORF1a and ORF1b),

intermittent ORFs between the spike glycoprotein (S) gene, envelope protein (E), membrane glycoprotein (M), nucleocapsid protein (N), and a 3' UTR ending with a poly-adenylated tail (Figure 1)[36,56].

Figure 1. The SARS-CoV-2 genome comprises of 13 to 15 open reading frames, coding for 27 to 29 different proteins. The genome contains a 5' UTR region, followed by a replicase and protease



encoding ORF (ORF1a and ORF1b), spike glycoprotein (S) gene, envelope protein I, membrane glycoprotein (M), nucleocapsid protein (N), and a 3' UTR ending with a poly-adenylated tail. The figure was generated using BioRender.

1.1.2.1.1. Non-Structural Proteins

The ORF1a-b gene complex encodes a polyprotein that gets auto-proteolyzed. The cleavage forms sixteen non-structural proteins (NSP; NSP1 to NSP16) when processed. These proteins assemble to produce the replicase and transcriptase complex (RTC) in addition to a combination of additional protein assemblies with complex roles[55]. The functional role of NSP1 is to inactivate host-cell translation and gene expression by promoting host mRNA degradation while resisting viral mRNA degradation[58]. NSP2 binds to specific and ubiquitous host proteins (prohibitin 1 and 2), which are known to regulate mitochondrial function, cellular replication, and many cellular functions[59]. Therefore binding to these cellular components will have consequential effects leading to cellular dysregulation. The NSP3, known as "papain-like proteinase, or PL^{PRO}", acts as one of the endoproteases responsible for the auto-cleavage of the ORF-1ab proteolytic processing[60]. The NSP4 protein is known to interact with NSP3 with a combined essential role in

viral replication and membrane rearrangement. However, the literature indicates that the two proteins may require host factors to allow these processes[61]. Like NSP3, NSP5 acts as an endoprotease, termed "main protease or 3-chymotrypsin-like protease; M^{PRO} or $3CL^{PRO}$", leading to the cleavage of 11 additional NSPs[62]. NSP6 in SARS-CoV-2 modulates autophagosome production, facilitating the assembly of viral replicase proteins, amongst other roles[63].

NSP7, NSP8, and NSP12 complex together to form the RdRp, which has a crucial role in catalyzing SARS-CoV-2 RNA genome replication[64]. The non-structural protein nine (NSP9) also functions within the RNA replication complex. According to the literature, NSP9 has no defined function; however, the protein putatively aids in facilitating RTC access to RNA during synthesis by binding to RNA and the NSP12 protein[65,66]. NSP10 complexes with the NSP14 and NSP16 to enhance the 3'-5' exoribonuclease, N7-methyltransferase, and 2'-O-Ribose-Methyltransferase activities, respectively. As generalized above, the NSP14 protein dual-functions as a ribonuclease that excises nucleotide mismatches starting from the 3'-end of the SARS-CoV-2 genome and catalyzes N7-methyltransferase action at the 5' cap of the viral genome when methylated by NSP16[67]. The function of the small 13-residue NSP11 peptide largely remains unknown. Literature shows variation in NSP11 necessity, depending on the pathogen. For example, mutations to the protein in murine hepatitis virus prevent replication, whereas, in avian Infectious bronchitis virus (IBV), the protein is dispensable for viral replication[68,69]. With variations in the necessity of NSP11 within coronaviruses, the function of NSP11 remains to be elucidated. Essential for replication, NSP13 also has dual functions. The first function is a double-stranded RNA unwinding helicase and the second as a 5'-triphosphatase, which plays a role in 5' capping of viral mRNA[70]. The non-structural protein 15 functions as a uridine-endoribonuclease[71]. One report identifies NSP15 as a viral RNA-degrading protein to evade host immune responses. In contrast, the same author

identifies the protein as essential for evading host immune recognition mechanisms, which is also the role of the 2'-O-methyltransferase non-structural protein 16[72,73].

1.1.2.1.2. Structural Proteins

The spike glycoprotein plays a primary role in SARS-CoV-2 pathogenesis and entry by acting as the mediating factor for cell entry[74]. The SARS-CoV-2 spike protein consists of a homotrimer, which, when subdivided into monomers, comprises two subunits (S1 and S2) of multiple domains with different functions. The subunits contain an N-terminal domain with a receptor-binding domain within a receptor binding motif (RBD-RBM), furin cleavage sites, fusion peptide, central helix, connecting domain, heptad repeat, a transmembrane domain, and a C-terminus cytoplasmic tail[75]. Upon receptor binding motif recognition and binding to the angiotensin-converting enzyme 2 (ACE2) receptor, the spike protein undergoes proteolytic cleavage separating the S1 and the S2 domains exposing the fusion peptide change, facilitating virion entry into host cells. As one of the major structural proteins of SARS-CoV-2, also providing the virus its corona name (crown of spike proteins), the spike protein is the primary target in host immune response, and also the immunogen present in various vaccine constructs including mRNA vaccines[75-77].

Another essential structural component, the membrane protein (M), is a membrane-spanning protein that binds to and interacts with the three other structural proteins (spike, envelope, and nucleocapsid proteins)[78]. For example, the M protein will bind with the N protein to enhance and promote viral assembly by stabilizing the N protein-gRNA complex[79]. The protein will also coordinate S protein anchorage to the viral membrane[80].

The envelope protein may not be essential for propagation depending on the coronavirus. For instance, in SARS-CoV, E protein deletions only decrease viral titers and cause morphological

changes within the viral capsid[81,82]. In SARS-CoV-2, the E protein has multiple functions, including aiding in the fusion of viral particles to host cells[83]. Other than structural functions, E protein aids viral assembly within the Endoplasmic Reticulum-Golgi (ER-Golgi) apparatus lumen, where whole virions are assembled and bud from the EG-Golgi[82]. Further, SARS-CoV-2 E protein may also function as a suppressor of the host-cell response, reducing host immunity and increasing viral pathogenesis[82,84]. Coronavirus E proteins also form ion pores within the viral membrane[85].

The SARS-CoV-2 nucleocapsid protein is a multifunctional protein[86]. Coronavirus N proteins are used in packing the gRNA into a helical compact ribonucleoprotein complex (RNP).[87] The protein complexes with genomic RNA via the N-terminus at the 3'-end of the gRNA, guiding rapid virion assembly in the ER-Golgi[88]. The nucleoprotein is co-localized in the cytoplasm and interacts with NSP13 (helicase) throughout RNA synthesis either by membrane-aided interactions or direct protein-protein interactions[89]. In coronaviruses, the N protein is also putatively known to play an essential role in viral pathogenesis[90].

1.1.2.1.3. Accessory Proteins

The SARS-CoV-2 expresses several accessory proteins; ORF- 3a, 3b, 6, 7a, 7b, 8, 9b, 9c, and 10. The structure and functions of most of these proteins in SARS-CoV-2 have yet to be solved. However, they can be putatively hypothesized/defined when looking at the biological processes in closely related coronaviruses[91]. In SARS-CoV-2, ORF3a interferes with host cell biological functions, including ion channel activity, reducing host cell function and increasing viral pathogenesis[92]. It can also induce a robust immune response, particularly triggering strong pro-inflammatory cyto/chemokines capable of causing a cytokine storm[93]. ORF3b is an immune modulator known to suppress host interferon response, and like ORF3a, it reduces host cell function and increases viral pathogenesis[94]. Also, an antagonist of interferon host response, SARS-

CoV-2 ORF6 will directly bind to STAT1, a human transcription factor, resulting in nuclear exclusion[95]. The OFR7a gene translates for a transmembrane protein that interacts with TAK1 leading to the activation of the NF-κB pathway, thereby increasing pro-inflammatory cytokine levels[96]. Also mediating the NF-κB pathway, ORF7b modulates TNF-α-induced apoptosis[97]. The function of ORF7b remains otherwise to be elucidated. ORF8 induces strong pro-inflammatory cytokine responses, reducing host cell response and increasing viral pathogenesis[98]. ORF9b also suppresses interferon I and III expressions by targeting multiple biochemical pathways[99]. Globally, most SARS-CoV-2 accessory proteins promote viral pathogenesis by suppressing innate antiviral immunity. It is suggested that ORF9c and ORF10, like many other accessory proteins, modulate interferon signaling and many other immune pathways[100,101].

1.1.2.2. Cell Entry

Functional interactions mediate SARS-CoV-2 cell entry between specific domains on the spike protein and its receptor, ACE2[74]. ACE2's primary function is homeostatic regulation of circulating angiotensin II, an effector metabolite of the Renin-Angiotensin-aldosterone system, increasing blood pressure, although it can regulate additional metabolites[102]. The ACE2 receptor is localized within the apical surface of epithelial lung alveolar cells and enterocytes of the small intestine[103,104]. Viral entry is initiated by binding the RBD's N-terminal domain on the S1 domain of the spike protein to the ACE2 receptor. Proteolytic cleavage of the S1 and S2 subunits is mediated by either of three proteases, transmembrane protease serine 2 (TMPRSS2), cathepsin or furin. The S1 subunit of the spike protein gets cleaved off of the viral membrane-bound S2 subunit and dissociates from the spike protein, exposing an S2 internally nested surface fusion peptide. The fusion peptide anchors to the host cell membrane following an S2 conformational change in its heptad repeat 1 region. The result of this conformational change leads to membrane fusion and

cellular uptake through membrane fusion pore formation and the release of viral RNA into the cytoplasm[74]. SARS-CoV-2 has more than one mechanism of entry within host cells. An alternative entry mechanism is ACE2-mediated endocytosis. Upon S1-S2 proteolytic cleavage, the virion is internalized as an endosomal product, traveling to the Golgi apparatus. Upon entry into the Golgi apparatus, the endosomal membrane is cleaved by Cathespin-L, releasing the viral RNA within the cytoplasm[105].

Although ACE2 is presumed to be the primary receptor by which SARS-CoV-2 enters the cell, a recent study identified CD209L/L-SIGN and CD209/DC-SIGN (Cluster of differentiation 209/ Dendritic cell-specific Intercellular adhesion molecule-3-Grabbing Non-integrin 1 and Cluster of differentiation 209/ Liver/Lymph node-specific Intracellular adhesion molecule-3-Grabbing Non-integrin, respectively) as alternative receptors leveraged by SARS-COV-2 for cell entry[106]. Evidence of multiple SARS-CoV-2 surface receptors suggests no single SARS-CoV-2 mechanism of entry exists.

1.1.2.3. Transcription and Replication

Upon fusion of the SARS-CoV-2 membrane to the cell capsid, genomic RNA (gRNA) is released into the cytosol, where replication of the positive-sensed RNA occurs. Recruited host cell ribosomes then translate the ORF1ab region of the gRNA, serving as an mRNA template for the ORF encoded proteins[107]. Resulting from translation is two polyproteins, pp1a and pp1ab, where the latter is translated from a -1 ribosomal reading frameshift[108]. After auto-proteolytic cleavage by PL^{PRO} and $3CL^{PRO}$, all sixteen non-structural proteins are cleaved from their respective polyproteins. NSP1 will rapidly promote host cell mRNA degradation while the other NSPs perform their functions, including forming the RTC[58].

The RTC complex, specifically the NSP12, NSP13, NSP14, and NSP16, encompasses the RNA-dependant RNA polymerase (RdRp), a helicase/phosphatase, a proof-reading exonuclease/methyltransferase, and another methyltransferase, engages in RNA-guided RNA synthesis. With the help of NSP7, NSP8 and NSP12, which form an RdRp holoenzyme, the coronavirus RTC will produce a full-length negative-sense anti-genome (genome complement). This anti-genome is then used as a template for synthesizing gRNA and associated subgenomic mRNA transcripts by the NSP7-8-12-13-14-16-complexed RNA-dependent RNA polymerase.

1.1.2.4. Tropism and Hosts

To understand appropriate pathogen-specific sample types used for infection/disease diagnosis, it is essential to understand the viral tropism and dissemination throughout the host. The distribution of SARS-CoV-2 receptors (i.e., ACE2, CD209L/L-SIGN, and CD209/DC-SIGN) for internalization (i.e., TMPRSS2 S protein priming) influences tropism and pathogenicity[109]. As mentioned above, ACE2 receptors are primarily found within the lung and small intestine tissue, whereas CD209/DC-SIGN and CD209L/L-SIGN receptors are found within macrophages, dendritic cells, liver, and lymph node cells. ACE2 receptors are also co-expressed with SARS-CoV-2 viral antigen during infection in multiple tissues, including the brain, trachea, kidney, pancreas, heart, and surprisingly, sweat glands and vascular endothelial cells in the skin suggesting viral presence in the above listed tissues[110-112]. The overlapping tropism of both receptors and the presence of viral antigen within the same tissues suggests that SARS-CoV-2 may produce a multi-organ infection. An early review of clinical samples for SARS-CoV-2 detection identified bronchoalveolar lavage fluid (BALF) with the highest detected positivity rate at 93%, followed by sputum (72%), nasal swabs (63%), pharyngeal swabs (32%) and feces (29%). In contrast, blood and urine have the lowest positivity rates (1% and 0%, respectively)[113]. Considering the physically

invasive approach to BALF collection, next best sample type for a rapid diagnostic assay would be sputum collections, nasal swabs, pharyngeal swabs, or nasopharyngeal swabs[114].

Putatively stated, SARS-CoV-2 mutations within the spike protein will affect S protein kinetics, more specifically binding affinity. These mutations aided in overcoming the species barrier with SARS-CoV, and the same mechanism would help promote SARS-CoV-2 adaptation[109,115]. Confirmed host range diversity of SARS-CoV-2 infection includes bats, felines (e.g., cats, lions), non-human primates, pangolins, mink, ferrets, hamsters, dogs, cervid, white-tailed deer, and likely many more[116]. With the diverse host range capable of amplifying SARS-CoV-2, the risk of zoonotic transmission and, subsequently, human-to-human transmission catalyzing the potential for spillover events.

*3.2.*1.2. Nipah Virus (NiV) Overview and Disease Epidemiology

In 1998/1999, a highly pathogenic novel paramyxovirus later termed Nipah virus (NiV), emerged in Malaysia and Singapore, resulting in 106 human deaths (105 in Malaysia, 1 in Singapore), which further resulted in the culling of millions of pigs[117]. Since then, near-annual infection events starting in 2001 have been recorded in Bangladesh. Most recently, an outbreak oIccured in Bangladesh between January and February of 2023, resulting in 11 fatalities[118]. Although live Nipah virus has only been isolated in Malaysia, Bangladesh, and India, serological evidence indicates that reservoirs of Nipah virus and zoonotic viral infections have been identified in neighboring countries, including Thailand, Cambodia, Vietnam, and China. Human case mortality varies from 40% to 75% depending on the isolates and infectious disease events[119]. This pathogen is listed by the World Health Organization as a pathogen of interest in the Top 10 Threats to Global Health (2019)[120].

The discovery of Nipah virus originates in Malaysia, stemming from an outbreak of initial unknown origin spanning 1998-1999. Primary clinical manifestation resembled Japanese encephalitis and Hendra virus, thus initially identified as a Hendra-like virus[121]. Early cases were found to have produced IgM antibodies against Japanese encephalitis virus (JEV). Considering how JEV is endemic to Malaysia, combined with clinical and serological evidence, the yet unidentified disease reinforced the potential of a JEV outbreak in the peninsular region[122]. Come December 1998, large clusters of similar cases started appearing throughout Malaysia. In March of 1999, the novel paramyxovirus was finally isolated from human cerebrospinal fluid, and it was officially proposed as the causative agent of the outbreak, then termed "Nipah virus" (eventually Nipah virus, strain "Malaysia" - NiV-MY)[123]. Within this first outbreak, 238 human cases were reported, affecting individuals directly implicated in pig farming (70% of cases). Of these human cases, 109 fatalities were reported demonstrating a 38.5% case fatality rate[121,124].

Significant associations between infections and contact with infected pigs were made by Parashar *et al.* eventually concluded that case patients were more than likely to have been in contact with pigs and/or assisting with pig-related housekeeping, husbandry, or slaughter[125]. Serological evidence identified swine as an effective virus-amplifying host due to rapid disease onset and spread between pigs[126]. It was determined that the presumed reservoir of Nipah virus is Pteropid bats, then transmitted to an intermediary porcine host followed by transmission from infected pigs to humans[124]. Initial transmission from Bats may result from viral shedding through fecal particles (guano), urine, and saliva. Commonly drunk in peninsular countries, date palm sap has been suspected as a transmission vehicle resulting in indirect transmission from bats to humans[127]. Limited evidence of human-to-human transmission of Nipah virus infection has been identified in the Malaysian outbreak; however, evidence exists within the Bangladesh and India

outbreaks. In the 2001 India outbreak, a patient admitted to a local hospital putatively initiated nosocomial transmission of NiV, infection another 11 patients, which subsequently infected a further 33 individuals[128]. More evidence of human-to-human transmission was verified in a 2004 outbreak in Bangladesh, with specific individual case-studies confirming the lateral transmission[127]. Further outbreak investigations also confirmed nosocomial and human-to-human transmission[129,130].

Near annual NiV outbreak events have occurred in Bangladesh since 2001, with over 200 individuals identified as infected with Nipah virus. The case fatality rate in Bangladesh was found to be >70% for the Bangladeshi strain (NiV-BD)[131]. Although genetically similar, pairwise identity between NiV-BD and NiV-MY genome sequences is >92%, distinguishing two specific genotypes. Also distinct from the NiV-MY outbreak, human-to-human transmission was key to spreading infection[127,132].

Periodically, Nipah virus outbreaks appear in India, with the first outbreak arising in early 2001. Sixty-six cases were presumed, with 45 deaths reported (~68% case fatality rate) within Siliguri, West Bengal, India[133]. Clinical disease presentation in India was very similar to the disease in Bangladesh. This pathophysiology was likely associated to the geographic proximity of Siliguri (India) and Faridpur (Bangladesh), one of the regions of the Bangladeshi outbreak, increasing the likelihood that the infecting strain of NiV was genetically very similar[128]. In addition, nosocomial infection, spreading to hospitalized individuals, family contact, and medical staff, was also identified[128]. In May 2018, another Nipah virus outbreak was identified in Kozhikode district, Kerala, India, with 23 cases and 21 casualties (91% case fatality rate)[134]. In September 2021, a single fatal case of NiV infection in a 12-year-old child was found in the same Indian state[135]. Phylogenetic analysis of samples obtained from the 2018-2019 outbreak and the

2021 case found >95% sequence identity within strains and ~96% homologous to the Bangladesh strain[136]. This difference in sequence similarity proposed the existence of a third Nipah virus genotype, “India” (NiV-I).

Further, putative evidence points toward a NiV-MY outbreak in the Philippines 15 years after the first NiV outbreak. Hendra virus, another member of the henipavirus genus, causes disease in horses and, rarely, humans. Similar to the original NiV-MY outbreak, humans infected with presumed NiV were associated with animal slaughter or consumption; this time, however, of horses in the Philippines[137]. Serological evidence showed anti-NiV antibodies in Cambodia, followed by isolating a genetically distinct Nipah virus from Lyle’s flying foxes (*Pteropus lylei*), closely related to NiV-MY[138,139]. However, the Cambodian isolate (CSUR381, Genbank Accession No.: MK801755) shares ~97% sequence identity to that of NiV-MY, phylogenetic analysis including NiV-MY, NiV-BD, NiV-I, therefore CSUR381 appears to be of a distinct genetic lineage[135,139]. Serological evidence also indicates potential Nipah virus presence in China, Vietnam, Thailand, and Indonesia[140-143]. Geographic distribution of pteropid bats is spread through the Indo-pacific region onward to eastern Africa, with suggestions of Wallace’s Line as the environmental border seperating NiV from Australia[144,145]. Moreover, serological evidence indicates that henipaviruses may be found in Pteropodid bats, expanding beyond just pteropid bats[145]. The geographical distribution of pteropid and non-pteropid bats may increase with global warming, increasing the risk of outbreak events in countries foreign to Nipah viruses.

Nipah virus is carried in a variety of hosts, including humans, swine, caddle, bats, cats, dogs, horses, and goats, with the primary reservoir being identified as pteropid bats[146-149]. Nipah virus transmission mechanism has not been established, although studies indicate that urofecal or salivary transmission is a potential transmission route. Historically, a common characteristic of

individuals infected with Nipah virus was the consumption of raw date palm sap[150]. This history provides a rationale for salivary and orofecal transmission, considering bat roosts have been found near date palm tree plantations, bats tend to bite into dates for consumption purposes and bat urinary and fecal matter has been detected in palm juice. Transmission through contact with infected tissues and fluids may occur, as evidenced by pig processing workers being infected through infected carcasses[151]. A study analyzed serological evidence from dogs and cats living near the infected neighborhoods, identifying both animals as having been in contact with the virus and developing an immune response against the virus[149,152]. Virus transfer of NiV from human to human is generally passed through a cough or sneeze droplets; also observed as a nosocomial infection phenomenon[153].

Nipah virus symptom manifestation is a severe respiratory illness and encephalitic disease[154]. Symptoms may start with headache, nausea, drowsiness, and vomiting, to name a few. Severe disease may result in neurological disorders, encephalitis, coma, respiratory complications leading to acute respiratory distress, and even death[155]. In addition, recovered patients, notably those who have previously lived with mild or asymptomatic cases of NiV infections, may be subject to relapsed or late-onset Nipah virus infection-induced encephalitis, occasionally resulting in death[156,157].

Recent (2018) clinical manifestations of patients diagnosed with Nipah virus infection broadly included severe encephalitis (83.3%) and bilateral pulmonary infiltrates (81.8%). Further manifestations of bradycardia and hypotension lead to acute respiratory distress[158]. Clinical features identified amongst pig farmers in the original NiV-MY outbreak also included acute encephalitis leading to a neurological disorder and decreased consciousness. Contrary to recent findings, previous NiV infection induced hypertension and tachycardia characteristic with

involuntary muscle contractions[119]. These findings suggest that Nipah virus infection may broadly affect the central nervous system, with underlying secondary disease manifestation that may vary from strain to strain.

Long-term sequelae of Nipah virus infection survivors having had encephalitis as a symptom included the development of major depressive disorder or depression. This altered psyche also induced personality changes and increased lethargy. Altered neurological function and cognitive impairment were also observed[159]. Relapsed or late-onset encephalitis inciting reactivation of latent Nipah virus infection was also identified[156,160].

There is no approved prophylaxis to NiV infection, with no available Nipah virus vaccines, although experimental antibody therapy used as passive prophylaxis produced partial protection in hamsters[161]. In addition, immunization with select Nipah virus proteins resulted in lethal infection prevention in the same animal model[162]. Although Nipah virus-infected patients rely heavily on intensive supportive care, active infections may be treated with Ribavirin; A clinical study showed that Ribavirin reduced Nipah virus infection mortality by 36%[163]. Due to the severity of the disease, combined with the fact that there are no approved prophylactic or immunizing mitigation measures, Nipah virus is deemed a risk group 4 (RG-4) pathogen requiring handling in a containment level 4 (CL4) facility.

Similar to SARS-CoV-2, Nipah virus surveillance and diagnostics rely on passive serological and molecular detection approaches. In response to the early 2000s NiV outbreaks, an indirect and a capture ELISA was developed to detect IgG and IgM anti-NiV antibodies, respectively[164]. Due to the short half-life of IgM antibodies, anti-NiV IgM detection helps identify arbitrarily recent immune responses to NiV infection. Conversely, IgG antibodies persist for several months, therefore used to identify historical NiV infections[165]. However, this diagnostic

approach is purely passive, highlighting the need for an active infection detection method, such as RT-qPCR. Also considered the "gold standard" in Nipah virus detection, several NiV RT-qPCR assays have been designed to detect the pathogen's genome. In addition, a primer/probe set designed to detect the NiV nucleoprotein has been adopted by the World Organization for Animal Health (WOAH – formerly the Office International des Epizooties, OIE) as the global diagnostic standard for molecular detection of the virus.

1.2.1. Nipah virus Viral Epidemiology and Evolution

The molecular evolution of Nipah viruses is not very expansive, with only two strains phylogenetically diverging from the original strain discovered in Malaysia (1998/1999). Bayesian phylogenetic analysis of evolutionary rate dated the most recent common ancestor to have been dated back to 1947 (95% highest posterior density, 1888-1988). The evolutionary rate/nucleotide mutation rate for the Nipah N gene is approximately $6.5x10^{-4}$ substitutions/site/year[166]. Generally stated, there are two main "clades", "strains" or "genotypes" (terms varying on literature source), although recently, a third was proposed[167] . In this thesis, genetic variants of Nipah viruses will be referred to as "strains" or "genotypes". The three genotypes are termed "Malaysia", "Bangladesh", and "India".

Nucleotide pairwise identity between the Malaysian and Bangladeshi genotypes is 91.8%, rendering a net-evolutionary nucleotide divergence of 8.2%, which underlines two distinct genetic lineages[167,168]. However, the pairwise identity between the Bangladesh and India strain has a net-evolutionary nucleotide divergence of only 1.96%, suggesting that NiV-I diverged from NiV-BD[167]. One unique NiV isolate from Cambodia (2003 - CSUR381), where no human Nipah virus infections have been reported, demonstrated a homologous sequence identity to NiV-MY isolates at 97.7%, therefore likely identifying CSUR381 as derived from NiV-MY[138,169-171]. However,

CSUR381 sequence identity was lower with NiV-BD isolates (91.4%-91.6%) and even less (91.3%) with a 2018 Kerela, India isolate later identified as NiV-I (Genbank Accession No.: MH396625.1)[167,169].

The pathogen with the highest nucleotide identity to Nipah virus, Hendra virus, has a nucleotide homology of approximately 70%. In contrast, the next nearest homologous neighbor to NiV is Cedar virus, another Henipavirus, with approximately 56% nucleotide homology[169,172]. There are only two other International Committee on Taxonomy of Viruses (ICTV)-confirmed henipaviruses, Mojiang virus and Ghanaian bat henipavirus[173,174]. However, recently novel henipaviruses have been identified in bats, including Angavokely virus, Daeryong virus, Gamak virus, Melian virus, Denwin virus, and a few select other henipaviruses[175-178]. Most recently, Langya henipavirus has been isolated and putatively, without completely abiding by Koch's postulates, identified as the causative agent of severe febrile disease in China[179]. Ancestral phylogenetic analysis of multiple bat-paramyxoviruses identified using deep-sequencing identified a potential most common henipavirus ancestor of African descent[180-182].

1.2.2. Nipah virus Biology

1.2.2.1. Genetic Biology

A part of the *Paramyxovidae* family, Nipah virus is a pleomorphic enveloped virus varying between 125 nm to 500 nm in size carrying a single, non-segmented, negative-sense single-stranded RNA genome[183]. Nipah viruses have a genome length of approximately 18.2 kb which is approximately 15%, or 2700 nt larger than other members of the *paramyxoviridae* family[184-186]. Within the *paramyxoviridae* family, all henipavirus genome lengths are multiples of six, following a rule known as "the rule of six". This multiplicity is required for each NiV nucleocapsid protein to associate with six RNA nucleotides to encapsulate the gRNA properly[187,188].

The Nipah virus genome encodes for 6 genes, which translates to 9 proteins. As described in Figure 2, from 3' to 5', the genome encodes monocistronic mRNA translating for the nucleoprotein (N), the phosphoprotein (P), the matrix protein (M), the fusion protein (F), the glycoprotein (G) and the RNA polymerase, also known as the large protein (L)[184]. The P gene also encodes V, C, and W proteins. The NiV RNA transcription complex consists of the large polymerase protein, the nucleocapsid protein, and the phosphoprotein. It can transcribe each gene from 3' to 5', although not produced in equimolar mRNA transcript quantities. There is a decreasing gradient in mRNA transcript quantity from the N protein to the L protein, whereas significant transcription attenuation is found at the M-F and G-L gene junctions[189].

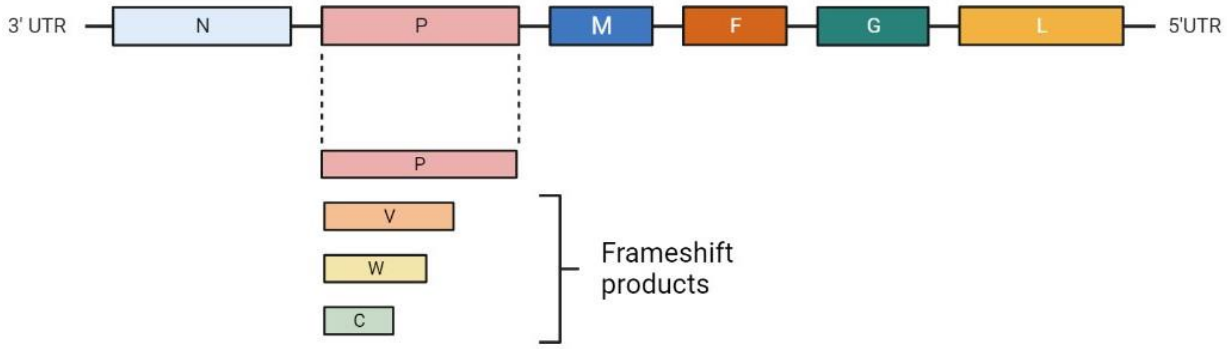


Figure 2. The Nipah virus genome encodes 6 genes, translating 9 proteins: nucleoprotein (N), phosphoprotein (P), matrix protein (M), fusion protein (F), glycoprotein (G) and RNA polymerase Upon framshift,, the P gene translates alternative products: V protein, W protein and C proteins. The figure was generated using BioRender.

1.2.2.2. Cell Entry

Nipah virus cell entry is very similar to that of SARS-CoV-2. Essential interactions mediate cell entry between the G and F surface proteins and either EphrinB2 or EphrinB3 surface receptors, enabling viral-cell fusion and syncytia, like the SARS-CoV-2 spike protein and the ACE2 receptor[191]. The glycoprotein binds to either receptor, inducing conformational changes within the G tetramer, which subsequently triggers the fusion protein-membrane binding, initiating viral

entry[192]. The F protein undergoes activation by endogenous proteolytic cleavage within the endosomal compartment, inducing a pre-hairpin intermediary formation containing an internally compartmentalized fusion peptide[193]. Upon F protein triggering by the G protein, the surface fusion peptide is then introduced into the host cell membrane, mediating virus-cell and cell-cell fusion[194]. Although some believe the mechanism to be pH-dependent (low pH), the mechanism by which the G protein induces F-triggering remains to be elucidated[195].

A suggested alternative entry mechanism for Nipah virus is that of macropinocytosis. Penet *et al.* 2009 presented evidence indicating that when the G protein binds to EphrinB2, the association mimics EphrinB4 binding, consequently transducing reverse signaling pathways, regulating cascades responsible for endocytosis[196]. Looking at the innate biological function of EphrinB2-EphrinB4 interactions during vasculogenesis, when complexed, they induce endocytosis of the complex, therefore supporting the rationale presented above[197,198].

1.2.2.3. Transcription and Replication

Understanding NiV transcription and replication and their respective product quantities allow for identifying the optimal gene target in molecular detection assays. As discussed within section 1.2.2.1., the viral replication complex, including the phosphoprotein, the polymerase protein, and the nucleoprotein-encapsidated negative-sense gRNA, is assembled and active within the cytoplasm, allowing for immediate transcription and replication upon cell entry. Transcription is initiated at a non-coding 3'-leader sequence producing a non-capped non-poly-adenylated transcript.

Subsequent 3' to 5' transcription starts with the N gene, producing a positive-sense monocistronic messenger RNA (mRNA) with a 5' methylguanosine cap and a 3'poly-adenylated tail[194]. Transcription is terminated and initiated at each gene junction, with transcriptional drop-

off observed as the complex transcribes onward 3' to 5' within intergenic regions[189]. To this extent, a decreasing gradient of mRNA transcripts is found from 3' to 5', with N gene mRNA being the most abundant and 5'-most L at the lowest abundance[194,199]. At the 3' end of the upstream gene, a gene end sequence terminates transcription, followed by a non-coding intergenic region, and then a 5' gene start sequence re-initiates transcription. Logically, at the 5' end of each mRNA is found a poly-uridine tract calling for methylation by the L protein.

In addition to producing monocistronic mRNA, the NiV RNA polymerase generates a polycistronic P gene mRNA transcript sub-encoding four proteins; P (direct reading frame), V (+1 reading frame), C (-1 reading frame) and W (+2 reading frame). The reading frame shift is caused by RNA polymerase stutter inserting non-template uridine, driving a frameshift in mRNA transcription and successive translation[194,200].

These primary transcripts are then translated to produce the proteins necessary for viral replication. Newly translated nucleoproteins and phosphoproteins complex and bind to the freshly generated transcripts at the 3' leader promoter sequence, coordinating antigenome synthesis starting at the 3'-leader promoter sequence; however, this antigenome is not transcribed. Used as a template to synthesize genomic RNA, the 3' end of the antigenome contains a negative leader, which promotes the 3'-end-initiated synthesis of negative-sense viral genomic RNA[194].

With the nucleoprotein's essential role of encapsidating genomic RNA, early NiV infection promotes transcription rather than replication, increasing intracellular levels of all proteins. Replication will only be initiated once a sufficient amount of N gene mRNA transcripts have been translated[194].

1.2.2.4. Tropism and Hosts

Originating in Pteropodid bats, Nipah virus tropism is consistent with the physiological distribution of EphrinB2 and EphrinB3 receptors. Belonging to the Receptor Tyrosine Kinase family, Ephrin receptors function as mediators to cell adhesion and repulsion. In addition, they are implicated in regulating and mediating cell migration, segmentation, and forming tissue boundaries[201-203]. Therefore, the physiological distribution of Ephrin receptors is widespread throughout the human body, with EphrinB2 and EphrinB3 primarily found within the neural circuit (synapses)[204]. The location of Nipah virus-binding receptors logically explains the pathophysiology of Nipah virus infections.

As mentioned above, Pteropodid bats, particularly the Pteropodinae, Rousettinae, and Eidolinae subgenera, serve as natural reservoirs for Nipah viruses[135,169,205]. Transmission from reservoir species to the primary host often occurs through contact with infected fecal matter, urine, or saliva from an infected bat, to a primary host. Although not well characterized nor having isolated live viruses from the host, various domestic animals, including cats and dogs, have been confirmed to have anti-NiV antibodies[149,206]. Experimental inoculation of cats demonstrated susceptibility, manifesting respiratory and neurological disease[207,208]. Notably, within the 1998/1999 Malaysia outbreak, pigs were identified as intermediate amplifying hosts; transmission from bats to pigs occurred through the abovementioned routes[209]. Unique to a 2014 outbreak in the Philippines, the most likely source of human NiV-like infection was through horses, identifying equine as a potential intermediate amplifying hosts[206]. Natural serological evidence of anti-NiV antibodies was identified in cattle and goats in Bangladesh[148,210]. Ducks and chickens were also identified as potential hosts illustrating increased risk factors for possible NiV infections [148].

African green monkeys, squirrel monkeys, mice, ferrets, and Syrian hamsters have all been experimentally inoculated, demonstrating various levels of susceptibility[211-217].

1.3. CRISPR-Associated Proteins (Cas Proteins)

1.3.1. CRISPR-Associated Proteins

Discovered by Drs. Emmanuelle Charpentier and Jennifer Doudna in 2011 and published in 2012, Clustered regularly interspaced short palindromic repeat-associated proteins (Cas) are adaptive prokaryotic immunomodulatory proteins only present in bacteria and archaea that play an essential role in adaptive bacterial immunity[218]. These proteins leverage a self-nonself discriminatory immune defense mechanism, enabling immune system memory to help defend against repeated infection with previously encountered pathogens[219,220]. The defense mechanism involves the incorporation of foreign DNA fragments, known as spacers, obtained through pathogen invasion, into host DNA cassettes, forming a CRISPR array. The host will then transcribe an oligonucleotide complementary to the foreign DNA sequence (known as a target sequence or spacer-targeting sequence) to form a single-guide RNA (sgRNA; also known as crRNA), which also contains a sequence of nucleotides (a motif) that specifically interacts with Cas protein amino acids. The sgRNA will subsequently complex with the complimentary Cas protein to form an active ribonucleoprotein (RNP). This RNP is guided to cleave any nucleic acid (spacer) that will bind to the target sequence, often cleaving collateral nucleic acids in the microenvironment depending on the Cas protein structure (figure 3). This defense mechanism is characterized by specific or non-specific cis or trans ribonucleic or deoxyribonucleic endonuclease activity depending on the nuclease[221]. These CRISPR-Cas proteins can be leveraged for gene editing and, recently, as a diagnostic tool. Although the principle is relatively straightforward, Cas proteins are

extensively diverse and numerous, with protein orthologs producing similar but slightly different guided cleavage activities varying by their respective microenvironments.

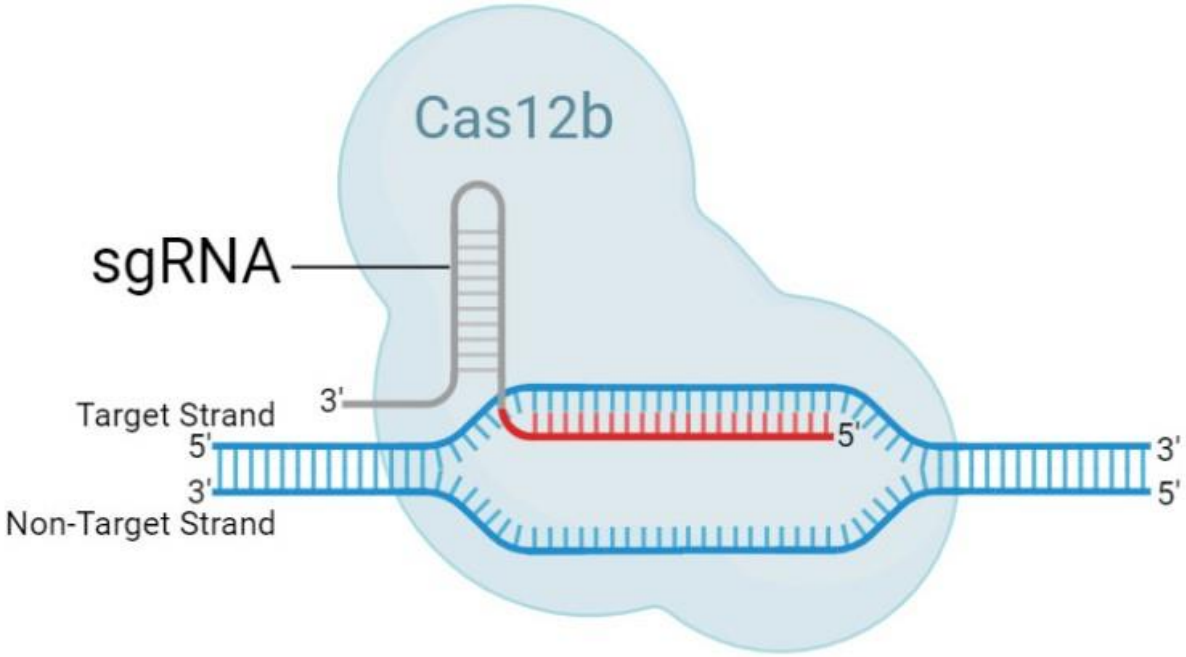


Figure 3. A single guide RNA consists of a singular strand with various regions. The target sequence or spacer targeting sequence (in red) will bind to a complimentary region (blue region bound to red) of single stranded or double-stranded nucleic acids. The grey region of the sgRNA will bind to the Cas protein to form an active ribonucleoprotein complex. The figure was generated using BioRender.

Except for Cas1 and Cas3, most Cas protein sequences are highly divergent, with varying roles and functions, forming different classes, types, and enumerations[219,220]. CRISPR proteins are classified according to frequency profiles of sequence alignments[219]. Another proposed approach to CRISPR-Cas protein classification is based on signatures within genes and elements in the Cas locus[223]. CRISPR-Cas proteins are divided into two classes (1 and 2), where class one includes multiple protein complexes and class two includes single protein effectors that are further type and subtype differentiated[224].

1.3.2. Diagnostic Potential of CRISPR-Associated Proteins

Recently the CRISPR toolbox has been leveraged beyond point mutations and gene knockouts using CRISPR-Cas9. Recently discovered CRISPR-Cas proteins, like Cas12, Cas13, Cas14, and ϕ, can be combined with various isothermal nucleic acid amplification methods, taking advantage of indiscriminate non-specific collateral nucleic acid cleavage upon spacer detection, resulting in turbidimetric, colorimetric or fluorometric pathogen detection. CRISPR-Cas12b, for example, has been leveraged to detect various viruses like SARS-CoV-2, Hepatitis B virus, Human adenovirus, and Herpes Simplex virus[225,226].

1.3.2.1. Cas12b, Cas13a, Cas14a and Cas ϕ Overviews

Several notable CRISPR-Cas proteins have been exploited for rapid nucleic acid detection, including type II Cas9 proteins, type V Cas12, Cas14, Cas ϕ, and type VI Cas13 effector proteins. Importantly, each of the above-listed Cas proteins acts using cis or trans, single-stranded or double-stranded DNA or RNA endonuclease activities, allowing for the specific selection and detection of nucleic acids.

CRISPR-Cas12 proteins are capable of cleaving single-stranded and double-stranded DNA. Historically, rapid diagnostic assays have used Cas12 proteins to diagnose both RNA and DNA pathogen infection, detecting either direct DNA amplification or, with the help of reverse transcription, generated cDNA amplification. With the emergence of SARS-CoV-2, Cas12a and Cas12b effectors have been used in conjunction with amplification assays, notably RT-LAMP, for rapid detection. For instance, Nobel-prize laureate Dr. Jennifer Doudna co-founded Mammoth Biosciences, which developed the DETECTR platform, an RPA-Cas12a assay capable of detecting pathogens at attomolar sensitivities[227]. Common Cas12 orthologs cited in literature have been purified from *Acidaminococcus sp.*, *Francisella novicida*, *Alicyclobacillus acidoterrestris*,

Alicyclobacillus acidiphilus, *Lachnospiraceae sp.* and *Brevibacillus sp.*[227-229]. To note, Cas12a is Mg2+-dependant, ensuring conformational changes within the RuvC domain, allowing for dsDNA cleavage, suggesting that magnesium or other metal ions are essential to Cas-protein modulation[230].

Cas13 proteins have also been leveraged for pathogen detection, displaying the same Mg^{2+}-dependence allowing for non-specific collateral cleavage[230]. Type VI Cas13 is an RNA-guided RNA endonuclease that has been used with cDNA amplification coupled with DNA-dependent RNA conversion techniques for direct RNA detection. For instance, Cas13a has been leveraged for amplification-free SARS-CoV-2 RNA detection [231,232]. However, an innate flaw of direct RNA detection are the RNAse-sensitive nucleic acids. Combining the thermal instability of RNA with the ubiquity of ribonucleases makes for a challenging assay environment prone to contamination and degradation.

The smaller-sized type V CRISPR-Cas14 protein is capable of PAM-free RNA-guided non-specific endoDNAse activity like Cas12 systems[224,233]. However, the approximate functional cleavage temperatures are the significant difference between the Cas12b used in STOPCovid and Cas14. For example, AapCas12b has optimal cleavage activity at approximately 60°C, whereas, within limited literature using Cas14, the protein is capable of collateral cleavage at 37°C[234,235]. Another small protein of approximately 70 kilodaltons, roughly half the molecular weight of Cas12, Cas ϕ is also capable of RNA-guided DNA recognition and cleavage[236]. Although requiring more research and development, these proteins may be helpful within the CRISPR-based diagnostic toolbox.

1.3.2.2. Cas12b Structure and Function

Cas12b (formerly C2c1) is a type V-b CRISPR-Cas RNA-mediated deoxyriboendonuclease capable of cleaving both single-stranded and double-stranded DNA[237]. Some members of type V-b CRISPR-Cas proteins are capable of site-specific DNA cleavage (e.g., *Alicyclobacillus acidoterrestris* Cas12b; AacCas12b and *Brevibacillus sp.* Cas12b; BrCas12b) guided by a protospacer adjacent motif (PAM) sequence; a PAM sequence being 2-6 nucleotides following the target sequence that interacts with a specific region within the Cas protein to either enable or disable nucleic acid modification. In contrast, other members of the same type group are capable of non-specific collateral cleavage not requiring a PAM sequence (e.g., *Alicyclobacillys* acidiphilus Cas12b; AapCas12b). Traditional Cas9 proteins contain two metal-ion-dependent nuclease cleavage domains termed HNH that generate single-strand breaks within a targeted region upstream of the base-paired with the sgRNA, and RuvC, which is capable of non-base paired non-targeted DNA cleavage[237,238]. Cas12b contains only the RuvC, which explains the non-specific endonuclease cleavage activity characteristic of this protein. Interestingly, in AacCas12b, the RuvC catalytic domain can target DNA and non-target DNA cleavage, generating a staggered double-strand DNA break providing seven nucleotide 5' overhangs[237]. Distinctly, AapCas12 does not have an identifiable CRISPR array (also termed a direct repeat sequence) but can function with the Alicyclobacillus macrosporangiidus Cas12b (AmCas12b) or the AacCas12 tracrRNA respectively[30,239]. Of the two, the AacCas12b sgRNA produces a more robust response in AapCas12b, likely due to a stronger hairpin at the 3' end of the AacCas12b sgRNA scaffold compared to that of the AapCas12g sgRNA scaffold (figure 4 and table 1 for complete AapCas12b scaffold sequence)[30]. The AacCas12b scaffold contains 111 nucleotides (nt), of which the crRNA region has a 20-nt guide region (target sequence) that will bind to the target DNA strand and a 14-nt repeat region that will bind to a 16-nt anti-repeat region of the 77-nt tracrRNA .

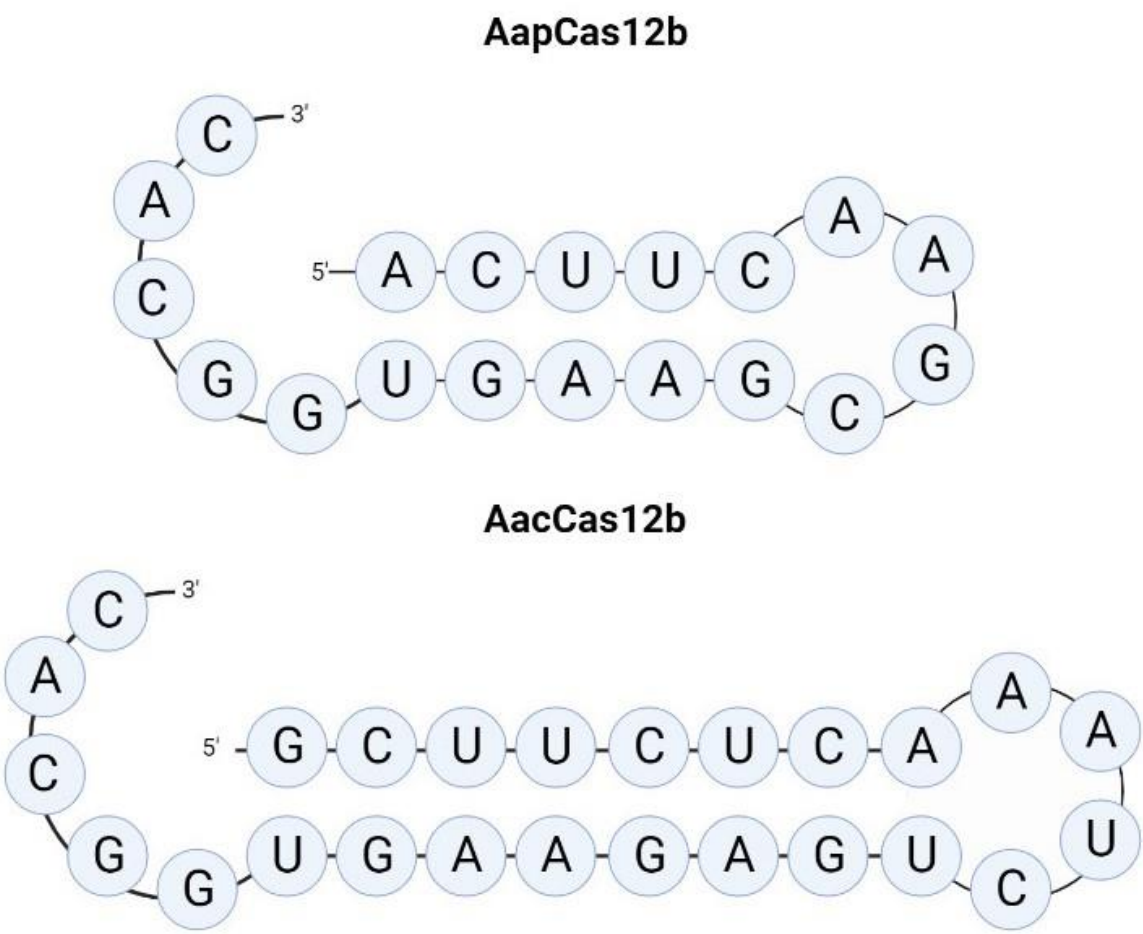


Figure 4. AapCas12b and AacCas12b sgRNA scaffolds share a high degree of homology although the AapCas12b scaffold is more rigid. Both scaffolds are functional at activating AapCas12b. The figure was generated using BioRender.

Table 1. AapCas12b complete sgRNA scaffold sequence.

Name	Nucleotide length	Sequence (5'->3')
AapCas12b	91	GUCUAGAGGACAGAAUUUUUCAACGGGUGUGCCAAUGGCCACUUUCCAG GUGGCAAAGCCCGUUGAGCUUCUCAAAUCUGAGAAGUGGCAC

Upon recognition of substrate DNA within the RuvC catalytic domain, three catalytic residues (Asp570, Gly848, and Asp977) are charged with positioning a scissile phosphate for cleavage. Ser899 and Arg911 will form a hydrogen-bond to the same scissile phosphate, followed by the insertion of the Tyr853 side chain between adjacent nucleotides of the scissile phosphate, creating a non-covalent pi-pi stack between aromatic rings, which interrupts the adjacent nucleotide stacking and subsequently cleaves the oligonucleotide[237]. These residues are found to

be highly conserved within the C2c1 family; therefore, they should be present in AapCas12b and display the same cleavage mechanism. Furthermore, mutations to these essential amino acids demonstrated decreased or complete loss of cleavage activity[237].

1.4. Diagnostics

1.4.1. Routine Molecular Diagnostics

1.4.1.1. Quantitative polymerase chain reaction (qPCR)

Polymerase chain-reaction (PCR) based diagnostics rely on targeted DNA amplification using thermal cycling to synthesize DNA. Developed in 1983, the technique cycles through three heating and cooling steps, including denaturation of target DNA from double-stranded to single-stranded , hybridization of primers to the denatured single-stranded DNA , and DNA polymerase-mediated primer extension[240]. The process can be adapted for detection of RNA samples by adding a reverse-transcriptase (RT) enzyme to convert RNA to cDNA, followed by DNA amplification.

PCR can be defined as quantitative (qPCR) with the real-time monitoring of fluorescent detection, allowing to quantitate PCR product through cyclic detection and cycle threshold definition. qPCR sample detection qPCR often relies on a Taqman technique in which a probe containing a 5'fluorophore moiety and a 3' quencher moiety is hydrolyzed by the 5'-3' exonuclease activity of *Taq* polymerase. Following the Förster resonance energy transfer (FRET) principle, the fluorophore is initially excited via the thermocycler light source and then detected by the instrument. Due to close proximity to the quencher, the fluorescent signal emission is inhibited until polymerase hydrolysis, where the quencher and fluorophore disperse, emitting a fluorescent signal. A thermal cycling spectrofluorometer measures this signal. However, there are alternative qPCR assays to Taqman probing, like SYBR green PCR or locked nucleic acids PCR.

As a molecular approach to SARS-CoV-2 diagnostics, RT-qPCR has its upsides. RT-qPCR assays are usually highly specific, sensitive, and robust, termed the "gold standard" of molecular diagnostics for RNA pathogens. For example, the Center for Disease Control and Prevention (CDC) SARS-CoV-2 N2 primer/probe set can detect 31.5 viral genome copies with a 100% positivity rate[241]. Moreover, as the name suggests, qPCR assays are quantitative, meaning they can quantify, within a range, the total amount of viral genome present in a sample, thus providing information on the viral load in a clinical sample. In addition, the CDC N2 primer/probe set is highly specific to SARS-CoV-2[241].

As a limitation to routine qPCR/RT-qPCR diagnostics, thermocyclers are usually quite expensive, ranging from $20,000 to nearly $100,000, and require a constant power supply (i.e., require being plugged into an outlet with stable power, typically 120V to 240V). Furthermore, PCR-based diagnostics require highly-trained laboratory technicians within a centralized laboratory and controlled conditions for clean and effective assay performance free of contaminants. Due to these requirements, the turnaround time from sampling to result output could take multiple days.

1.4.2. Non-Routine Molecular Diagnostics

1.4.2.1. Reverse-Transcriptase Loop-Mediated Isothermal Amplification (RT-LAMP)

RT-LAMP-based nucleic acid amplification can be separated into two steps, as described in figure 5: Reverse-transcription and amplification. Firstly, sample RNA is reverse-transcribed, using a reverse-transcriptase, generating complementary deoxyribonucleic acid (cDNA). Secondly, the cDNA is then amplified by polymerase amplification. Compared to PCR polymerase amplification which requires thermal cycling, LAMP amplification does not require thermal cycling to allow for DNA denaturation, primer hybridization, and strand extension. Amplification

is permitted due to a keynote feature necessary for the DNA polymerase: a high strand-displacement activity leads to bypassing DNA denaturation at 95°C. The standard primer annealing temperature is approximately 60°C, and extension can be performed at various temperatures, depending on the DNA polymerase. This assay uses a homolog of *Bacillus Stearothermophilus* DNA polymerase I large fragment to amplify cDNA. A synthetic reversibly-bound aptamer proprietary to New England BioLabs is bound to this DNA polymerase, which releases at temperatures above 45°C, whereas the enzyme's optimal temperature is 60°C. The aptamer allows thermal stability at temperatures below 45°C (if left at 25°C for two hours, the enzyme will not lose activity) which prevents the enzyme from prematurely initiating extension. This enzyme also lacks 5' to 3' exonuclease activity.

Unique to RT-LAMP, amplification requires three primer pairs, F3-B3 (forward and backward third primers), FIP-BIP (forward and backward inner primers), and LF-LB (loop forward and backward primers). FIP and BIP each contain two distinct binding regions: a sense-binding region and an antisense dumbbell-folding binding region. First, the FIP primer's sense region binds to the target DNA, initiating complementary strand synthesis. Next, the F3 primer binds to the target DNA, initiating strand displacement synthesis. This step produces a FIP-linked complementary DNA strand which forms a 3' stem-loop due to the antisense binding region within the FIP. This half-dumbell-shaped single-stranded complementary DNA strand serves as a template for BIP-B3-initiated DNA synthesis, resulting in a dumbbell-shaped single-stranded DNA amplicon. This amplicon then undergoes self-primed DNA synthesis forming a stem-loop DNA amplicon. The stem-loop DNA amplicon serves as a template for LAMP cycling, where the FIP primer hybridizes to the complementary regions within the loop, initiating strand displacement synthesis. The product of this amplification is an intermediate-shaped one-gapped stem-loop DNA

and a loop formed at the opposite end via the BIP sequence. This structure then undergoes BIP-primed strand displacement amplification[242]. The end product of LAMP is a mixture of strand-displaced and self-primed DNA synthesis cycling through FIP and BIP-primed synthesis forming a multitude of stem-loop and dumbbell-shaped amplicons of various sizes.

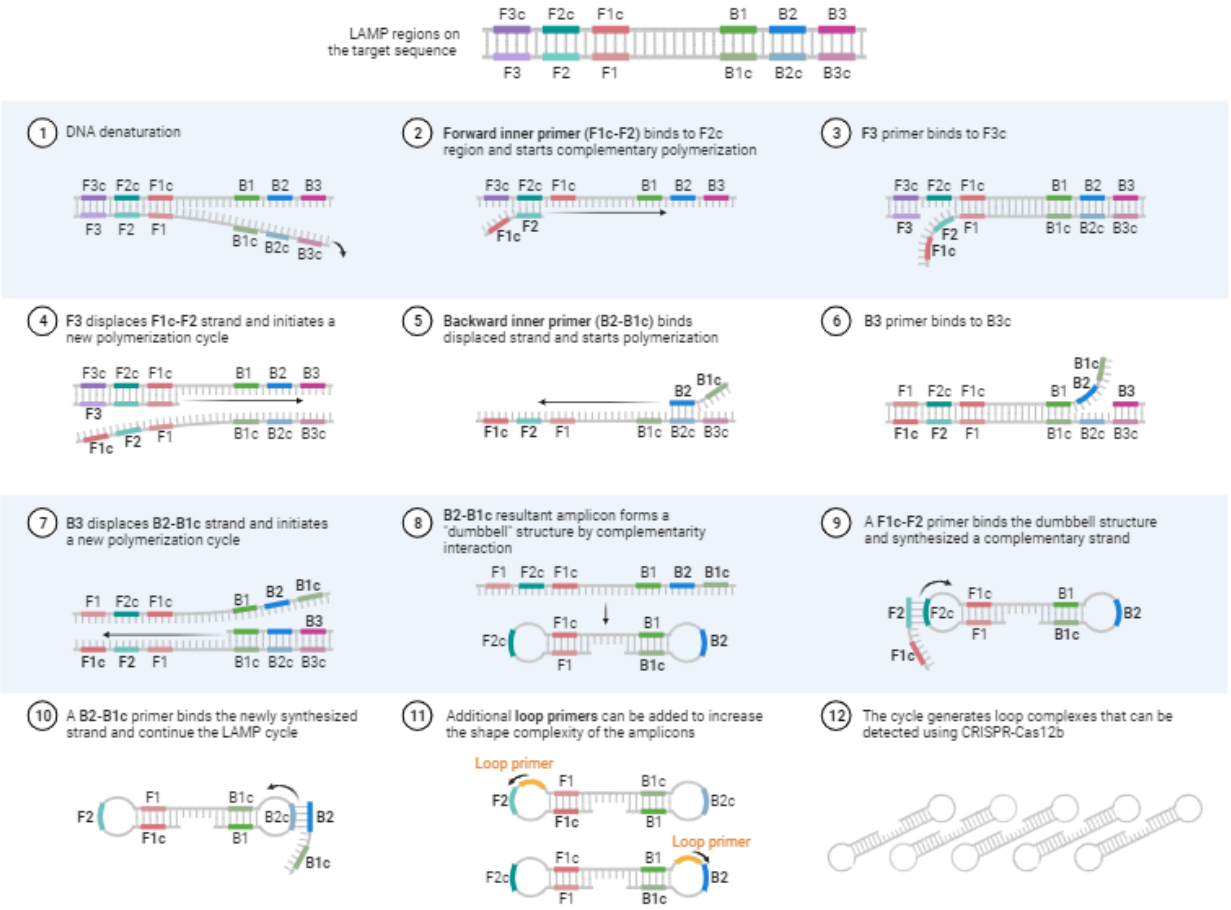


Figure 5. Loop-mediated isothermal amplification of SARS-CoV-2 commences with the reverse transcription of the SARS-CoV-2 target region RNA to cDNA (not demonstrated in the figure). The complementary DNA is subsequently amplified via FIP-BIP and F3-B3 primer pairs. The resulting amplicon self-primes subsequent amplification whilst leveraging the use of LF and LB primers to further amplify the genetic product. The figure was generated using BioRender.

Due to having three primer sets, or six individual primers, RT-LAMP should theoretically have increased specificity to the targeted pathogen, however is also susceptible to artefactual complications. RT-LAMP is also prone to non-specific amplification due to these primers' increased potential for off-target binding. This loss of specificity increases the likelihood of false-positive results or amplification of highly homologous pathogens (i.e., same species, different

strain)[244-246]. Despite the potential pitfalls of RT-LAMP, SARS-CoV-2 RT-LAMP assay specificities have <90% specificity, comparable to that of qPCR[30,247]. Contrary to qPCR's sensitivity in detecting SARS-CoV-2 (>95%), RT-LAMP alone only has a sensitivity of <60%, leaving a gap in sensitive diagnostics with RT-LAMP as a molecular diagnostic approach[247]. Moreover, in contrast to qPCR assays, RT-LAMP-based molecular diagnostics are challenging to design as quantitative, limiting the assay's diagnostic capability. However, combined with CRISPR-Cas systems, RT-LAMP Cas assays have increased sensitivity to RT-LAMP alone[30,247].

Regardless of the few limitations of RT-LAMP, the isothermal nucleic acid amplification approach to rapid and sensitive diagnostics makes sense both in terms of costs and assay performance. Conventional rapid antigen tests and RT-LAMP Cas12b assays cost less than $10 to assemble and perform. However, the benefit of using a CRISPR-based diagnostic approach is that molecular detection is more sensitive and specific while utilizing low-cost equipment when compared to rapid antigen tests. In a laboratory setting, an isothermal fluorometer like the Dialunox ESEQuant TS2.x is perfect for consistent and high-quality fluorescent measurements and costs less than $12,000 CAD. Some laboratories have successfully performed RT-LAMP Cas12b diagnostic assays using simple approaches like a thermal block, water baths, commercially-available sous-vide cookers, and even in combination with lateral flow strips[30].

1.4.2.2. Recombinase Polymerase Amplification (RPA)

Recombinase polymerase amplification (RPA, figure 6) is another isothermal DNA amplification method that can be leveraged for specific and sensitive low-temperature molecular diagnostics. In RPA, when in the presence of Adenosine 5'-triphosphate (ATP) and crowding agents like polyethylene glycol, a recombinase protein (T4 UvsX) binds to primers forming an RNP complex. The RNP complex then scans dsDNA looking to bind to a primer-complementary

sequence, promoting strand invasion once aligned. Next, single-stranded binding proteins (gp32 SSB) bind to the displaced ssDNA strands to stabilize and aid in this strand displacement and prevent primer ejection through branch migration. UvsY, a recombination-mediating protein, promotes efficient UvsX strand invasion by stimulating UvsX DNA-dependent ATPase (helicase) activity while recruiting and stimulating dissociation of ssDNA-gp32 SSB complexes[248]. Upon UvsX-mediated dsDNA strand separation, a DNA polymerase also characterized by strong strand displacement activity (usually *Bacillus subtilis* DNA polymerase I large fragment) binds to the 3'-end of the primer, commencing amplification cycling. RPA can also be adapted to amplify RNA-transcribed cDNA products by starting with a reverse-transcription step[249,250].

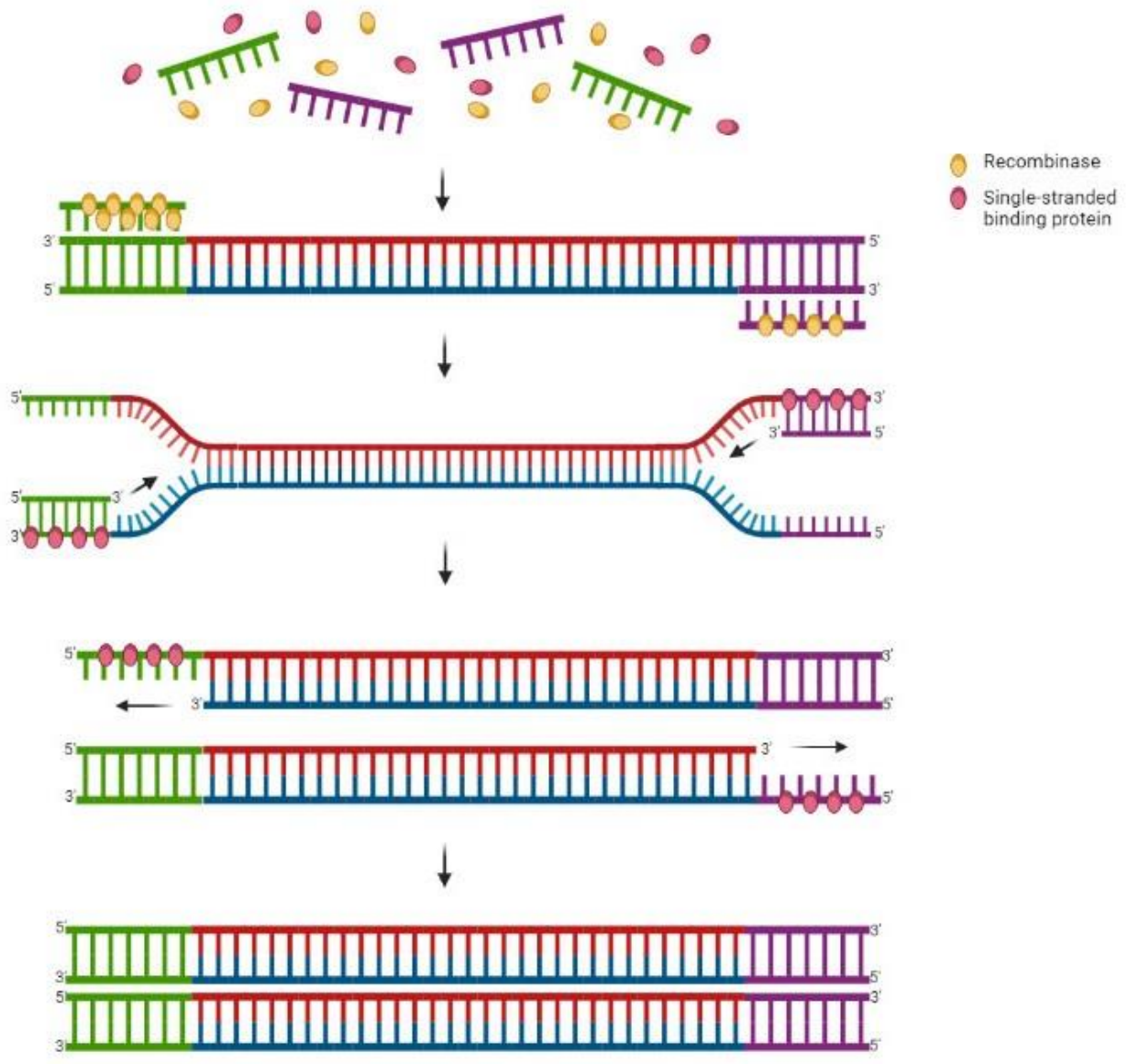


Figure 6. Recombinase polymerase amplification of a DNA product starts with ribonucleoprotein formation of a recombinase enzyme with primers. This RNP then scans for a primer complementary region. Once aligned, the RNP in conjunction with single-stranded binding proteins promotes strand invasion and primer binding. Upon binding, a DNA polymerase initiates 3'-cyclic amplification. The figure was generated using BioRender.

This pre-amplification can be coupled with various deoxy/riboendonucleases, including Cas12b and Cas13a, depending on the amplicon format (RNA or cDNA), for nucleic acid detection via fluorometry. If cDNA is the end-product amplicon, Cas12b can be used directly to detect the amplicon; however, if Cas13a is used, RNA must be the end-product amplicon. Therefore, a T7

RNA polymerase catalyzes RNA transcription from a cDNA amplicon, which the Cas13a protein can subsequently recognize for RNA detection (Li *et al.,* 2023). The entire assay can be performed between 37°C-42°C.

1.4.2.3. CRISPR-Cas-based molecular detection

Cas proteins are activated upon binding with a complementary short palindromic repeat region forming a stem loop. This hairpin structure varies from Cas-ortholog and can occasionally activate more than one Cas protein. For instance, the *Alicyclobacillus acidoterrestris* Cas12b repeat sequence can bind and activate the *Alicyclobacillus acidiphilus* Cas12b ortholog, likely due to having similar thermal stability properties and being harbored in similar microenvironments[30]. As mentioned above, magnesium is essential in activating Cas12 structure catalytic domains. Therefore, for fluorometric detection, the only micro-environmental necessity left for diagnostic detection is the introduction of a nucleic acid reporter labeled with a quenched fluorophore. When target nucleic acid binds to the spacer region of the sgRNA, the RuvC domain is conformationally activated and capable of cleaving all single-stranded and double-stranded DNA present, including added reporter DNA. Once the reporter is cleaved, the fluorophore is unquenched, thereby emitting a detectable fluorescence.

Common CRISPR-Cas proteins like AapCas12b, AsCas12a, LbaCas12a, LbuCas13a, LwaCas13a, PsmCas13b, and various Cas9 proteins can be obtained commercially through large international manufacturers and distributors like New England Biolabs, and locally in Canada from source companies like SignalChem Lifesciences Corporation. In addition, all other reagents needed to perform CRISPR-based molecular detection are readily available, making CRISPR-based diagnostic assays viable as a point-of-care detection method.

1.5. Nucleic Acid Extraction Strategies

1.5.1. Organic extraction

Common organic extraction methods for RNA extraction and isolation from a pathogen are phenol-guanidine isothiocyanate-based/phenol-chloroform-based extractions, also known as triphasic extractions[252]. Triphasic extractions isolate DNA, RNA, and proteins, leveraging their respective polarities in phenol and water to separate each. Triphasic extractions are efficient in producing pure RNA elutions, although not without drawbacks. Due to the requirement of isolating specific solution phases, there are successive chances to contaminate isolated phases with molecules supposedly isolated within another layer phase. In addition, elution volume loss is inevitable with organic-phase extractions as it is difficult to mechanically separate one phase from another, thus not having total nucleic acid representation. Organic phase extractions also use chlorinated and phenol-containing organic reagents, which are known inhibitors to amplification assays[253]. Ultimately, due to highly laborious and manually intensive steps, organic extractions are nearly impossible to automate or simplify for use in point-of-care.

1.5.2. Silica-Membrane Column Extractions

Although silica-membrane column extractions may be laborious and manually intensive, they are simple, requiring minimal setup and cost. Like organic extractions, silica-membrane column extractions leverage nucleic acid polarities to isolate and purify total nucleic acids from a sample. Under high salt conditions, negatively charged RNA and/or DNA will bind to a positively charged silica membrane, isolating the nucleic acids from the remaining sample matrix. Then, nucleic acids are eluted using a lowly-ionic elution solution like water or tris-EDTA buffer[254]. Although about 5%-10% of isolated nucleic acids remain trapped in the spin column, losses are minimal, proving an ideal nucleic acid extraction method[255]. In addition, contaminants within the

nucleic acid elution are generally minimal when using a silica-membrane column, allowing for an efficient extraction protocol. Column extractions are commonly used in the point-of-care as they are inexpensive and efficient; however, they are not usually compatible with an automated extraction system considering they require multiple centrifugation steps before elution. Another limit to this approach is that the column pore sizing limits the nucleic acid product size and quantity therefore limiting the total quantity of end-product isolated from the extraction.

1.5.3. Paramagnetic Particle Extractions

Conventional magnetic particles isolate nucleic acids from various sample types, including lysed virus, tissue homogenates, propagation media, wastewater, and more. Magnetic beads with an iron oxide core can bind nucleic acids using attractive forces; however, they generally cause nucleic acid aggregation. The magnetic nanoparticles are often surface-modified by silanisation and other modifications allowing for specific nucleic acid interactions and preventing such aggregates[256]. These magnetic particles can be isolated using an external magnetic field, ultimately enriching the end-product elution. This approach to nucleic acid isolation is ideal due to the separation of RNA/DNA from matrix contaminants which may affect purity or inhibit nucleic acid amplification methods.

1.5.3.1. Ceres Magnetic NanoTrap Technology for SARS-CoV 2 Extractions

Magnetic hydrogel particles (NanoTrap particles) developed by Ceres Nanosciences, Inc. and the National Center for Biodefense and Infectious Diseases (George Mason University, Manassas, VA, USA) are capable of binding to whole viruses rather than nucleic acids for complete viral isolation and enrichment. These beads function by an affinity capture of various biological agents, including viruses, proteins, and bacteria. The NanoTrap particles are based on a cross-linked N-isopropyl acrylamide core capable of being customized with affinity-bait

modifications like acrylic acid, vinyl sulfonic acid, and Cibacron Blue F3G-A thus preferentially binding to specific analytes[257,258]. These NanoTrap particles allow for simple sample washing, isolating viral particles from inhibitory substances present in sample matrices, followed by direct extraction from the beads or a detergent-based water elution of the viral particles from the beads, avoiding the need for ethanol-based washes. Residual ethanol from these extractions can often strongly inhibit amplification assays[259]. This extraction approach can also be performed and completed within 20 minutes of sample collection, which is ideal for point-of-care applications.

1.6. STOPCovid

STOPCovid was developed with the collective efforts of researchers from the Massachusetts Institute of Technology, Harvard University, Broad Institute of MIT, and Harvard and many more collaborators; and as a part of Dr. Julia Joung's Doctor of Philosophy dissertation. The first iteration of the assay, known as STOPCovid.v1, leverages RT-LAMP amplification of a highly conserved region within the N gene of SARS-CoV-2 with *Alicyclobacillus acidiphilus* Cas12b fluorometric and lateral flow virus detection. The protocol included a virus lysis step using 10X QuickExtract Plant DNA extraction solution (Lucigen Corporation, Custom order) heated at 22°C, 60°C, or 95°C for 5 to 10 minutes. The reagents used in the assay consist of water, $MgSO_4$, Cas12b, a sgRNA, a Tween-20-based amplification buffer, dNTPs, a DNA polymerase I, a reverse-transcriptase, RT-LAMP primers, a reporter DNA, taurine and proteinase K inhibitor. The reagents in the extraction protocol consist of the QuickExtract Plant DNA extraction solution, water, magnetic beads, and proteinase K inhibitor.

The second iteration of the assay, STOPCovid.v2 also developed by Joung and colleagues leverages the same RT-LAMP-Cas12b formulation with select modifications: a reduction of Cas12b and sgRNA concentrations from 500 nM per reaction to 31.25 nM, an increase in reporter

DNA concentration from 125 nM per reaction to 250 nM per reaction, and a non-obligatory addition of proteinase K inhibitor. The considerable modification to the protocol comes from adapting a magnetic bead-based enrichment extraction using in-house laboratory-developed magnetic beads and complex chemical mixtures (the 10X QuickExtract Plant DNA extraction solution). The extraction consists of adding a sample into the DNA extraction mixture containing the magnetic beads and incubating for 15 minutes, followed by the 60°C RT-LAMP Cas12b assay for a predetermined duration. Finally, the extraction proceeded with the SARS-CoV-2 N gene RT-LAMP Cas12b assay and fluorescent or lateral flow detection.

1.6.1. STOPCovid Protocol Limitations

The originators of the STOPCovid.v2 protocol devised an assay that can rapidly, sensitively, and specifically detect SARS-CoV-2 using RT-LAMP Cas12b technology. By leveraging the CRISPR toolbox, researchers developed an alternative diagnostic test detecting SARS-CoV-2 nucleic acids. The development of this assay was fast-tracked, unveiling select complications with the data presented by Dr. Julia Joung and colleagues. Upon review of the method, potential intervention points were identified in optimizing, improving and validating the already impressively effective nascent molecular detection method.

The primary issue with this assay is the lack of validation and optimization data. The original protocol contains twelve reagents, all of which are listed in table 2 including all reagents used in the optimized extraction and RT-LAMP Cas12b protocol. Joung *et al.* presented only critically essential data guided toward validating the functionality of the assay without guiding the reader through the optimization of the assay. This lack of data highlights the need for additional insight into potential intervention points that may improve assay sensitivity or specificity. For example, at the time of publication (October 2020), the most common SARS-CoV-2 variants were

the Alpha, Beta, and Gamma variants. In contrast, the most pathogenic and contagious variants (Delta and Omicron, amongst more) were only first listed in October 2020 and September 2021, respectively[46]. With this information, the STOPCovid.v2 protocol was validated to detect timely relevant variants, opening up a gap in data confirming assay specificity to globally relevant variants.

Table 2. Reagents used in the SARS-CoV-2 rapid enrichment-extraction and N gene RT-LAMP Cas12b assay. Bolded reagent titles were used in the STOPCovid protocol.

Step	Reagent	Catalogue Number	Manufacturer	Final Assay Concentration or Volume	Additional Information
Extraction	Nanotrap Microbiome A particles	44202	Ceres Nanosciences, Inc.	10 µL	-
	1X Phosphate-Buffered Saline, Without Magnesium or Calcium	311-010-CL	Wisent Bioproducts	1X	-
	Thermolabile Proteinase K	P8111S	New England Biolabs, Inc.	1.5 µL or 0.18 Units	-
	Extraction/elution buffer	See additional Information	In-house	-	See Appendix 5.5. for formulation
Extraction and RT-LAMP Cas12b	**Proteinase K Inhibitor**	539470	Millipore Sigma	1X	See Appendix 5.5. for formulation
RT-LAMP Cas12b	**UltraPure DNAse/RNAse-Free Distilled Water**	10977015	ThermoFisher Scientific	-	-
	Magnesium Sulfate ($MgSO_4$) Solution	B1003S	New England Biolabs, Inc.	9 mM	MgSO4 comes with the purchase of the polymerase and reverse-transcriptase.
	AapCas12b	Custom Order	New England Biolabs, Inc.	31.25 nM	-
	single-guide RNA	Custom Order	Integrated DNA Technologies	31.25 nM	-
	Brij-35 Reaction Buffer	See additional Information	In-house	1X	See Appendix 5.5. for formulation
	Deoxynucleotide (dNTP) Solution Mix	N0447L	New England Biolabs, Inc.	1.4 mM	-
	Bst 2.0 WarmStart DNA Polymerase	M0538L	New England Biolabs, Inc.	16 Units	-
	WarmStart RTx Reverse Transcriptase	M0380L	New England Biolabs, Inc.	15 Units	-
	10X Primer Pool	Custom Order	Integrated DNA Technologies	1X	See Appendix 5.5. for formulation
	Reporter DNA	Custom Order	Integrated DNA Technologies	250 nM	-
	Taurine	86329	Millipore Sigma	50 mM	-
	Dithiothreitol	P1171	Promega	2 mM	-

Besides SARS-CoV and MERS-CoV, the described protocol does not validate cross-reactivity against other human-infecting coronaviruses like HCoV-229E, HCoV-NL63, HCoV-OC43, HCoV-HKU1, and other closely related coronaviruses with zoonotic potential. Additionally, the assay was mainly validated using virus-like particles (VLPs) and synthetic SARS-CoV-2 N gene oligonucleotides. VLPs and synthetic oligonucleotides provide idealized conditions restructured to purified target RNA oligonucleotides, reducing the risk of non-specific amplification and off-target effects, which is a concern when using RT-LAMP. However, such conditions over-emphasize the realistic detection limit and sensitivity. Considering AapCas12b can only detect the inputted RNA, which, in this instance, is limited to the SARS-CoV-2 N gene oligonucleotide region, detection is idealized at only detecting one genome region without risk of specificity-loss through primer misbinding. Therefore, using infectious SARS-CoV-2 virus and SARS-CoV-2 RNA is ideal for validating actual assay performance. In addition, the authors developed an internal control leveraging RT-LAMP to amplify and detect glyceraldehyde-3-phosphate dehydrogenase (GAPDH) or beta-actin (ACTB). However, the fluorometric detection of these controls relies upon nucleic acid detection using a non-specific SYTO-9 dye that binds to all RNA and DNA, which is prone to false positive results due to the lack of specificity.

Finally, the authors reason that in-house laboratory-developed magnetic beads used for sample enrichment are significantly cheaper and more easily modified than commercial options. This reasoning is not entirely accurate considering production involves more laborious procedures that limit the point-of-care applicability of their assay whereas commercially available options can be purchased in large quantities at significantly reduced costs, following stringent manufacturer quality control and limiting potential variability. Commercially available magnetic beads such as NanoTrap Magnetic Virus Particles (Ceres Nanosciences, Inc.) are not significantly costly, and the

unit cost vastly decreases when ordered in larger quantities. Scaled production and bulk ordering are standard in developing a rapid diagnostic assay, reducing and maintaining a low unit cost while using extensively validated magnetic particles instead of laboratory-developed magnetic particles. To add to these costs, the authors use a custom ordered 10X concentration of QuickExtract Plant DNA extraction solution at a 1:1 ratio of sample, costing approximately $350 USD for only 5 mL. Combining the cost of the magnetic bead preparation with the extraction solution adds significant overhead to sample processing.

1.6.2. Conservation analysis of the RT-LAMP Primers and AapCas12b target site

In May 2020, authors of the STOPCovid protocol performed a conservation analysis of the SARS-CoV-2 RT-LAMP Cas12b primers and single-guide RNA. The analysis was completed by globally aligning the oligonucleotides with over 31,000 genome sequences obtained from the Global Initiative on Sharing Avian Influenza Data (GISAID) database[30]. The alignments indicated that the primers and the sgRNA were perfectly conserved in ≥99.5% of SARS-CoV-2 genomes.

Since then, new variants, including but not limited to the Beta, Gamma, Delta, and Omicron variants, have been discovered, introducing novel nucleotide mutations/substitutions and indels within the same targeting region. Therefore, an updated conservation analysis was completed by Dr. Julie Chen (Public Health Agency of Canada), aligning the same primers and sgRNA to over 7,000,000 SARS-CoV-2 genome sequences obtained from the same GISAID database. The results of this alignment indicated that the updated conservation rate for the F3, B3, FIP, BIP, LF, LB, and sgRNA remained ≥99% conserved. These results suggest that although new virus variants have emerged since the initial design of these primers, the use of the STOPCovid primers with variants that Joung and colleagues have not confirmed should, remain effective in pathogen detection.

1.7. Ma *et al.* 2019's Nipah Virus RT-LAMP

After an extensive literature search citing no point-of-care diagnostic assays and with the recurrence of Nipah virus outbreaks, the need for rapid molecular diagnostic testing for Nipah virus infection is only increasing. Since the first mention of Nipah virus on PubMed in 1999, various molecular diagnostic polymerase chain reaction assays have been developed detecting all known strains of NiV. However, there is a distinct lack of rapid, deployable molecular diagnostic assays that do not rely on expensive PCR equipment and protocols. One manuscript described a reverse-transcription loop-mediated isothermal amplification assay detecting all known Nipah virus strains in 2019[286]. Since then, there have not been any additional publications describing the development of rapid molecular diagnostic methods for Nipah virus.

Ma and colleagues used a unique RT-LAMP formulation, including enhancement strategies like the use of betaine, a Triton X-100-based polymerase amplification buffer (1X ThermoPol Reaction Buffer, New England Biolabs, Cat. No.: B9004S), a magnesium sulfate concentration of 6 mM and approximately the same primer ratios and enzymes as the STOPCovid assay. The primary pathogen detection method qualitatively interpreted turbidity using a real-time turbidimeter or adding a pH-sensitive calcein indicator for colorimetric detection. The assay targeted a conserved region with the NiV N gene and could detect all known strains of NiV (two strains known at that time). The assay did not cross-react with highly homologous pathogens like Hendra virus, Newcastle disease virus, Japanese encephalitis virus, or Influenza A virus. The assay was capable of detecting approximately 100 pg of Nipah pseudovirus RNA, which, when considering the Nipah genome length of roughly 18.2 kilobases, is equivalent to the range of $9.7x10^6$ to $1.0x10^7$ genome copies.

1.8. Isothermal amplification and CRISPR enhancement strategies

The optimization of the SARS-CoV-2 RT-LAMP Cas12b assay developed by Joung *et al.* termed STOPCovid was investigated to verify if further increases in assay performance were possible compared to the original publication's claimed version. Twelve components within the SARS-CoV-2 RT-LAMP Cas12b assay can be evaluated as potentially optimizable; Reaction buffer, deoxyribonucleotide triphosphate (dNTP), $MgSO_4$, a polymerase, a reverse transcriptase, primers, a Cas12b protein, a reporter DNA, taurine, Proteinase K inhibitor and double-distilled water (ddH_2O). In this project, the approach to optimizing the RT-LAMP Cas12b assay started with evaluating core components necessary for RT-LAMP Cas12b assay functionality, including the titration of dNTP, $MgSO_4$, AapCas12b, and the AapCas12b sgRNA. The next step was to identify the optimal formulation for the RT-LAMP reaction buffer by substituting the detergents used to stabilize and reduce secondary structure formations, titrate the optimal pH for enzymatic activity, and nucleoprotein complex collateral cleavage. Commercially available and published formulations were also trialed to identify an optimal candidate buffer formula.

Reverse transcriptases and DNA polymerases alternative to those used in STOPCovid were explored as potential options that may improve RNA-cDNA conversion or DNA amplification. Once these critical components to the reaction were optimized, additional parameters identified through literature search that could potentially improve the were iteratively analyzed seeking to improve the assay; including but not limited to the use of poly-thymine-linked primers, the use of 4 vs. 6 primers, L-proline/bovine serum albumin, dithiothreitol and helicases as assay enhancers.

1.9. Hypothesis

The primary focus of this graduate work follows an exploratory hypothesis diving into the optimization and translation/development of rapid and sensitive RT-LAMP Cas12b diagnostics. The SARS-CoV-2 RT-LAMP Cas12b assay developed by Joung and colleagues provides potential opportunities to optimize a functional RT-LAMP Cas12b protocol. In contrast, the imminent need for rapid NiV diagnostics is heightened by near-annual outbreaks in the Eastern hemisphere. Due to this thesis being a methods-based exploration that requires step-by-step interpretation, the results and the discussion sections will contain similar content reasoning and explanations, which may be repetitious.

1.10. Rationale

CRISPR-associated protein-based isothermal rapid diagnostics is collectively a nascent and revolutionary field in rapid molecular diagnostics at the point-of-need. Many diagnostic platforms have been developed recently for the detection of SARS-CoV-2, Zika virus, Dengue virus, Crimean-Congo Hemorrhagic Fever virus, among others, leveraging the CRISPR toolbox and isothermal amplification methods. Notably, RT-LAMP and RPA coupled with DNA or RNA endonucleases like Cas12b and Cas13a can be used for the rapid and sensitive fluorometric detection of genomic nucleic acids. The assay format can be designed with programmable pathogen specificity. This molecular diagnostic approach often demonstrates a limit of detection, sensitivity, and specificity similar to that of polymerase chain reactions. Emerging and re-emerging infectious disease outbreaks require rapid, portable, and simple diagnostics methods. There is a critical gap in Canada's capacity to respond to these high impact events. In turn, developing highly specific, sensitive, and rapid pathogen molecular detection assays is crucial.

Currently, there are limited SARS-CoV-2 and no Nipah virus diagnostic assays utilizing CRISPR technology at the point-of-need.

1.11. Aim

Adapt and optimize parameters to improve the SARS-CoV-2 N gene RT-LAMP Cas12b assay for detection of SARS-CoV-2 in both animals and humans. This assay will be adopted for use as a functional point-of-care assay detecting Nipah virus.

1.12. Objectives and Outcomes

Objective 1:

Optimize the SARS-CoV-2 RT-LAMP Cas12b assay to obtain as close to an ideal detection limit of 1 genome copy per microliter with the lowest time-to-detection possible.

Outcome 1:

The SARS-CoV-2 RT-LAMP Cas12b assay metrics were enhanced by substituting Tween 20 with Brij-35 as the detergent in the amplification buffer, increasing the $MgSO_4$ concentration and by adding dithiothreitol as a chemical enhancer to the reaction. The limit of detection obtained was 50 genome copies per microliter

Objective 2:

Translate SARS-CoV-2 RT-LAMP Cas12b assay to detect all strains of Nipah virus available at the National Centre for Foreign Animal Diseases (NCFAD).

Outcome 2:

The SARS-CoV-2 RT-LAMP Cas12b was successfully translated to detect all strains of Nipah virus stored at the NCFAD by designing and using NiV-specific RT-LAMP primers and a sgRNA with a spacer targeting the NiV N gene.

Objective 3:

A) Develop and optimize a rapid RNA extraction protocol for SARS-CoV-2 and verify functionality with Nipah virus.

B) Complete validation required for the development of a rapid diagnostic kit.

Outcome 3:

3A) A simple, inexpensive, and rapid RNA enrichment-extraction protocol was developed and optimized using affinity virus capture beads, detergents, and a thermolabile proteinase K (TLPK) to disrupt the viral envelope and degrade the nucleocapsid, releasing viral RNA.

3B) Validation requirements have been established between the NCFAD and are currently in progress.

2. Materials and methods

2.1. Nuclease-Free Workflow

To ensure a nuclease-free workflow, the biosafety cabinet or RNA workstation was sprayed with Nuclease Decontamination Solution (Integrated DNA Technologies, Cat. No.: 11-05-01-01), given a one-minute contact period, then wiped with a WypAll disposable wipe to remove any remaining solution. Sample or reagent aliquots and storage tubes were kept sterile and limited to being opened in nuclease-decontaminated cabinets or workstations. Assumptions were made that all reagents received directly from manufacturers were already nuclease-free, thus only opened

within nuclease-decontaminated cabinets or workstations and transferred to sterile storage tubes as needed. As an exceptional circumstance, UltraPure DNAse-RNAse-Free Distilled Water (Thermo Fisher Scientific, Cat. No.: 10977023) was purchased as an extra precaution due to water being the primary RNA elution solution and core buffer solvent. In addition, pipettes dedicated to CRISPR research were purchased to limit potential cross-contamination from pipettes used for routine clinical diagnostics and other research activities.

2.2. Handling and Removal of Samples from High Containment

For safe handling of live SARS-CoV-2 and MERS-CoV, all cell infections and Ceres MNP extractions were performed in CL3ag. All NiV cell infections and Ceres extractions were performed in a containment level 4 facility to handle the live Nipah virus safely. Samples were inactivated according to the National Centre for Foreign Animal Disease (NCFAD) Standard Operating Procedures (SOPs) to remove samples from high containment facilities for safe handling and analysis. Samples destined for RNA extraction were aliquoted in TriPure Isolation Reagent (Millipore Sigma, Cat. No.: 116671465001), then transferred from CL3ag or CL4 to containment level 3 (CL3). Samples containing virus-infected cells (e.g., plaque assays) were fixed with 10% formalin removed after twenty-four hours to CL3 for analysis.

2.3. Cell Lines, Maintenance, Virus propagation

Vero E6, Vero 76 (both African green monkey kidney cells), and Vero E6 TMPRSS2 (Human transmembrane serine protease 2-expressing African green monkey kidney cells, obtained from the Japan Cell Culture Bank) were maintained in Dulbecco's modified eagle medium (DMEM; Wisent Bio Products, Cat. No.: 319-016-CL) supplemented with 10% Characterized Fetal Bovine Serum (FBS; Cytiva HyClone™ Laboratories Inc., Cat. No.: SH30071) and 1X penicillin-streptomycin (Wisent Bio Products, Cat. No.: 450-201-EL). Cells were seeded and

maintained at 37°C and 5% CO_2 until ≤90% confluency in a cell culture-designated incubator. Cell density was quantified using a Trypan Blue dead cell exclusion dye (Invitrogen, Cat. No.: 15250061) on the Nexcelom Cellometer Auto T4 automated cell counter (Nexcelom Bioscience). Cells were passaged daily or weekly, depending on purpose and use. Nutrient-depleted media was first removed to pass cells, followed by a Dulbecco's phosphate-buffered saline (DPBS: Wisent Bio Products Cat. No.: 311-425-CL) wash. Cells were then trypsinized with 0.25% Trypsin/EDTA (Wisent Bio Products, Cat. No.: 325-043-CL) and observed through microscopy to ensure cell detachment. Cells were then resuspended in nutrient-filled DMEM to neutralize trypsin activity and divided accordingly.

Viral inoculum was prepared in serum-free DMEM, incubated on susceptible cells for one hour, followed by the addition of maintenance DMEM at reduced serum conditions (2%). All experiments using live infectious SARS-CoV-2 and MERS-CoV were conducted in a containment level 3-agriculture facility (CL3ag). Work within the CL3ag laboratory at the NCFAD followed all institutional SOPs. All experiments using live infectious Nipah viruses were conducted in a CL4 laboratory at the NCFAD following the institutional SOPs.

2.4. Viruses and RNA

SARS-CoV-2 – Wuhan 1 variant (Hu-1, Accession No. : SARS-CoV-2 isolate hCoV-19/Canada/ON-VIDO-01/2020, GISAID Accession No.: EPI_ISL_425177; 4th passage on Vero E6 cells), SARS-CoV-2 – Delta variant (Vero E6 cells), and SARS-CoV-2 – Omicron variant (Vero TMPRSS2 cells) were kindly gifted from the Public Health Agency of Canada. SARS-CoV-2 viruses were amplified, purified, aliquoted, and stored at -70°C until future use.

Nipah virus – Malaysia genotype (NiV-MY; 4th passage on Vero 76 cells, isolated from pig lung) and recombinant Nipah virus – Bangladesh genotype (rNiV-BD; generated and kindly

gifted by Dr. Darwyn Kobasa (Public Health Agency of Canada), based on Accession No.: AY988601, JN808863 and JN808857) were amplified, purified, aliquoted and stored at -150°C until future use.

RNA used for cross-reactivity testing was obtained through historical extraction catalogs stored at the NCFAD. Samples were stored at -70°C until RT-LAMP Cas12b testing.

2.5. Plaque Assays

Plaque assays were performed to determine the titers of infectious viruses in cells and their supernatants of stocks destined for RNA extraction. Forty-eight well plates were seeded with the desired cell line and incubated at 37C with 5% CO_2 until ≥90% confluency. Virus stocks were initially serially diluted in serum-free DMEM. Cells were then washed with serum-free DMEM, followed by incubation with 75 uL or 100 uL of diluted virus (plaque count was adjusted depending on the volume of virus added) in a cell culture-designated humidified incubator. Samples were run in triplicate to ensure virus titer accuracy. Following the incubation period, 0.5 mL of 1.75% carboxymethylcellulose (CMC) was added to each well, and the plate was incubated for three days. After three days of incubation, the plates were fixed with 10% formalin and removed from CL3ag as per 2.1.. In CL3, fixed cells were washed with water, dried, then stained with 0.5% Crystal violet (Ricca Chemical, Cat. No.: 3235-4) for forty-five minutes. Stained plates were washed with water and dried; plaques were then counted under a microscope to determine infectious titers. Infectious virus titers were used to standardize the number of infectious particles, in plaque-forming units (PFU) per ml, to be used when spiking saliva or viral transport medium (VTM).

2.6. Ultracentrifugation Virus Concentration

A modified sucrose-ultracentrifugation protocol was performed to purify and concentrate infectious SARS-CoV-2 particles, to be tested for protease viral lysis efficacies. After SARS-CoV-2 propagation, culture supernatants were harvested and centrifuged at room temperature at 180 g/min for 5 minutes to purge the sample from cellular debris. 20 mL of the purified supernatant was gently layered on top of 8 mL of equilibration buffer containing 20% sucrose (Fisher Scientific, Cat. No.: S5-500), Tris-HCl (Invitrogen, Cat. No.: 15567-027), NaCl (Invitrogen, Cat. No.: AM9757),EDTA (Ambion, Inc., Cat. No.: 9262) and 18-ohm water within an Open-Top Thinwall Ultra-Clear centrifugation tube (Beckman Coulter, Cat. No.: 344058). Ultracentrifugation was performed in a Beckman Coulter XPN-100 Ultracentrifuge using the SW 32 Ti swinging bucket rotor at 27000 rpm (12300 RCF) for two hours at 4°C. Supernatants were then removed, and the viral pellet was resuspended in 200 µL of Qiagen protease buffer (contents listed in 2.8.3.). Concentrated virus samples were then aliquoted and stored at -70°C. Aliquots were randomly selected to have the virus titer quantified by plaque assay (as described in 2.5).

2.7. Clinical Swab and Mock Clinical Sample Preparation

Archived mink and deer swab samples used to validate the SARS-CoV-2 RT-LAMP-Cas12b assay were initially processed as diagnostic submissions to the NCFAD Special Pathogens Unit. Processing included identification of SARS-CoV-2 positive or negative-status using RT-qPCR (see 2.11.). To mimic a swabbed sample, Viral Transport Medium (Corning Incorporated, Cat. No: 25-500-CI) was spiked with pre-calculated concentrations of SARS-CoV-2-infected cell culture media. Clinical mimic samples were directly used fresh and not stored in a freezer (frozen) to validate efficacy of the in-house-developed enrichment-extraction protocol.

2.8. RNA Extractions

2.8.1. QIAamp Viral RNA Mini Kit (Qiagen, Cat No.: 52904)

RNA extractions using the QIAamp Viral RNA Mini Kit was performed following the protocol as described by QIAGEN and/or by modifying select extraction steps. Samples inactivated in TriPure Isolation Reagent were first mixed with cold 70% ethanol at a 1:1 ratio and thoroughly mixed by pipette. Samples were then transferred to RNeasy Mini spin columns and centrifuged at ≥8000 x g for 30 seconds using an Eppendorf 5415 R Centrifuge. Samples were then washed 3 times with RW1 buffer (Qiagen, Cat No.: 1053394) to remove unwanted biomolecules and then spun at ≥8000 x g for 30 seconds. Three subsequent washes with Qiagen RPE buffer (Qiagen, Cat No.: 1018013) were performed to remove trace salts left from the previous wash, spun at ≥8000 x g for 30 seconds. The columns were then spun dry at 15000 x g for 1 minute to remove residual buffer. RNA was then eluted from the column by adding 30-50 µL of nuclease-free water and spun at ≥8000 x g for 1 minute. Eluted RNA was stored at -70°C until future use.

2.8.2. MagMAX™ CORE Nucleic Acid Purification Kit (Applied Biosciences, Cat. No.: A32702)

RNA extractions using the MagMAX™ CORE Nucleic Acid Purification Kit followed a protocol developed in-house after extensive literature searches of publications using the same kit. MagMAX™ CORE RNA purifications were performed on the Thermo Scientific™ KingFisher™ Duo Primer Purification System. Eluted RNA was stored at -70°C until future use.

2.8.3. In-house developed SARS-CoV-2 Rapid Extraction using Nanotrap® Magnetic Virus Particles (Ceres Nanosciences, Inc., Cat. No.: 44202)

RNA extractions using MNPs followed a protocol heavily modified from an existing Ceres Nanosciences, Inc. (Protocol No.: I-057, custom request for protocol) protocol. To start, 10 µl of

MNPs were added to 990 µL of sample (saliva or spiked VTM), briefly vortexed to homogenize, and incubated at room temperature for 10 minutes. The samples were then placed on a magnetic rack (Invitrogen DynaMag™, Thermo Fisher Scientific, Cat. No.: 12321) for 3 minutes to separate the MNPs from the supernatant. The supernatant was then carefully discarded without disturbing the MNP pellet. 500 µL of 1X DPBS (without calcium and magnesium) was added to MNPs to resuspend and to wash the beads from any residual sample matrix, then the sample was placed on a magnetic rack for 30 seconds to separate the MNPs from wash. Wash supernatant was then carefully discarded without disturbing pellet. Pellet was then resuspended in 45 µL of Qiagen extraction solution containing 10 mM Tris-Cl pH 8.0 (Thermo Fisher Scientific, Cat. No.: AM9855G), 50 mM KCl (Thermo Fisher Scientific, Cat. No.: AM9640G), 1.5 mM $MgCl_2$ (Thermo Fisher Scientific, Cat. No.: AM9530G), 0.45% Tween 20 (Thermo Fisher Scientific, Cat. No.: 28320), 0.5% Triton X-100 (Thermo Fisher Scientific, Cat. No.: 85111) and 0.18 U (1.5 µL) Thermolabile proteinase K (New England BioLabs, Cat. No.: P8111S), gently pipette-mixed and incubated at room temperature for 2.5 minutes to lyse the virus. Directly after the 2.5-minute lysis incubation, 5 µL of Proteinase K Inhibitor solution (preparation described in appendix 5.5.) (PKI; Millipore Sigma, Cat. No.: 539470-10MG) was added to inhibit remaining protease activity and to prevent accidental downstream AapCas12b degradation. Samples were then placed on a magnetic rack for 30 seconds to separate the MNPs from the extraction solution containing PKI, acting as the eluent solution. Supernatant was then collected and stored at -70°C until future use.

2.9. RNA Quantification

RNA isolated and purified using the techniques described in 2.8.1. and 2.8.2. were quantified using a NanoDrop One Microvolume UV-Vis Spectrophotometer (Thermo Fisher Scientific, Cat. No.: ND-ONE-W), measuring nucleic acid sample absorbance at 260 nm to

calculate RNA concentration in nanogram per microliter (ng/µL). RNA sample absorbance and concentrations were measured by adding 1 µL of sample on the reader. RNA quantification following the NanoTrap Magnetic Virus Particle extraction was not possible as the spectrophotometer was located in the primary CL3 laboratory space, whereas the MNP extraction was conducted in CL3ag. The MNP extracted RNA could not be removed for quantification due to NCFAD institutional SOPs regarding safety testing and safe removal of samples from CL3ag being limited to internally validated protocols.

2.10. RT-LAMP Cas12b assay

RT-LAMP Cas12b normally operates between 55°C-70°C and Cas12b proteins function around the 60°C temperature point. The thermal profile of this assay, as visualized in appendix 5.1. was held continuous at 60°C for one hour, although select optimization steps increased the assay time in hopes of visualizing late cycle amplification. Generally, sixty fluorescent measurement cycles were applied to the thermal-fluorometer, irrespective of the device, corresponding to one minute intervals in fluorescence measurements (1 cycle was equivalent to 1 detection minute). The SARS-CoV-2 RT-LAMP Cas12b primer set and sgRNA used in this assay and in STOPCovid v2 can be found in appendix 5.3.2., including the poly-thymine-linked forward and backward inner primers described in 3.2.1.4.1. The selected N gene primer set and sgRNA sequences used in the assay targeting Nipah virus are found in appendix 5.3.3..

The RT-LAMP-Cas12b reagent setup can be visualized in appendix 5.5. This appendix describes the individual preparation of the 15.4 µM AapCas12b stock dilution, the E gene sgRNA, the Brij-35 reaction buffer, the 10X primer pool, the 10 µM reporter DNA working stock, the 500 mM taurine working stock, the 10X proteinase K inhibitor solution, and the 100 mM DTT solution. An overview of the entire RT-LAMP Cas12b assay setup is also included in appendix 5.4.

2.10.1. RT-LAMP Cas12b Primer and sgRNA Design

Suggested parameters from Lucigen Corportation were taken into consideration when designing RT-LAMP primers. The parameters were as followed:

1. Maximum amplicon length ≤ 280 base-pairs.
2. Avoid runs of 3 or more singular base-pair type and multi-dinucleotide repeats.
3. Primers should be of similar melting temperatures (±5°C).
4. Primers are not to be complementary to each other.
5. Use the largest ΔG for dimer analysis (min. -3.5).
6. Use the smallest ΔG for primer ends (max of -4).
7. Hairpins should have a melting temperature lower than the annealing temperature (on average between 55°C and 65°C).
8. Mutations/degeneracies in 5'-ends of F3, B3, F2 and B2 primers will least impact primer performance.
9. Mutations/degeneracies in 3'-ends of F1c and B1c will impact primer performance.
10. Internal primer mutations/degeneracies will least impact primer erformance.

Degeneracies were introduced in select primers to ensure full sequence coverage, improving the likelihood of successful amplification, detection and increasing target region specificity. Degeneracies in primers used for isothermal amplification coupled with CRISPR detection have proven to broaden strain coverage and detection. In regard to sgRNA, literature suggests conventional target region length appears to be strictly 20 nucleotides[260]. Potential implications to oversized target regions would include steric hindrance on the CRISPR-Cas protein. However, data collected at the NCFAD (not included) suggests that the target region limited to 20 nucleotides in length is not critical (NiV N gene sgRNA spacer targeting region

consists of 23 nucleotides in length). Considering the potential effects on the Cas protein, the longest sgRNA design length is 23 nts and the shortest is 20 nts. NiV RT-LAMP primers were designed using the NEB LAMP Primer Design Tool (New England Biolabs), a free open-access primer design tool that enables specific primer design parameters. The single-guide RNA target regions were designed by hand using Geneious Prime once the RT-LAMP primer designs were finalized.

2.10.2. Optimized One-Pot Reverse-Transcriptase Loop-Mediated Isothermal Amplification-AapCas12b collateral cleavage and fluorescent detection

The one-pot SARS-CoV-2 and Nipah virus RT-LAMP-Cas12b reaction performs at a total volume of 50 µL. The assay is modular in a way where the total reagent volume can vary from 45 µL to 49 µL and the input of extraction template/extracted RNA can vary between 1 µL to 5 µL, ultimately making an final volume of 50 µL per reaction. Working within a PCR workstation, nuclease-free water (Thermo Fisher Scientific, Cat. No.: 10977023), 9 mM Mg_2SO_4 solution (New England Biolabs, Cat. No.: B1003S), 31.25 nM AapCas12b (New England Biolabs, Custom order), 31.25 nM sgRNA (Integrated DNA Technologies, Custom order), 1X Brij-35 Buffer, 1.4 mM deoxyribonucleotide (dNTP) solution mix (New England Biolabs, Cat. No.: N0447L), 6.4 units of Bst 2.0 WarmStart® DNA Polymerase (New England Biolabs, Cat. No.: M0538L), 6 units of WarmStart® RTx Reverse Transcriptase (New England Biolabs, Cat. No.: M0380L), 1X primer pool, 250 nM reporter DNA (Integrated DNA Technologies, Custom order), 50 mM Taurine (Millipore Sigma, Cat. No.: 86329), 1X proteinase K inhibitor solution and 2 mM DTT was added to the appropriate-sized tube, while on ice, on a 96-well cooler block or a benchtop cooler (Fisher Scientific, Cat. No.: 15-350.61). All reagents were thawed at room-temperature and kept on a benchtop cooler to prevent precipitation or loss of component integrity before being added to the

master mix. After combining the RT-LAMP-Cas12b reagents, forming the master mix, 1 µL to 5 µL of RNA was added to the reagent master mix and samples were placed within one of the thermal-fluorometers described in 2.10.3.. The reaction was performed as per 5.1..

2.10.3. Fluorometers

Two fluorometers were used for fluorescent detection of RT-LAMP Cas12b: CFX96 Touch Real-Time PCR Detection System (Bio-Rad) and ESEQuant TS2.4 tube scanner (Dialunox). The CFX96 platform was primarily used for RT-LAMP-Cas12b optimization using extracted nucleic acids, whereas the ESEQuant platform was used in high-containment primarily when extracting nucleic acids from live pathogens, and directly performing RT-LAMP Cas12b on nucleic acid samples that have not been extracted according to National Centre for Foreign Animal Disease (NCFAD) Standard Operating Procedures (SOPs). The unit readout for the Bio-Rad platform is measured in relative fluorescence units and the unit readout for the Dialunox platform is registered in millivolts (mV). The ESEQuant platform is portable and versatile, user-friendly and functional at the point-of-care, making it an ideal device to be used for isothermal fluorometric detection in high-containment laboratories.

2.11. SARS-CoV-2 RT-qPCR

The SARS-CoV-2 RT-qPCR protocol used the N2 primer/probe set (appendix 5.3.1) designed by the Center for Disease Control and Prevention (U.S.A). RT-qPCR reactions were performed on an Applied Biosystems 7500 Real-time PCR system using TaqPath 1-step RT-qPCR Master mix (Thermo Fisher Scientific, Cat. No: A15299). Cycle threshold was calculated using the Applied Biosystems 7500 Software automatic threshold calculation using a standard curve of diluted SARS-CoV-2 N gene dsDNA gBlock (Integrated DNA Technologies). The RT-qPCR assay was used to validate the integrity and the quantity of nucleic acids obtained by extraction, as

well as a confirmatory measure validating that the nucleic acids extracted were in fact from SARS-CoV-2.

2.12. Statistical Analysis

3. GraphPad Prism v.9.0.2 (GraphPad Software Inc., San Diego, CA. USA) was used for statistical analysis of data acquired with RT-LAMP Cas12b assays. Plots and graphs were also generated using the software. Significance of differences in interpreted data generated with the RT-LAMP Cas12b assay was calculated using *Student's* paired *t* test, where a p value less than 0.05 was defined as statistically significant.

3. Results

Although not necessary for optimization and validation of assay, most steps regarding optimization and validation have been tested in technical and/or biological triplicates, on differing days. Replicates of assays where optimization attempts appeared unsuccessful or did not noticeably improve the assay were not re-run as duplicates and triplicates. The assays were performed using no template controls (NTC; double-distilled water - ddH_2O) and often, a positive control consisting of high concentration ($\geq 10^5$ genome copie/µL) SARS-CoV-2 or NiV RNA extracted using in-house validated extraction protocols like those described in 2.8.. These were completed to ensure proper validation when presenting data which may be used in clinical applications. Considering multiple replicates on differing days is required for a complete validation package, testing with human and animal samples is still in progress.

3.1 Virus propagation

The SARS-CoV-2 RT-LAMP Cas12b assay was validated and optimized using three SARS-CoV-2 viruses obtained by the NCFAD as kind gifts from the Public Health Agency of Canada (PHAC):

1. SARS-CoV-2 Strain : Wuhan-1
2. SARS-CoV-2 Strain : Delta
3. SARS-CoV-2 Strain : Omicron

The NiV RT-LAMP Cas12b assay was developed, optimized and validated using two different genotypes.

1. Nipah virus genotype Malaysia
2. Recombinant Nipah virus genotype Bangladesh

3.2. SARS-CoV-2 RT-LAMP Cas12b

3.2.1. Iterative Optimization Metrics

The metrics interpreted in RT-LAMP Cas12b are as follows:

1. Signal Maximum; most elevated relative fluorescent unit (RFU) detected by the fluorometer, which provides insight on assay sensitivity. Increases in signal maxima allow for potential improvements in detecting samples with low genome copy quantities.
2. End-point fluorescence; the last relative fluorescent unit reading detected by the fluorometer within the designated RT-LAMP Cas12b timeframe. Provides the same insight as the signal maximum considering there is very little difference between signal maximum and end-point fluorescence, unless mentioned otherwise.

3. Detection time; the earliest time point surpassing the minimum positive threshold (τ; simply referred to as the threshold). Provides insight on the reaction speed.
4. Time to half of the maximum fluorescence; the median of the entire range of the relative fluorescent units detected by the fluorometer. Indirectly provides insight on reaction efficiency.

The cutoff point of a negative test was established as the mean of all NTC RFUs plus three standard deviations of the NTCs. A raw fluorescent unit detected above the τ is considered SARS-CoV-2 or NiV positive whereas a raw fluorescent unit detected below the τ is considered negative.

3.2.1.1. Core Assay Conditions

3.2.1.1.1. New England Biolabs AapCas12b-sgRNA Titration and comparison to SignalChem AapCas12b

The AapCas12b and N gene sgRNA were both titrated at equimolar concentrations to validate and potentially optimize the RNP complex concentration needed for effective detection of SARS-CoV-2 RNA. The AapCas12b and the sgRNA were titrated from 10 nM per reaction to 75 nM, including 31.25 nM established by Joung *et al.* as the optimal concentration in the STOPCovid.v2 protocol. An upper limit of 75 nM was set due to the increased assay cost when significantly increasing reagent concentrations. The data previously obtained by Joung *et al.* suggests that non-specific detection is increased as the sgRNA concentration increases, therefore a maximal limit was set in an attempt to minimize or prevent these potential effects. This upper limit was also chosen to limit costs for Cas12b; 75 nm of Cas12b would more than double the concentration of protein used, doubling protein costs alone. All other conditions within the RT-LAMP Cas12b assay were kept unaltered and constant as described in the STOPCovid protocol.

Results from the titration of both reagents revealed that the optimal concentration for RNP complexes was well established in the STOPCovid.v2 protocol (Fig.7). The ideal concentration of

N gene sgRNA and AapCas12b is between 30 and 40 nM, at equimolar concentrations. Non-equimolar concentrations were not tested, but mathematical modelling found in literature suggests equimolar concentrations as optimal. Low standard deviations in the signal maxima were obtained within this range. A wide range of Cas12b-sgRNA concentrations that provide the similarly elevated detection times, with little variation in signal maximum is ideal in the context of point-of-need by allowing room for variation when the test is performed in the field. With the results presented, AapCas12b and the corresponding sgRNA were kept constant at 31.25 nM.

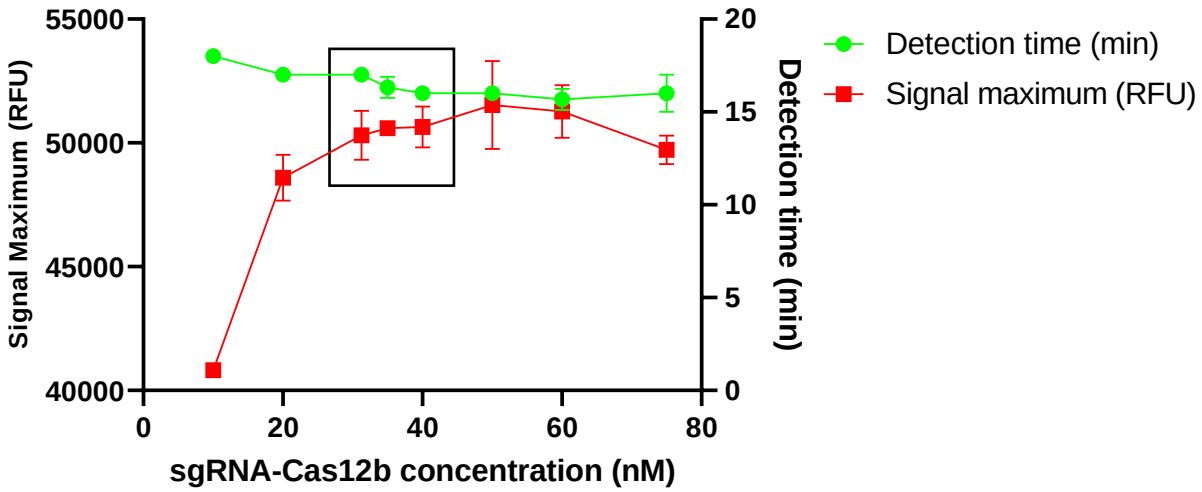


Figure 7. The titration of the New England Biolabs Inc. AapCas12b enzyme and the SARS-CoV-2 N gene sgRNA at equimolar concentrations, from 10 nM to 75 nM. The results with error bars are means of three technical replicates (n=3) and the error bars represent the standard deviations.

As a follow-up to identifying the optimal concentration of AapCas12b using the protein manufacturered by New England Biolabs, comparisons to Cas12b orthologs would have provided insight as to which Cas12b may exhibit the most robust and sensitive transcleavage activity. Unfortunately, attemps to acquire *Alicyclobacillus acidoterrestris* Cas12b and *Brevibacillus sp.* Cas12b were unsuccessful and in-house generation of the protein was not feasible.

As an alternate avenue, another manufacturer, SignalChem Lifesciences Corporation, was contracted to generate and purify the same protein, AapCas12b. Comparing one protein to the same made from another manufacturer leverages the potential in finding a protein generated with better activity, purity and more streamlined production processes that may have less detrimental effects on protein integrity and activity. SignalChem Lifesciences Corporation was selected as it focuses on research and development of recombinant proteins and the company is based in Richmond, British Columbia, making it an ideal source for local reagent manufacturing for a national supply chain. Herein, the SignalChem AapCas12b protein was also titrated at equimolar concentrations with the SARS-CoV-2 N gene sgRNA in an attempt to identify the locally-manufactured protein's optimal concentration. Seen in figure 8, the protein exhibited approximately the same trends in signal maxima and detection times as the New England Biolabs protein (see fig.7). The main difference observed was a decrease in total signal maximum across the range of Cas12b-sgRNA concentrations, where the New England Biolabs protein signal maximum ranged from approximately $4.8x10^4$ RFU to $5.1x10^4$ RFU when using 20 nM equimolar and the SignalChem protein ranged from approximately $3.8x10^4$ RFU to $4.3x10^4$ RFU. The detection times varied by only a few minutes between the two proteins, demonstrating that the transcleavage are of similar activity and could likely be used interchangeably with little effect on the signal maxima.

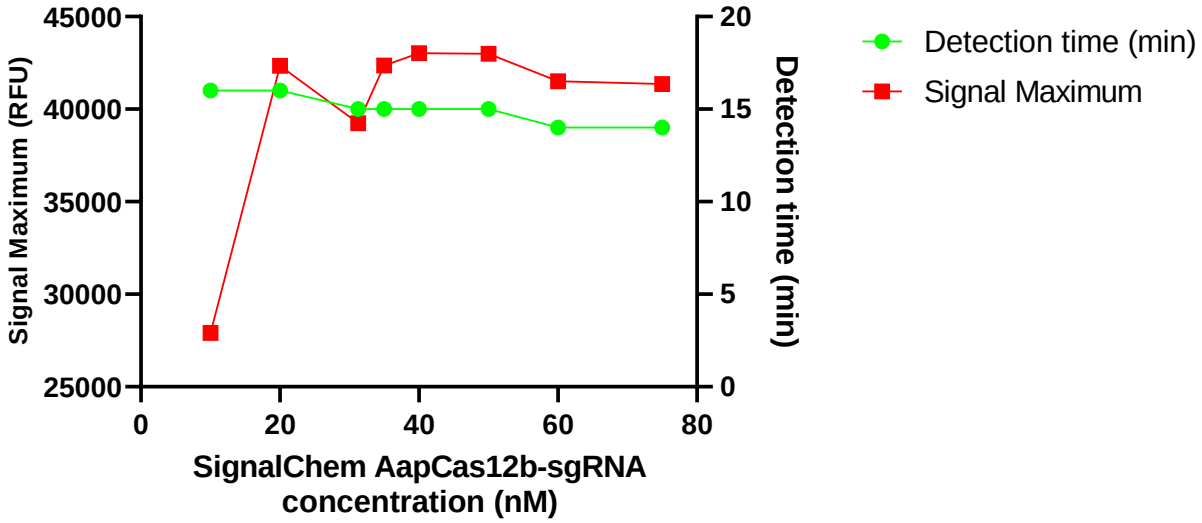


Figure 8. The titration of the SignalChem Lifesciences Corporation AapCas12b enzyme and the SARS-CoV-2 N gene sgRNA at equimolar concentrations, from 10 nM to 75 nM. The results are means of three technical replicates (n=3).

3.2.1.1.2. dNTP Titration

A SARS-CoV-2 RT-LAMP Cas12b assay was performed with the titration of the deoxyribonucleotides to identify the optimal concentration of dNTPs required for reverse transcription and amplification of the N gene amplicon. According to the STOPCovid protocol, optimal dNTP concentration per reaction is 1.4 mM. The titration range was selected from 0 mM, 0.5 mM, 1 mM, 1.4 mM, 2 mM, and 3 mM. If the signal maximum trended upward beyond 3 mM dNTP, with an inverse trend in detection time or time to reach half of the maximum fluorescence, a wider range would then be tested. Results indicated when decreasing dNTP concentrations below 1.4 mM, the detection time and the time to half of the maximum fluorescence increased significantly (Fig.9B-C). However, when decreasing concentrations below 1.4 mM dNTP, the signal maximum increases slightly (Fig.9A). When considering the disparity between the signal maxima at 1 mM, 1.4 mM and 2 mM with increased detection times from 1.4 mM to 1 mM, the optimal dNTP concentration was determined to be approximately 1.4 mM.

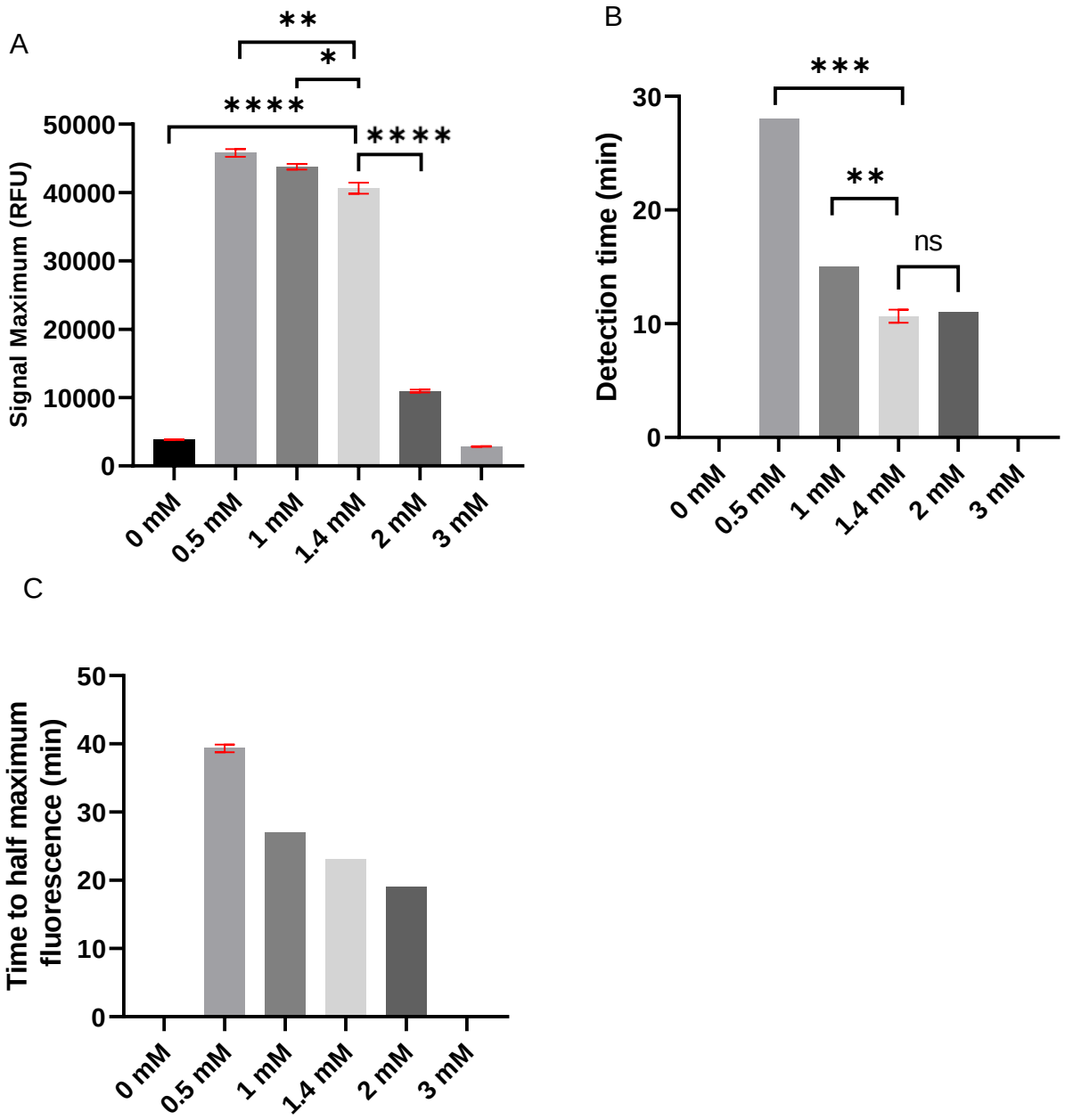


Figure 9. A) Signal maxixmum of the titration of dNTP from 0 mM to 3 mM in the SARS-CoV-2 N gene RT-LAMP Cas12b assay. B) Detection time of the the titration of dNTP from 3 mM to 0 mM in the SARS-CoV-2 N gene RT-LAMP Cas12b assay. C) Times to reach half of the maximum fluorescence of the the titration of dNTP from 3 mM to 0 mM in the SARS-CoV-2 N gene RT-LAMP Cas12b assay. The results with error bars are means of three technical replicates (n=3) repeated in biological triplicate and the error bars represent the standard deviations.

3.2.1.1.3. $MgSO_4$ Titration

Magnesium sulfate was titrated within the one-pot reaction to identify the optimal concentration of Mg^{2+} necessary for an effective combination of Cas12b collateral cleavage, DNA polymerase and reverse transcriptase enzymatic activities. Initial titration included a wide range of Mg^{2+} concentrations including 0 mM, 4 mM, 8 mM, 12 mM and 25.5 mM. Signal maxima were statistically significant when elevated at 8 and 16 mM of $MgSO_4$ compared to when no Mg^{2+} was added (Fig.10A). Detection was kept within twenty minutes at 4 mM and 8 mM (Fig.10B), although no amplification was detected at the 4 mM. The time to reach half of the maximum fluorescence was nearly halved (~20 minutes) at 8 mM in comparison to that of 16 mM (Fig.10C) at approximately 40 minutes. These results cumulatively indicate that there is reduced assay efficiency and detection time from 8 mM to 16 mM, however there may be a more narrow optimal concentration within that range.

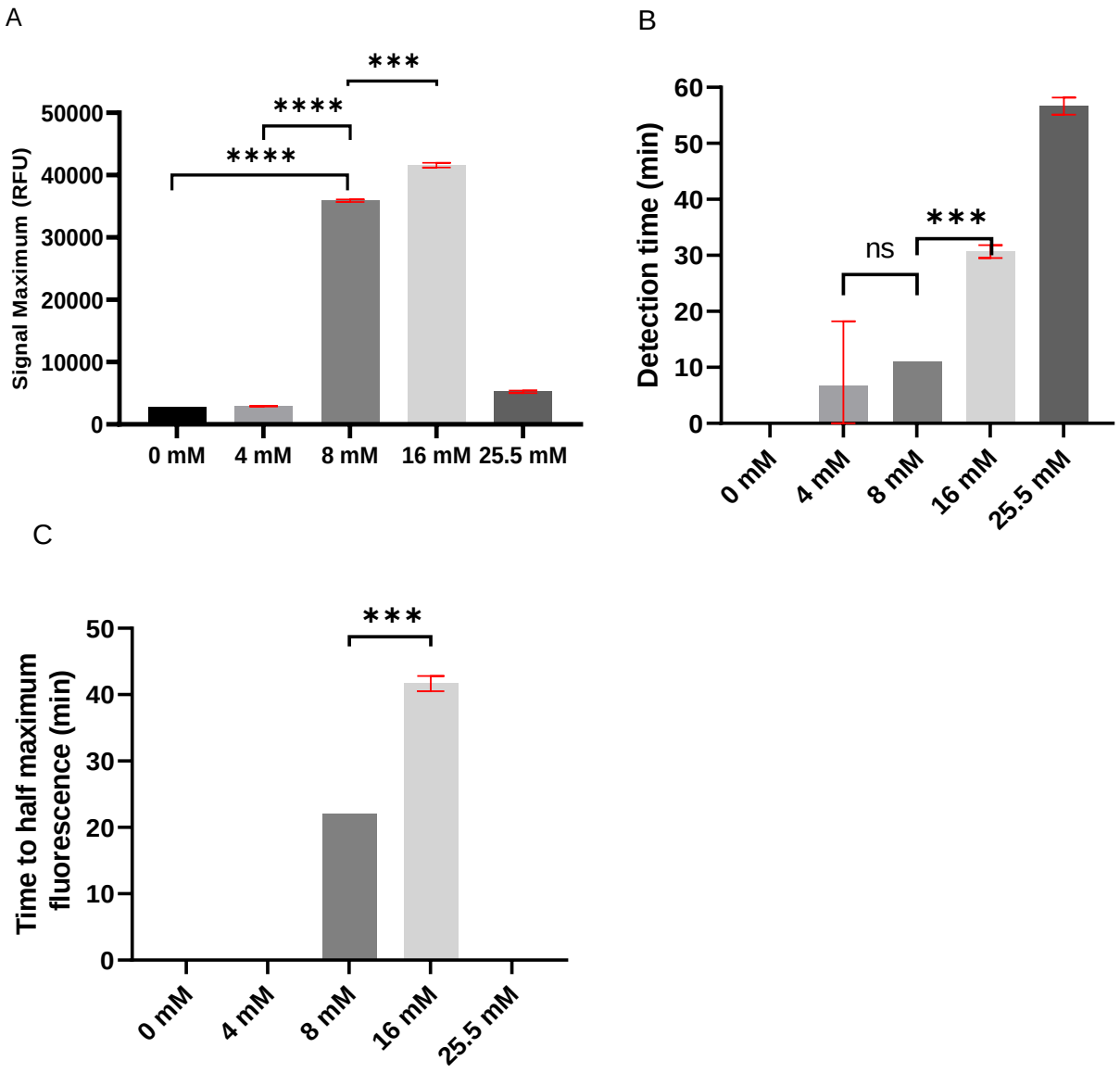


Figure 10. The titration of $MgSO_4$ from 0 mM mM to 25.5 mM in the SARS-CoV-2 N gene RT-LAMP Cas12b assay identified that between 8 and 16 mM, the assay generated A) the most elevated signal maxima, B) a progressive decrease in detection time when decreasing the $MgSO_4$ concentration and, C) a detectable time to half of the maximum fluorescence. The results with error bars are means of three technical replicates (n=3) repeated in biological triplicate and the error bars represent the standard deviations.

$MgSO_4$ was titrated further ranging from 8 mM to 12 mM at 0.5 mM intervals. There is an observable upward-trend within the range of 8 mM to 9.5 mM, with signal maxima increasing when augmenting the metal ion concentrations up to 9.5 mM (Fig.11A). This increase in signal maximum suggests a potential increase in assay sensitivity by allowing for the detection of lower quantities of nucleic acids that may elicit weaker fluorescent signals. The detection time and the time to reach half of the signal maximum within the same range is also statistically significant, although only increasing by a few minutes (Fig.11B-C). At concentrations above 9.5 mM, increases in detection times and times to reach half of the maximum fluorescence suggest that these concentrations will negatively affect the assay performance. Furthermore, these results also suggest that the optimal $MgSO_4$ concentration lies between 8 mM and 9 mM. Moving forward, 9 mM was used as an optimized parameter to ensure that there is a sufficient amount of cofactor available for use by three separate Mg^{2+}-requiring proteins and enzymes without negatively affecting assay performance.

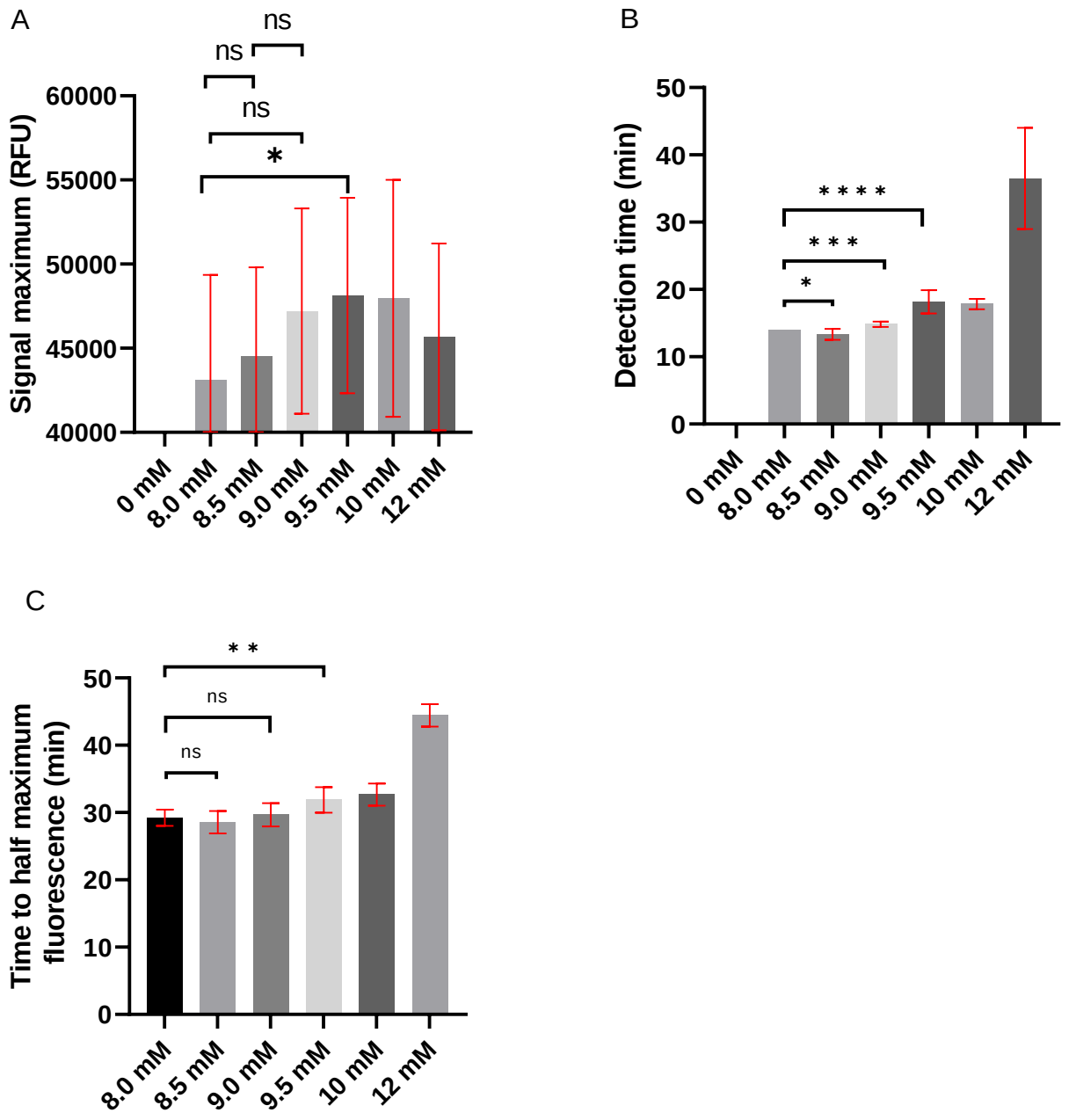


Figure 11. The titration of $MgSO_4$ from 25.5 mM mM to 0 mM in the SARS-CoV-2 N gene RT-LAMP Cas12b assay identified that between 8 and 16 mM, the assay generated A) the most elevated signal maxima, B) a progressive decrease in detection time when decreasing the $MgSO_4$ concentration and, C) a detectable time to half of the maximum fluorescence. The results with error bars are means of three technical replicates (n=3) repeated in biological triplicate and the error bars represent the standard deviations.

3.2.1.1.4. Temperature Gradient of the SARS-CoV-2 RT-LAMP Cas12b Assay

A temperature gradient ranging from 56.0°C to 66.0°C was applied to the SARS-CoV-2 N gene RT-LAMP-Cas12b assay to identify the optimal operating temperatures for both the nucleic acid transcription-amplification reactions and AapCas12b-based collateral cleavage.

Throughout the entirety of the temperature range applied to the RT-LAMP Cas12b assay, the signal maximum does not significantly increase, remaining stable around 40,000 RFU, with no statistically significant increases in the fluorescent signal when testing the assay at 60°C when compared to that of temperature emitting the most elevated fluorescent signal (Fig.12A). However, when increasing from 56.0°C to 66.0°C, the detection time and the time to half of the maximum fluorescence is significantly decreased, with the minimum detection times reached at 64.3°C (Fig.12B-C). These results suggest that at 60.0°C, as established by Joung *et al.*, the assay is tolerant and permissible to micro-environmental fluctuations in temperature.

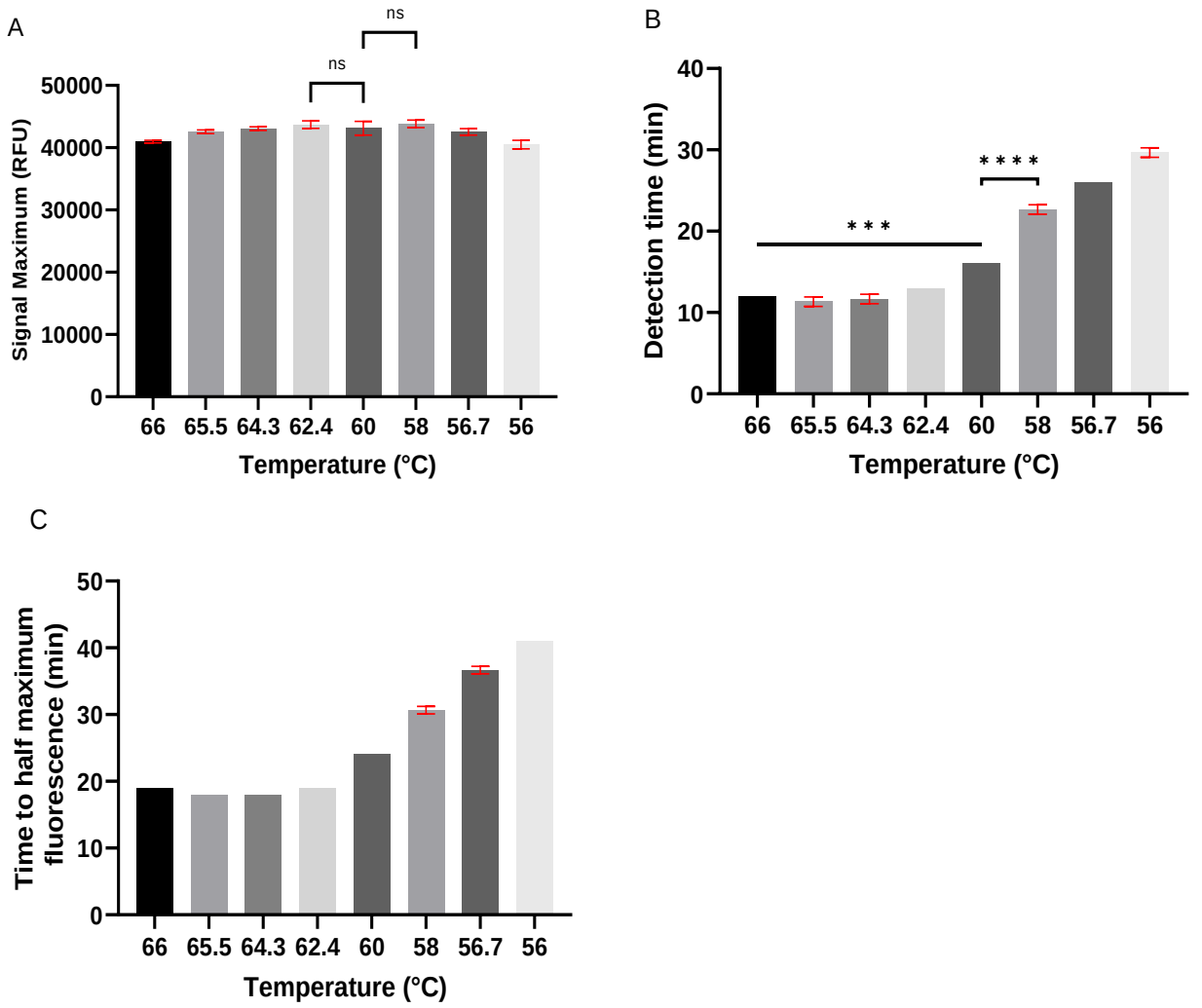


Figure 12. A) Signal maximum when applying a temperature gradient from 66°C to 56°C for the SARS-CoV-2 N gene RT-LAMP Cas12b assay. B) Detection time when applying a temperature gradient from 66°C to 56°C for the SARS-CoV-2 N gene RT-LAMP Cas12b assay. C) Times to reach half of the maximum fluorescence when applying a temperature gradient from 66°C to 56°C for the SARS-CoV-2 N gene RT-LAMP Cas12b assay. The results with error bars are means of three technical replicates (n=3) and the error bars represent the standard deviations.

3.2.1.2. RT-LAMP Reaction Buffer

3.2.1.2.1. Three Non-Ionic Detergents Within the Reaction Buffer

To identify the most efficacious detergent at reducing secondary structures and destabilizing dsDNA in the RT-LAMP Cas12b reaction thus improving reaction kinetics, three non-ionic detergents were titrated from 0.5%, down to 0% and individually added to the assay. These detergents are a part of what makes up the reaction buffer, which is a buffer comprising of essential amplification enabling, stabilizing and enhancing reagents. The three detergents in question were Tween 20, Triton X-100 and Brij-35.

As illustrated in figure 13A, most of the reactions using Brij-35 as the detergent elicited large increases in signal maxima in comparison to the reactions using Tween 20 or Triton X-100. The disparity between the signal maxima obtained when using Brij-35 at 0.5% or 0.2% is large when comparing to the buffer used in the STOPCovid assay (Tween 20 at 0.1%). There were no statistically significant differences in assay detection times and times to reach half of the maximum fluorescence (Fig.13B-C) other than what is believed to be an outlying increase in detection time and time to reach half of the maximum fluorescence when using Triton X-100 at 0.5%.

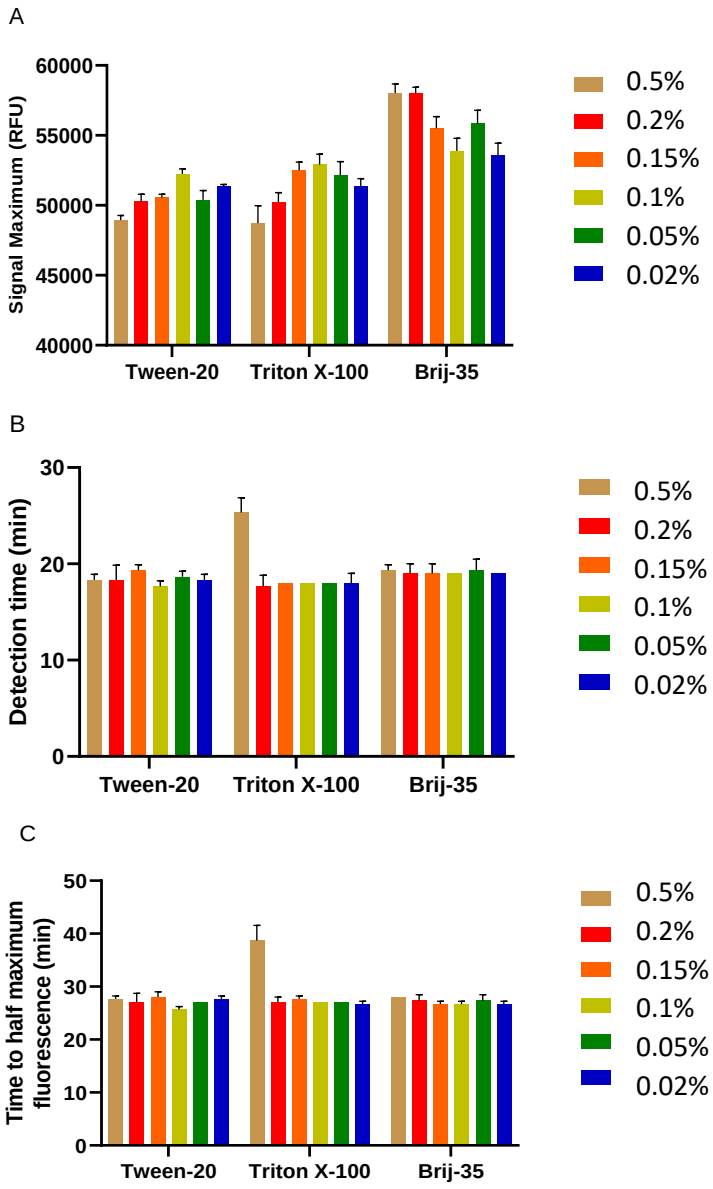


Figure 13. A) Differences between the signal maxima of three non-ionic detergents (Tween-20, Triton X-100 and Brij-35) titrated from 0% to 0.5% in the RT-LAMP reaction buffer, identifying Brij-35 as a candidate for elevating the signal maximum. B) Differences in detection times of Tween-20, Triton X-100 and Brij-35 did not identify a candidate significantly improving rapid detection. C) Differences in times to reach half of the maximum fluorescence of the three detergents did not identify a candidate significantly improving assay kinetics. The results with error bars are means of three technical replicates (n=3) and the error bars represent the standard deviations.

3.2.1.2.2. Published LAMP Buffers

The effects from using the STOPCovid RT-LAMP buffer was also compared to other published RT-LAMP assay buffers containing distinct characteristics. The first candidate buffer was produced by Abbasi *et al.* in 2016 for the detection of Leishmania DNA. The unique components to this buffer is the uniquely elevated Tween 20 concentration being 1% final concentration, and the inclusion of KCl (Potassium chloride - 10 mM). Conversely, the second candidate buffer, made by Ali *et al.* in 2020 to detect SARS-CoV-2, uses the exact formulation as that of the STOPCovid protocol, but includes an even more concentrated amount of KCl at 50 mM (Table 3).

Table 3. Published LAMP reaction buffer consitutents

Reagent	Working concentration	Author
Tris-HCl (pH 8.8)	20 mM	Abassi *et al.* 2016
KCl	10 mM	
$(NH_4)_2SO_4$	10 mM	
$MgSO_4$	8 mM	
Tween-20	1%	
Tris-HCl (pH 8.8)	20 mM	Ali *et al.* 2020
KCl	50 mM	
$(NH_4)_2SO_4$	10 mM	
$MgSO_4$	2 mM	
Tween-20	0.1%	

Successful amplification and detection was recorded when using Abbasi's buffer and Ali's buffer, however only one buffer was deemed to produce efficient amplification and detection comparable to the STOPCovid buffer (1% Tween 20 in Fig.13A-B)(Fig.14A-B). The buffer generated by Abbasi and colleagues produced amplification commencing around 30 minutes (Fig.14B), which is significantly less rapid than 20-minute detection with the STOPCovid buffer,

delaying the time to half of the maximum fluorescence significantly (Fig.14C). Also noted was the variability of replicate signal maxima (Fig.14A). These results imply that the Abbasi buffer is not suitable for this assay due to potential inconsistencies in nucleic acid detection when varying cp numbers, and this variability may be impacted by the 1% working concentration of Tween-20 added to the amplification buffer (end concentration). The amplification and detection generated by Ali and colleagues produced suitable detection, however was not better than the STOPCovid buffer. The Signal maximum generated was lower than that of the STOPCovid buffer by approximately half, whereas the detection time and efficiency was increased compared to that of the STOPCovid buffer by over ten minutes. Therefore, none of the two published alternative buffers trialed using the STOPCovid protocol improved the reaction.

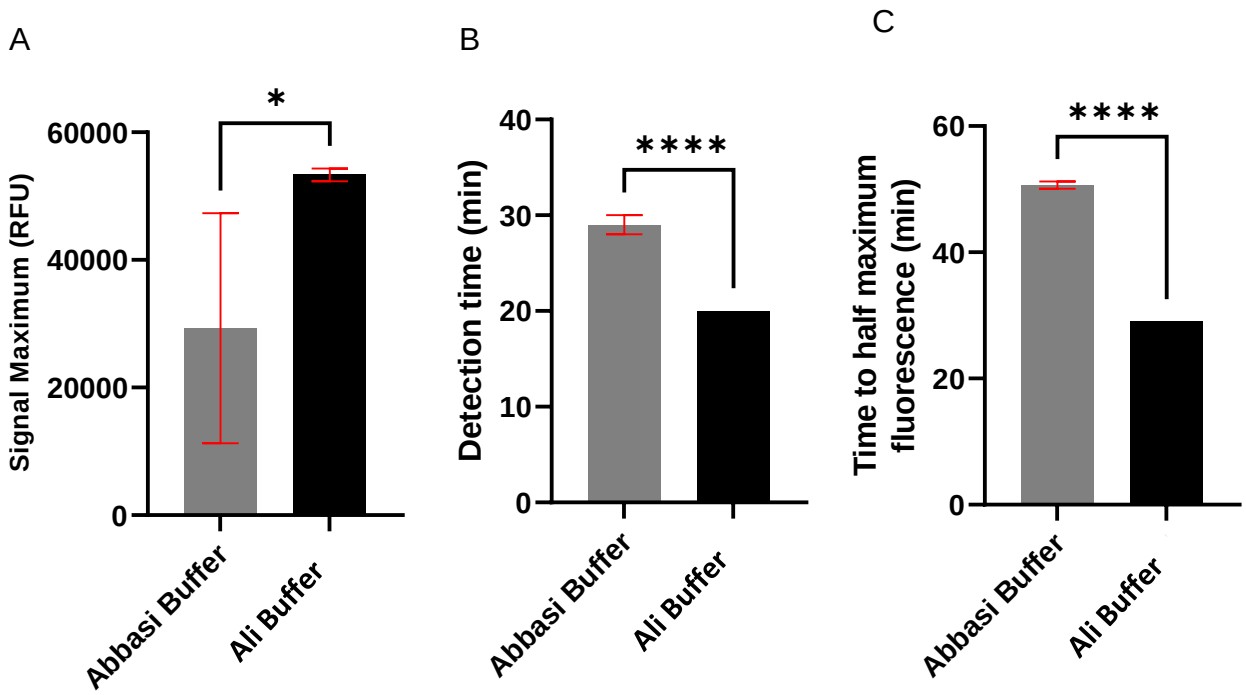


Figure 14. Two published RT-LAMP buffers with different chemistries than that of the STOPCovid protocol generated A) decreased signal maximum, B) detection times and, C) times to reach half of the maximum fluorescence when compared to the STOPCovid reaction kinetics and signal maximum in figure 13. The results with error bars are means of three technical replicates (n=3) and the error bars represent the standard deviations.

3.2.1.2.3. Commercially Available Amplification Buffers

Four commercially available buffers used for common enzymatic reactions (PCR and restriction digestions), and/or isothermal amplification assays were tested using the STOPCovid protocol with the only modification being the buffer in question. It is important to note that the buffers are mainly proprietary, therefore buffer reagents and concentrations were not deciphered. The first buffer consisted of a 10X Isothermal Amplification Buffer (New England BioLabs Inc., Cat. No.: B0537S) which, as per the manufacturer, has been optimized for isothermal amplification. The second, CutSmart Buffer (New England BioLabs Ltd., Cat. No.: B7204S – Discontinued – now B6004S, now uses recombinant albumin), is a unique buffer containing bovine serum albumin (BSA), an enzyme stabilizer typically used for digestion reactions and that has been previously cited in CRISPR-based reactions. The final two buffers, 10X DNA Polymerase Buffer B (Lucigen, Cat. No.: Not Available) and 10X Bsm Buffer (Thermo Fisher Scientific, Cat. No.: Not Available) are buffers that are sent with their respective enzymes and that are used for amplification assays. The results in figure 15A show that three of the four new buffers effectively produced conditions viable for RT-LAMP Cas12b nucleic acid amplification and cleavage leading to pathogen detection. Three of four new buffers produced small increases in signal maxima when compared to the signal obtained when using the STOPCovid buffer. The buffer producing weakly positive signal just barely detectable above the minimum threshold was the outlying buffer not conventionally used in amplification systems, CutSmart Buffer, although suggested in literature (Fig.15B)[261]. Other than the CutSmart buffer, the other buffers produced a microenvironment where amplification and Cas12b-mediated detection of SARS-CoV-2 was effective and only varying by a few minutes, even when compared to the STOPCovid buffer (Fig.15C). The same trend was observed with the times to reach half of the maximum fluorescence

(Fig.15D). Due to there not being any improvement over the use of the STOPCovid buffer, none of the commercial buffers were persued further.

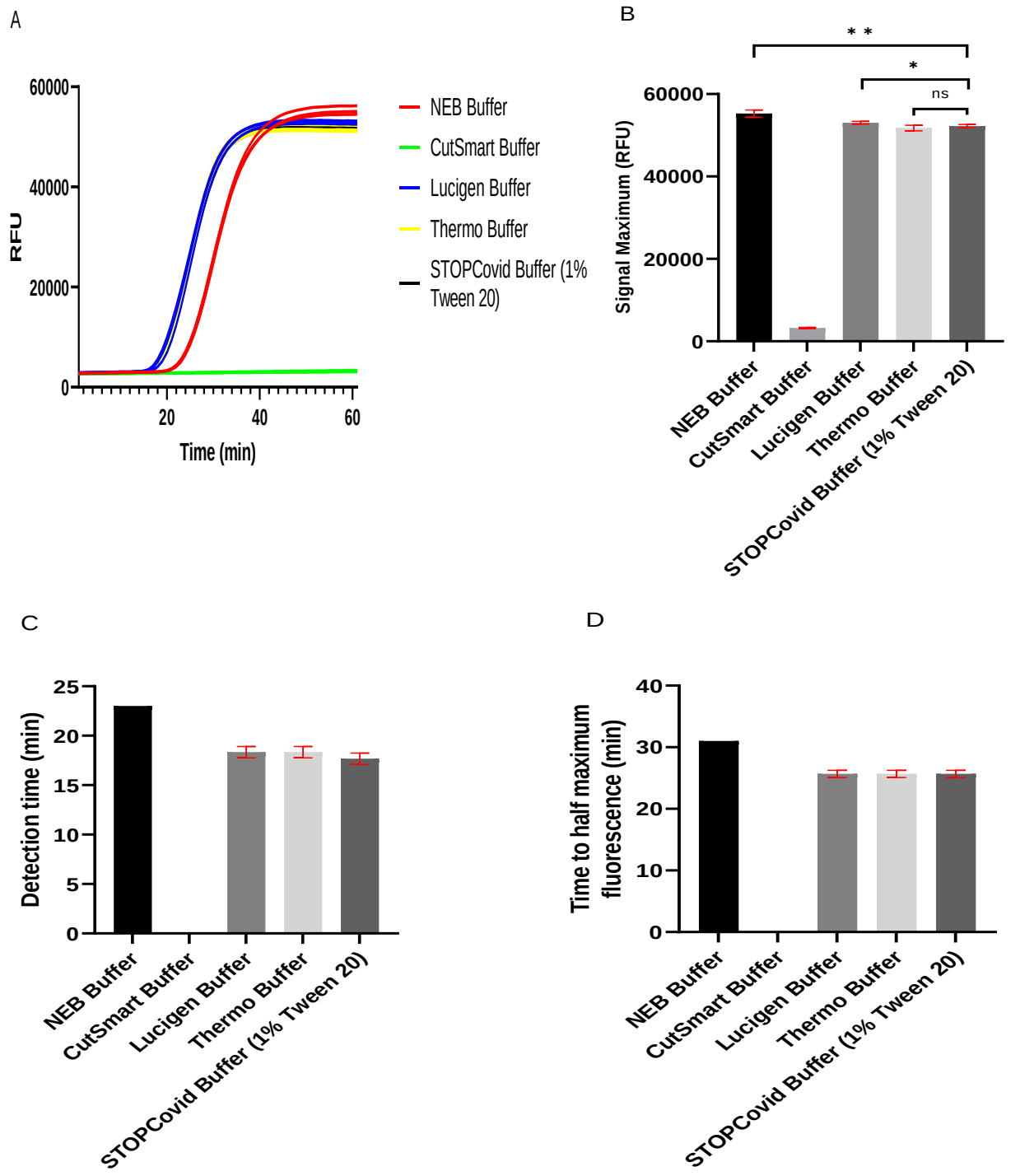


Figure 15. A) SARS-CoV-2 N gene RT-LAMP Cas12b assay kinetic profile using four commercially available buffers, NEB Buffer, CutSmart Buffer, Lucigen Buffer and Thermo Buffer, including the STOPCovid buffer. B) Differences in signal maxima of the commercially available amplification buffers when compared to the STOPCovid buffer chemistry. C) Differences in SARS-CoV-2 detection times. D) Differences in the time to reach half of the maximum fluorescence. The results with error bars are means of at least three technical replicates (n=3) and the error bars represent the standard deviations.

3.2.1.2.4. Comparison of Each Optimal Buffer Condition

When evaluating the optimal buffers results shown in 3.2.1.2.1. to 3.2.1.2.3, there are five standout candidates: Brij-35 buffer at 0.2% and at 0.5%, the buffer produced by Ali *et al.*, the buffer from Lucigen Inc. and the buffer from Thermo Fisher Scientific. A side-by-side comparison of each of the results can be directly made as they were all performed at the same time using the same reagents. Directly looking at the curves in figure 16A, all buffer conditions successfully amplify and detect SARS-CoV-2 RNA using the N gene RT-LAMP Cas12b assay. Looking at the metrics in depth, both Brij-35-containing buffers produce a significantly more elevated signal maximum (Fig.16B) whereas the other buffers do not when compared to the STOPCovid buffer. There is only one significant increase in detection time when compared to the STOPCovid buffer, and that is with the Ali *et al.* published buffer (Fig.16C). There is also only one buffer that produces a significant increase in signal maximum while also not having a statistically significant increase in time to reach half of the maximum fluorescence, and that is the Brij-35 at 0.2% (Fig.16D). When combining the specific positive applications of the Brij-35 buffer, a solution containing 0.2% Brij-35 appears to be the optimal buffer detergent when performing the SARS-CoV-2 N gene RT-LAMP Cas12b assay.

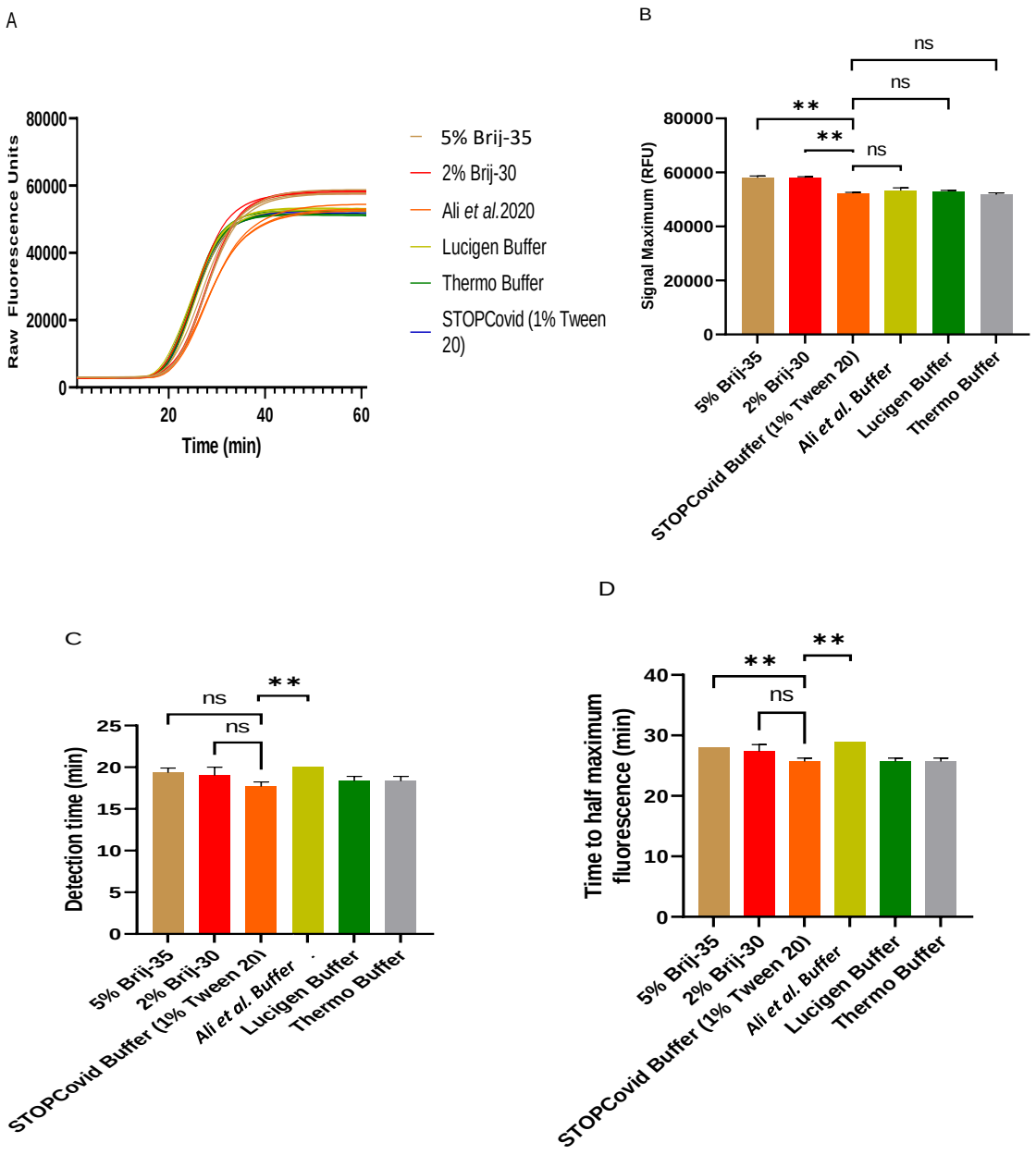


Figure 16. A) Summary of the SARS-CoV-2 N gene RT-LAMP Cas12b assay kinetic profiles using each of the optimal buffer formulations when testing the non-ionic detergents, the published buffers and the commercially available amplification buffers. B) Differences in signal maxima of the optimal buffer formulations when compared to the STOPCovid buffer. C) Differences in SARS-CoV-2 detection times. D) Differences in the time to reach half of the maximum fluorescence. The results with error bars are means of at least three technical replicates (n=3) and the error bars represent the standard deviations. The results with no error bars correspond to results that obtained the same metric in each replicate.

3.2.1.2.5. Optimal Reaction Buffer pH

Changes in hydrogen potential (pH) affect protein-protein and protein-nucleic acid interactions, having effects on protein conformation from protonation and deprotonation of essential structural and catalytic residues. With the detergent change from 1% Tween 20 to 2% Brij-35, the objective of this step in optimization is to verify the optimal pH conditions relative to using a new detergent, which may alter the reaction pH. The hypothesis here is that an alteration in the RT-LAMP Cas12b assay chemistry would subsequently require pH readjustment. Literature states that Cas proteins have a wide functional pH range from pH 1.0 to pH 12.0[262]. This optimal activity pH range leaves room for identifying the delicate balance in pH where the Cas12b protein, the DNA polymerase I and the reverse-transcriptase have the most synergy in amplifying and detecting SARS-CoV-2 RNA. The STOPCovid protocol, which uses Tween-20, identified an optimal reaction pH of 8.8. Literature suggests that AapCas12b is optimally active in basic environments, which is why a scale going from pH 7.8 to 10.0 was selected, including an outlying pH of 12.0 to look at extreme pH measures.

The reaction buffer was made as per appendix 5.6.. The pH was measured using a Mettler-Toledo SevenExcellence S400 Benchtop pH/mV Meter calibrated with pH 4.0, pH 7.0 and pH 10.0 electrochemistry buffer solutions (Fisher scientific, Cat. No.: SB101-500, SB107-500 and SB115-500, respectively). The pH was adjusted using 1N NaOH for basic conditions and 5N HCl for acidic conditions. The native buffer pH (not pH-buffered) was approximately 8.2. The buffer was then divided into two aliquots, one of which was either acidic-buffered and the other basic-buffered to control and minimize the effects that Cl^- and/or Na^+ may inadvertently carry on the reaction.

End-point fluorescence is stable at just above 40,000 RFU from pH 8 to pH 9.2 then reduces significantly beyond pH 9.2 (Fig.17A.). This change in signal amplitude suggests that beyond pH 9.2, functional enzymatic and protein activities are altered and may result in stochastic results, which is observed. Increased detection time and time to reach half of the maximum signal fluorescence is also noticed at more elevated pH values (Fig.17B-C). Considering these stark changes in detection parameters, the lowest and most stable detection time and time to half of the maximum fluorescence is narrowed to a range of pH 8.2 to approximately 9.2. A pH of 8.8 was selected as buffer pH to prevent any batch-effects from slight pH variation in scaled production if the assay were to be used at the point of care due to flexibility result output if there were to be any variation in batch production. This pH would also allow uncertainty from random variables.

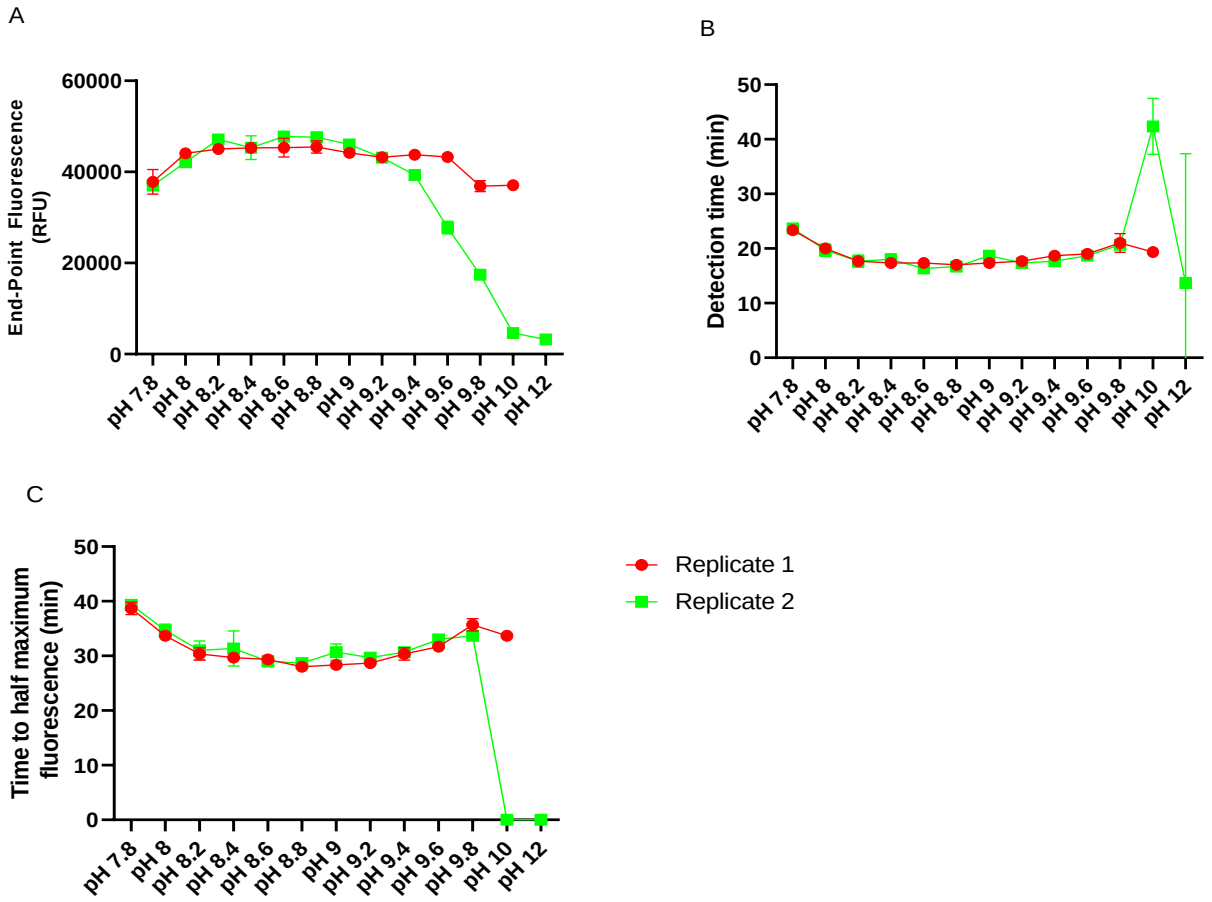


Figure 17. A) Mean signal maximum profile of the optimized SARS-CoV-2 RT-LAMP Cas12b assay when titrating the pH of the 2% Brij-35 buffer. B) Mean detection time profile of the optimized SARS-CoV-2 RT-LAMP Cas12b assay when titrating the pH of the 2% Brij-35 buffer. C) Mean times to reach half of the maximum fluorescence of the optimized SARS-CoV-2 RT-LAMP Cas12b assay when titrating the pH of the 2% Brij-35 buffer. These are means of at least three technical replicates (n=3) of two biological repeats (n=2) and the error bars represent the standard deviations. Results that have a time to half of maximum fluorescence at 0 minutes are considered at infinity as the reactions did not occur.

3.2.1.3. Reaction Enzymes

3.2.1.3.1. DNA Polymerase Titration and Comparison

To successfully amplify native genomic DNA or complimentary DNA using loop-mediated isothermal amplification, the DNA polymerase must have a high strand displacement activity. As discussed in 1.5.2.1., LAMP requires DNA polymerase-mediated double-stranded DNA-strand displacement to be able to amplify dumbbell and looped/hairpined nucleic acids. The optimal enzymatic activity is required to be within 50°C to 70°C to be compatible with RT-LAMP and with Cas12b.

This attempt in optimizing the SARS-CoV-2 RT-LAMP looked at titrating four DNA polymerases that have high strand displacement activity and optimal activities within the same temperature range as AapCas12b to identify the optimally amplifying enzyme. A control Taq DNA polymerase was included to confirm that an enzyme without strand displacement activity would not be useful for this application. The first enzyme, Bst 2.0 WarmStart DNA polymerase, is the original polymerase used in the STOPCovid protocol which has a reversibly-bound aptamer which inhibits any activity at temperatures lower than 45°C; The second enzyme, Bst 3.0 DNA polymerase is a LAMP-optimized enzyme (according to the manufacturer); the third, Bst DNA polymerase – Exonuclease minus comes from the same *Bacillus stearothermophilus* DNA polymerase I large fragment but is made by a different manufacturer than the first two enzymes; the fourth is a DNA polymerase I from *Bacillus smithii*, and lastly, the fifth enzyme is a DNA polymerase from *Thermus aquaticus* exhibiting 5’ to 3’ exonuclease activity and no strand displacement activity. To identify the ideal DNA polymerase for the RT-LAMP Cas12b reaction, each individual enzyme was titrated within manufacturer suggested ranges. Each enzyme was carefully selected considering the specific enzymatic requirements as listed above.

As seen in figure 18, most enzymes were capable of producing a detectable signal within the entire manufacturer suggested titration range. The time to half of the maximum fluorescence of the optimal concentration of each enzyme increases in comparison to the results obtained by the enzyme used in the STOPCovid protocol. This indicates that the enzyme most capable at harboring the earliest efficient amplification for Cas12b cleavage is the New England Biolabs Bst 2.0 WarmStart DNA Polymerase at 320 U/mL.

The same enzyme produces a significantly more elevated signal maximum of nearly 50,000 RFU, greater than its nearest neighbour at approximately 40,000 RFU suggesting that this enzyme is capable of producing the most amplicon which is detected by Cas12b through collateral cleavage. The Bst 2.0 WarmStart enzyme produced the most rapid detection time when used at 320 U/mL. Lucigen's enzyme also produces non-specific amplification in its no template control, eliminating its applicability in the context of this assay (data not shown). The New England Biolabs 3.0 DNA Polymerase and the Thermo Fisher Scientific Bsm DNA polymerase produce a slightly more elevated signal maximum, but also produces longer detection times and times to reach half of the maximum fluorescence. The SignalChem Taq plus enzyme produced, as expected, no detectable amplification, which can likely be attributed to the lack of strand displacement activity. Therefore, the optimal enzyme for the SARS-CoV-2 N gene RT-LAMP Cas12b assay is the New England BioLabs Bst 2.0 WarmStart DNA polymerase at a concentration of 320U/mL, as previously established in the STOPCovid protocol.

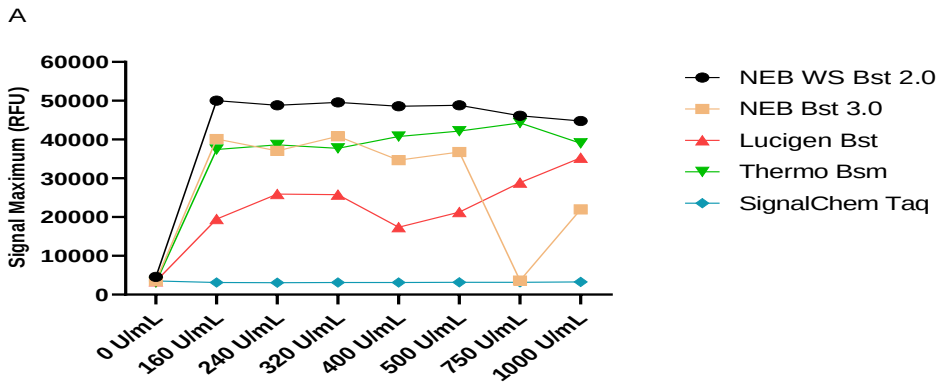


Figure 18. SARS-CoV-2 N gene RT-LAMP Cas12b assay kinetic profile testing five DNA polymerases of varying strand displacement activity: NEB Bst 2.0 WarmStart DNA polymerase, NEB Bst 3.0 DNA polymerase, Lucigen Bst DNA polymerase – Exonuclease minus, ThermoFisher Scientific Bsm DNA polymerase and SignalChem Lifesciences Corp. Taq polymerase.

3.2.1.3.2. Reverse Transcriptase Titration and comparison

In this optimization attempt, four reverse transcriptases were tested; The first enzyme is the original New England BioLabs WarmStart RTx Reverse Transcriptase, which has an optimal activity within 45°C to 65°C. The second enzyme is from Lucigen, RapiDxFire Thermostable Reverse Transcriptase, with an optimal activity within 55°C to 80°C. The remaining two enzymes are from ThermoFisher Scientific: Maxima H Minus Reverse Transcriptase which has an optimal activity up to 65°C, and SuperScript IV Reverse Transcriptase, with 100% activity at 50.0°C and 70% activity at 65°C.

Result in figure 19A indicated that there was no detectable amplification with the use of the Lucigen RapiDxFire enzyme when titrated within the manufacturer's recommended range. All three other enzymes produced very similar signal maxima, with no significant variance within. Signal maxima were held consistent within approximately 180 U/mL to 400 U/mL with little variance between enzyme raw fluorescent units. Between approximately 150 U/mL and 500 U/mL, all three enzymes provided stable, consistent amplification efficiency, although the New England BioLabs enzyme produced overall lower times to half of the maximum fluorescence in comparison to the two others (Fig.19C). Detection times varied as enzyme concentrations were titrated, although the WarmStart enzyme appeared to produce more consistent detection times throughout the enzyme concentration range, and generally, was lower than the two other enzymes (Fig.19B). With that said, the most robust, consistent and efficient enzyme for the SARS-CoV-2 RT-LAMP Cas12b assay is the New England BioLabs WarmStart RTx Reverse Transcriptase at a concentration of 300 U/mL, as established by the STOPCovid protocol.

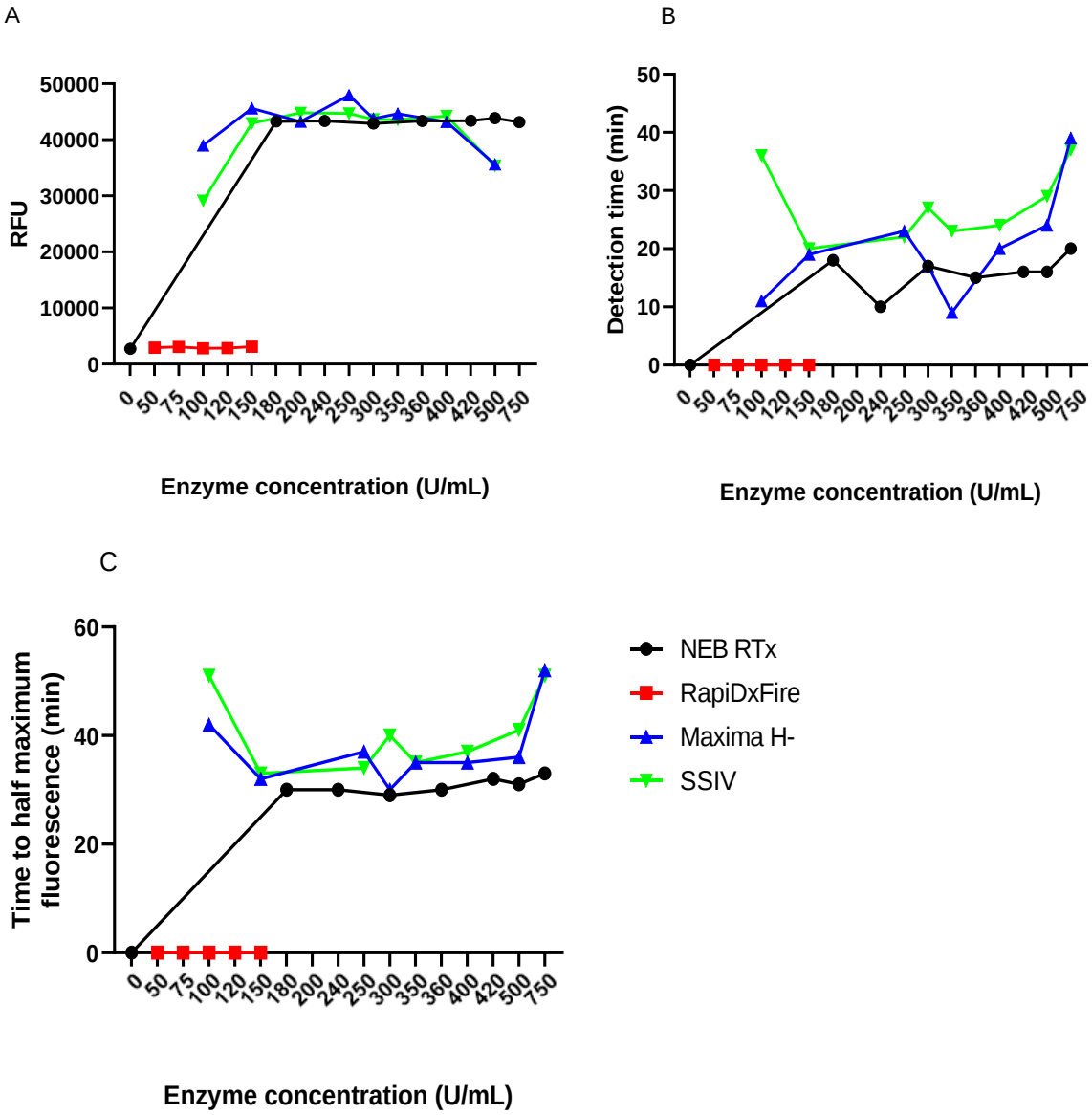


Figure 19. A) SARS-CoV-2 N gene RT-LAMP Cas12b assay signal maximum profile when titrating four different reverse-transcriptases with optimal activities around 60°C: NEB WarmStart RTx Reverse Transcriptase, Lucigen RapiDxFire Thermostable Reverse Transcriptase, ThermoFisher Scientific Maxima H Minus Reverse Transcriptase and SuperScript IV Reverse Transcriptase. B) Differences in SARS-CoV-2 detection times. C) Differences in the time to reach half of the maximum fluorescence. This assay was performed with one replicate due to the assay complexity, therefore technical replicates would be useful to further validate this data.

3.2.1.4. Additional Parameters

3.2.1.4.1. Effect of Poly-T Linked FIP and BIP Primer

Poly-thymine (poly-T) linkers between the 1c and 2 regions of the forward inner and backward inner primer were incorporated into the SARS-CoV-2 RT-LAMP FIB and BIP primers (see 5.3.2. for primer sequences) in an attempt to improve amplicon folding in a dumbbell/hairpin shape. The self-folding self-priming dumbbell structure is necessary for LAMP amplification, and literature suggests that a flexible linker between the two regions improves folding efficiency[263]. Other than one primer pool containing the modified poly-T primers, the assay followed identical conditions outlined in the STOPCovid protocol.

Results indicated that the decrease in signal maximum when using the poly-T linker was statistically significant (Fig.20A), whereas the differences in the detection times and the times to half of the maximum fluorescence were not statistically significant (Fig.20B-C) when compared to the parameters established by the non-linked primer reaction. In this assay, the use of poly-thymine linkers do not suggest any improvement to the folding of the amplicon secondary structure, which would theoretically aid in improving amplification efficiency, speed and, potentially, yield. Technically, the introduction of a poly(5)-thymine stretch between the 2c and 1 regions of the inner increased the time to reach half of the maximum fluorescence, therefore reduced the amplification efficiency of the assay. Further studies including varying the size of the poly-T linkers are needed to cover a larger spectrum of candidate primers that may improve the thermodynamic and kinetic properties of the amplification. What can be concluded from these results are that a poly(5)-thymine linker reduces SARS-CoV-2 N gene RT-LAMP Cas12b amplification potential.

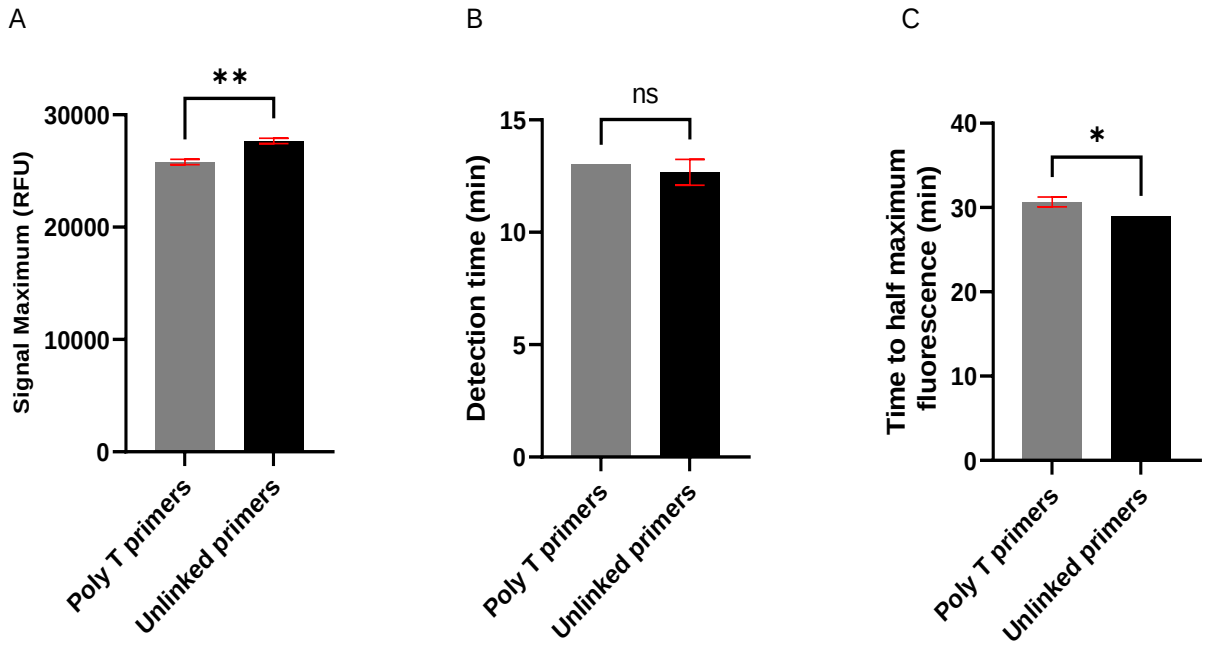


Figure 20. A) Signal maximum comparison when using SARS-CoV-2 N gene RT-LAMP Cas12b forward and backward inner primers containing poly-thymine linkers between the complementary and self-binding primer regions compared to using standard unlinked primers. B) Detection time comparison when using SARS-CoV-2 N gene RT-LAMP Cas12b forward and backward inner primers containing poly-thymine linkers between 1c and 2 regions of the primers compared to using standard unlinked primers. C) Times to reach half of the maximum fluorescence comparison when using SARS-CoV-2 N gene RT-LAMP Cas12b forward and backward inner primers containing poly-thymine linkers between 1c and 2 regions of the primers compared to using standard unlinked primers. The results with error bars are means of three technical replicates (n=3) and the error bars represent the standard deviations.

3.2.1.4.2. Use of 4 Primers vs. 6 Primers in RT-LAMP Cas12b

First published in 2000, Notomi *et al.* showed that loop-mediated isothermal amplification can be performed using four primers with successful target amplification[242]. Two years later, the originators of the method published again stating that six primers can be used to accelerate LAMP reactions[264]. Two simple RT-LAMP Cas12b reactions were performed, one using four primers (F3, B3, FIP & BIP) and the other using six (F3, B3, FIP, BIP, LF & LB) to identify the kinetic differences of using the two primer combinations in the SARS-CoV-2 N gene RT-LAMP Cas12b assay. The assay was also performed at twice the duration of a standard assay (120 minutes) for the purpose of potentially detecting delayed amplification when using four primers. A large quantity of SARS-CoV-2 RNA (10^6 cp/µL) was added to the reactions to ensure that if detectable amplification occurs, it will be registered by the fluorometer.

With the use of six primers, the SARS-CoV-2 N gene RT-LAMP Cas12b assay detected SARS-CoV-2 RNA rapidly within less than 20 minute, eliciting a strong signal maximum at 40,000 RFU (Fig.21A-B). Conversely, one of three technical replicates of the assay using 4 primers demonstrated a slight but not statistically significant signal increase beyond baseline amplification, although did not appear as a sigmoidal amplification curve (data not included). Data in Figure 21C confirms the significant difference in times to reach half of the maximum fluorescence, as the variance in the starting signal and signal is so minimal that the time to half of the maximum fluorescence is near zero. There is no statistical significance in detection time between the two pools only because the variance in times surpassing the threshold is elevated, which significantly increases the standard deviation, subsequently skewing the statistic. An approach to avoid scenarios similar to this where a potential false positive may occur when baseline fluorescence is considered a positive result would be by increasing the standard deviations

included in the threshold calculation. Overall, it appears that when using four primers for this assay, amplification is significantly delayed if at all even amplifying, highlighting the importance of the loop primers in loop-mediated isothermal amplification.

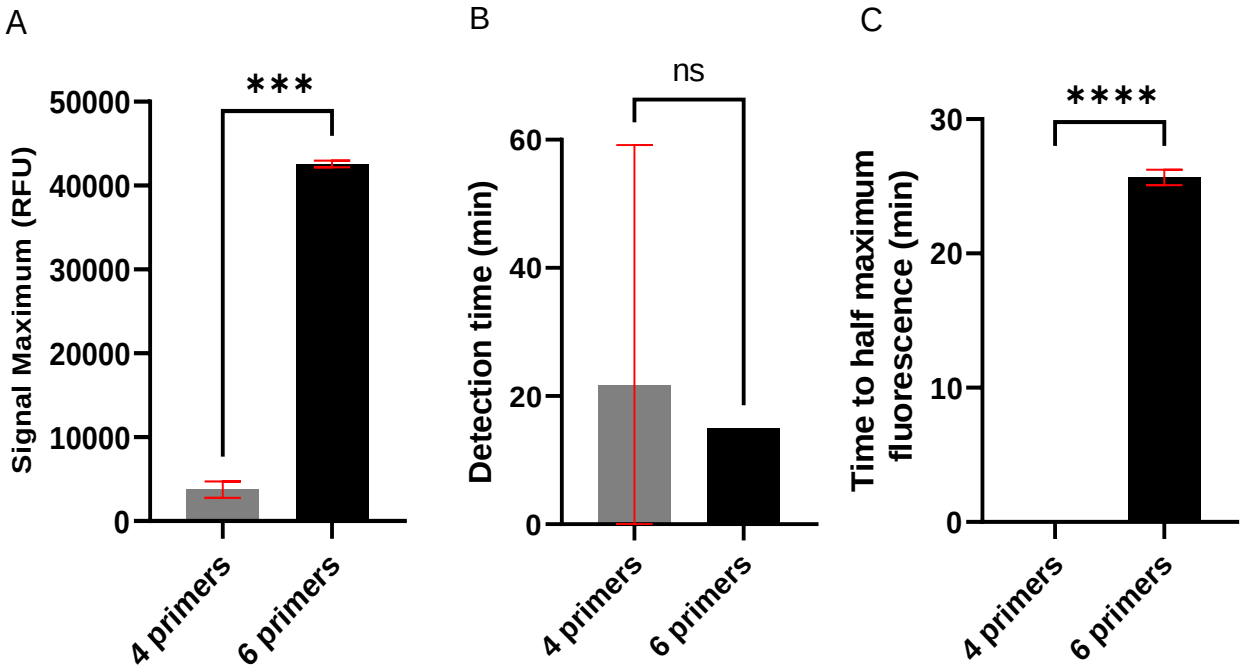


Figure 21. A) Signal maximum when using 4 or 6 primers in the SARS-CoV-2 N gene RT-LAMP Cas12b assay. B) Detection time when using 4 or 6 primers in the SARS-CoV-2 N gene RT-LAMP Cas12b assay. C) Times to reach half of the maximum florescence when using 4 or 6 primers in the SARS-CoV-2 N gene RT-LAMP Cas12b assay. The results with error bars are means of three technical replicates (n=3) and the error bars represent the standard deviations.

3.2.1.4.3. Pre-Incubation of AapCas12b with sgRNA, $MgSO_4$ and Nuclease-Free H_2O and Two-Week Storage of a Pre-Assembled Master Mix

In theory, pre-incubating the Cas12b protein with its essential Mg^{2+} cofactor and single-guide RNA to form the active ribonucleoprotein prior to being added to the one-pot RT-LAMP Cas12b reaction could improve collateral cleavage activity by ensuring that the most possible RNPs are associated prior to detection. The reasoning is that if the three components were added all at once in the one-pot reaction, the magnesium may not as efficiently bind to the Cas protein due to competing enzymes, DNA polymerase and reverse transcriptase, both also requiring Mg^{2+} as a cofactor catalyzing their respective reactions.

After pre-incubating the three components for a duration of 10 minutes at room-temperature, followed by being added to the RT-LAMP Cas12b assay, the assay signal maximum was increased by more than 27% of that obtained by directly combining all reagents (Fig.22A). A slight but statistically significant delay in detection time and the time to half of the maximum fluorescence was observed for the same pre-incubated reaction (Fig.22B-C).

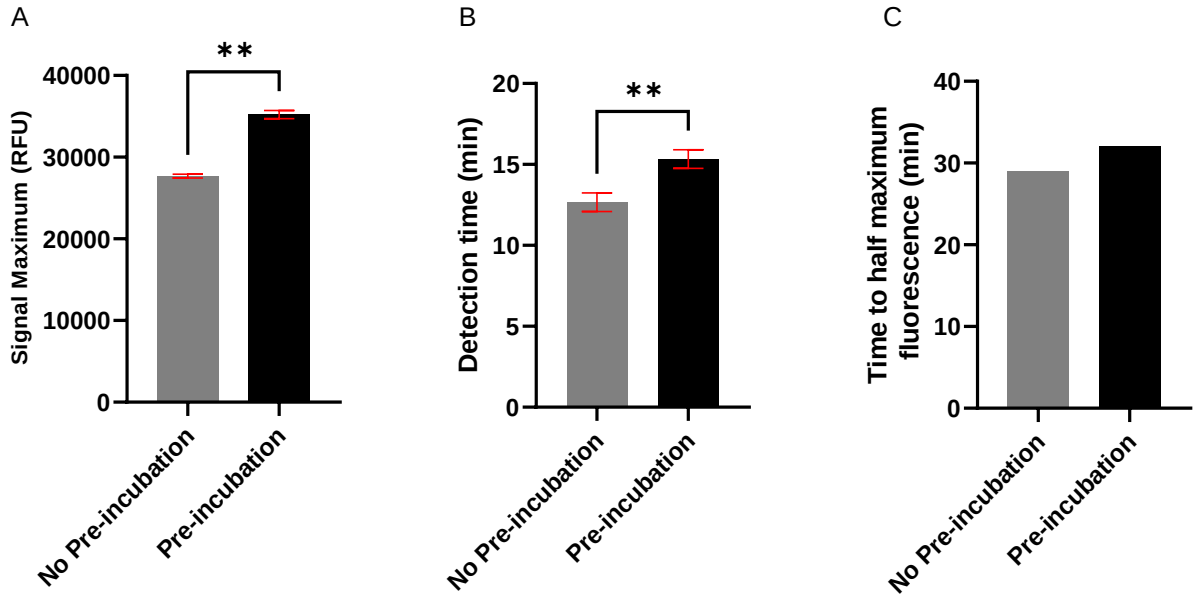


Figure 22. A) Signal maximum when pre-incubating the AapCas12b with $MgSO_4$ and the N gene sgRNA for 10 minutes at room temperature prior to performing the RT-LAMP Cas12b assay and without pre-incubation of these reagents prior to performing the RT-LAMP Cas12b assay. B) Detection time when pre-incubating the AapCas12b with $MgSO_4$ and the N gene sgRNA for 10 minutes at room temperature prior to performing the RT-LAMP Cas12b assay and without pre-incubation of these reagents prior to performing the RT-LAMP Cas12b assay. C) Times to reach half of the maximum fluorescence when pre-incubating the AapCas12b with $MgSO_4$ and the N gene sgRNA for 10 minutes at room temperature prior to performing the RT-LAMP Cas12b assay and without pre-incubation of these reagents prior to performing the RT-LAMP Cas12b assay. The results with error bars are means of three technical replicates (n=3) and the error bars represent the standard deviations.

Considering the significant increase in signal maximum when pre-incubating the reaction mixture before combining the remaining reagents, it was prudent to combine all RT-LAMP Cas12b reagents and allow a certain incubation period to see if there would be any improved effects in signal maxima like when pre-incubating for 10 minutes at room temperature. To do so, and to maintain all possible variables, one large master mix was produced and divided into two lots. The first lot was immediately tested using SARS-CoV-2 RNA that was initially diluted, divided and frozen into two aliquots, controlling the same amount of freeze-thaw cycles, and genome copy numbers that would be used for testing. The second lot was placed at -20°C for two weeks, an acceptable timeframe considering the duration of research for a graduate thesis. When the two week period passed, the buffer was thawed and tested using the second aliquot of the same RNA used in the first run. The purpose of testing the two week freeze of the RT-LAMP Cas12b master mix was to observe effects on reagent integrity having been frozen as a master mix.

Results for the two week incubation period are simple; There was very little statistical variance in signal maximum and none for the detection times and times to reach half of the maximum fluorescence when comparing the reaction using the fresh and frozen master mix aliquots (Fig.23A-C). There was no noticeable improvement in signal maximum, indicating that to obtain signal maximum enhancement, the Cas12b protein must be isolated with magnesium ions and a binding single-guide RNA prior to being added into the RT-LAMP reaction.

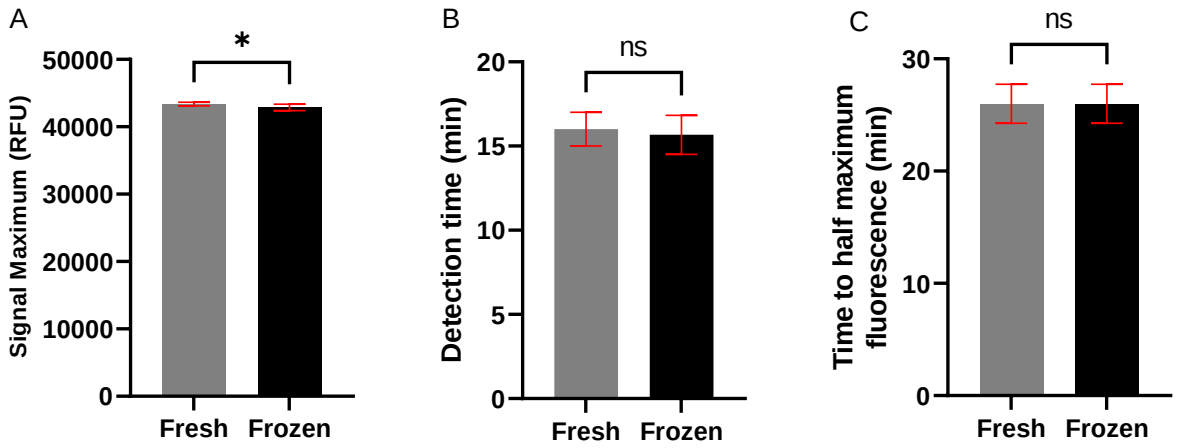


Figure 23. A) Signal maximum when freezing the SARS-CoV-2 N gene RT-LAMP Cas12b master mix prior to performing the assay and without freezing the master mix prior to performing the assay. B) Detection time when freezing the SARS-CoV-2 N gene RT-LAMP Cas12b master mix prior to performing the assay and without freezing the master mix prior to performing the assay. C) Times to reach half of the maximum fluorescence when freezing the SARS-CoV-2 N gene RT-LAMP Cas12b master mix prior to performing the assay and without freezing the master mix prior to performing the assay. The results with error bars are means of three technical replicates (n=3) and the error bars represent the standard deviations.

3.2.1.4.4. RT-LAMP Cas12b Chemical Enhancers

3.2.1.4.4.1. L-Proline, Bovine Serum Albumin and Synergistic Enhancement

Herein, both reagents were checkerboard-titrated at select concentrations based on those used in Li *et al.* 2021 describing the enhanced reactions with L-proline and BSA[287]. The assay was only performed once due to elevated cost of performing multiple technical and biological replicates, and a complex and time consuming assay setup. Initial results suggest that BSA may improve signal maximum. The addition of 10 µg/mL BSA without any L-proline appears to significantly improve the signal maximum in comparison to the assay without any of the two enhancers (Fig.24A) although replicates are needed to establish statistical significance. L-proline alone, however, appears to decrease assay signal maximum while clearly increasing detection time; presumably interfering with amplification or detection whereas BSA does not appear to affect detection time (Fig.24B).

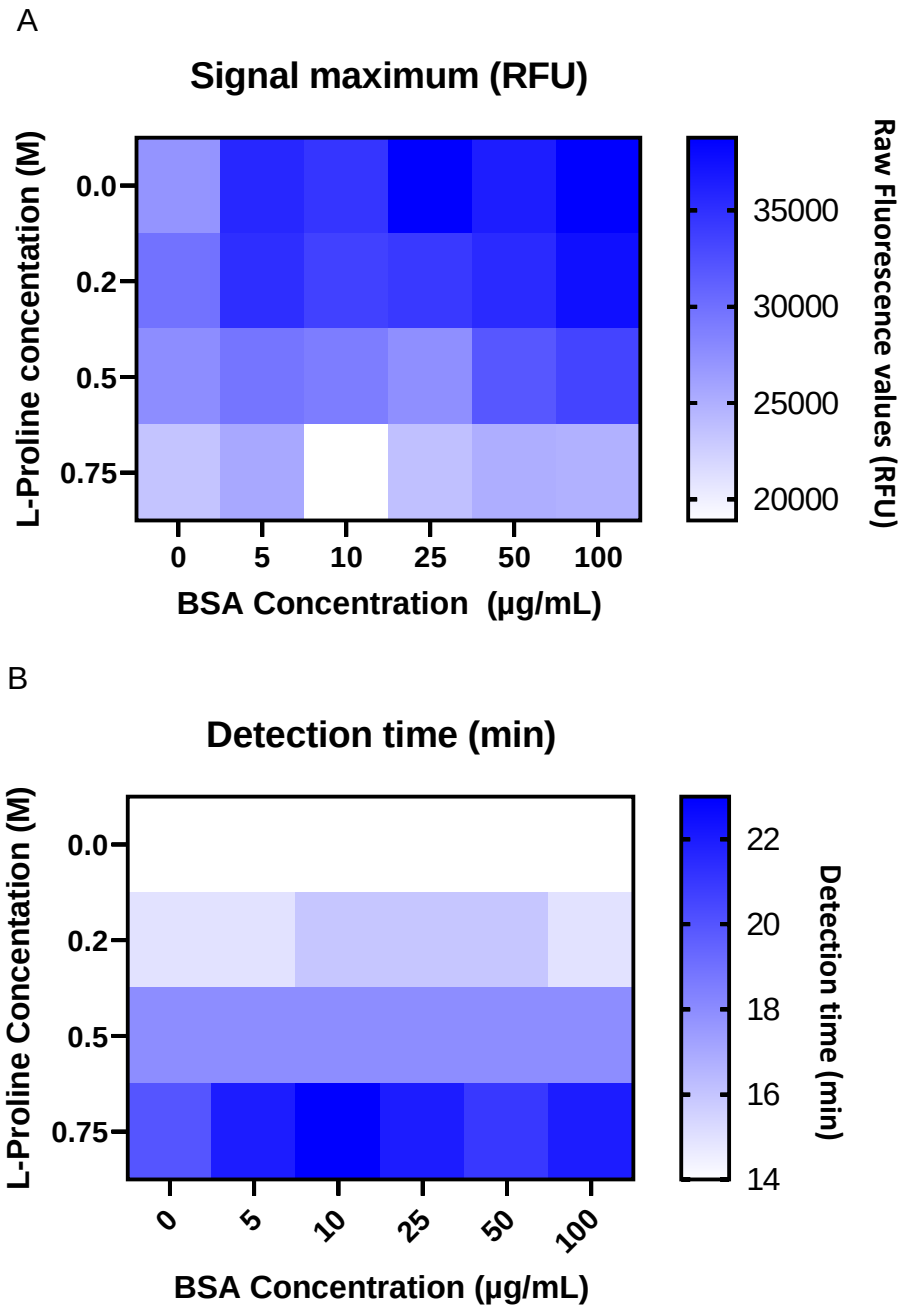


Figure 24. A) Signal maximum of the SARS-CoV-2 N gene RT-LAMP Cas12b assay when checkerboard titrating and adding bovine serum albumin and L-proline to the assay as potential chemical enhancers. B) Detection time of the SARS-CoV-2 N gene RT-LAMP Cas12b assay when checkerboard titrating and adding bovine serum albumin and L-proline to the assay as potential chemical enhancers. C) Times to reach half of the maximum fluorescence when checkerboard titrating and adding bovine serum albumin and L-proline to the assay as potential chemical enhancers. The results with error bars are means of three technical replicates (n=3).

With these suggestive results of BSA improving the SARS-CoV-2 N gene RT-LAMP Cas12b assay when used at 10 µg/mL, a confirmatory assay was performed in technical triplicate comparing reactions containing the above mentioned BSA concentration to a reaction without bovine serum albumin. The replicates produced significant decrease in signal maximum using BSA as an enhancer observed when compared to the neat reaction (Fig.25), suggesting that further investigation would be needed to validate the reagent as an enhancement additive. For the purpose of improving the RT-LAMP Cas12b, with such insignificant enhancement the reagent was not persued further as an additive to the assay.

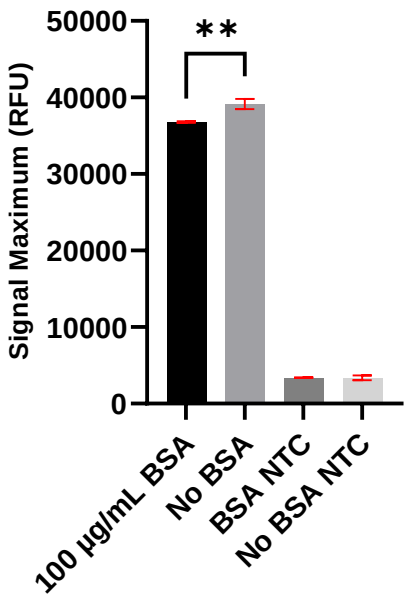


Figure 25. Signal maxima of replicates of the potentially BSA-enhanced SARS-CoV-2 N gene RT-LAMP Cas12b assay at 10 µg/mL in comparison to a non-chemically enhanced assay. The results with error bars are means of three technical replicates (n=3) and the error bars represent the standard deviations.

3.2.1.4.4.2. Dithiothreitol Titration to Reduce Nucleic Acid Secondary Structures

Dithiothreitol (DTT), commonly used in enzyme stability buffers as a redox agent, was titrated as a potential supplementary enhancement reagent to the SARS-CoV-2 N gene RT-LAMP Cas12b assay. The titration of DTT from 0 mM to 10 mM generates a stable signal maximum range in each biological replicate (Fig.26A). The detection time also appears to trend downward (decrease) as DTT concentration increases (Fig.26B). Although not statistically significant, the trend also appears as such for the time to reach half of the maximum fluorescence (Fig.26C). Overall, the addition of DTT does not appear to negatively affect the SARS-CoV-2 N gene RT-LAMP chemistry. It is evident that incorporation of a range of redox agent concentrations agent has little to no effect on Cas12b protein activity, and enzymatic activities. Considering these results, and that New England Biolabs have validated the storage of AapCas12b at 2 mM of DTT (see appendix 5.6. for AapCas12b storage solution), moving forward 2 mM DTT per reaction was included as a precautionary measure to reduce RNA secondary structure formation while stabilizing AapCas12b.

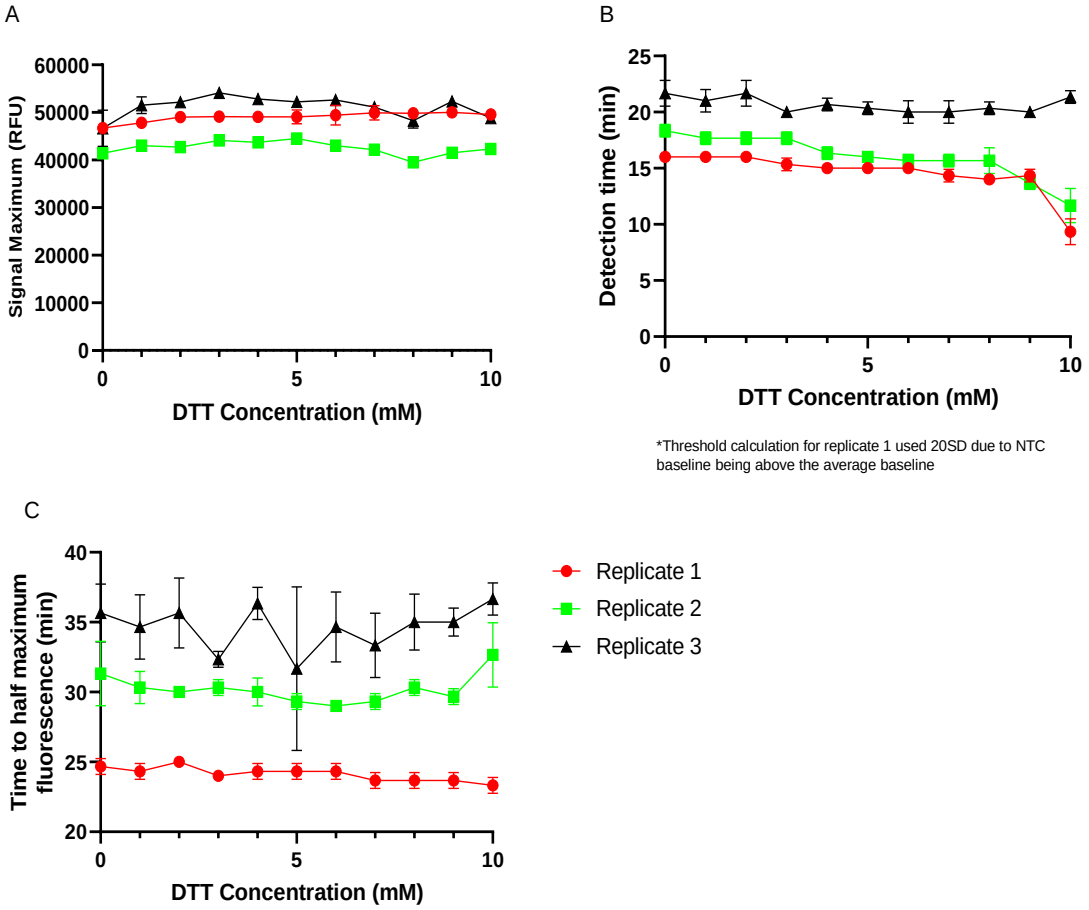


Figure 26. A) Biological triplicates of the signal maximum when titrating dithiothreitol from 10 mM to 0 mM into the SARS-CoV-2 N gene RT-LAMP Cas12b assay. B) Biological triplicates of the detection time when titrating dithiothreitol from 10 mM to 0 mM into the SARS-CoV-2 N gene RT-LAMP Cas12b assay. C) Biological triplicates of the times to reach half of the maximum fluorescence when titrating dithiothreitol from 10 mM to 0 mM into the SARS-CoV-2 N gene RT-LAMP Cas12b assay. The results with error bars are means of three biological replicates repeated in technical triplicate (n=3x3) and the error bars represent the standard deviations.

3.2.1.4.5. Nuclease-shielded sgRNA

A nuclease-shielding modification proprietary to Integrated DNA Technologies was added to the 3’ and 5’ ends of the SARS-CoV-2 N gene sgRNA in an attempt to mitigate sgRNA degradation by nucleases ubiquitously present in most microenvironments. The objective was to identify and assess potential effects on assay parameters due to this modification.

Upon signal detection, there was no statistically significant difference in detection time between the assay using the unaltered sgRNA and the assay using the ALT-R-modified sgRNA (Fig.27A). Increases in time to half of the maximum fluorescence and signal maximum was observed upon usage of the modified guide, therefore reducing assay efficiency and likely lightly reducing assay sensitivity (Fig.27B-C). This does not absolutely disregard the potential application of a nuclease-protected sgRNA in RT-LAMP Cas12b assays, however the concept was not explored further in this application.

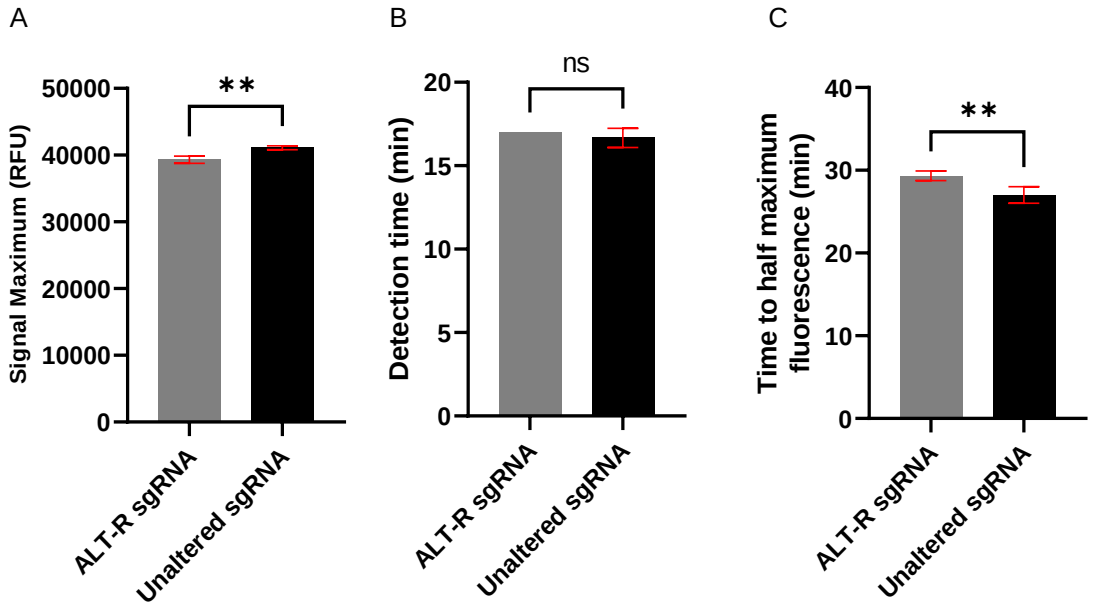


Figure 27. A) Signal maximum when using an ALT-R-modifed SARS-CoV-2 N gene sgRNA or an unmodified SARS-CoV-2 N gene sgRNA when performing the SARS-CoV-2 N gene RT-LAMP Cas12b assay. B) Detection time when using an ALT-R-modifed SARS-CoV-2 N gene sgRNA or an unmodified SARS-CoV-2 N gene sgRNA when performing the SARS-CoV-2 N gene RT-LAMP Cas12b assay. C) Times to reach half of the maximum fluorescence when using an ALT-R-modifed SARS-CoV-2 N gene sgRNA or an unmodified SARS-CoV-2 N gene sgRNA when performing the SARS-CoV-2 N gene RT-LAMP Cas12b assay. The results with error bars are means of three technical replicates (n=3) and the error bars represent the standard deviations.

3.2.1.4.6. Adding a Helicase to Reduce Nontemplate amplification

A thermostable Tte UvrD Helicase (New England Biolabs, Cat. No.: M1202S) was added to the SARS-CoV-2 RT-LAMP Cas12b assay at 10 ng/reaction and 20 ng/reaction, as per the manufacturer's recommendations. Supplemented ATP helps with adequate helicase function, therefore 1 mM of ATP (New England Biolabs, Cat. No.: P0756S) was included per helicase-containing reaction, again as per the manufacturer's recommendations.

Supplementing the SARS-CoV-2 RT-LAMP Cas12b reaction with 10 ng of helicase and 1 mM of ATP did not significantly increase signal maximum but did significantly increase the time to reach half of the maximum fluorescence (Fig.28A-B). There was, however, only a one minute decrease in the detection time when going from no helicase to 10 ng of the enzyme (Fig.28C). This decrease in detection time without effects on signal maximum suggest that the helicase may be slightly interfering with normal helicase-free amplification by reducing available reagents, or crowding the reaction. This effect is further observed when adding 20 ng of helicase with significantly decreased signal maxima, detection times and with the time to reach half of the maximum fluorescence. Ultimately, the addition of a helicase and ATP to the RT-LAMP Cas12b reaction appears to be detrimental to SARS-CoV-2 detection. The decrease is logical due to the innate hydrolysis of ATP by the helicase to drive its function, which releases hydrogen ions in the reaction. These hydrogen atoms would lower the reaction pH which, as per the results in 3.2.1.2.5., a more acidic microenvironment which will reduce signal maxima obtained by RT-LAMP Cas12b.

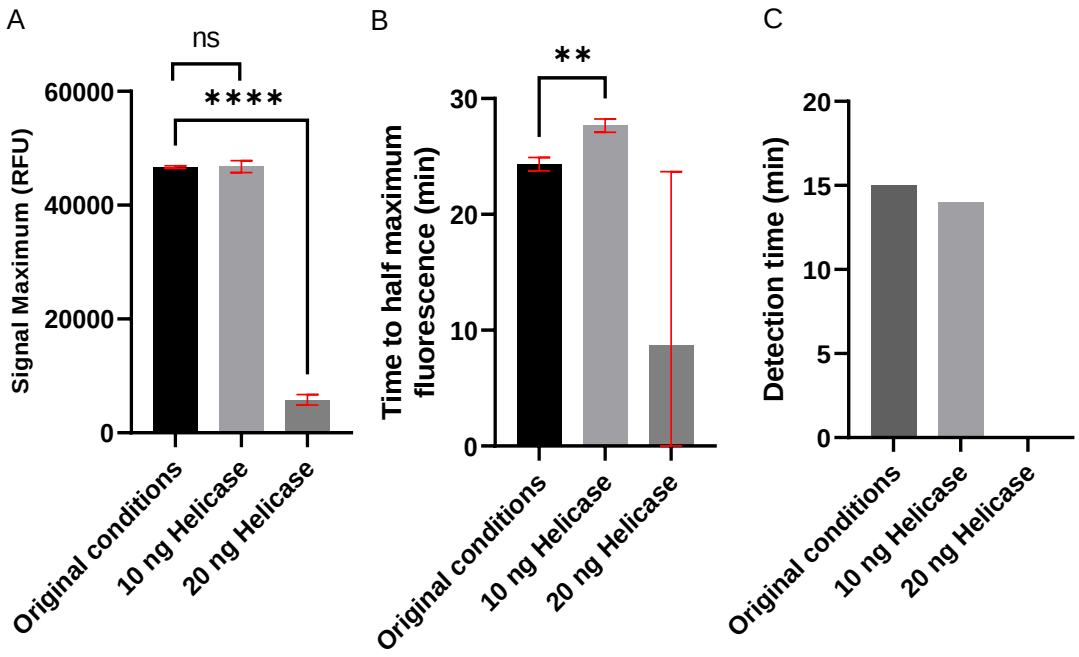


Figure 28. A) Signal maximum when adding 0 ng. 10 ng or 20 ng of Tte UvrD Helicase with 1 mM of ATP to the SARS-CoV-2 N gene RT-LAMP Cas12b assay. B) Detection time when adding 0 ng. 10 ng or 20 ng of Tte UvrD Helicase and 1 mM of ATP to the SARS-CoV-2 N gene RT-LAMP Cas12b assay. C) Times to reach half of the maximum fluorescence when adding 0 ng. 10 ng or 20 ng of Tte UvrD Helicase and 1 mM of ATP to the SARS-CoV-2 N gene RT-LAMP Cas12b assay. The results with error bars are means of three technical replicates (n=3) and the error bars represent the standard deviations.

3.2.1.4.7. Effects of Reporter Fluorophore on SARS-CoV-2 N gene RT-LAMP Cas12b

Previous literature suggests that differences in fluorophore photon emission levels may affect assay sensitivity. A *Brevibacillus sp.* Cas12b assay targeting SARS-CoV-2 reported that FAM and HEX reporter DNA exhibit significantly more elevated signal maxima than Cy5 at equal concentrations, thus increasing assay sensitivity. In the author's hands, FAM emitted a more elevated RFU signal maximum than HEX when cleaving a 8-mer poly-thymine DNA reporter upon SARS-CoV-2 detection [228]. Using the SARS-CoV-2 N gene RT-LAMP AapCas12b assay, FAM and HEX relative fluorescence emissions were compared using equal quantities of FAM and HEX connected to a 5-mer poly-thymine linked to a quencher. Shown in figure 29, and opposite to the results obtained in the BrCas12b-based assay, the 5-mer poly-thymine connected to HEX emitted more than 1.6X the signal maximum obtained when using a 5-mer poly-thymine connected to FAM. These results are suggestive that using HEX as the fluorophore linked to a 5-mer poly-thymine may increase assay sensitivity when detecting low quantity nucleic acid samples. Baseline or background fluorescence levels are also lower when using the HEX fluorophore, which allows for more easily differentiable negative-to-positive results. These results are also suggestive that CRISPR-Cas proteins have varying affinities to cleave certain DNA products, which has extensively been confirmed in literature[266,267].

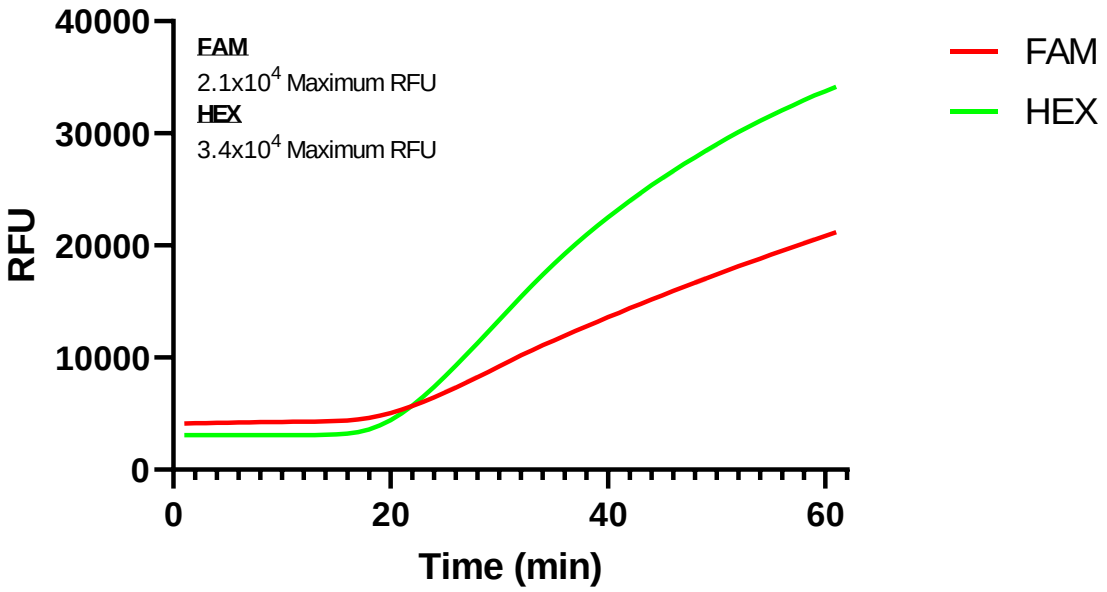


Figure 29. Mean kinetic profile and signal maxima of the SARS-CoV-2 N gene RT-LAMP Cas12b assay when using two different DNA reporters containing the fluorophores FAM or HEX. The fluorescent profiles of each fluorophore are means of three technical replicates (n=3).

3.2.2. Validation and Performance Characteristics

3.2.2.1. Specificity to SARS-CoV-2 Variants

The SARS-CoV-2 RT-LAMP Cas12b assay was not only validated for diagnostic detection of the original Wuhan-1 strain of the virus, but for the detection of the most prevalent variant, Omicron variant and a lesser prevalent Delta strain. The assay conditions tested two conditions, high nucleic acid content (1000 genome copies/µL) to replicate a sample that may have high viral titers and low nucleic acid copies (300 genome copies/µL) to replicate a sample that may have low viral titers. It is recognized that a 3-fold difference is not necessarily significant, however RT-LAMP based detection is not on a linear scale, therefore subtle changes in nucleic acid concentrations will have a significant effect on detection capabilities.

As expected, all three variants were detected with the STOPCovid assay, although with differences in detection time and signal maximum for the Delta and Omicron strains when compared to the Wuhan-1 strain (Figure 30). Although the detection times differed, actual detection only increased by 5-6 minutes. The detection time variability could potentially be attributed to sequence specificity of the sgRNA or RT-LAMP primers guided to the Wuhan-1 variant. Moreover, detection stochasticity could be attributed to sample integrity due to age and unknown quantities of freeze-thaw cycles on the RNA used as the Delta and Omicron RNA used here was gifted from the Public Health Agency of Canada whereas the Wuhan-1 RNA was freshly extracted from viral stocks.

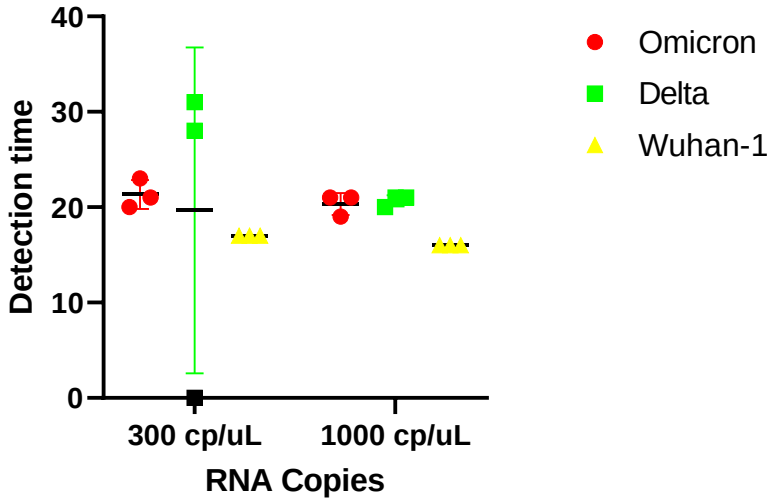


Figure 30. Detection times of the SARS-CoV-2 Wuhan-1, Delta and Omicron strains when using the N gene RT-LAMP Cas12b assay.

3.2.2.2. Cross-Reactivity to Homologous and Pathologically Similar Agents

Testing was performed on nucleic acids of homologous and pathophysiologically similar agents to SARS-CoV-2 to ensure the the SARS-CoV-2 N gene RT-LAMP Cas12b does not cross-react and detect unintended pathogens. The primary pathogens of interest were SARS-CoV-1, MERS, HCoV-229E, HCoV-NL63, HCoV-OC43 and HCoV-HKU1, although HCoV-HKU1 nucleic acid was not obtainable. Other animal viruses, including avian and porcine coronaviruses, viruses not known to infect humans, and one human respiratory pathogen was tested for cross-reactive nucleic acid detection. These pathogens include Transmissible gastroenteritis virus (TGEV), Porcine endemic diarrhea virus, Infectious bronchitis virus, Influenza A virus subtype H7N9 and pandemic Influenza A virus subtype H1N1. Futher testing of common human respiratory pathogens including but not limited to Respiratory syncytial virus, Human metapneumoviruses, Human parainfluenzaviruses, rhinoviruses, H5N1 avian influenza and *Streptococcus pneumoniae* are recommended and would cover a larger panel of potential cross-reacting pathogens that cause pathophysiologically similar illnesses. However, these pathogens were not available for testing at the NCFAD.

There was no indication of amplification within any of the tested pathogens other than the positive control, which was RT-qPCR-confirmed SARS-CoV-2 RNA (Fig.31). One of three replicates of TGEV Purdue Strain indicated an increase in signal beyond 50 minutes of amplification. Due to the lack of homology within all of the primers/sgRNA to the TGEV Purdue genome and to the fact that only one of three replicates showed sign of amplification, this signal can likely be attributed to accidental SARS-CoV-2 genome contamination within the well or incidental false positivity although less likely considering the 100% positive predictive value presented by Joung and colleagues. Although the data is not included in this thesis, results obtained

by Dr. Guodong Liu from the Special Pathogens Program at the Public Health Agency of Canada, confirmed there is no cross-reactivity to HCoV-229E, HCoV-NL63 and HCoV-OC43.

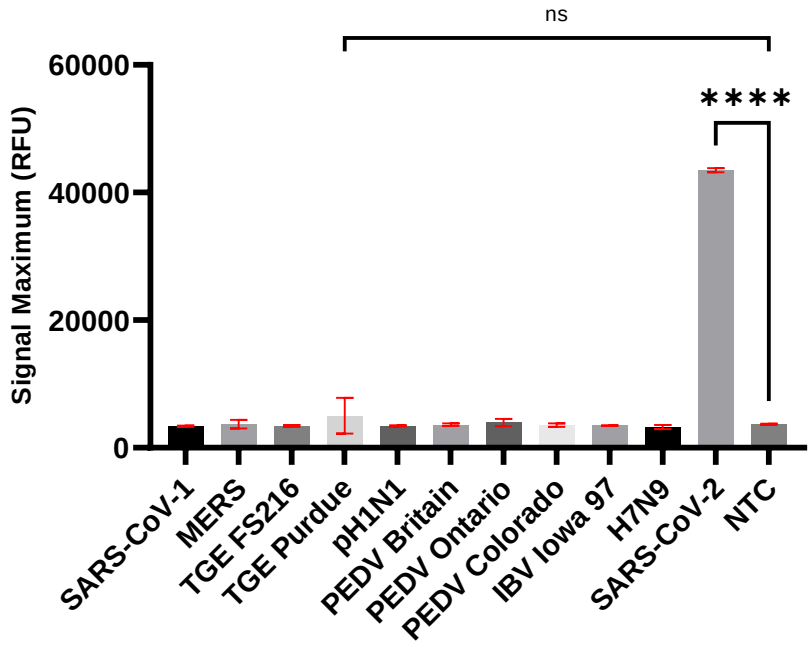


Figure 31. Signal maxima of the SARS-CoV-2 N gene RT-LAMP Cas12b assay cross-reactivity testing against SARS-CoV-1, MER-CoV, Transmissible gastroeneteritis virus, Influenza A virus H1N1, Porcine epidemic diarrhea virus, Infectious bronchitis virus and avian influenza A virus H7N9. The results with error bars are means of three technical replicates (n=3) and the error bars represent the standard deviations.

3.2.2.3. SARS-CoV-2 Genome Limit of Detection Without Enrichment Extraction

The limit of detection was defined as the lowest concentration of nucleic acids detected at which 100% of the replicates surpassed the detection threshold. The optimized SARS-CoV-2 N gene RT-LAMP Cas12b assay was tested with a dilution series of SARS-CoV-2 RNA initially quantified as per section 2.9. then diluted from 1000 cp/µL to 1 cp/µL. All technical and biological replicates were detected down to 50 cp/µL (Fig.32). At 10 and 1 copies per microliter, select replicates were not detected. With these results, the optimized SARS-CoV-2 RT-LAMP Cas12b assay was confirmed to have a detection limit of at least 50 cp/µL.

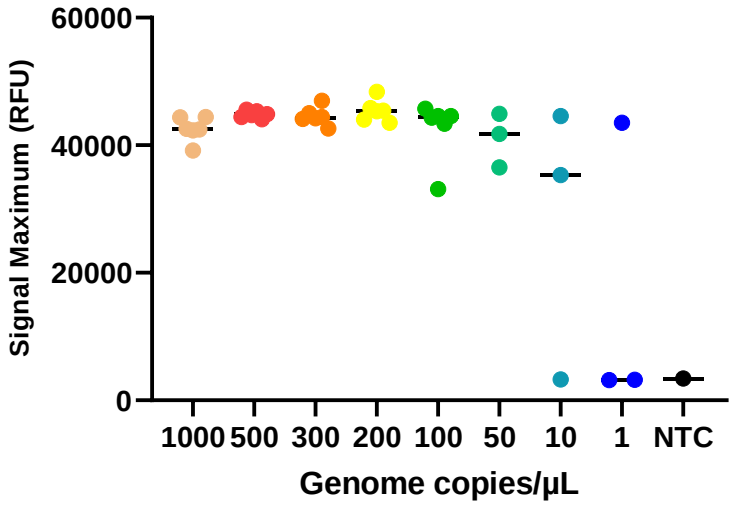


Figure 32. Signal maxima of SARS-CoV-2 RNA titrations from 1000 cp/µL to 1 cp/µL, detected via the SARS-CoV-2 N gene RT-LAMP Cas12b assay without nucleic acid enrichment-extraction to verify the assay limit of detection. The center bands of each RNA titration are means of at least three technical replicates (n=3).

3.2.2.4. Limit of Detection Reproducibility

To validate the limit of detection established in 3.2.2.3., the optimized STOPCovid assay LOD repeatability was extensively tested with ten assay replicates inputted with 50 cp/µL of SARS-CoV-2 RNA. The ten SARS-CoV-2-positive technical replicates were performed using RNA that was extracted and purified using the QIAamp Viral RNA Mini Kit (see 2.8.1), quantified following the protocol in 2.9., then diluted to 50 cp/µL. To ensure that no false positive results were obtained, ten no-template controls were included by adding nuclease-free water as RNA template instead of SARS-CoV-2 RNA. All ten positive replicates were detected with very little variability in signal maxima (Fig.33). Only one of the ten "no template control" technical replicates surpassed the positive threshold value. These results indicate that the SARS-CoV-2 N gene RT-LAMP limit of detection can confidently and repeatedly be detected using AapCas12b.

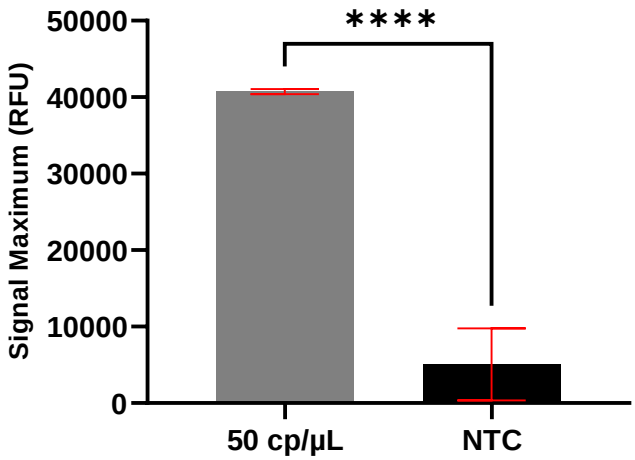


Figure 33. Signal maxima of 10 SARS-CoV-2 RNA controls at 50 cp/µL and 10 no template controls used to validate the reproducibility of the limit of detection of the SARS-CoV-2 N gene RT-LAMP Cas12b assay. The results with error bars consist of ten replicates (n=10) and the error bars represent the standard deviations.

3.2.2.5. Analytical Characteristics (Sensitivity, Specificity & Predictive Values)

To assess the analytical performance of the SARS-CoV-2 N gene RT-LAMP Cas12b assay, RT-qPCR-confirmed negative and positive clinical deer and mink nasal swabs submitted at the National Centre for Foreign Animal Diseases for clinical diagnostics were tested using two different conditions. The first assay condition consisted of using 49 µL of total master mix and adding 1 µL of extracted template RNA, and the second condition consisted of reducing the ddH_2O/ reaction further to 5.66 µL and increasing the RNA template/reaction to 5 µL (table . The concept of increasing the total RNA template added to the reaction is to identify the optimal amount of input RNA available to the RT-LAMP Cas12b reaction while attempting to identify a volume threshold of residual contaminants and/or reagents in the extraction eluent that minimally affect the reaction. The RNA extractions were performed using the extraction protocol developed in 3.4.

Using 1 µL of RNA elution, the mink samples had 100% sensitivity, specificity, positive and negative predictive values, whereas deer swabs had only 44% sensitivity, 89% specificity, 80% positive and 61.5% negative predictive values. Increasing template to 5 µL of RNA elution, mink samples had a slight reduction in sensitivity to 89%, and a drastic decrease in specificity to 56%, changing the predictive values to 66.7% positive and 83.3% negative predictive values. Deer however, increased in positivity to 67%, decreased to 67% specificity and 66.7% positive and negative predictive values (Table 4).

Table 4. Analytical sensitivity, specificity, positive predictive value and negative predictive value of the SARS-CoV-2 N gene RT-LAMP Cas12b assay testing mink and deer nasal swabs. Tables 3A, 3B and 3C used 1 µL of RNA template extracted using the rapid enrichment-extraction protocol whereas tables 3D, 3E and 3F used 5 µL of RNA template. RT-qPCR was not completed in parallel due to logistical constrains in CL3Ag.

A

1 µL - Total Mink & Deer				
	Infection status			
	Pos.	Neg.	Total	Predictive value
Pos.	13	1	14	93
Neg.	5	17	22	77
Total	18	18		
	Sensitivity	Specificity		
	72	94		

B

1 µL - Mink				
	Infection status			
	Pos.	Neg.	Total	Predictive value
Pos.	9	0	9	100
Neg.	0	9	9	100
Total	9	9		
	Sensitivity	Specificity		
	100	100		

C

1 µL - Deer				
	Infection status			
	Pos.	Neg.	Total	Predictive value
Pos.	4	1	5	80
Neg.	5	8	13	62
Total	9	9		
	Sensitivity	Specificity		
	44	89		

D

5 µL - Total Mink & Deer				
	Infection status			
	Pos.	Neg.	Total	Predictive value
Pos.	14	7	21	67
Neg.	4	11	15	73
Total	18	18		
	Sensitivity	Specificity		
	78	61		

E

5 µL - Mink				
	Infection status			
	Pos.	Neg.	Total	Predictive value

Pos.	8	4	12	67
Neg.	1	5	6	83
Total	9	9		
	Sensitivity	**Specificity**		
	89	56		

F

5 µL - Deer				
	Infection status			
	Pos.	**Neg.**	**Total**	**Predictive value**
Pos.	6	3	9	67
Neg.	3	6	9	67
Total	9	9		
	Sensitivity	**Specificity**		
	67	67		

*Results may be skewed as they were performed when troubleshooting SARS-CoV-2 contamination issues; repeated experiments are required for further validation.

3.3. Nipah virus RT-LAMP Cas12b

3.3.1. P, F, G, M and N Gene Primer and sgRNA Designs

The primer design parameters outlined in 2.10.1. were taken into consideration when designing the Nipah virus RT-LAMP assay. Five distinct genes were targeted with the hopes of identifying a candidate primer set capable of reliably detecting the pathogen: the phosphoprotein gene, the fusion glycoprotein gene, the glycoprotein gene, the matrix gene and the nucleoprotein gene. In literature there is just one example of a Nipah virus RT-LAMP; designed in 2019 by Ma and colleagues, the assay leverages colorimetric detection based on pH changes from RT-LAMP amplification. With primers targeting the N gene, Ma and colleagues validated the detection of NiV-M and NiV-B, the two known genotypes in 2019. This was made possible by incorporating nucleotide degeneracies within five of the six primers to ensure complete coverage of NiV strains. The Ma *et al.* primer set was included in this trial to see if the only published NiV RT-LAMP primer set would be a candidate for coupling with CRISPR-based detection. All primer sets and sgRNA sequences described in this thesis can be found in appendices 5.3.2 and 5.3.3.. All known Nipah virus strains have relatively highly conserved genomes, making pan-genome sgRNA and primers possible. Although the RT-LAMP primers retained degeneracies to allow for complete strain coverage, the single-guide RNA did not require any degeneracies due to the presence of a 100% homologous twenty to twenty-three nucleotide stretch being found within the central region of the N gene RT-LAMP amplicon. This was the case for the each of the sgRNAs designed for each NiV RT-LAMP primer set.

3.3.2. Iterative Optimization

3.3.2.1. Core Assay Conditions

3.3.2.1.1. Primer Selection Based on Temperature Gradient of the NiV RT-LAMP Cas12b Assay

The selection process for the NiV RT-LAMP primer and Cas12b sgRNA sets were based on the largest and most functional/versatile temperature range demonstrating effective amplification and detection. A characteristic important to this selection is that the candidate primer and sgRNA set can produce the most elevated signal maximum, demonstrating the likelihood to detect the lowest concentration of NiV RNA. Likely the most crucial parameter to a well-designed and ideal primer set is the most rapid time to detection. Each primer set was tested following the original STOPCovid protocol for RT-LAMP Cas12b setup.

Two thousand genome copies per microliter was added to each RT-LAMP Cas12b reaction containing different primer/sgRNA set, fixing and standardizing the quantity of nucleic acid detected within each assay condition. A temperature gradient was applied to each primer set, ranging from 56.0°C to 66°C to identify the optimal amplification temperature, Cas12b cleavage temperature and to verify if there would be any effect on negative controls (nuclease-free water instead of RNA).

The green curves in each of figures 34A-C clearly demonstrate a signal maximum and a signal minimum for each temperature point of each of the M, N and G genes. There were no significant signal maxima nor minima detected within the P and F primer/sgRNA sets suggesting that the primer set was not effective for amplification, therefore those two gene targets were omitted from further evaluation. Looking at the detection times (red curves) of these three select primer sets, the N gene elicited the lowest time to detection and the most elevated signal maximum (Fig.34B), idealizing this primer/sgRNA set as the gene target. The N gene primer set displayed

the largest functional amplification and detection range, with five temperatures from 56.0°C to 62.4°C emitting signal maxima at more than $4x10^4$ relative fluorescence units, being detected within 25 minutes. In comparison, the M and G genes elicited a more narrow range; The M gene detected four replicates between $3x10^4$ RFU-$4x10^4$ RFU, detected within 40 minutes, at four temperature points, and the G gene detected three replicates at more than $4x10^4$ RFU within the same timeframe as the N gene. This wide range is important in the context of point-of-care applications due to the fact that rapid diagnostics may be performed in very limited settings where environmental temperature and power supply may affect actual instrument output temperature. A large range in assay functionality allows for temperature flexibility in point-of-care settings. Considering how the N gene and the G gene primer sets produced very similar detection times and signal maxima, but the N gene set generated a wide temperature range where the RT-LAMP Cas12b reaction amplified and detected efficiently, the N gene primer/sgRNA set was pursued for the development of this assay.

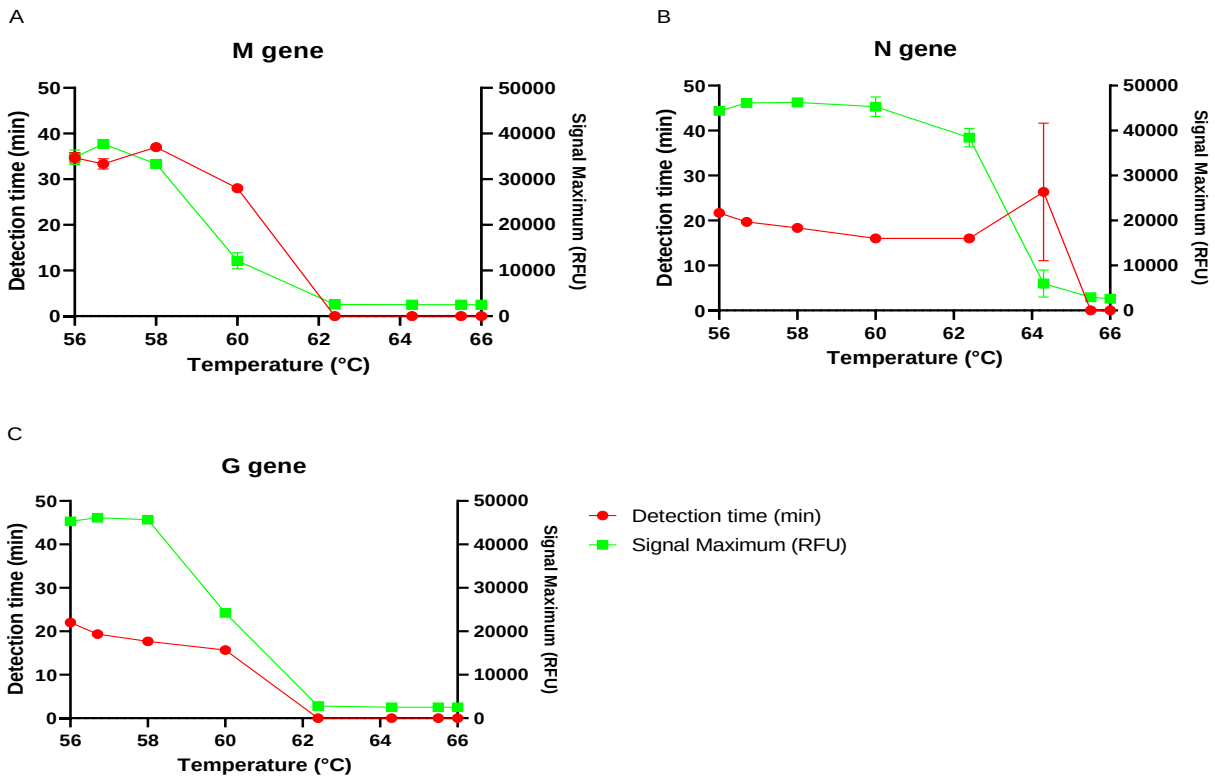


Figure 34. A) Signal maximum and detection time of the Nipah virus RT-LAMP Cas12b assay when using the matrix gene primer set and single-guide RNA at temperatures ranging from 66C°C to 56°C. B) Signal maximum and detection time of the Nipah virus RT-LAMP Cas12b assay when using the nucleoprotein gene primer set and single-guide RNA at temperatures ranging from 66C°C to 56°C. C) Signal maximum and detection time of the Nipah virus RT-LAMP Cas12b assay when using the glycoprotein gene primer set and single-guide RNA at temperatures ranging from 66C°C to 56°C.

3.3.2.1.2. AapCas12b-sgRNA Titration

The concentrations of sgRNA and Cas12b established in the STOPCovid protocol would potentially require optimization for the Nipah virus-targeting assay, which uses a completely new primer and sgRNA set. Changes in primers will affect amplification efficiency which, downstream, will affect the amount of sgRNA needed for ribonucleoprotein complex formation, RNA scanning, detection and non-specific collateral cleavage. These combinations of changes will, like mentioned above, likely alter Cas12b-sgRNA complex temperament, therefore require re-optimization. Like the SARS-CoV-2 sgRNA and Cas12b titration series, the reagents were titrated at equimolar concentrations from 10 nM to 75 nM per reaction. Non-specific collateral cleavage of reporter DNA upon NiV-MY RNA detection was registered at all equimolar concentrations of sgRNA-Cas12b. The most elevated signal maximum was registered when employing 60 nM of the two reagents, which is nearly double the molar concentration used in the STOPCovid protocol (31.25 nM) (Fig.35A). The signal maxima elicited a positive trending increase from lower to higher concentrations of sgRNA and Cas12b, with the maximum obtained at 60 nM. A slight decreasing trend was noted in the time to detection, from 10 nM to 75 nM, with the minimal detection time also being at 60 nM of the two reagents (Fig.35B). Within the context of a rapid and inexpensive diagnostic assay to be used at the point of care, the optimal concentration for these reagents will be where the concentrations are at their lowest, with little to no change within increased and decreased concentrations. Taking this metric into consideration, 60 nM of AapCas12b and 60 nM of N gene sgRNA was the optimal concentration for maximal signal and minimal time to detection, doubling the necessary concentration when compared to the SARS-CoV-2-detecting assay.

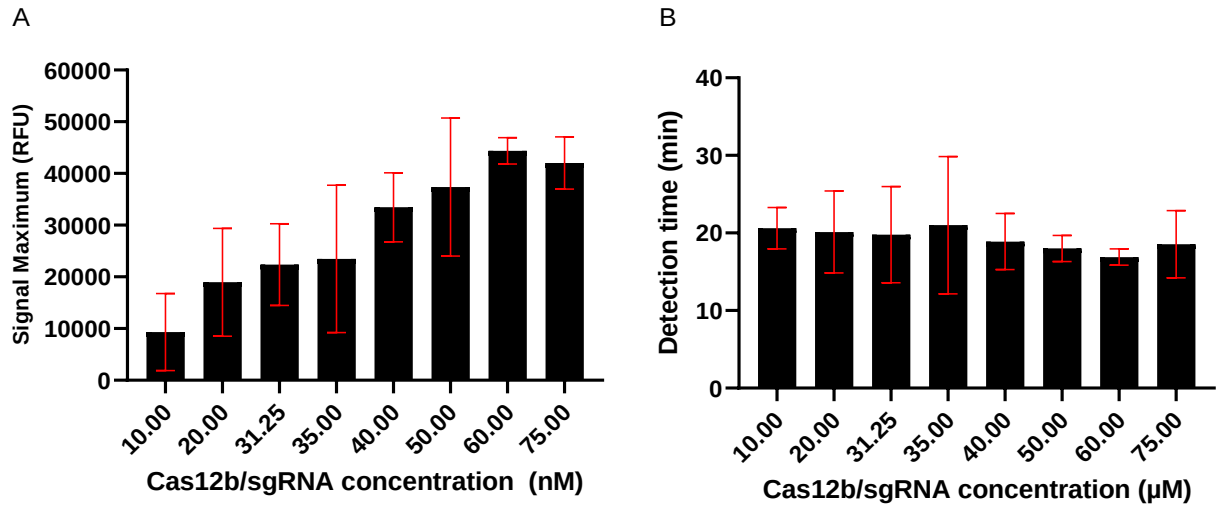


Figure 35. A) Signal maximum of the the titration of the New England Biolabs Inc. AapCas12b enzyme and the Nipah virus N gene sgRNA at equimolar concentrations 10 nM to 75 nM. B) Detection time of the titration of the New England Biolabs Inc. AapCas12b enzyme and the Nipah virus N gene sgRNA at equimolar concentrations from 10 nM to 75 nM. The results with error bars are means of at least three technical replicates (n=3) and the error bars represent the standard deviations.

3.3.2.2. Additional Optimization

One of the objectives of this thesis was to demonstrate translatability of the SARS-CoV-2 RT-LAMP Cas12b assay to detect another pathogen. This meant to demonstrate that CRISPR-based molecular diagnostic approaches are modular and can be rapidly modified in a "plug-and-play" manor for the development of molecular diagnostic assays targeting discriminate pathogens of interest. Herein, without overly complicating optimization at this stage, the Nipah virus RT-LAMP Cas12b assay was selectively optimized in an attempt to improve the current format following similar improvement points identified within the SARS-CoV-2 assay. These improvement points include the verification as to which detergent may be most ideal for RT-LAMP amplification using Nipah virus-targeting primers, the optimal pH of said buffer once the detergent has been optimized and the validation of DTT as a potential chemical enhancer that can stabilize and deter secondary structure formation within NiV RNA.

3.3.2.2.1. Three Non-Ionic Detergents Within the Reaction Buffer

Considering one of the functions of adding detergents to an amplification assay is to reduce secondary structures in nucleic acids, and in the context of RT-LAMP, these secondary structures can be found in the input template and the overfolded amplicon, the three non-ionic detergents were re-titrated from 5% to 0.2% to identify the optimal concentration for use with NiV RNA and N gene amplicon. Restricting the upper limit at 5% detergent was due to the reagent stock concentration ranging from 10% to 35%, which consequently does not allow for adequate volume considering the added reagents needed to generate the buffer.

Broadly, all three conditions were capable of detecting Nipah virus RNA within thirty minutes and with $3x10^4$ RFU to nearly $4.5x10^4$ RFU as signal maxima (Fig.36A-C). When using Brij-35 as detergent from 0.2% to 5%, signal maxima were more stochastically detected the more

detergent added. With this regard, at 0.2 to 1% detergent, signal maximum replicate groupings were tight and lowly variable. Detection times, from 0.2% to 5%, were kept to approximately 20 minutes or less. Again within the range of 0.2% to 1%, detection time replicate groupings were tight and lowly variable (Fig.36A). When using Triton X-100 as detergent, signal maxima where much more stochastic than Brij-35 throughout the entire detergent concentration range (Fig.36B). The more elevated the concentration of triton X-100, the lower was the signal maximum whereas the maximum was obtained at 1%. Detection times were equally as stochastic within the same range of concentration, varing from close to 10 minutes to nearly 30 minutes before detection. The variability of these two parameters suggest that triton X-100 may not be suited for the assay. Interestingly the same can be said when using tween 20 as detergent. As the tween 20 concentration decreased from 5% to 0.2%, signal maxima and detection times were more stochastic in replicability, even at 1% which is the concentration used in the STOPCovid protocol (Fig.36C). Due to the variability in the detection times and signal maxima when using triton X-100 and tween 20, and the accuracy of the results when using 1% down to 0.2% of Brij-35, Brij-35 at 1% was the detergent concentration selected for further validation of the STOPCovid protocol. Concordant with the results obtained when optimizing the STOPCovid protocol, brij-35 appears to produce the most elevated, precise and accurate results. The only difference between the optimized SARS-CoV-2 assay and the NiV assay is that the former uses a 2% Brij-35 buffer and the latter uses a 1%.

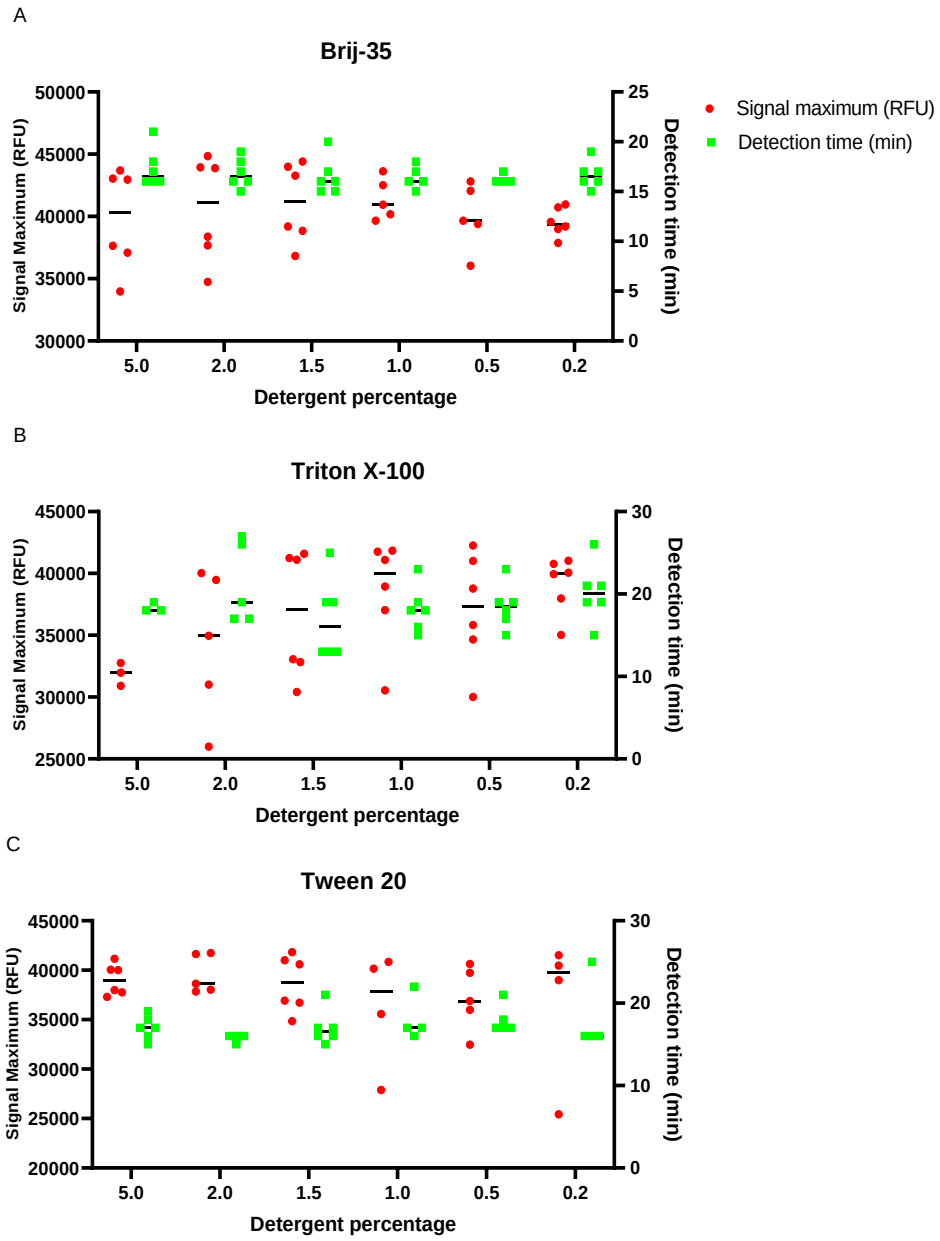


Figure 36. A) Signal maximum and detection time of the Nipah virus N gene RT-LAMP Cas12b assay when titrating Brij-35 as the detergent in the RT-LAMP reaction buffer. B) Signal maximum and detection time of the Nipah virus N gene RT-LAMP Cas12b assay when titrating Triton X-100 as the detergent in the RT-LAMP reaction buffer. C) Signal maximum and detection time of the Nipah virus N gene RT-LAMP Cas12b assay when titrating Tween-20 as the detergent in the RT-LAMP reaction buffer. The center bands of each detergent percentage are means of at least three technical replicates (n=3).

3.3.2.2.2. Optimal Reaction Buffer pH

Like with the SARS-CoV-2 N gene RT-LAMP Cas12b assay where the detergent used was changed from tween 20 to Brij-35 and the optimal pH was reestablished, nearly the same change was made with the Nipah virus-targetting assay. In this context, the reaction buffer detergent was changed from 1% tween 20 (STOPCovid assay) to 2% Brij-35 (Optimized SARS-CoV-2 assay) to 1% Brij-35 in the NiV assay. For the same purpose as stated in 3.3.2.2.2., the pH was retitrated in hopes of identifying the optimal condition for the now Nipah virus N gene RT-LAMP Cas12b assay. A 2% Brij-35 buffer lot was buffered as described in the SARS-CoV-2 pH optimization section using NaOH or HCl and the pH was varied from 8.2 to 11.3. A sharp decrease in signal maximum was observed, as per figure 37A, from a pH of 8.2 to 9.3 whereas an increase in time to reach half of the maximum fluorescence was observed up until a pH of 9.3 (Fig.37C). Above pH 9.3, the times to reach half of the maximum fluorescence was significantly reduced. Stochasticity in detection times was observed at pH values of 9.3 and higher (Fig.37B), suggesting that the functional pH range would be defined between 8.2 and 9.0. Considering the most elevated signal maximum was obtained at a pH of 8.2, combined with producing the lowest detection time, the 2% Brij-35 buffer was kept at a pH of 8.2.

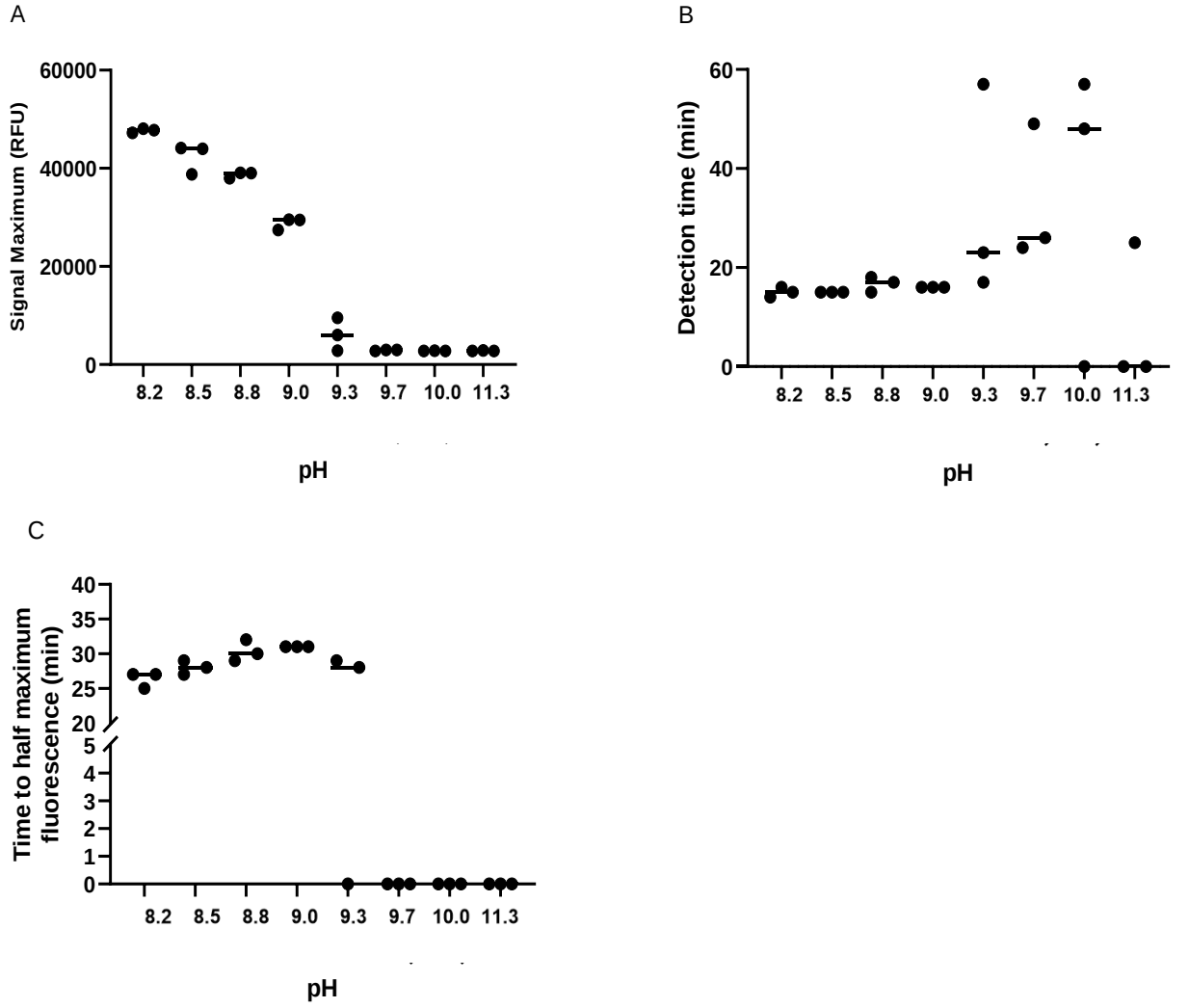


Figure 37. A) Signal maximum of the Nipah virus N gene RT-LAMP Cas12b assay when using Brij-35 at 1% in the reaction buffer titrated from pH 8.2 to 11.3. B) Detection time of the Nipah virus N gene RT-LAMP Cas12b assay when using Brij-35 at 1% in the reaction buffer titrated from pH 8.2 to 11.3. C) Times to reach half of the maximum fluorescence of the Nipah virus N gene RT-LAMP Cas12b assay when using Brij-35 at 1% in the reaction buffer titrated from pH 8.2 to 11.3. The center band of each pH value is mean of three technical replicates (n=3).

3.3.2.2.3. Addition of DTT to Reduce NiV Genome Secondary Structures

Similar to the SARS-CoV-2 RT-LAMP Cas12b DTT optimization where dithiothreitol was titrated from 0 mM to 25 mM, dithiothretol was titrated from 0.1 mM to 2 mM at 0.5 mM intervals with outlying 4 mM, 6 mM and 12 mM concentrations to cover a large concentration range in an attempt to optimize redox conditions for Nipah virus secondary structures. The results obtained here are very similar to those obtained in 3.2.1.4.4.2.. Throughout the spectrum of concentrations, signal maxima were not enhanced significantly, only slightly reduced at higher DTT concentrations (6 mM and 12 mM) (Fig.38A). The detection time when 2 mM DTT, 12 mM DTT and 0 mM DTT only varied by minutes, with only a minute difference in detection time from 0 mM to 2 mM (concentration used in the optimized SARS-CoV-2-detecting assay) (Fig. 38B). The benefit in using DTT at 2 mM outweighs the minimal-to-none decrease in performance, thus 2 mM was also used in the Nipah virus N gene RT-LAMP Cas12b assay. We reasoned the DTT will prevent the risk of secondary structure formation that may prevent or inhibit effective RT-LAMP amplification and CRISPR-Cas function.

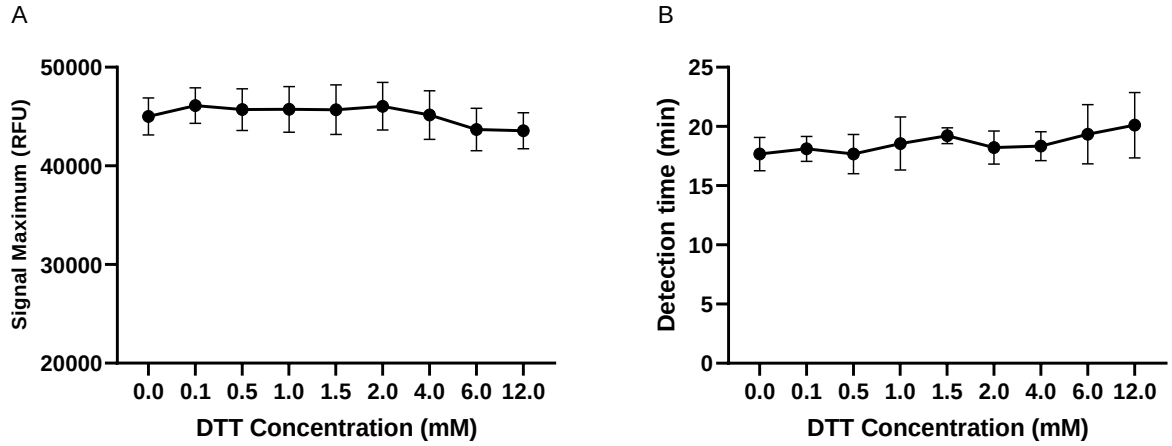


Figure 38. A) Mean signal maximum of the Nipah virus RT-LAMP Cas12b assay when titrating dithiothreitol from 0 mM to 12 mM. B) Mean detection time of the Nipah virus RT-LAMP Cas12b assay when titrating dithiothreitol from 0 mM to 12 mM. The results with error bars are means of three technical replicates (n=3) and the error bars represent the standard deviations.

3.3.3. Validation and Performance Characteristics

3.3.3.1. Specificity to Nipah Genotypes

Like the SARS-CoV-2 specificity validation, the NiV assay was also conducted using two test conditions: high nucleic acid content (10^4 genome copies/µL) and low nucleic acid copies (10^3 genome copies/µL). These conditions were set to ensure that, regardless of the strain, at low viral load the pathogen strain will be detected.

The results in figures 39A demonstrate that both the Malaysia and Bangladesh genotypes are being detected, with NiV-BD producing a slightly more elevated signal maximum. Conversely, NiV-MY is detected slightly more rapidly than NiV-BD (Fig.39B). Adequate detection of both genotypes and considering the sequence homology between the Bangladesh and India strains, suggests that the India strain would also be detected. At low genome copy numbers (10^3 cp/µL), the assay stochastically detects both genotypes, which is consistent with results obtained in 3.3.3.3. where a limit of detection of 5000 cp/µL was established.

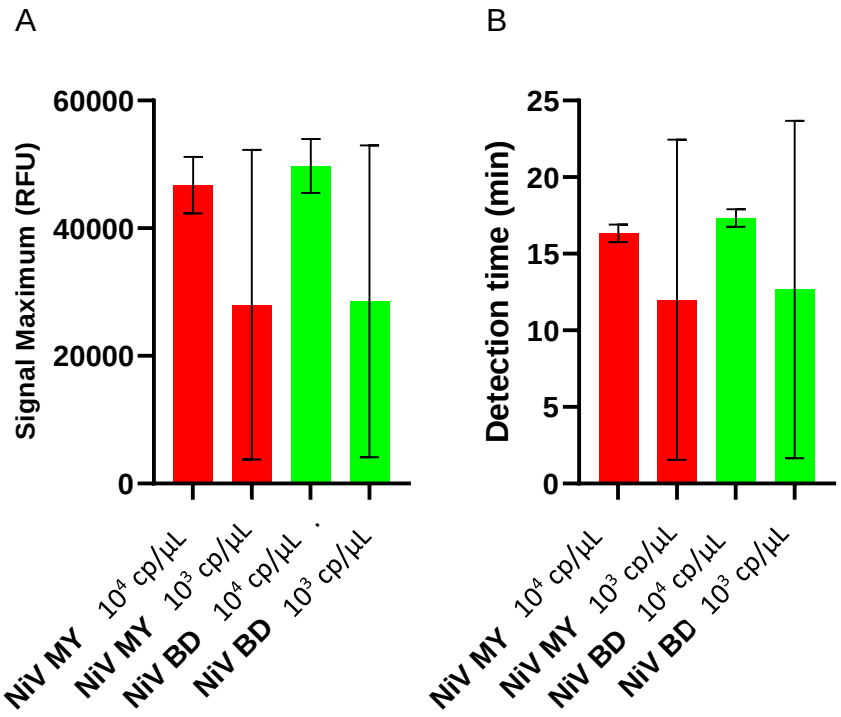


Figure 39. A) Signal maximum of the Nipah virus N gene RT-LAMP Cas12b assay when testing the Malaysia and Bangladesh genotypes at 10^4 and 10^3 cp/µL, respectively. B) Detection times of the Nipah virus N gene RT-LAMP Cas12b assay when testing the Malaysia and Bangladesh genotypes at 10^4 and 10^3 cp/µL, respectively**.** The results with error bars are means of at least three technical replicates (n=3) and the error bars represent the range.

3.3.3.2. Cross-Reactivity to Homologous and Pathologically Similar Agents

The NiV N gene RT-LAMP Cas12b assay was tested for cross-reactivity to select etiologically similar or current global pandemic agents, including SARS-CoV-2, Influenza A virus subtype H5N1, and the nearest non-Nipah henipavirus, Hendra virus. Newcastle Disease virus was also included in the cross-reactivity testing to verify if the assay would cross-react outside of the Henipavirus genus but within the *Paramyxoviridae* family. Futher testing of common neurotropic viruses including but not limited to Japanese Encephalitis virus, Rabies virus, Venezuelan equine encephalitis virus, polioviruses, coxsackieviruses and more would cover a larger panel of potential cross-reacting pathogens that cause pathophysiologically similar illnesses. However, these pathogens were not available for testing at the NCFAD. NiV-B RNA was included as a positive control confirming Nipah virus detection with RT-LAMP Cas12b and a no-template control (water) was added to monitor for false positivity. All RNA was extracted from cell-culture infected samples of high viral titer. Extraction eluents were not diluted, therefore each RNA sample used in this test was at an elevated quantity of nucleic acid.

No foreign nucleic acids were detected, although beyond 45 minutes, low signals beyond the baseline threshold were detected for Influenza A virus H5N1 (Fig.40). As anticipated, the positive control was rapidly detected, and the no template control was not detected. These results conclude that the NiV N gene RT-LAMP Cas12b is non-reactive to current pandemic agents, the most homologous non-nipah henipavirus, and with another member of the *Paramyxoviridae* family. Biological replicates of this assay performed on individual days were not necessary; three technical replicates for each pathogen were performed.

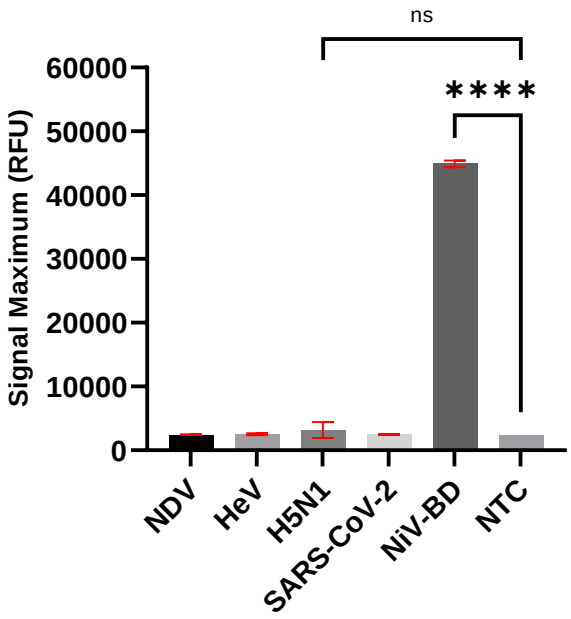


Figure 40. Signal maxima of the Nipah virus N gene RT-LAMP Cas12b assay cross-reactivity testing against Newcastle Disease virus, Hendra virus, Influenza A virus H5N1, SARS-CoV-2 and Nipah virus genotype Bangladesh. The results with error bars are means of three technical replicates (n=3) and the error bars represent the standard deviations.

3.3.3.3. Nipah virus Genome Limit of Detection

The definition of the limit of detection remained the same as described in 3.2.2.3.. The validation of the limit of detection for NiV RT-LAMP Cas12b assay remains in progress. Data collected throughout the optimization and validation of the assay suggests that the LOD is at least at the 10^3 order of magnitudes genome copies per microliter.

3.3.3.4. Limit of Detection Reproducibility

To validate the tentative LOD of the NiV RT-LAMP Cas12b assay, ten technical replicates of NiV MY RNA diluted to $5x10^3$ cp/µL and 10 technical NTC replicates were tested following the optimized conditions. To remain consistent with the methods in the SARS-CoV-2 validation, the diluted NiV RNA was also extracted and purified using the QIAamp Viral RNA Mini Kit (as per 2.8.1.) and quantified following the protocol in 2.9.. Nuclease-free water was added as no template control. As per figure 41, all ten NiV-positive samples were effectively detected with statistical significance in contrast to no detection, and subsequently no false positivity within the ten NTC replicates.

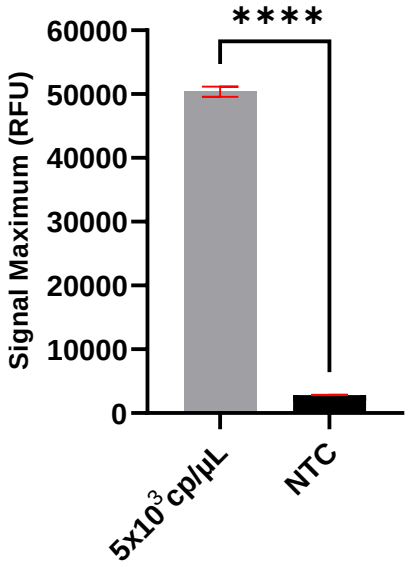


Figure 41. Signal maxima of 10 Nipah virus RNA controls at $5x10^3$ cp/µL and 10 no template controls used to validate the reproducibility of the limit of detection of the Nipah virus N gene RT-LAMP Cas12b assay. The results with error bars consist of ten replicates (n=10) and the error bars represent the standard deviations.

3.4. Rapid RNA Extraction protocol

Ceres magnetic NanoTrap Technology was first extensively used at the Canadian Science Center for Human and Animal Health with the emergence of the SARS-CoV-2 pandemic. The beads were primarily used within the Wastewater Monitoring Program for COVID-19 (Public Health Agency of Canada) to concentrate and enrich large volume (liters)-low viral titer wastewater samples so they could be sequenced and surveilled. The decision to use these beads for rapid sample enrichment was founded on the successful implementation within the PHAC, and the idea to extract nucleic acids directly from the beads came from historically successful protocols internal to Ceres Nanosciences Incorporated (Protocol No. I057). The main difference between this extraction protocol, the STOPCovid.v2 extraction protocol and Protocol No. I057 is that in this extraction, the beads bind to viral particles directly through affinity binding and the extraction is directly performed on the beads using enzymatic lysis, whereas the STOPCovid.v2 protocol uses nucleic acid-binding beads after chemical lysis. The original direct capture, enrichment and extraction method as developed by Ceres Nanosciences included washing the bead-bound virus from the sample matrix with a detergent-based wash followed by a heat-lysis extraction. In this novel protocol, a simple commercially available non-detergent based wash was used to wash the bead-bound virus from the sample matrix without accidentally eluting the viral particles from the beads (commonly eluted by detergents). Protocol I057 used heat-lysis-based extraction which is not conducive to point-of-care applications due to the need of high-temperature thermal capacities, Instead, this assay uses a thermolabile enzyme functional between 20°C and 40°C and a detergent-based extraction/elution buffer to permeate the viral envelope and to degrade the viral protein capsid. It is to note that not all of the extraction protocol optimization steps were performed in biological triplicate on three separate days. This limitation is due to the lack of feasibility in regard

to time and materials, performing manual extractions within a containment level 3+ laboratory, and having to perform RT-LAMP Cas12b fluorometric detection on a device only capable of measuring fluorescence in twelve reactions at once.

3.4.1. Optimization Guided for SARS-CoV-2 RNA Extractions

3.4.1.1. Identifying the Optimal Proteinase K Enzyme for RNA Extraction Using a SARS-CoV-2 Recombinase Polymerase Amplification Assay Coupled with Cas13a

A very simple early trial was performed using the STOPCovid format of the RT-LAMP Cas12b assay to identify the optimal protease capable of being used for viral extraction. Three enzymes were screened from literature as potential candidates to be used in the extraction protocol, although the protocol described in 3.4. had not yet been established: Qiagen Protease (Cat. No.: 19157), New England Biolabs Proteinase K (Cat. No. 10012S) and New England Biolabs Thermolabile Proteinase K (Cat. No.: P8111S). The preliminary trial followed a simple extraction protocol: spiking a saliva sample with a predetermined high concentration of ultracentrifuged SARS-CoV-2, titrating the proteases from 0.5 µL to 5 µL and titrating the Qiagen protease buffer from 25 µL to 29.5 µL for a total extraction volume of 50 µL. Once the extraction was set up, the enzymes were activated at their respective optimal temperatures for 15 to 20 minutes varying on manufacturer recommendations. The enzymes were subsequently inactivated at their respective heat inactivation temperatures for 10 to 15 minutes varying on manufacturer recommendations. Theoretically at this point in the extraction, nucleic acids should be released from the viral particle due to envelope and capsid degradation. Five microliters of post-extraction mix was added to the SARS-CoV-2 RT-LAMP Cas12b assay and run for five hours at 60°C on an ESEQuant TS2.4 and analyzed.

The Qiagen protease effectively released SARS-CoV-2 nucleic acids and this was demonstrated by Cas12b detection when using 0.5 µL and 1.5 µL of enzyme whereas 5 µL demonstrated to be too concentrated. The NEB proteinase k did not demonstrate a similar trend; all replicates went undetected, The NEB thermolabile proteinase K (TLPK) showed effective RNA detection only when using 5 µL of enzyme. The Qiagen protease extraction produced detectible quantities of RNA at a signal maximum just below 800 mV after approximately one hour of run time whereas the TLPK produced detectable quantities after only approximately thirty minutes, with nearly 1.5X the signal maximum obtained via the qiagen protease extraction. Though a positive control was not detected due to an error in RNA dilutions generating an over-dilute template, post-assay data collected from optimization and subsequent assay performance increases confidence in the collected data. With these results, the thermolabile proteinase K was explored in depth. As the dataset testing various proteases is not complete, the results are suggestive and not complete, therefore the figures to this data were not included in this thesis.

3.4.1.2. Thermolabile Proteinase K Titration and Incubation Period

Following the discovery of the direct enrichment-extraction protocol established by Ceres Nanosciences Inc., the core protocol described in 2.8.3. was established with key logical modifications to directly extract samples using an isothermal approach. The primary modification is from using a heat-lysis-based extraction to an enzymatic extraction using a thermolabile proteinase K from New England Biolabs, lysing virus directly from beads without elution.

The commercially available thermolabile proteinase K was titrated from 7 µL to 0.5 µL to identify the optimal enzyme concentration for degradation of the viral envelope and capsid post-magnetic NanoTrap enrichment. New England Biolabs defines 1 µL to be equivalent to 0.12 units of thermolabile proteinase K. With the eluent fixed at a volume of 50 µL, and with the addition of

5 µL of 10X proteinase K inhibitor (PKI), the volumes of extraction buffer/eluent varied from 38 µL to 44.5 µL. The sample incubation period was fixed at 10 minutes to ensure full enzymatic degradation. The enzyme's functional volume ranged from 0.5 µL to 7 µL without significant changes in detection time (Fig.42B). Conversely, the signal maximum demonstrated a stable trend when increasing TLPK when starting from 0.5 µL (Fig.42A). Logically the decrease in the standard deviation error bar trend in signal maximum may in part be explained by the decrease in extraction buffer volume when increasing the protease volume (to maintain a 50 µL extraction volume), which consequently means decreased available reagents enhancing enzymatic activity. Therefore, a reduced signal maximum would occur due to less efficient cleavage-mediated detection by Cas12b. It is to note, however, that the ESEQuant TS2.x systems are prone to stochastic signal detection. Identical replicates may have signal maxima that differ by several hundred millivolts.

When using 1 µL and 1.5 µL of TLPK, the nearest increase and decreased enzyme volumes only slightly vary in signal maxima. Using 1.5 µL of TLPK allows for more permissible enzyme available for virus lysis without affecting detection parameters. With the combined allowance for variability in results and enzyme available for extraction, 1.5 µL of TLPK is the ideal volume of enzyme to be added to the 50 µL total volume enrichment-extraction. The added volume of 1.5 µL of TLPK builds potential buffer room for even more virus-concentrated samples.

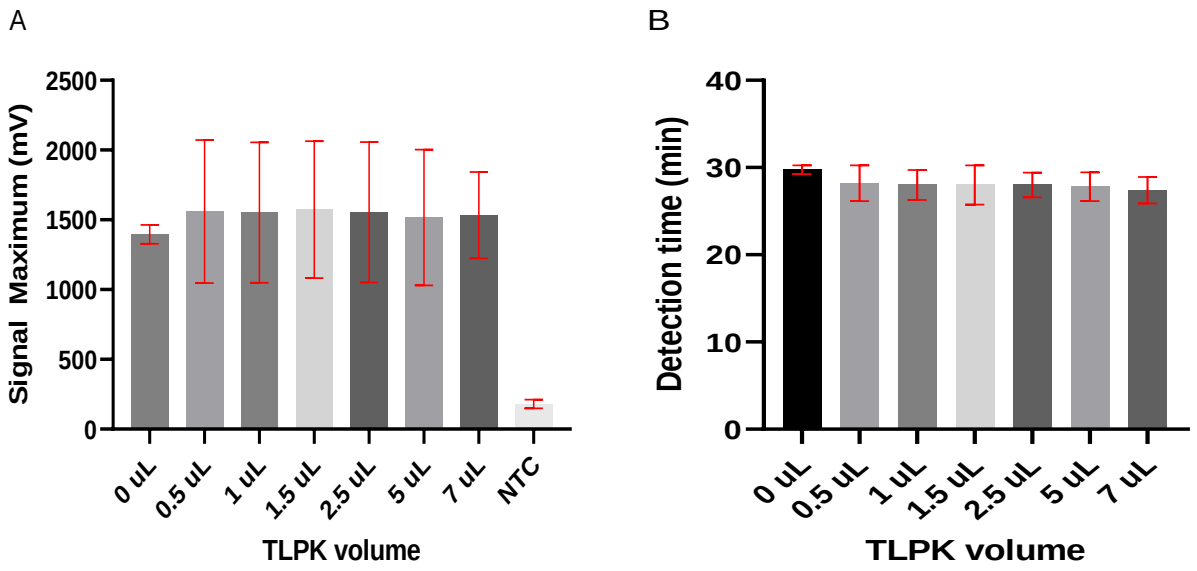


Figure 42. A) Signal maxima generated by the SARS-CoV-2 N gene RT-LAMP Cas12b assay using a titrated range, from 0 µL (0 Units) to 7 µL (0.84 Units, as defined by the manufacturer) of thermolabile proteinase K in the SARS-CoV-2 rapid enrichment-extraction. B) Detection times generated by the SARS-CoV-2 N gene RT-LAMP Cas12b assay using a titrated range, from 0 µL to 7 µL of thermolabile proteinase K in the SARS-CoV-2 rapid enrichment-extraction. The results with error bars consist of the mean of three independent experiments, each with three technical replicates (n=3) and the error bars represent the standard deviations.

As a follow-up test, the enzyme-sample incubation period was incrementally adjusted from 10 minutes, 7.5 minutes, 5 minutes and 2.5 minutes to identify how long it was needed for effective viral degradation followed by Cas12b-mediated detection using 1.5 µL of TLPK. Each incubation period was detected at the same cycle timepoint, with elevated signal maxima (Fig.43), indicating that only a short 2.5 minute incubation period is necessary for sufficient enzymatic lysis. Therefore, the incubation data presented is suggestive that a duration of 2.5 minutes is sufficient for SARS-CoV-2 extractions. Biological replicates are needed to further validate these results.

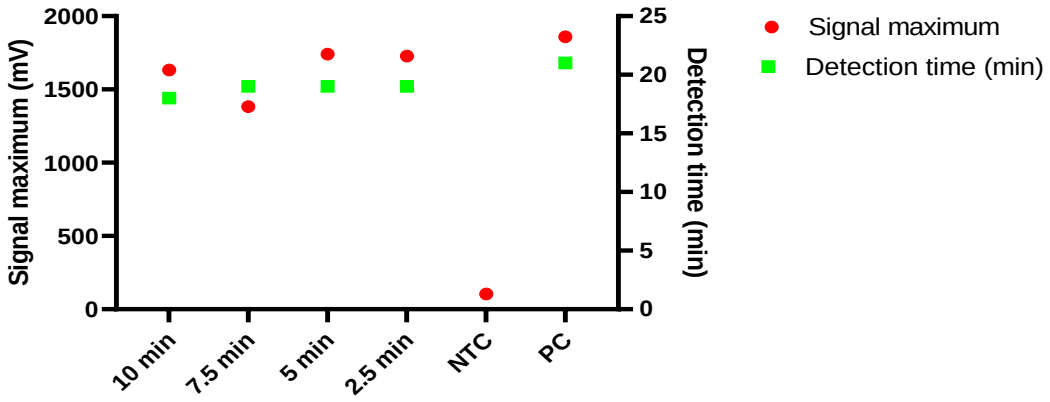


Figure 43. Signal maximum and detection time of the SARS-CoV-2 N gene RT-LAMP Cas12b assay upon using RNA product extracted from four identical spiked samples extracted with 1.5 µL of TLKP at four different incubation periods, 10 minutes, 7.5 minutes, 5 minutes and 2.5 minutes.

3.4.1.3. Proteinase K Inhibitor Titration

The proteinase K inhibitor (PKI) was integrated based on the fact that if the objective of the RT-LAMP Cas12b assay were to be used at the point-of-care, an added step of thermal inactivation would require more complex instrumentation whereas a proteinase K inhibitor can be applied at room temperature. A 10X PKI solution described in appendix 5.6. was also added to the enrichment extraction protocol following the 2.5-minute TLPK incubation. This step was to ensure that after viral lysis, there was no active TLPK in the template transfered to the RT-LAMP Cas12b reaction. Moreover, the addition of the proteinase K inhibitor removes the need to heat-inactivate the enzyme prior to the template addition. The 10X PKI solution was titrated within the 50 µL elution at eight final concentrations using 1.4X, 1.2X, 1X, 0.8X, 0.6X, 0.4X 0.2X and 0X, then 1 µL of template was added to the SARS-CoV-2 N gene RT-LAMP Cas12b assay for detection. There were no significant trends in signal maxima or detection times when varying the PKI concentration, although a noticeable drop in signal maximum was observed when no proteinase K inhibitor was added to the elution (Fig.44). This can likely be attributed to Cas12b degradation by the TLPK, which reduces the amount of collateral cleavage within the reaction. Moving forward, a 1X concentration of PKI per extraction was chosen as it is the same concentration used within the STOPCovid protocol. To mitigate possible downstream protease contamination or accidentally not entirely inactivating TLPK in an extraction elution, the 1X concentration of proteinase K inhibitor solution added to the RT-LAMP Cas12b assay also remained.

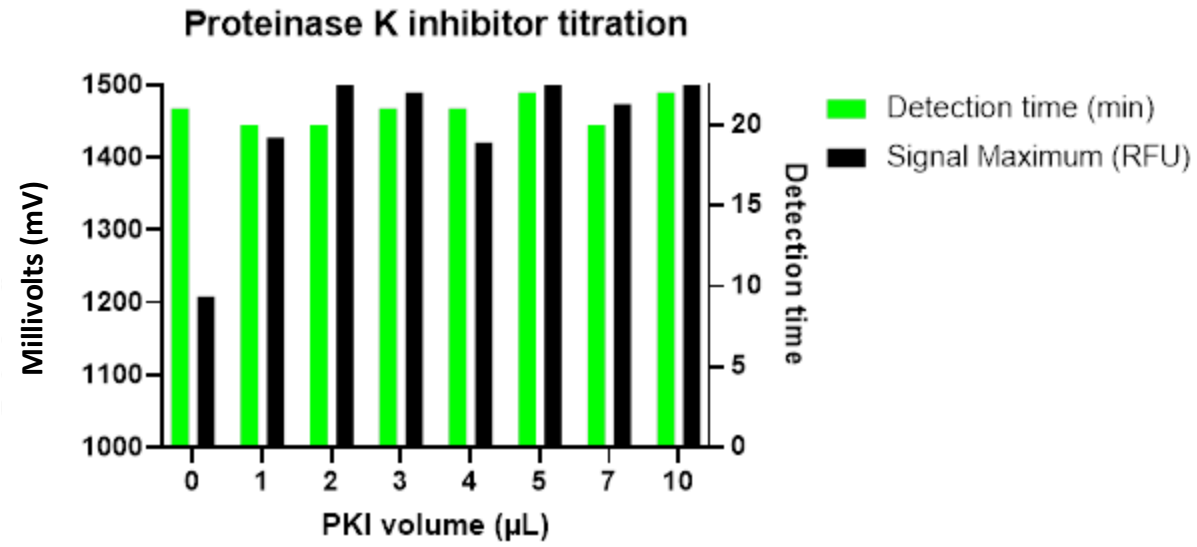


Figure 44. Detection times and signal maxima of a titration series of Proteinase K inhibitor added to the SARS-CoV-2 extractione-elution buffer prior to being added to the SARS-CoV-2 N gene RT-LAMP Cas12b assay.

3.4.1.4. Pre-incubation of Thermolabile Proteinase K with the Extraction/Elution buffer

According to collaborators at the National Research Council of Canada, a microfluidic chip system designed for rapid diagnostic purposes can only reliably flow 30 µL or more fluid within a microfluidic channel without causing issues with pressure and capillary flow. The initial design of this assay resuspended the virus-containing magnetic NanoTrap Particles in 43.5 µL of extraction buffer, followed by the addition of a small volume of 1.5 µL of TLPK, then proceeding with the 2.5 minute incubation period. To comply with microfluidic system requirements, the subsequent addition of the elution buffer and TLPK was compared to a pre-incubated system where a solution of 43.5 µL of extraction buffer was pre-mixed with 1.5 µL of TLPK 24 hours prior to use and frozen at -20°C to mimic storage conditions. The TLPK-buffer mix was then thawed at room temperature the following day and used following the in-house designed SARS-CoV-2 RNA extraction protocol. There were no significant differences in signal maxima and detection times obtained by samples extracted using the subsequent reagent addition and the samples extracted using the pre-incubated enzyme-extraction solution (Fig.45A-B). These results indicate that the storage of TLPK in extraction buffer as an injectable 45µL volume of enzyme-extraction solution would be suitable for a microfluidic system designed with the SARS-CoV-2 N gene RT-LAMP Cas12b assay.

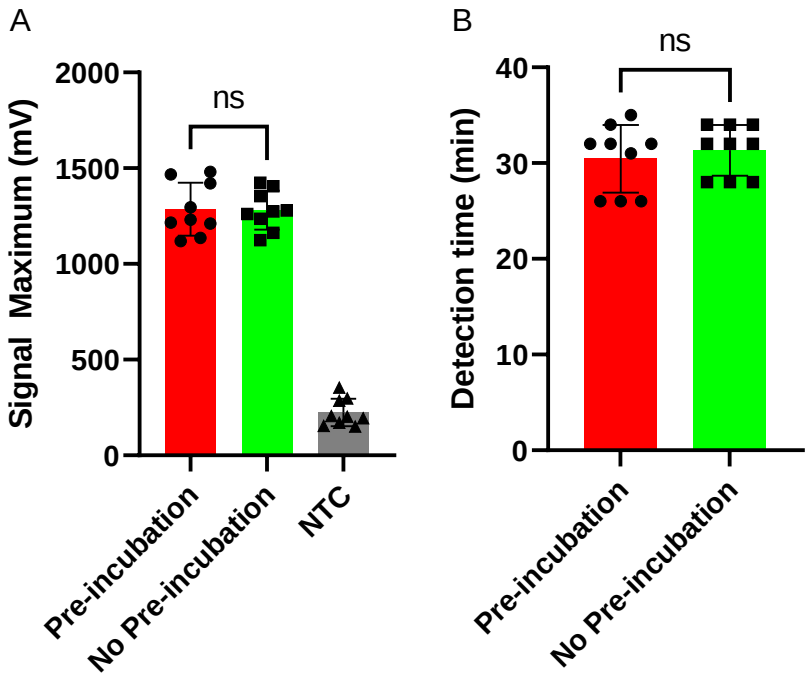


Figure 45. A) Signal maximum when pre-incubating the TLPK with the extraction/elution buffer prior to RNA extraction and performing SARS-CoV-2 N gene RT-LAMP Cas12b assay and, without pre-incubation. B) Detection time when pre-incubating the TLPK with the extraction/elution buffer prior to RNA extraction and performing SARS-CoV-2 N gene RT-LAMP Cas12b assay and, without pre-incubation. The results with error bars are means of three independent experiments with three technical replicates (n=3x3) and the error bars represent the standard deviations.

3.4.1.5. Magnetic NanoTrap Particle Titration

The magnetic NanoTrap particles and viral titers were checkerboard-titrated from the manufacturer suggested 100 µL down to 10 µL and from 500 PFU/sample to 10 PFU/sample to see if reduced NanoTrap quantities would still capture and concentrate enough virus, allowing for detection. This titration series was only performed once to provide insight for an ideal magnetic NanoTrap particle quantity range, then subsequent replicates were adjusted using a more narrow MNP and viral titer range

Titrating the MNPs from 100 µL to 10 µL and the viral titer from 500 PFU/sample to 10 PFU/sample yielded interesting results. A 10-fold reduction in quantity of magnetic NanoTrap particles from 100 µL to 10 µL produced similar detection times, and the 10 µL volume-point produced a statistically significantly more elevated signal maximum, indicating that 10 µL of MNPs may suffice in this extraction system (visual data not available as concording data was saved on a device that has been corrupted).

As a follow-up to the checkerboard titration two quantities of MNPs, 100 µL and 10 µL were compared and contrasted at 100 PFU/sample and 10 PFU/sample. In both bead volumes at 100 PFU/sample and 10 PFU/sample, there was no stastical difference in signal maxima (Fig. 46A-B). At 10 PFU, however, there was a slight statistically significant increase in detection time from using 100 µL to 10µL (Fig.46C-D). With 10 µL of magnetic NanoTrap particles being effective at detecting SARS-CoV-2 at low concentrations having negligible effects on detection time and no effect on signal maxima, the rapid extraction protocol proceeded to use the lower volume of MNPs.

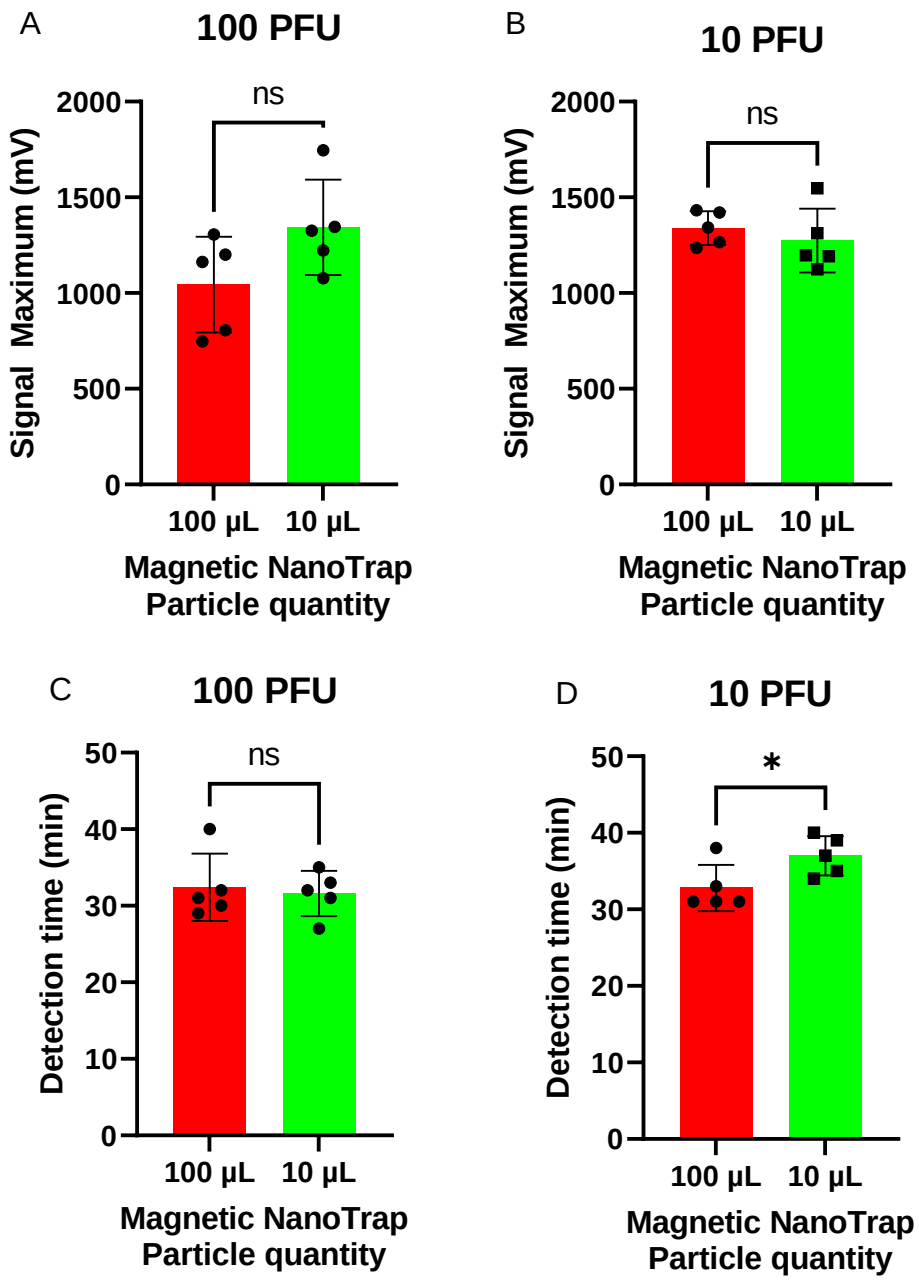


Figure 46. A) Signal maximum of the SARS-CoV-2 RT-LAMP Cas12b using identical SARS-CoV-2 samples spiked with 100 PFU and extracted with 100 µL of MNP or 10 µL of MNP. B) Signal maximum of the SARS-CoV-2 RT-LAMP Cas12b using identical SARS-CoV-2 samples spiked with 10 PFU and extracted with 100 µL of MNP or 10 µL of MNP. C) Detection time of the SARS-CoV-2 RT-LAMP Cas12b using identical SARS-CoV-2 samples spiked with 100 PFU and extracted with 100 µL of MNP or 10 µL of MNP. D) Detection time of the SARS-CoV-2 RT-LAMP Cas12b using identical SARS-CoV-2 samples spiked with 10 PFU and extracted with 100 µL of MNP or 10 µL of MNP. The results with error bars are means of five replicates (n=5) and the error bars represent the standard deviation.

3.4.2. Validation and Performance Characteristics Based on SARS-CoV-2 Extractions

3.4.2.1. Bead Binding Capacity to Mixed Virus Samples

As recent as November 2022, Ceres Nanosciences Inc. disclosed that the magnetic Nanotrap particles are not limited to binding enveloped viruses, as previously thought. In a meeting with Ceres Nanosciences Inc, chief Business Officer, Dr. Robbie Barbero disclosed that the beads are capable of binding a variety of non-enveloped viruses, bacteria and proteins. This may have implications in reducing binding capacity when a complex sample matrix is used for viral detection. To interpret the effects of a complex viral sample containing multiple viruses, a side-by-side comparison was made using a sample spiked with three enveloped viruses, SARS-CoV-2, MERS-CoV and Rift-Valley fever virus, and an identical sample spiked only with an identical quantity of SARS-CoV-2. A reduction in detection may indicate that coinfections would have the potential in reducing the efficacy of the SARS-CoV-2 enrichment-extraction.

A slight statistically insignificant reduction in detection time was noticed in the pooled sample in comparison to the detection time of the same quantity of SARS-CoV-2 alone (Fig.47A). The same trend was also noticed for the signal maximum and time to reach half of the maximum fluorescence, though with only little statistical significance (Fig.47B-C). These results suggest that coinfections may reduce assay sensitivity if the coinfected viral load is high enough and the SARS-CoV-2 viral load is low enough, though more in depth studies are needed.

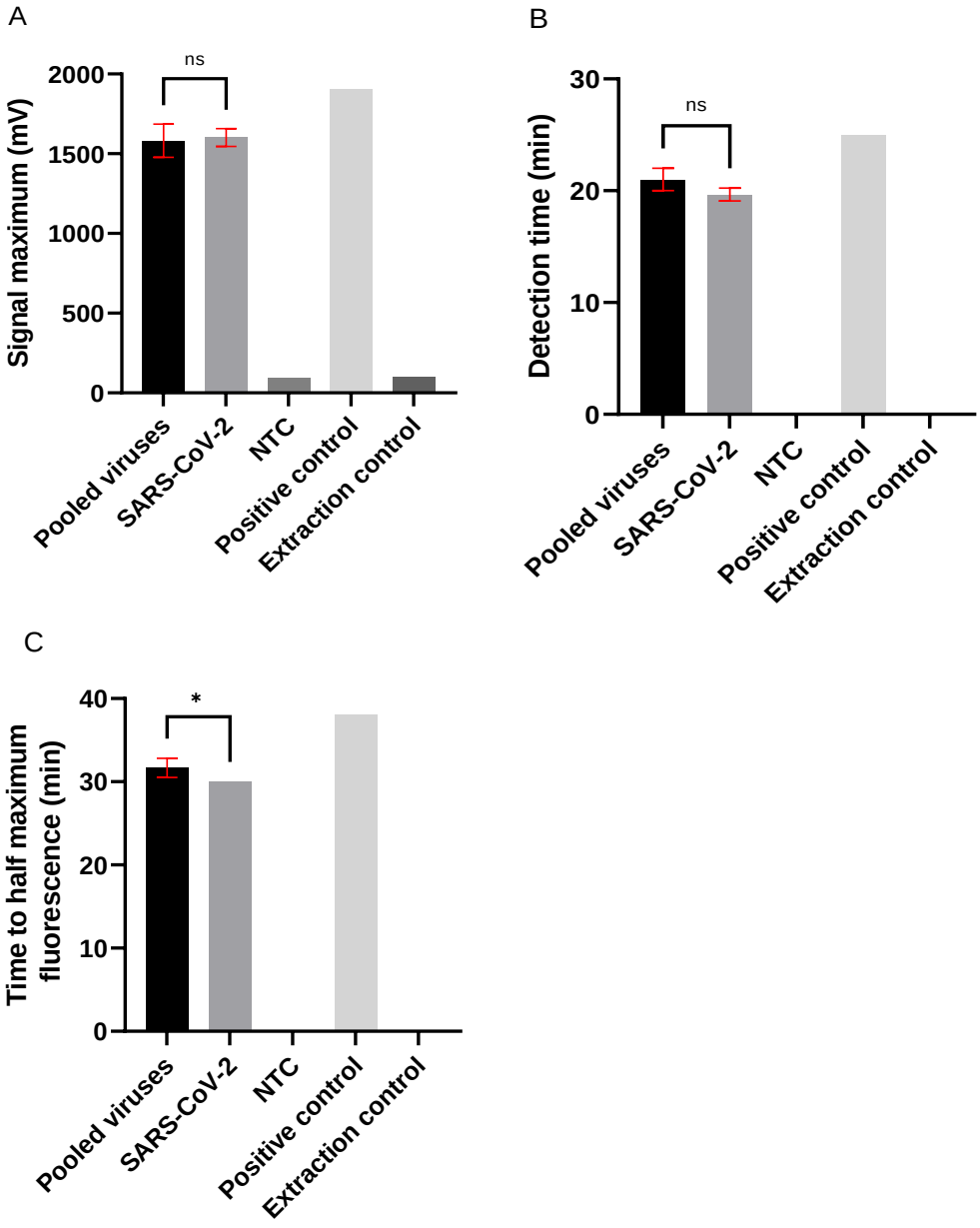


Figure 47. A) Comparison of signal maxima generated from extracting samples pooled with SARS-CoV-2, MERS-CoV and Rift-Valley fever virus to samples only containing SARS-CoV-2 at equal concentrations as the pooled samples. B) Comparison of detection times generated from extracting samples pooled with SARS-CoV-2, MERS-CoV and Rift-Valley fever virus to samples only containing SARS-CoV-2 at equal concentrations as the pooled samples. C) Times to reach half of the maximum fluorescence generated from extracting samples pooled with SARS-CoV-2, MERS-CoV and Rift-Valley fever virus to samples only containing SARS-CoV-2 at equal concentrations as the pooled samples. The results with error bars are means of at least three replicates (n=3) and the error bars represent the standard deviation.

3.4.3. Use of the Rapid RNA Extraction Protocol on Nipah viruses

3.4.3.1. Enrichment Extraction Limit of Detection Using Plaque Forming Units Per Sample

A brief trial of the in-house developed enrichment-extraction protocol optimized for SARS-CoV-2 detection was attempted for the detection of Nipah virus. The foreseeable optimization parameters for translating this protocol from one pathogen to another would lie within the enzyme used, the enzyme concentration and the enzyme incubation period. As mentioned in the introductory chapter, Ceres Nanosciences Inc. claims that the magnetic NanoTrap particles bind to enveloped viruses. Also mentioned in the same chapter, SARS-CoV-2 and Nipah virus are enveloped viruses, suggesting that the affinity-ligand adapted magnetic particle should be capable of binding both viruses. Testing the limit of detection of Nipah virus following the in-house designed enrichment-extraction protocol coupled with the NiV N gene RT-LAMP Cas12b assay will hint the functionality of this assay when changing the pathogen of interest. To ensure the highest likelihood of virus binding to the NanoTrap particles, NiV-Malaysia was titrated from $1x10^5$ PFU/sample down to an expected detection range between 6250 PFU/sample to approximately 78- PFU/sampled, based on the NiV N gene RT-LAMP Cas12b limit of detection.

Initial results demonstrated that Nipah virus was stochastically detected, and not effectively detected in replicate samples at $1x10^5$ PFU/sample, but detected in select lower concentration samples (data not included). After careful brainstorming, is is thought that these erroneous results may not be due to the reaction chemistry and function, but more to be made by within the physical mechanics of performing the RT-LAMP Cas12b in CL4. A possible source of error would be the difficulty of pipetting small volumes (< 2 µL) whilst wearing CL4 personal protective equipment, including multiple layers of thick gloves and a pressurized protective suit. Small volumes of viral inoculum were calculated for the dilutions of spiked volumes to preserve viral stock quantities.

Small volumes of sample eluent was also used for the template addition post-extraction, inducing the potential for physical error. Repeated experiments are in progress with updated dilutions less prone to error and increases in template volumes for the RT-LAMP Cas12b assay.

4. Discussion

4.1. Summary

The objective of this investigation was to explore the optimization potential of the STOPCovid RT-LAMP Cas12b to improve its performance characteristics further. This investigation also aimed at translating the functional SARS-CoV-2 assay to detect Nipah virus at the highest possible sensitivity and specificity. With collaborators' help, we also sought to produce a rapid and sensitive diagnostic assay capable of being used at the point of care, using and costing a minimum in resources.

It was determined that the original SARS-CoV-2 N gene RT-LAMP Cas12b assay developed by Joung and colleagues was thoroughly optimized and, in our hands, only slightly optimized further. Herein, we also provide supportive data validating the usability and feasibility of this assay at the point-of-care. The assay detecting SARS-CoV-2 can be directly modified to detect other pathogens of interest, including Nipah virus. The Nipah virus N gene RT-LAMP Cas12b assay can detect two NiV strains with high sensitivity in less than forty-five minutes. In addition to the RT-LAMP Cas12b assays, a rapid, inexpensive, and functional enzymatic-enrichment extraction protocol was capable of isolating SARS-CoV-2 and extracting nucleic acids directly from the magnetic NanoTrap particles. Unfortunately, the extraction protocol could not adequately isolate NiV RNA from spiked VTM samples, leaving room for improvement in future directions toward producing a rapid NiV RNA extraction. These findings demonstrate the ease and

utility of isothermal amplifying CRISPR-Cas-based molecular diagnostic assays and its potential for translatable detection of targeted pathogens.

4.2. Key Findings

4.2.1. Increased signal maxima in the STOPCovid.v2 is generated with the increase in $MgSO_4$ concentration, the addition of Dithiothreitol, and the substitution of Tween 20 with Brij-35 in the RT-LAMP buffer.

Conventional optimization includes the titration of various reagents and conditions used in an assay to identify parameters that improve in comparison to the original format. The STOPCovid assay consists of twelve different reagents; Most are diluted to specific concentrations before adding them to the reaction or are diluted in buffers comprising reagent mixtures. Therefore the permutations of reagent mixtures are above what is feasibly possible to attempt and complete to optimize. Optimizing the reaction's main components is the most effective approach to identifying and improving potential reaction-modulating reagents and enhancers. In this endeavour, testing was conducted in an attempt to mainly improve assay sensitivity. Specificity was not evaluated under each condition evaluated as it would not be feasible in the time-frame of this project. It is acknowledged that improvements in sensitivity may compromise specificity and this has been kept into consideration throughout the duration of the project.

Multiple cited publications refer to using RT-LAMP primers at 1.6 µM, 0.4 µM and 0.2 µM for the FIB and BIP, LF and LB, and the F3 and B3 primers, respectively, per reaction, therefore well establishing the optimal primer concentrations used for this amplification method. Moreover, amplification is initialized using F3 and B3 primers but is exponentially amplified by primarily using the loop and inner primers upon refolded amplicon formation. Furthermore, without the use of loop primers, the amplification still occurs, and when adding LF and LB primers,

the amplification yield is increased. With this reasoning, the use of highly concentrated inner primers, mid-concentrated loop primers, and lowly concentrated outer primers is validated, which is why this parameter was not studied.

The SARS-CoV-2 N gene RT-LAMP Cas12b optimization started with the titration of AapCas12b produced by two manufacturers, New England Biolabs and SignalChem LifeSciences Corporation. The starting conditions for CRISPR-Cas13a detection of SARS-CoV-2 consist of the protein and the sgRNA in equimolar concentrations, whereas the same rationale was also used for the RT-LAMP Cas12b assay[268]. Herein we titrated at equimolar AapCas12b and an N-gene-targeting sgRNA concentration to identify the optimal concentration providing the most elevated signal maximum with the lowest detection time. The reagents were titrated from 10 nM, capped at 75 nM to limit reagent cost for a point-of-care assay. As established within the STOPCovid protocol, 31.25 nM and 35 nM produced the most elevated signal maximum, although detecting SARS-CoV-2 RNA one minute later than the more elevated concentrations. To avoid potential issues with non-specific primer binding due to high concentrations of sgRNA and to reduce the assay cost, adding the ribonucleoprotein complex at the concentration established in STOPCovid is sufficient for robust detection of SARS-Cov-2 RNA. A candidate Cas12b protein manufactured by a Canadian corporation was proposed as a potential alternative to the enzyme provided by New England Biolabs to ease the difficulty of exporting the reagent from the United States of America to Canada. Removing Canada's dependence on international suppliers will help strengthen the supply chain for a "made in Canada" solution. The SignalChem protein was capable of detecting SARS-CoV-2 following the same kinetics as the New England Biolabs protein throughout enzyme titration, albeit generating a slightly reduced signal maximum and a delayed time to reach half of the maximum fluorescence.

As promising as are these results, NCFAD requested a custom order for AapCas12b from the manufacturer. SignalChem produced and purified the enzyme, although without having done so before with any Cas protein, leaving room for optimization of the expression and purification process. Since the purchase, SignalChem has developed an *in vitro* diagnostics products section focusing on the development of isothermal amplification and CRISPR-associated proteins, which is promising for Canadian collaboration to help produce locally made and assembled CRISPR-based diagnostic assays at the point of care.

Following the titration of Cas12b and the sgRNA, magnesium ions were titrated as $MgSO_4$, which disassociates into Mg^{2+} and SO_4^{2-} when dissolved in water. DNA synthesis is catalyzed by DNA Polymerase I, which relies on Mg^{2+} as an essential cofactor transitioning the enzyme from a closed to an open catalytic state[269]. These magnesium ions are also critical to RNA to cDNA translation by reverse transcriptase and for type V CRISPR-Cas systems, making it an essential parameter for optimization[230,270]. The initial $MgSO_4$ concentration used in the STOPCovid protocol was 8 mM. Here, it was found that the reaction performed well within a wide range of $MgSO_4$ concentrations and optimally between 8 mM and 9 mM. A slight but not statistically significant increase in signal maximum was observed when increasing the $MgSO_4$ concentration from 8 mM to 9 mM. With this observation noted, this protocol continued with the more elevated concentration to ensure the most potential in obtaining the most elevated signal maximum cumulatively.

Literature states that RT-LAMP amplification can generally be optimized between 55°C and 70°C and that Cas12b has an optimal trans cleavage within a wide range of temperatures. To validate the optimal assay temperature of 60°C established by Joung and colleagues, a temperature gradient from 56°C to 66°C was applied using a BioRad CFX96 thermal cycler to identical

replicates to observe the effects on RT-LAMP amplification and Cas12b detection. Differences in signal maxima were nearly minimal within the whole temperature range, indicating that there was CRISPR-mediated trans cleavage within a broad range of temperatures. However, detection times and time to reach half of the maximum fluorescence followed a decreasing trend from 56°C to 66°C. This inversely proportionate trend in temperature and time indicates that the optimal amplification temperature, where there is early rapid amplicon production detected by Cas12b, is optimal at warmer temperatures, with the lowest detection time ranging from 64.2°C to 65.6°C. The most elevated signal maximum was obtained at 62.4°C, with only minutes in detection time reduction compared to the 64.2°C measurements. As it is a delicate balance between improving detection time and signal maxima, the ideal temperature would be 62.4°C. However, at 60°C, there is room for uncertainty in signal maxima, with the next higher and lower signal maxima not significantly different and without substantially affecting the detection time. The assay temperature established in the STOPCovid protocol is justifiably an adequate performing temperature; therefore, this assay used 60°C as its thermal profile.

RT-LAMP relies on an amplification buffer that consists of Tris-HCl, $(NH_4)_2SO_4$, $MgSO_4$, Tween 20, and water. Tris-HCl is commonly used at low concentrations in amplification assays to maintain a stable pH in the microenvironment. The ammonium sulfate improves assay sensitivity and prevents false negatives in amplification, whereas magnesium ions act as essential cofactors for amplification and detergents are used to reduce secondary structures in nucleic acids[271,272]. In this study, ammonium sulfate concentrations were not titrated for each buffer but remains a consideration for future potential assay improvements. Considering the assay's overall Mg^{2+} content is modulated by the direct input of 100 mM $MgSO_4$ to a final concentration of 9 mM (buffer magnesium content is negligible in comparison to directly inputted $MgSO_4$), the

optimization factor in the buffer may rely on the detergent used. Herein, several conditions were explored to identify the ideal buffer combination. Three non-ionic detergents, Tween 20, Brij-35, and Triton X-100, were titrated from 0.5% to 0.2% while fixing the concentrations of the other reagents to identify detergent creating the most optimal amplification microenvironment. Two published buffers were also selected as potential candidates that may improve the RT-LAMP Cas12b assay. The buffer made by Abbasi *et al.* differs from the STOPCovid buffer with the incorporation of potassium chloride and slight modifications in reagent concentrations[273]. The use of potassium chloride may neutralize standing negative repulsive charges in nucleic acid backbones, which would affect primer annealing to its target-binding region[274]. In combination with ammonium sulfate, the aqueous NH_4^+ destabilizes hydrogen bonds in mismatched annealed primers, improving primer specificity. Uniquely, the Abbasi buffer also uses Tween 20 at 1%, which according to the literature, seems high and may be a mistake where the authors meant 1% at 10X concentration or 0.1% at 1X concentration. The buffer made by Ali *et al.* differs from the STOPCovid buffer only by the incorporation of 50 mM KCl per reaction. Several easily accessible commercial buffers commonly used for polymerase chain reaction-based amplification that are sent with commercially available enzymes were tested for effectiveness in an RT-LAMP Cas12b setting. Of the detergent titrations from 0.5% to 0.2%, Brij-35 produced significantly higher signal maxima across all concentrations than the 0.1% Tween 20 used in STOPCovid. These results are suggestive that Brij-35 improves the environment in which amplification occurs, likely by stabilizing enzymes interactions and reducing secondary structures in RNA and cDNA, allowing for more efficient amplification. These results were not performed in thrice on three separate days due to the cost in reagent usage, leaving room for further data validation. However, due to the

statistical increase in signal maximum in comparison to the conditions followed in the STOPCovid protocol, it was deemed that Brij-35 likely foundationally improves assay performance.

Both published buffers had detectable SARS-CoV-2 detection signals but without improvement in all parameters compared to using the STOPCovid buffer. As expected, the Abbasi buffer produced significantly reduced signal maxima, with significantly decreased detection times and times to reach half of the maximum fluorescence. As hypothesized, this may be due to an accidental typographical error in the manuscript describing the detergent concentration at 10X concentration rather than at 1X; no attempts were made to contact manuscript technical services to verify this. Three of the four commercial buffers also produced detectable SARS-CoV-2 detection signals without improvement compared to using the STOPCovid buffer. Literature suggests that CRISPR-based nucleic acid detection may be enhanced when using New England Biolabs' CutSmart Buffer, a buffer commonly used for enzymatic digestions[261]. In this assay, CutSmart buffer appears to prevent Cas12b-mediated detection completely. The complete reduction in amplification or inhibited detection was not investigated further. Considering each buffer modification, going from Tween 20 to Brij-35 at 0.2% to 0.5% improves signal obtention in this SARS-CoV-2 RT-LAMP Cas12b assay; therefore, the assay was continued at 0.2% Brij-35.

Four commercial DNA polymerases with high strand displacement activity and lacking 5' to 3' exonuclease activity were then respectively titrated, fixing all other RT-LAMP Cas12b reagent concentrations with the hopes of identifying an enzyme that would amplify more rapidly and yield more amplicon. A more rapid amplification would be detectable with improvements in detection time, and an increased amplicon yield would be detected with enhancements to the signal maximum. The Lucigen Bst DNA polymerase improved all parameters but also increased no

template control background to an unmanageable background signal. As for the other two enzymes, signal maxima were enhanced, but detection times were not. It is hypothesized that the reduced signal maximum of the WarmStart enzyme compared to that of the other enzymes may be due to the partial inhibitory effect of the reversibly-bound aptamer that increases the enzyme's thermal stability. The hypothesis is founded around the idea that the aptamer inhibits preemptive amplification because it remains bound to the enzyme until the complex reaches a 45°C dissociation temperature, as stated by the manufacturer. Regardless, the thermal stability of this enzyme and its functional parameters promote it as the ideal enzyme to be used at the point of care. The titration of a control enzyme commonly used in PCR, Taq Polymerase (SignalChem Lifesciences Corporation, Cat. No.: TQ02-E311), was included confirming that an enzyme with 5' to 3' exonuclease activity and no strand displacement activity is not capable of amplifying nucleic acids using loop-mediated isothermal amplification. Future studies could involve quantitative analysis of nucleic acid yields obtained by each enzyme, however in the context of such a rapidly evolving test, direct inpretation of RT-LAMP Cas12b detection was sufficient.

Including the reverse-transcriptase used in the original STOPCovid protocol, four reverse-transcriptases with optimal functional transcription near 60°C were titrated to identify an optimal enzyme compatible with the RT-LAMP Cas12b system. The only criterion required for a reverse-transcriptase to be used for RT-LAMP Cas12b is to have an optimal reverse transcription activity between 50°C and 70°C, ideally close to 60°C, to be compatible with RT-LAMP and Cas12b. All enzymes were titrated as per manufacturer-suggested concentration ranges. Expectedly, none of the reverse transcriptases produced significantly higher signal maxima as the enzyme function is only to convert RNA to cDNA. Therefore, it was expected that there would be a direct effect on detection time due to the variances in reverse transcription rate. The lowest mean detection time

across all enzyme concentrations was obtained using the New England Biolabs WarmStart RTx reverse transcriptase. Maxima H Minus reverse transcriptase produced the next lowest mean detection time. This increase in detection time can likely be attributed to the enzyme's optimal temperature for reverse transcription being 50°C but functional up to 60°C. The same can be said about the SuperScript IV reverse transcriptase.

Interestingly, the thermostable RapiDxFire reverse transcriptase, active between 37°C and 80°C, and optimal at the latter, did not aid in producing Cas12b-detectable amplicon. This lack of detection may be due to the need to expand the enzyme titration range as there is little literature using this enzyme; however, due to high costs for such a low quantity of enzyme, this line of investigation was not further studied. Globally, the DNA polymerase and the reverse transcriptase used in the STOPCovid assay produced the most optimal results compared to comparable commercial counterparts, at a reasonable cost, with the added benefit of being thermostable up to 45°C.

Several parameters were explored based on literature suggestions as potential enhancement strategies for isothermal nucleic acid amplification and CRISPR-based nucleic acid detection. Taking a thermodynamic approach to improve RT-LAMP amplification, adding poly-thymine linkers between the -1c and -2 regions of the inner primers supposedly affects the microenvironmental entropy in favor of efficient amplification. Interestingly, there was no significant effect on detection time but a slightly significant effect on the time to reach half of the maximum fluorescence and the signal maximum in favor of the non-linked primers. In this context, adding the poly-thymine linker may not be thermodynamically necessary or advantageous for the adequate amplification and refolding of nucleic acid amplicons. However, as literature demonstrates, these result do not absolutely confirm that a poly-thymine or poly-nucleotide linker

is disadvantageous to all RT-LAMP Cas12b assays. Building on the approach of primer functionality in isothermal amplification, historical LAMP assays were designed without loop-forward and loop-backward primers and only improved with the addition of these two supplementary primers. It turns out that RT-LAMP did not yield detectable quantities of cDNA when using four primers, highlighting the necessity of the loop primers in increased amplicon yields typical of this RT-LAMP Cas12b assay.

One parameter not directly mentioned in literature as a potential enhancement point to Cas-12b-mediated detection is the pre-incubation of the Cas12b protein with its native cofactor and single-guide RNA before being added to the RT-LAMP Cas12b master mix. The hypothesis driving this step as a potential enhancement strategy is based on increasing the probability of all Cas12b proteins forming optimal ribonucleoprotein complexes due to having a maximal amount of magnesium ion available for proper protein folding. This added step increased signal maxima by more than 27%, which is expected if more Cas12b-sgRNA complexes are present within a mixture ready for non-specific collateral cleavage upon target recognition. However, in the context of a point-of-care assay, pre-incubating a specific subset of reagents before adding them to a master mix increases the potential for mistakes, contamination, and the need for a technician to perform this extra step. In the context of point-of-care applications, a preincubated mixture of this sort is not feasible due to the added time it would take to pre-incubate before the remaining master mix preparation, therefore a pre-incubation step in the master mix preparation was not included for the remainder of the optimization of this assay.

With this in mind, producing a master mix containing the entire one-pot RT-LAMP Cas12b reagents that could be stored for extended periods would help reduce the intervention points listed above. In addition, this stored master mix may add to the optimal RNP complex formation due to

extended Cas12b exposure to essential components. Upon preparing a fresh lot of RT-LAMP Cas12b, one half was stored at -20°C for two weeks before moving forward with the SARS-CoV-2 N gene RT-LAMP Cas12b assay while the other half continued directly with the assay. To control the replicability of both reactions, RT-qPCR-confirmed SARS-CoV-2 RNA extracted and purified using the Qiagen QIAamp Viral RNA Kit was stored at -70°C before performing both assays. Storing the RNA before use controls the concentration and the number of freeze-thaw cycles the RNA would be submitted to, producing identical templates for both reactions. The results were highly similar when using a freshly prepared RT-LAMP Cas12b master mix and a two-week frozen master mix. Surprisingly, the signal maximum was not increased with the direct production of the RT-LAMP Cas12b master mix followed by freezing, which was the conceptualized idea when pre-incubating the $MgSO_4$, AapCas12b, and the N gene sgRNA.

Enhancement strategies in the nascent field of CRISPR-based diagnostics are minimal due to the naivety in understanding specific molecular interactions that can increase CRISPR-Cas non-specific collateral cleavage. Current findings suggested that bovine serum albumin and L-proline improve Cas12a and Cas13a trans cleavage, suggesting that it would similarly enhance Cas12b trans cleavage. BSA has been conventionally used as a thermal stabilizer for enzymatic digestions and has been explored in PCR amplification assays, and L-proline is known to decrease DNA melting temperature[275,276].

Contrary to the findings obtained by Li and colleagues in 2021, BSA appeared to improve signal maximum in the SARS-CoV-2 N gene RT-LAMP Cas12b, whereas L-proline did not. There were also no detected synergistic improvements with the combined addition of both reagents at their respectively titrated concentrations. Unfortunately, a replicate assay testing 10 µg/mL of BSA

showed no improvement over the control assay without BSA; therefore, neither BSA nor L-proline was added as a chemical enhancer to the SARS-CoV-2 RT-LAMP Cas12b assay.

Ubiquitously used as a redox agent capable of disrupting secondary structure formations in nucleic acids, dithiothreitol was titrated in the SARS-CoV-2 RT-LAMP Cas12b assay using elevated RNA concentrations with the hopes of observing improvements in assay metrics. This would be beneficial to the reaction due to DTT reducing potential secondary nucleic acid structures. The hypothesis behind why and how the addition of DTT could be beneficial stems from the in-house rapid nucleic acid extraction protocol; The extraction is quick and contains all nucleic acid present in the sample, including but not limited to the genomic RNA, copy-genomic RNA and subgenomic messenger RNA, which may covalently bind together to form secondary structuring which could interfere with normal polymerase amplification and CRISPR-based detection.

Another factor that may influence secondary structure formation is the extraction buffer/elution which consists of Tris-Cl (pH 8.0), KCl, $MgCl_2$, Tween-20 (pH 5-7) and Brij-35 (pH 5.0-8.0). These reagents likely reduce the microenvironmental pH below 8.0, whereas the optimal nucleic acid unfolding pH is generally alkaline above 8.0. The introduction of DTT into the pH 8.8 RT-LAMP Cas12b assay in combination with 60°C primer annealing, amplification and detection adds precaution, ensuring proper unfolding of nucleic acids, allowing for efficient RNA scanning by the active RNP complex.

Unfortunately, no statistical improvements were registered when adding up to 10 mM of DTT per 50 µL reaction. Although there were no noticeable improvements, DTT still serves a useful function of disrupting potential secondary structure formation in nucleic acids, especially if nucleic acid quantities are significantly elevated with the enrichment extraction protocol. Two

micromolars of DTT was chosen as the concentration added per reaction as it is the concentration that New England Biolabs have validated as non-detrimental to Cas12b storage.; along with Tris-HCl, NaCl, glycerol, and water, the Cas12b storage buffer contains 2 mM of DTT.

Integrated DNA Technologies offers 5' and 3' sgRNA chemical modifications termed ALT-R, which are used as preventative barriers to nuclease degradation. The modifications are proprietary; therefore, the specific chemical changes to the sgRNA are unknown. Considering how nucleases are ubiquitous and how the SARS-CoV-2 enhancement-extraction does not have preventative measures against ribonucleases, it is prudent to have safeguards against the potential degradation of an essential ribonucleic acid that may be subject to degradation. There must not be any adverse effects on assay metrics (i.e., detection time, signal maximum, and time to reach half of the maximum fluorescence) to evaluate if the ALT-R chemical modifications could be beneficial adequately. Interestingly, each metric was negatively affected by the incorporation of 5' and 3' ALT-R chemical modifications, therefore, was not subjected to further investigation due to likely reducing sensitivity and, potentially, the limit of detection. There is no directly identifiable explanation for why the modification reduced the assay performance within each metric. One could hypothesize that the 5'-end modification located on the direct-repeat region that directly binds to AapCas12b may effect Cas-mediated non-specific cleavage due to steric hindrance in the RuvC domain. Another hypothesis explaining this detriment in assay function may be founded by the effect of the 3'-end modification affecting sgRNA annealing to its' targeting region.

The last potential enhancement point in the SARS-CoV-2 RT-LAMP Cas12b was the incorporation of a helicase and ATP to the RT-LAMP Cas12b reaction in hopes of reducing secondary structure formation due to improperly hybridized primers and also to enhance amplification yield by unwinding tightly bound RT-LAMP amplicons that have seen subjected to

multiple amplification cycles. Some manuscripts stipulate that including a helicase to isothermal amplification reduces non-specific primer binding that can lead to non-specific amplicon generation[265]. Helicase functions by unwinding double-stranded DNA, which may be useful in both reducing steric hindrance of overwound LAMP amplicons having gone through multiple amplification cycles with the DNA polymerasae, and by unwinding non-specific primer binding. Conversely, this double-strand DNA unwinding activity may also be detrimental to RT-LAMP by unwinding dumbbell/hairpin structure formations necessary for exponential amplification when employing self-priming amplification. With the inclusion of degeneracies in the SARS-CoV-2 N gene RT-LAMP primers, the possibility of non-specific interactions and amplification is more likely.

Unfortunately, there was no enhancement to the detection time, signal maximum, or the time to reach half of the maximum fluorescence at the manufacturer-suggested concentrations of helicase and ATP. The hypothesized reasoning would be due to changes in pH due to ATP hydrolysis and the release of free hydrogen, acidifying the reaction and reducing Cas12b activity in acidic environments.

Ultimately, the assay designed and developed by researchers at the Broad Institute of MIT and Harvard developed a highly sensitive and robust molecular diagnostic assay. However, of all the parameters tested in this thesis, only a few could slightly improve assay metrics. The results demonstrate that more research is needed to identify improvement and enhancement methods used in CRISPR-Cas diagnostic systems. See appendix 5.4. for the updated table of reagents used and their respective concentrations, as optimized in this project.

4.2.2. The optimized SARS-CoV-2 RT-LAMP Cas12b assay can detect relevant virus variants without cross-reacting to homologous coronaviruses and pathophysiologically relevant pathogens.

Although the STOPCovid protocol designates that the assay does not cross-react against highly homologous SARS-CoV and MERS-CoV, many other relevant coronaviruses were not validated for cross-reactivity. Four more common human coronaviruses are globally dispersed and cause more disease cases than SARS-CoV and MERS-CoV; they are HCoV-OC43, HCoV-NL63 and HCoV-229E, and less commonly HCoV-HKU1[277]. To add to the list of globally relevant coronaviruses, many animal coronaviruses like Transmissible gastroenteritis virus (of porcine origin), Porcine epidemic diarrhea virus (of porcine origin), and Infectious bronchitis virus (of avian origin) may cause similar pathophysiology in their respective host species. Moreover, many human and animal respiratory pathogens that cause similar illness and may cross-react were not available at the NCFAD therefore not tested.

Moreover, in May 2020, Joung and colleagues, authors of the STOPCovid.v2 protocol, aligned the primers and the sgRNA-spacer targeting region to only approximately 30,000 SARS-CoV-2 sequences available on the GISAID database interpreting at least 99.5% conservation. In May 2020, there were only a handful of known SARS-CoV-2 genetic variants; none of which are predominantly circulating in September 2022 or available at the NCFAD (wet-lab conclusion period for this thesis). Therefore, the specificity of the STOPCovid assay or the capability of detecting early variants of concern circulating in the timeframe of this thesis was not possible.

Graciously performed and provided by Dr. Julie (Chih-yu) Chen at the National Microbiology Laboratory (Public Health Agency of Canada) in March 2022, an updated conservation analysis of the same primer and sgRNA-spacer targeting regions was completed using an updated 7,000,000 human SARS-CoV-2 genome sequences from the same GSAID

database. Two years since the STOPCovid protocol was publicly released, and with the evolution of hundreds of new SARS-CoV-2 variants and respective genome sequences, the primer set and sgRNA remain conserved above 99%. At the time of the updated sequence conservation analysis, the most relevant variants were Omicron and Delta (pre-BA.4-5 Omicron subvariants), citing the importance of validating the STOPCovid assay's ability to detect these two variants of concern.

Cross-reactivity testing was performed using highly concentrated and undiluted RNA elutions from various pathogens stored at the National Centre for Foreign Animal Diseases. Results indicate that the STOPCovid assay does not cross-react to detect human coronaviruses, selected animal coronaviruses, and pathogens causing similar pathophysiology. Furthermore, specificity to relevant SARS-CoV-2 variants confirmed that the assay is specific to the SARS-CoV-2 viruses, capable of detecting the pre-BA.4 and 5 Omicron, Delta, and Wuhan-1 variants.

The STOPCovid protocol claims a limit of detection of 250 genome copies per sample (or 83 copies per mL of VTM) using a lateral-flow format of the assay and a limit of detection of 100 genome copies per sample (or 33 copies per mL of VTM) using a fluorescent readout. The lateral flow approach follows the identical STOPCovid protocol other than using a biotinylated reporter DNA rather than a quenched reporter. The lateral flow strip binds to the cleaved fluorescein reporter using a gold-labeled fluorescein isothiocyanate antibody after Cas12b-mediated detection. Describing the limit in a format of genome copies per sample and per mL of VTM may appear convoluted, considering standard literature uses genome copy per reaction or copies per sample distinct volume sample (Ex.: 100 genome copies per 1 mL sample). In addition, these results are restrictive to an idealized setting due to using synthetic SARS-CoV-2 genomes and virus-like particles, as discussed Joung *et al*. In this optimized fluorescent-readout format of the STOPCovid assay, using full-length authentic SARS-CoV-2 genomes, a realistic limit of detection of 50

genome copies/µL was established at varying sensitivities and specificities depending on the total volume of RNA elution added to the assay. These values may be questioned and would likely require further investigation due to recurring SARS-CoV-2 genome contaminations in the NCFAD CL3 laboratory space around when clinical SARS-CoV-2 samples were being tested. Contamination was also observed in the diagnostic SARS-CoV-2 N gene-targeting RT-qPCR assay and was subsequently confirmed upon sequencing pooled no-template controls that appeared positive for the virus. One factor indicating that the clinical data obtained at the NCFAD may contain contaminations relies on the fact that the data obtained at the Broad Institute of MIT and Harvard and the University of Washington had the assay at a positive predictive value of 100% using human clinical samples. A counterargument to consider is how the clinical data presented here is from naturally deceased deer carcasses that may have blood and other coagulated analytes that may not usually be found in the sample type and that could interfere with extraction effectiveness, RT-LAMP function and CRISPR-based detection. Similar complications often arrive with PCR-based assays, supporting the idea that sample integrity likely had an affect on the results obtained here. Moreover, the integrity of the samples may be reduced based on the sample type, storage prior to arriving at the NCFAD and due to age.

4.2.3. SARS-CoV-2 N gene RT-LAMP Cas12b detects clinical mink and deer samples at reduced sensitivity and specificity than human clinical samples tested by Joung *et al*.

Optimizing the SARS-CoV-2 N gene RT-LAMP Cas12b assay provided insight into real limits of detection, sensitivities, and specificities using live virus and not synthetic or surrogate-viral particles. Furthermore, the analytical parameter data presented above, studying and validating the potential use of this assay within a One Health lens, bridges the gap between human and animal

health by combining the Broad Institute, National Centre for Foreign Animal Diseases and Public Health Agency of Canada data.

Combining data obtained at the Broad Institute of MIT and Harvard and the University of Washington, the STOPCovid protocol testing human clinical samples produces a sensitivity of 84.3%, a specificity of 100%, positive and negative predictive values of 100% and 68.7%, respectively. Drastic variations in sensitivity and specificity depending on species samples and RNA volume added to the RT-LAMP Cas12b assay were noted when performing the assay at the NCFAD using RT-qPCR confirmed positive and negative clinical deer and mink samples. Sensitivity, in our hands, ranged from 100% to 44%, a significant difference from the 84% obtained at both American institutions. The same considerable variation was observed with the specificity; both American institutions obtained 100% specificity, whereas a range from 100% down to 56% was obtained at the National Centre for Foreign Animal Diseases. A notable and logical observation from performing the diagnostic testing on animal samples was that the more dense and generally dirty the sample matrix, the less likely the RT-LAMP Cas12b would properly detect SARS-CoV-2 RNA. When testing “dirty”deer nasal swabs containaing nasal secretions, blood, nucleases, proteases and other potential amplification inhibitors found in carcass swabs, 3 or 5 of 9 samples were tested as false negatives depending on the template input quantity. When testing mink nasal swabs, which produce a clear, orange, or pink translucent sample matrix, there was only one false negative. False positives, however, if compared to the 100% positive predictive value obtained by Joung *et al.* (no false positives), may be attributed to RNA contaminations in the SARS-CoV-2 N gene RT-LAMP Cas12b assay. At the time of this data collection, the Special Pathogens Unit speculated the NCFAD had contaminants in various nucleic acid amplification assays, including the diagnostic standard RT-qPCR. After thoroughly cleaning the molecular

workstation with bleach and ethanol, replacing the pipettes and tips with new and unused materials, and having an alternative technician perform the diagnostic set-up, no-template controls were assayed to verify if a false positive would be detected (data not included). All three controls turned positive. The three controls were subsequently pooled and sent to the Genomics Unit at the NCFAD for sequencing. Results confirmed that there was amplification and detection of a SARS-CoV-2 N gene amplicon, confirming the suspicion of contamination. The Special Pathogens Unit increased cleaning procedures, including thorough use of nuclease sprays, after performing all molecular assays to combat this contamination issue. As another mitigation attempt, and due to the large permutations of possible reagents being contaminated, all new isothermal amplification and CRISPR reagents were purchased. All buffers and mixes were made in containment level 2, where SARS-CoV-2 genomic RNA should not be present for research purposes, before being brought into higher containment for RT-LAMP Cas12b master mix assembly.

Clinical human samples are currently being tested using the optimized SARS-CoV-2 N gene RT-LAMP Cas12b assay at NCFAD. Based on the positive predictive values from Broad Institute and the University of Washington, and the hypothesized sample cleanliness, it is anticipated that human clinical samples with have a more elevated positive predictive value than those obtained using deer and mink samples, therefore producing less false-positive results; This data remains to be collected.

4.2.4. The optimized SARS-CoV-2 N gene RT-LAMP Cas12b assay is directly translated to detect the Nipah virus N gene, generating a novel Nipah virus molecular diagnostic assay.

The requirements to translate the optimized SARS-CoV-2 N gene RT-LAMP Cas12b assay to detect Nipah virus was to design RT-LAMP primer sets and single-guide RNA oligonucleotides capable of detecting Nipah virus Malaysia, Bangladesh, and India. Primer sets were designed using

a free online software from New England Biolabs that allows custom primer design parameters based on user and assay specifications (e.g., total assay Mg^{2+} concentration). The single-guide RNAs were designed once the primer sets were set. The design parameters taken into consideration when designing the spacer region of the sgRNA was the location being within the -F1c and -B1c regions of the internal primers to optimize the sgRNA's ability to detect a non-hybridized LAMP amplicon formation, avoiding poly-adenine and poly-thymine tracts which increase the sgRNA rigidity and having a 20 to 23 nucleotide spacer-targeting region to prevent steric hindrance on the Cas12b protein. Four primer sets were designed to bind, amplify and detect the P, F, G, and M genes individually, and one set was selected from literature targeting the N gene. Most of the primers required degeneracies to accommodate binding and subsequent amplification to various NiV genotypes. The reaction chemistry used for the Nipah virus RT-LAMP Cas12b assay consisted of the optimized STOPCovid assay, with the only substitutions being the primers and the single-guide RNA.

Upon testing each primer and sgRNA set, most amplified NiV-MY RNA with varying amplitudes and detection times. These parameters mainly varied depending on the assay temperature. Three of the primer sets (M and G gene targets), including the published N gene primer set, were able to amplify NiV RNA. Amplification was confirmed using Nipah virus N, M, and G gene-targeting single-guide RNAs, identifying a novel nucleic acid detection method targeted towards Nipah virus. Of the three functional RT-LAMP Cas12b primer sets, the N gene targeting set produced statistically significantly more rapid detection times and signal maxima within a more extensive range of assay temperatures than the M and G gene-targeting counterparts. With these significant assay parameters, the N gene RT-LAMP primers designed by Ma and colleagues in conjunction with the newly designed N gene sgRNA were chosen as the primer-

sgRNA set to be used for the optimization of this assay moving forward. The N gene sgRNA and the Cas12b protein were then titrated at equimolar concentrations to identify the optimal quantity of individual reagents forming active ribonucleoprotein complexes used to detect NiV N gene amplicon. Due to the differences in the amplification curves when comparing the SARS-CoV-2 and NiV assays, changes in active ribonucleoprotein complexes available for detection could primarily affect the assay detection time and signal maximum. Therefore the objective of this titration was to find the concentration with the most significant signal maximum amplitude and the most rapid detection time. Although it was hypothesized that the Cas12b-sgRNA concentration would differ from the concentration used with the STOPCovid assay, the NiV RT-LAMP Cas12b assay could detect NiV-MY RNA from 20 nM up to 75 nM of equimolar reagents. The optimal detection times and signal maxima were similar to the STOPCovid assay, within 30 nM and 40 nM; therefore, the assay continued using 31.25 nM Cas12b. An approximate concentration of 30 nM of Cas12b and sgRNA appears to be a stable trend across various literature sources focused on Cas12b-based detection[30,278].

In the interest of time, select iterations of optimization assays performed for the SARS-CoV-2-targeting assay were also performed with the NiV-targeting assay. Optimization included the non-ionic detergents used in the reaction buffer when amplifying the NiV genome, titrating the buffer pH to identify the optimal Cas12b cleavage in the presence of NiV amplicon, and the titration of dithiothreitol to reduce NiV RNA secondary structures. Identical to the optimized STOPCovid protocol, the optimal non-ionic detergent for the NiV N gene RT-LAMP Cas12b assay is 1% Brij-35 without any modification to the remaining buffer chemistry. The optimal reaction pH and DTT concentration are identical to those used in the STOPCovid protocol. These results highlight that the optimized assay can likely be directly translated to detect various

pathogens with minimal optimization. The only parameters that would need modification for alternate pathogen detection would be the RT-LAMP primer designs, the spacer-targeting region sequence within the sgRNA, and potentially the AapCas12b-sgRNA concentrations. The assay can also be directly translated to detect various pathogens containing DNA genomes. One approach to optimizing LAMP consists of removing the reverse-transcription step, re-optimizing the $MgSO_4$ concentration needed for the DNA polymerase and the Cas12b protein, re-evaluate the DNA polymerase quantity required, and re-optimize the dNTP concentration needed for DNA polymerase-driven cDNA synthesis.

4.2.5. 2000-fold improvement in sensitivity from the colorimetric Nipah virus N gene RT-LAMP assay to a CRISPR-Cas12b assay.

The NiV N-gene RT-LAMP assay developed by Ma *et al.*in 2019 leverages colorimetric detection using a calcein indicator. Sensitivity testing established a limit of detection of approximately 100 pg of total NiV pseudovirus RNA. Considering that the average NiV genome length is approximately 18.2 kb, 100 pg of NiV pseudo viral RNA equals $9.7x10^6$ to $1.0x10^7$ genome copies.

When validating the performance of the NiV N gene RT-LAMP Cas12b assay, Nipah virus Malaysia RNA was extracted using the various extraction protocols described in 2.8.. Genome copies were then diluted in series from 250,000 genome copies per reaction (5000 cp/µL) down to 1953 genome copies per reaction (39 cp/µL) and tested in triplicate on three separate days. The detection of seventy-five percent of replicates was set as an arbitrary detection limit threshold for the NiV assay. Seven out of nine replicates, or 77.8%, were effectively detected when 5000 genome copies were added to the reaction. These results indicate a 1940-to-2000-fold increase in sensitivity compared to the colorimetric output using RT-LAMP without CRISPR-mediated

detection. According to Guillaume *et al.* 2004, the detection limit of the NiV N gene RT-qPCR, which is used as the NiV diagnostic standard in the Special Pathogens Unit (NCFAD), is of a sensitivity of 1 PFU[279]. To correlate NiV-MY plaque-forming units to genome copies, 1 PFU is equivalent to approximately 1000 genome copies[189]. With this logic, the NiV N gene RT-LAMP Cas12b assay should be capable of detecting five plaque-forming units of NiV-MY. The hypothesized PFU detection limit was tested using the rapid enrichment-extraction protocol developed and optimized for SARS-CoV-2. Nipah virus RNA was not detected at low PFU concentrations, whereas 1 mL samples spiked with 10^5 plaque-forming units were detected. These results indicate that the extraction protocol designed for SARS-CoV-2 requires re-evaluation and optimization for translation to Nipah virus. Logically, the optimization parameters mainly requiring optimization would be the protease, the protease concentration, the protease incubation period, and the concentration of detergents present in the extraction buffer to permeate and disrupt the viral envelope. It would be prudent to perform the SARS-CoV-2-optimized extraction and RT-qPCR on the eluent to confirm that the extraction functions on this particular pathogen. At the NCFAD, the lack of a thermal cycler in the BSL4 facility and how the extraction protocol has not been confirmed and safety-tested for removal of the eluent from higher to lower containment limits efficient assay development and validation. The functionality of the isothermal magnetic NanoTrap particle enrichment and enzymatic extraction protocol on Nipah viruses remains to be elucidated. It is noted that only while writing this thesis the author noticed that the Nipah virus N gene RT-LAMP FIB and BIP primers designed by Ma *et al*. both contain a poly-thymine linker sequence between the -1c and -2 regions. The utility and increased function of this modification also remain to be elucidated.

After testing the Nipah virus assay for cross-reactivity to highly homologous pathogens, including Hendra virus and Newcastle Disease virus or pathogens that cause similar disease manifestation, it was confirmed that the NiV-targeting assay could confidently identify the pathogen of interest. Moreover, RNA from Nipah virus Malaysia and a recombinant Nipah virus Bangladesh were tested using the NiV RT-LAMP Cas12b assay, detecting both accurately and timely. Ultimately it can be hypothesized that Nipah virus India would also be detected using the NiV RT-LAMP Cas12b assay. This idea is supported by the fact that the N gene amplicon region of Nipah virus Bangladesh and India strains are highly homologous (Fig.49), although this remains to be confirmed. NCFAD access to other meningoencephalitic or neurotropic pathogens were limited, however further testing of these pathogens should be performed to confirm that the assay does not cross-react to a large range of pathophysiolocially similar pathogens.

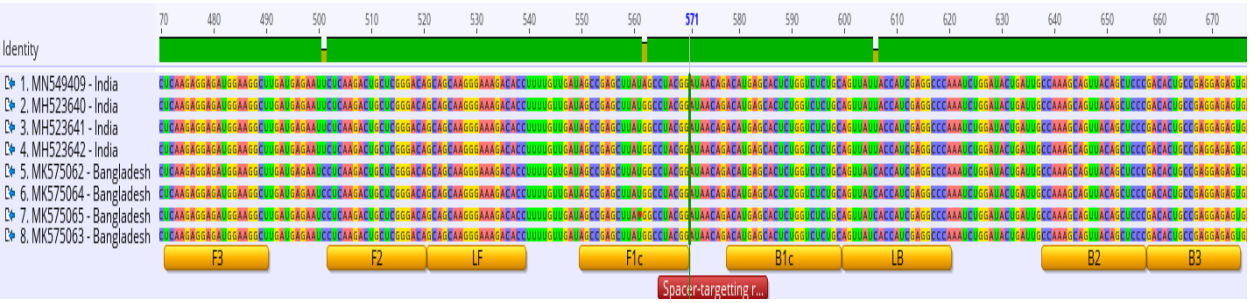


Figure 48. Genome alignment of select Nipah virus India and Bangladesh strain N gene sequences within the RT-LAMP N gene amplicon region demonstrating highly homologous intraspecies genome sequences.

4.2.6. SARS-CoV-2 RNA is easily extracted and enriched using inexpensive and accessible commercial reagents at room temperature.

Conventional RNA extraction methods include harsh chemicals and expensive reagents, often requiring sophisticated equipment that require a centralized and constant energy source. RNA used to validate the SARS-CoV-2 and Nipah virus assays were extracted using the QIAamp Viral RNA Mini Kit or the MagMax CORE Nucleic Acid Purification Kit, which cost $314 for 50

preparations and $784 for 100 preparations, respectively. These extraction protocols are time-consuming, taking over an hour to perform.

To this regard, a rapid extraction protocol using basic and inexpensive commercially available reagents was developed and optimized explicitly for SARS-CoV-2. Furthermore, the simplicity of the extraction protocol means that it may be compatible with extracting RNA from various pathogens. Therefore, the optimization of this protocol was guided toward SARS-CoV-2, but may also be modulated to extract nucleic acids from other pathogens of interest. The optimization comprised of identifying the optimal magnetic NanoTrap particle concentration to enrich SARS-CoV-2 virion, identifying the optimal protease (and concentration) for viral capsid degradation, incubation periods of the said enzyme, the ideal concentration of Proteinase K inhibitor to prevent post-extraction RT-LAMP Cas12b protein degradation, and more.

One plaque-forming unit is the limit of detection when combining the SARS-CoV-2-optimized enrichment-extraction protocol with the SARS-CoV-2 N gene RT-LAMP Cas12b assay. A wide range of equivalencies of SARS-CoV-2 genome copies to PFU ratios have been reported, from 10^3-10^6 genome copies:1 PFU. However, SARS-CoV-2 Wuhan-1, deemed more infectious per particle, has a ratio of 360:1. The enrichment-extraction limit of detection results is generally consistent with the SARS-CoV-2 RT-LAMP Cas12b assay limit of detection when using purified SARS-CoV-2 RNA.

To study the effects on SARS-CoV-2 detection, multi-coinfected samples containing various high-titered enveloped viruses (MERS-CoV and Rift Valley fever virus) and low-titered SARS-CoV-2 virus were tested using the SARS-CoV-2 assay. A slight decrease in signal maximum was observed when multiple viruses were present in the sample, but no change in detection time was reported. Therefore, due to the minimal effect on detection when testing high-

titered coinfected samples, minimal impact would be expected when detecting SARS-CoV-2. Moreover, the Magnetic NanoTrap particle virion retention/binding capacity is significantly more than all three pathogens' combined inputted viral load.

4.3. Conclusions and Future Directions

The primary finding in this investigation is that the SARS-CoV-2 N gene RT-LAMP Cas12b assay, termed STOPCovid (v1 and v2), may be improved through rigorous and specific optimization approaches. However, the assay presents a robust and sensitive amplification platform for molecular diagnosis of COVID-19. The novel finding elaborated in this thesis is that the optimized one-pot STOPCovid chemistry can be directly translated to detect another pathogen of interest, Nipah virus.

The optimization of the STOPCovid protocol used to detect SARS-CoV-2 has not been previously investigated, nor has the development of a Nipah virus-targeting RT-LAMP Cas12b nucleic acid detection assay. Various sources present isothermal nucleic acid amplification enhancement strategies, whereas CRISPR-Cas-mediated detection enhancement strategies are limited in literature[280]. Some RT-LAMP enhancement strategies rely on the reduction and destabilization of secondary structures in nucleic acids using helicases, L-proline, and dithiothreitol[281,282]. Other approaches rely on enzyme stabilizers to increase enzymatic activity, stability, production, and reproducibility with bovine serum albumin[283]. Literature sources cite L-proline and BSA as enhancement strategies to CRISPR-Cas trans cleavage and the original STOPCovid.v1 protocol describes having tested the Hamptons Research Solubility and Stability Screen to scan for chemical additives that improve the entire reaction, having found taurine as an enhancer[261,284].

The literature cites CRISPR-detection-based isothermal amplification assays capable of detecting the Ebola virus, Lassa virus, Zika virus, Dengue virus, SARS-CoV-2, Crimean Congo hemorrhagic fever virus, and more. However, of these high-consequence pathogens, nucleic acid detection methods for Nipah virus, a high-consequence pathogen with epidemic potential, have only been developed using a PCR-based, genome sequencing-based, and one RT-LAMP (colorimetric) based approach. This investigation demonstrated that the optimized STOPCovid protocol was successfully modulated to detect Nipah virus, presenting a fourth approach to NiV nucleic acid detection with a sensitivity similar to RT-qPCR and significantly more sensitive than the colorimetric NiV RT-LAMP assay. However, the assay designed to detect Nipah virus could benefit from future additional enhancement and optimization with the hopes of obtaining an assay with sensitivities similar to RT-qPCR.

This investigation lays the cornerstone to show that the assay developed by Joung and colleagues is well-suited as a modular platform that can be adapted to detect RNA-genome pathogens and, with modifications to the assay, DNA-genome pathogens. The research in this thesis opens the door to many other avenues for future isothermal amplification assay and CRISPR-based assay developments. Many conditions could be investigated to validate further and to optimize the current SARS-CoV-2 and Nipah virus N gene RT-LAMP Cas12b assays, namely repeated experiments to confirm that specific parameters are effective as they've been described above. Repeating the detergent titrations, for example, would validate further that Brij-35 would effectively be a more proper alternative detergent in the amplification buffer mix or testing various metal ions as cofactors to CRISPR-mediated detection in hopes of identifying the optimal ion additive. Investigations into reducing loop-mediated isothermal amplification operation temperatures from 60°C to 37°C using phosphorothioated primers show promise with the

integration of Cas12 or Cas14 proteins that are functional at lower temperatures[285]. This investigation would lead to decreased energetic requirements and could potentially be driven using body heat (i.e., holding the reaction tube in one's hand). As developed in the STOPCovid protocol, a lateral flow assay would be another potential avenue to develop the Nipah virus N gene further RT-LAMP Cas12b assay. Further explorations regarding the effect of complex sample matrices (e.g., blood, deceased animal swabs, bacterial contaminants, proteinaceous contaminants, etc.) would also aid in better understanding the functionality and applicability of Ceres Magnetic NanoTrap particles.

5. Appendices

5.1. RT-LAMP Cas12b Thermal Profile

Thermal Profile:
Isothermal
60°C/60 min
Cycles : 60x (1min*)
***Collection of Fluorescence; 1 cycle is equivalent to 1 minute**

5.2. Calculation examples

5.2.1. RNA Dilution Calculations

$$\frac{cp}{\mu L} = \left(\frac{(RNA\ concentration\ in\ ng/\mu L) * (N_A)}{(Average\ MW\ ssRNA) * (10^9)}\right.$$

$N_A = 6.022x10^{23}$

Average MW of ssRNA = (genome nt length * 320.5)

Average SARS-CoV-2 genome length used = 29782 nucleotides

Average NiV genome length used = 18253 nucleotides

5.3. Oligonucleotide sequences

5.3.1. CDC N2 RT-qPCR

Oligonucleotide Type	Name/Abbreviation	Sequence (5'->3')	Fluorophore/Quencher	Reference
Forward Primer	2019-NCOV_N2 FOR	TTACAAACATTGGCCGCAAA	N/A	Lu *et al.* 2020
Reverse Primer	2019-NCOV_N2 REV	GCGCGACATTCCGAAGAA	N/A	
Probe	2019-NCOV_N2 PR	ACAATTTGCCCCCAGCGCTTCAG	FAM/BHQ1	

Table 5. CDC N2 RT-qPCR primers and probe sequences used to validate the integrity and the quantity of nucleic acids obtained by extraction, as well as a confirmatory measure validating that the nucleic acids extracted were in fact from SARS-CoV-2.

5.3.2. Joung *et al.* SARS-CoV-2 RT-LAMP Cas12b oligonucleotides including the poly-thymine FIP and BIP and the ALT-R sgRNA

Table 6. Primer and single-guide RNA sequences used in the STOPCovid protocol, also used in the optimized STOPCovid protocol.

Oligonucleotide Type	Name / Abbreviation	Sequence (5'-->3')	Fluorophore/Quencher	Reference
Forward third primer	F3	GCTGCTGAGGCTTCTAAG	N/A	Joung *et al.* 2020
Reverse third primer	B3	GCGTCAATATGCTTATTCAGC		
Forward inner primer	FIP	**GCGGCCAATGTTTGTAATCAGT**AGACGTGGTCCAGAACAA*		
Backward inner primer	BIP	**TCAGCGTTCTTCGGAATGTCGC**TGTGTAGGTCAACCACG*		Designed in-house
Poly-thymine forward inner primer	FIP-T	GCGGCCAATGTTTGTAATCAGT**TTTTT**AGACGTGGTCCAGAACAA**		
Poly-thymine backward inner primer	BIP-T	TCAGCGTTCTTCGGAATGTCGC**TTTTT**TGTAGGTCAACCACG**		Joung *et al.* 2020
Loop forward primer	LF	CCTTGTCTGATTAGTTCCTGGT		
Loop backward primer	LB	TGGCATGGAAGTCACACC		
AapCas12b SARS-CoV-2 N gene single-guide RNA	N gene sgRNA	GUCUAGAGGACAGAAUUUUUCAACGGGU**GUGCC**AAUGGCCACUU UCCAGGUGGCAAAGCCCGUUGA**GCUUCUCAAAU**CUGAGAAGUGGC ACCGAAGAACGCUGAAGCGCUG***		
HEX-linked reporter DNA	Reporter DNA	TTTTT	HEX/IAbkFQ	Designed in-house
FAM-linked reporter DNA	Reporter DNA	TTTTT	FAM/IAbkFQ	

*The bold region highlights the -1c region of the primer and the normal font region highlights the -2 region of the primers.

**The bold region highlights the poly-thymine linker region between the -1c and -2 regions of the primers.

***The black highlight covers the tracrRNA; The bolded region covers a 16-nucleotide anti-repeat region which folds together to form a hairpin; The red highlight covers a 24 nucleotide repeat region from the tracrRNA; The green highlight covers a 20 nucleotide spacer-targetting region.

5.3.3. Ma *et al.* Nipah Virus RT-LAMP oligonucleotides and in-house designed NiV N gene sgRNA

Table 7. Nipah virus N gene RT-LAMP Cas12b primer and single-guide RNA sequences.

Oligonucleotide Type	Name/Abbreviation	Sequence (5'->3')	Reference
Forward outter primer	F3	TCARGAGGAGATGGAAGGCT	Ma *et al.* 2019
Backward outter primer	B3	ACTYTCCTCGGCAGTGTC	
Forward inner primer	FIP	CCGTAGGCCRTAAGCTCGGCTCTC AARACTGCTCGRGACA	
Backward inner primer	BIP	ACATGAGCACYCTGGTCTCTGCGG GAGCTGTAACTGCTTTRG	
Loop forward primer	LF	GGTGTYTTKCCCTTGCTGC	
Loop backward primer	LB	AGTTATCACCATCGAGGCCCA	
single-guide RNA	sgRNA	GUCUAGAGGACAGAAUUUUUCAACGGGUGUGCCAAUGGCCA CUUUCCAGGUGGCAAAGCCCGUUGAGCUUCUCAAAUCUGAGA AGUGGCAC**CUACGGAUAACAGACAUGAGC***	In-house

*Bold region corresponds to the NiV target sequence.

5.4. SARS-CoV-2 N gene RT-LAMP Cas12b Worksheet

Enter # rxns (10% extra)			1	
Component	**[Initial]**	**[Final]**	**Vol/rxn (uL)**	**V_f (uL)**
ddH2O*	-	-	9.66	9.66
Mg2SO4	100 mM	9 mM	4.5	4.5
NEB AapCas12b	1.54 µM	31.25 nM	1.02	1.02
N gene sgRNA	1 µM	31.25 nM	1.57	1.57
Buffer	10X	1X	5	5
dNTPs	10 mM	1.4 mM	7	7
Bst 2.0 DNA Polymerase	8000U/mL	320U/mL	2	2
RTx RTase	15000U/m	300U/mL	1	1
10 X primer pool	10X	1X	5	5
Reporter DNA	10 µM	250 nM	1.25	1.25
Taurine	500 mM	50 mM	5	5
Proteinase K Inhibitor	10X	1X	5	5
DTT	100 mM	2 mM	1	1
Total volume (pre-RNA)			49	49
RNA (µL)*			1	50

*ddH2O volume can be adjusted to increase RNA template addition up to 5 µL.

Title :
Analyst :
Date :

Notes :

Thermal Profile:
Isothermal
60°C/60 min
Cycles : 60x (1min*)
***Collection of Fluorescence**

5.5. Reagents and solution preparations

10X 2% Brij-35 reaction buffer

A 10X concentration stock of 2% Brij-35 can be generated by mixing the following reagents in a 50 µL falcon tube.

Reagents	Stock Concentration	10X Concentration	Volume (mL)
Tris-HCl	1 M	0.2 M	10
$(NH_4)_2SO_4$	2 M	0.1 M	2.5
Mg_2SO_4	1M	0.02 M	1
Brij-35	30%	2%	3.33
Nuclease-free water	-	-	33.17
		Total volume	50 µL

10X Primer pool

1. Reconstitute the lyophilized RT-LAMP Cas12b primers, as per the manufacturer's designation, to 100 µM using nuclease-free water.
2. In the same aliquot, dilute the F3 and B3 primers to 2 µM, the FIP and BIP primers to 16 µM and the LF and LB primers to 4 µM.

This will generate a 10X primer pool. When diluted into the RT-LAMP Cas12b reaction, primers will be at a final concentration of 1X.

Proteinase K inhibitor

1. Dissolve 10 mg of Proteinase K Inhibitor with 150 µL of dimethylsulfoxide (DMSO), generating a master stock.
2. Dilute the master stock at 1:100 using nuclease-free water to generate working aliquots of 10X concentration.

When diluted into the RT-LAMP Cas12b reaction, Proteinase K inhibitor will be at a final concentration of 1X.

5. References

1 Wudiri, G. A. *et al.* Molecular requirement for sterols in herpes simplex virus entry and infectivity. *J Virol* **88**, 13918-13922 (2014). https://doi.org:10.1128/JVI.01615-14

2 *WHO Coronavirus (COVID-19) Dashboard*, <https://covid19.who.int/> (2023).

3 Torres-Ibarra, L. *et al.* SARS-CoV-2 infection fatality rate after the first epidemic wave in Mexico. *Int J Epidemiol* **51**, 429-439 (2022). https://doi.org:10.1093/ije/dyac015

4 Said, A. S. A. *et al.* Monotherapy versus polytherapy of enoxaparin and hydroxychloroquine for the treatment of COVID-19: A randomized controlled clinical trial. *Pharm Pract (Granada)* **21**, 2777 (2023). https://doi.org:10.18549/PharmPract.2023.1.2777

5 Rothrock, S. G., Weber, K. D., Giordano, P. A. & Barneck, M. D. Meta-analyses do not establish improved mortality with ivermectin use in COVID-19. *Am J Ther* **29**, e237-e244 (2022). https://doi.org:10.1097/mjt.0000000000001477

6 Zhu, W. *et al.* Identification of SARS-CoV-2 3CL protease inhibitors by a quantitative high-throughput screening. *ACS Pharmacology & Translational Science* **3**, 1008-1016 (2020). https://doi.org:10.1021/acsptsci.0c00108

7 Kabinger, F. *et al.* Mechanism of molnupiravir-induced SARS-CoV-2 mutagenesis. *Nat Struct Mol Biol* **28**, 740-746 (2021). https://doi.org:10.1038/s41594-021-00651-0

8 WHO, M. T. WHO recommends against the use of convalescent plasma to treat COVID-19. https://www.who.int/news/item/07-12-2021-who-recommends-against-the-use-of-convalescent-plasma-to-treat-covid-19

9 Chen, L. *et al.* Co-infecting pathogens can contribute to inflammatory responses and severe symptoms in COVID-19. *J Thorac Dis* **14**, 355-370 (2022). https://doi.org:10.21037/jtd-21-1284

10 Linton, N. M. *et al.* Incubation period and other epidemiological characteristics of 2019 novel Coronavirus infections with right truncation: A statistical analysis of publicly available case data. *J Clin Med* **9** (2020). https://doi.org:10.3390/jcm9020538

11 Backer, J. A., Klinkenberg, D. & Wallinga, J. Incubation period of 2019 novel coronavirus (2019-nCoV) infections among travellers from Wuhan, China, 20-28 January 2020. *Euro Surveill* **25** (2020). https://doi.org:10.2807/1560-7917.ES.2020.25.5.2000062

12 Zhang, J. *et al.* Evolving epidemiology and transmission dynamics of coronavirus disease 2019 outside Hubei province, China: a descriptive and modelling study. *Lancet Infect Dis* **20**, 793-802 (2020). https://doi.org:10.1016/S1473-3099(20)30230-9

13 Nishiura, H., Linton, N. M. & Akhmetzhanov, A. R. Serial interval of novel coronavirus (COVID-19) infections. *Int J Infect Dis* **93**, 284-286 (2020). https://doi.org:10.1016/j.ijid.2020.02.060

14 Backer, J. A. *et al.* Shorter serial intervals in SARS-CoV-2 cases with Omicron BA.1 variant compared with Delta variant, the Netherlands, 13 to 26 December 2021. *Euro Surveill* **27** (2022). https://doi.org:10.2807/1560-7917.ES.2022.27.6.2200042

15 Byrne, A. W. *et al.* Inferred duration of infectious period of SARS-CoV-2: rapid scoping review and analysis of available evidence for asymptomatic and symptomatic COVID-19 cases. *BMJ Open* **10**, e039856 (2020). https://doi.org:10.1136/bmjopen-2020-039856

16 Cevik, M. *et al.* SARS-CoV-2, SARS-CoV, and MERS-CoV viral load dynamics, duration of viral shedding, and infectiousness: a systematic review and meta-analysis. *Lancet Microbe* **2**, e13-e22 (2021). https://doi.org:10.1016/S2666-5247(20)30172-5
17 Suzuki, R. *et al.* Attenuated fusogenicity and pathogenicity of SARS-CoV-2 Omicron variant. *Nature* **603**, 700-705 (2022). https://doi.org:10.1038/s41586-022-04462-1
18 Ito, K., Piantham, C. & Nishiura, H. Relative instantaneous reproduction number of Omicron SARS-CoV-2 variant with respect to the Delta variant in Denmark. *Journal of Medical Virology* **94**, 2265-2268 (2022). https://doi.org:10.1002/jmv.27560
19 Nishiura, H. *et al.* Relative reproduction number of SARS-CoV-2 Omicron (B.1.1.529) compared with Delta variant in South Africa. *Journal of Clinical Medicine* **11** (2021). https://doi.org:10.3390/jcm11010030
20 Ruan, F. *et al.* An outbreak of the COVID-19 Omicron variant—Zhuhai City, Guangdong Province, China, January 13, 2022. **4**, 1-3 (2022). https://doi.org:10.46234/ccdcw2022.032
21 Barnard, R. C., Davies, N. G., Pearson, C. A., Jit, M. & Edmunds, W. J. J. m. Projected epidemiological consequences of the Omicron SARS-CoV-2 variant in England, December 2021 to April 2022. (2021). https://doi.org/10.1101/2021.12.15.21267858
22 Ranjan, R. Omicron impact in India: Analysis of the ongoing COVID-19 third wave based on global data. (2022). https://doi.org/10.1101/2022.01.09.22268969
23 Du, Z. *et al.* Reproduction number of the Omicron variant triples that of the Delta variant. *Viruses* **14** (2022). https://doi.org:10.3390/v14040821
24 Society, R. A. P. *COVID-19 Vaccine Tracker*, <https://www.raps.org/news-and-articles/news-articles/2020/3/covid-19-vaccine-tracker> (2022).
25 Arnaout, R. *et al.* SARS-CoV-2 Testing: The limit of detection matters. *bioRxiv* (2020). https://doi.org:10.1101/2020.06.02.131144
26 Eckert, K. A. & Kunkel, T. A. DNA polymerase fidelity and the polymerase chain reaction. *PCR Methods Appl* **1**, 17-24 (1991). https://doi.org:10.1101/gr.1.1.17
27 Núñez, I., Belaunzarán-Zamudio, P. F. & Caro-Vega, Y. Result turnaround time of RT-PCR for SARS-CoV-2 is the main cause of COVID-19 diagnostic delay: A country-wide observational study of Mexico and Colombia. *Rev Invest Clin* **74**, 071-080 (2022). https://doi.org:10.24875/ric.21000542
28 Luo, X. *et al.* Digital CRISPR/Cas12b-based platform enabled absolute quantification of viral RNA. *Anal Chim Acta* **1192**, 339336 (2022). https://doi.org:10.1016/j.aca.2021.339336
29 Sam, I. K. *et al.* TB-QUICK: CRISPR-Cas12b-assisted rapid and sensitive detection of Mycobacterium tuberculosis. *J Infect* **83**, 54-60 (2021). https://doi.org:10.1016/j.jinf.2021.04.032
30 Joung, J. *et al.* Detection of SARS-CoV-2 with SHERLOCK one-pot testing. *N Engl J Med* **383**, 1492-1494 (2020). https://doi.org:10.1056/NEJMc2026172
31 Wernike, K. *et al.* Multi-species ELISA for the detection of antibodies against SARS-CoV-2 in animals. *Transbound Emerg Dis* **68**, 1779-1785 (2021). https://doi.org:10.1111/tbed.13926
32 Ruantip, S. *et al.* Self-enhancement lateral flow immunoassay for COVID-19 diagnosis. *Sens Actuators B Chem* **389**, 133898 (2023). https://doi.org:10.1016/j.snb.2023.133898
33 Itoh, K. *et al.* False positive results in severe acute respiratory coronavirus 2 (SARS-CoV-2) rapid antigen tests for inpatients. *J Infect Chemother* **27**, 1089-1091 (2021). https://doi.org:10.1016/j.jiac.2021.03.011

34 Jegerlehner, S., Suter-Riniker, F., Jent, P., Bittel, P. & Nagler, M. Diagnostic accuracy of a SARS-CoV-2 rapid antigen test in real-life clinical settings. *Int J Infect Dis* **109**, 118-122 (2021). https://doi.org:10.1016/j.ijid.2021.07.010

35 Cubas-Atienzar, A. I. *et al.* Limit of detection in different matrices of 19 commercially available rapid antigen tests for the detection of SARS-CoV-2. *Scientific reports* **11**, 18313 (2021). https://doi.org:10.1038/s41598-021-97489-9

36 Zhu, N. *et al.* A novel Coronavirus from patients with pneumonia in China, 2019. *The New England journal of medicine* **382**, 727-733 (2020). https://doi.org:10.1056/NEJMoa2001017

37 Wu, F. *et al.* A new coronavirus associated with human respiratory disease in China. *Nature* **579**, 265-269 (2020). https://doi.org:10.1038/s41586-020-2008-3

38 Zhou, P. *et al.* A pneumonia outbreak associated with a new coronavirus of probable bat origin. *Nature* **579**, 270-273 (2020). https://doi.org:10.1038/s41586-020-2012-7

39 Lu, R. *et al.* Genomic characterisation and epidemiology of 2019 novel coronavirus: implications for virus origins and receptor binding. *Lancet* **395**, 565-574 (2020). https://doi.org:10.1016/S0140-6736(20)30251-8

40 Worobey, M. *et al.* The Huanan Seafood Wholesale Market in Wuhan was the early epicenter of the COVID-19 pandemic. *Science* **377**, 951-959 (2022). https://doi.org:10.1126/science.abp8715

41 Nair, A. N., Anand, P., George, A. & Mondal, N. A review of strategies and their effectiveness in reducing indoor airborne transmission and improving indoor air quality. *Environ Res* **213**, 113579 (2022). https://doi.org:10.1016/j.envres.2022.113579

42 Meister, T. L. *et al.* Low risk of SARS-CoV-2 transmission by fomites - a clinical observational study in highly infectious COVID-19 patients. *The Journal of infectious diseases* (2022). https://doi.org:10.1093/infdis/jiac170

43 Rambaut, A. *et al.* A dynamic nomenclature proposal for SARS-CoV-2 lineages to assist genomic epidemiology. *Nat Microbiol* **5**, 1403-1407 (2020). https://doi.org:10.1038/s41564-020-0770-5

44 Organization, W. H. *WHO announces simple, easy-to-say labels for SARS-CoV-2 Variants of Interest and Concern*, <https://www.who.int/news/item/31-05-2021-who-announces-simple-easy-to-say-labels-for-sars-cov-2-variants-of-interest-and-concern> (2021).

45 Center, J. H. U. o. M. C. R. *COVID-19 Map*, <https://coronavirus.jhu.edu/map.html> (2023).

46 Organization, W. H. *Tracking SARS-CoV-2 variants*, <https://www.who.int/activities/tracking-SARS-CoV-2-variants> (2023).

47 Mohandas, S. *et al.* Pathogenicity of SARS-CoV-2 Omicron (R346K) variant in Syrian hamsters and its cross-neutralization with different variants of concern. *EBioMedicine* **79**, 103997 (2022). https://doi.org:10.1016/j.ebiom.2022.103997

48 Motozono, C. *et al.* SARS-CoV-2 spike L452R variant evades cellular immunity and increases infectivity. *Cell host & microbe* **29**, 1124-1136 e1111 (2021). https://doi.org:10.1016/j.chom.2021.06.006

49 Wang, Q. *et al.* Antibody evasion by SARS-CoV-2 Omicron subvariants BA.2.12.1, BA.4 and BA.5. *Nature* **608**, 603-608 (2022). https://doi.org:10.1038/s41586-022-05053-w

50 Houhamdi, L. *et al.* Characteristics of the first 1119 SARS-CoV-2 Omicron variant cases, in Marseille, France, November-December 2021. *J Med Virol* **94**, 2290-2295 (2022). https://doi.org:10.1002/jmv.27613

51 Newsroom, C. *First confirmed case of Omicron variant detected in the United States*, <https://www.cdc.gov/media/releases/2021/s1201-omicron-variant.html#:~:text=The%20individual%20was%20a%20traveler,contacted%20and%20have%20tested%20negative.> (2021).
52 Wang, S. *et al.* Molecular evolutionary characteristics of SARS-CoV-2 emerging in the United States. *J Med Virol* **94**, 310-317 (2022). https://doi.org:10.1002/jmv.27331
53 Duchene, S. *et al.* Temporal signal and the phylodynamic threshold of SARS-CoV-2. *Virus Evol* **6**, veaa061 (2020). https://doi.org:10.1093/ve/veaa061
54 Wu, A. *et al.* Genome composition and divergence of the Novel Coronavirus (2019-nCoV) originating in China. *Cell host & microbe* **27**, 325-328 (2020). https://doi.org:10.1016/j.chom.2020.02.001
55 Gordon, D. E. *et al.* A SARS-CoV-2 protein interaction map reveals targets for drug repurposing. *Nature* **583**, 459-468 (2020). https://doi.org:10.1038/s41586-020-2286-9
56 Kim, D. *et al.* The architecture of SARS-CoV-2 transcriptome. *Cell* **181**, 914-921 e910 (2020). https://doi.org:10.1016/j.cell.2020.04.011
57 Rastogi, M., Pandey, N., Shukla, A. & Singh, S. K. SARS coronavirus 2: from genome to infectome. *Respir Res* **21**, 318 (2020). https://doi.org:10.1186/s12931-020-01581-z
58 Huang, C. *et al.* SARS coronavirus nsp1 protein induces template-dependent endonucleolytic cleavage of mRNAs: viral mRNAs are resistant to nsp1-induced RNA cleavage. *PLoS pathogens* **7**, e1002433 (2011). https://doi.org:10.1371/journal.ppat.1002433
59 Signorile, A., Sgaramella, G., Bellomo, F. & De Rasmo, D. Prohibitins: A critical role in mitochondrial functions and implication in diseases. *Cells* **8** (2019). https://doi.org:10.3390/cells8010071
60 Lei, J., Kusov, Y. & Hilgenfeld, R. Nsp3 of coronaviruses: Structures and functions of a large multi-domain protein. *Antiviral research* **149**, 58-74 (2018). https://doi.org:10.1016/j.antiviral.2017.11.001
61 Sakai, Y. *et al.* Two-amino acids change in the nsp4 of SARS coronavirus abolishes viral replication. *Virology* **510**, 165-174 (2017). https://doi.org:10.1016/j.virol.2017.07.019
62 Tomar, S. *et al.* Ligand-induced dimerization of Middle East Respiratory Syndrome (MERS) Coronavirus nsp5 protease (3CLpro): Implications for nsp5 regulation and the development of antivirals. *The Journal of biological chemistry* **290**, 19403-19422 (2015). https://doi.org:10.1074/jbc.M115.651463
63 Abdelkader, A. *et al.* In-Silico targeting of SARS-CoV-2 NSP6 for drug and natural products repurposing. *Virology* **573**, 96-110 (2022). https://doi.org:10.1016/j.virol.2022.06.008
64 Kirchdoerfer, R. N. & Ward, A. B. Structure of the SARS-CoV nsp12 polymerase bound to nsp7 and nsp8 co-factors. *Nature Communications* **10** (2019). https://doi.org:10.1038/s41467-019-10280-3
65 Sutton, G. *et al.* The nsp9 replicase protein of SARS-coronavirus, structure and functional insights. *Structure* **12**, 341-353 (2004). https://doi.org:10.1016/j.str.2004.01.016
66 Yan, L. *et al.* Cryo-EM Structure of an extended SARS-CoV-2 replication and transcription complex reveals an intermediate state in cap synthesis. *Cell* **184**, 184-193 e110 (2021). https://doi.org:10.1016/j.cell.2020.11.016

67 Ferron, F. *et al.* Structural and molecular basis of mismatch correction and ribavirin excision from coronavirus RNA. *Proceedings of the National Academy of Sciences* **115** (2017). https://doi.org:10.1073/pnas.1718806115

68 Deming, D. J., Graham, R. L., Denison, M. R. & Baric, R. S. Processing of open reading frame 1a replicase proteins nsp7 to nsp10 in Murine Hepatitis virus Strain A59 replication. *Journal of virology* **81**, 10280-10291 (2007). https://doi.org:10.1128/jvi.00017-07

69 Fang, S. G., Shen, H., Wang, J., Tay, F. P. L. & Liu, D. X. Proteolytic processing of polyproteins 1a and 1ab between non-structural proteins 10 and 11/12 of Coronavirus infectious bronchitis virus is dispensable for viral replication in cultured cells. *Virology* **379**, 175-180 (2008). https://doi.org:10.1016/j.virol.2008.06.038

70 Shu, T. *et al.* SARS-Coronavirus-2 Nsp13 Possesses NTPase and RNA helicase activities that can be inhibited by bismuth salts. *Virologica Sinica* **35**, 321-329 (2020). https://doi.org:10.1007/s12250-020-00242-1

71 Kim, Y. *et al.* Tipiracil binds to uridine site and inhibits Nsp15 endoribonuclease NendoU from SARS-CoV-2. *Commun Biol* **4**, 193 (2021). https://doi.org:10.1038/s42003-021-01735-9

72 Deng, X. *et al.* Coronavirus nonstructural protein 15 mediates evasion of dsRNA sensors and limits apoptosis in macrophages. *Proceedings of the National Academy of Sciences of the United States of America* **114**, E4251-E4260 (2017). https://doi.org:10.1073/pnas.1618310114

73 Deng, X. & Baker, S. C. An "Old" protein with a new story: Coronavirus endoribonuclease is important for evading host antiviral defenses. *Virology* **517**, 157-163 (2018). https://doi.org:10.1016/j.virol.2017.12.024

74 Jackson, C. B., Farzan, M., Chen, B. & Choe, H. Mechanisms of SARS-CoV-2 entry into cells. *Nat Rev Mol Cell Biol* **23**, 3-20 (2022). https://doi.org:10.1038/s41580-021-00418-x

75 Yadav, R. *et al.* Role of structural and non-structural proteins and therapeutic targets of SARS-CoV-2 for COVID-19. *Cells* **10** (2021). https://doi.org:10.3390/cells10040821

76 Baden, L. R. *et al.* Efficacy and safety of the mRNA-1273 SARS-CoV-2 vaccine. *The New England journal of medicine* **384**, 403-416 (2021). https://doi.org:10.1056/NEJMoa2035389

77 Polack, F. P. *et al.* Safety and efficacy of the BNT162b2 mRNA Covid-19 vaccine. *The New England journal of medicine* **383**, 2603-2615 (2020). https://doi.org:10.1056/NEJMoa2034577

78 Neuman, B. W. *et al.* A structural analysis of M protein in coronavirus assembly and morphology. *J Struct Biol* **174**, 11-22 (2011). https://doi.org:10.1016/j.jsb.2010.11.021

79 Astuti, I. & Ysrafil. Severe Acute Respiratory Syndrome Coronavirus 2 (SARS-CoV-2): An overview of viral structure and host response. *Diabetes Metab Syndr* **14**, 407-412 (2020). https://doi.org:10.1016/j.dsx.2020.04.020

80 Arndt, A. L., Larson, B. J. & Hogue, B. G. A conserved domain in the coronavirus membrane protein tail is important for virus assembly. *Journal of virology* **84**, 11418-11428 (2010). https://doi.org:10.1128/JVI.01131-10

81 Schoeman, D. & Fielding, B. C. Coronavirus envelope protein: current knowledge. *Virol J* **16**, 69 (2019). https://doi.org:10.1186/s12985-019-1182-0

82 Ruch, T. R. & Machamer, C. E. The coronavirus E protein: assembly and beyond. *Viruses* **4**, 363-382 (2012). https://doi.org:10.3390/v4030363

83 Boson, B. *et al.* The SARS-CoV-2 envelope and membrane proteins modulate maturation and retention of the spike protein, allowing assembly of virus-like particles. *J Biol Chem* **296**, 100111 (2021). https://doi.org:10.1074/jbc.RA120.016175
84 DeDiego, M. L. *et al.* Severe acute respiratory syndrome coronavirus envelope protein regulates cell stress response and apoptosis. *PLoS Pathog* **7**, e1002315 (2011). https://doi.org:10.1371/journal.ppat.1002315
85 Westerbeck, J. W. & Machamer, C. E. A Coronavirus E protein is present in two distinct pools with different effects on assembly and the secretory pathway. *J Virol* **89**, 9313-9323 (2015). https://doi.org:10.1128/JVI.01237-15
86 McBride, R., van Zyl, M. & Fielding, B. C. The coronavirus nucleocapsid is a multifunctional protein. *Viruses* **6**, 2991-3018 (2014). https://doi.org:10.3390/v6082991
87 de Haan, C. A. & Rottier, P. J. Molecular interactions in the assembly of coronaviruses. *Adv Virus Res* **64**, 165-230 (2005). https://doi.org:10.1016/S0065-3527(05)64006-7
88 Spencer, K. A. & Hiscox, J. A. Characterisation of the RNA binding properties of the coronavirus infectious bronchitis virus nucleocapsid protein amino-terminal region. *FEBS Lett* **580**, 5993-5998 (2006). https://doi.org:10.1016/j.febslet.2006.09.052
89 Denison, M. R. *et al.* The putative helicase of the coronavirus mouse hepatitis virus is processed from the replicase gene polyprotein and localizes in complexes that are active in viral RNA synthesis. *J Virol* **73**, 6862-6871 (1999). https://doi.org:10.1128/JVI.73.8.6862-6871.1999
90 Nakanaga, K., Yamanouchi, K. & Fujiwara, K. Protective effect of monoclonal antibodies on lethal mouse hepatitis virus infection in mice. *J Virol* **59**, 168-171 (1986). https://doi.org:10.1128/JVI.59.1.168-171.1986
91 Gorkhali, R. *et al.* Structure and function of major SARS-CoV-2 and SARS-CoV proteins. *Bioinform Biol Insights* **15**, 11779322211025876 (2021). https://doi.org:10.1177/11779322211025876
92 Kern, D. M. *et al.* Cryo-EM structure of SARS-CoV-2 ORF3a in lipid nanodiscs. *Nat Struct Mol Biol* **28**, 573-582 (2021). https://doi.org:10.1038/s41594-021-00619-0
93 Zhang, J. *et al.* Understanding the role of SARS-CoV-2 ORF3a in viral pathogenesis and COVID-19. *Front Microbiol* **13**, 854567 (2022). https://doi.org:10.3389/fmicb.2022.854567
94 Konno, Y. *et al.* SARS-CoV-2 ORF3b Is a potent interferon antagonist whose activity is increased by a naturally occurring elongation variant. *Cell reports* **32**, 108185 (2020). https://doi.org:10.1016/j.celrep.2020.108185
95 Miyamoto, Y. *et al.* SARS-CoV-2 ORF6 disrupts nucleocytoplasmic trafficking to advance viral replication. *Communications biology* **5**, 483 (2022). https://doi.org:10.1038/s42003-022-03427-4
96 Nishitsuji, H., Iwahori, S., Ohmori, M., Shimotohno, K. & Murata, T. Ubiquitination of SARS-CoV-2 NSP6 and ORF7a Facilitates NF-kappaB Activation. *mBio* **13**, e0097122 (2022). https://doi.org:10.1128/mbio.00971-22
97 Yang, R. *et al.* SARS-CoV-2 Accessory protein ORF7b mediates tumor necrosis factor-alpha-induced apoptosis in cells. *Frontiers in microbiology* **12**, 654709 (2021). https://doi.org:10.3389/fmicb.2021.654709
98 Kohyama, M. *et al.* SARS-CoV-2 ORF8 is a viral cytokine regulating immune responses. *International immunology* (2022). https://doi.org:10.1093/intimm/dxac044

99 Han, L. *et al.* SARS-CoV-2 ORF9b antagonizes type I and III interferons by targeting multiple components of the RIG-I/MDA-5-MAVS, TLR3-TRIF, and cGAS-STING signaling pathways. *J Med Virol* **93**, 5376-5389 (2021). https://doi.org:10.1002/jmv.27050
100 Dominguez Andres, A. *et al.* SARS-CoV-2 ORF9c Is a membrane-associated protein that suppresses antiviral responses in cells. *bioRxiv : the preprint server for biology* (2020). https://doi.org:10.1101/2020.08.18.256776
101 Li, X. *et al.* SARS-CoV-2 ORF10 suppresses the antiviral innate immune response by degrading MAVS through mitophagy. *Cellular & molecular immunology* **19**, 67-78 (2022). https://doi.org:10.1038/s41423-021-00807-4
102 Turner, A. J. in *The protective arm of the renin angiotensin system (RAS)* 185-189 (2015).
103 Hamming, I. *et al.* Tissue distribution of ACE2 protein, the functional receptor for SARS coronavirus. A first step in understanding SARS pathogenesis. *The Journal of pathology* **203**, 631-637 (2004). https://doi.org:10.1002/path.1570
104 Salamanna, F., Maglio, M., Landini, M. P. & Fini, M. Body localization of ACE-2: On the trail of the keyhole of SARS-CoV-2. *Frontiers in medicine* **7**, 594495 (2020). https://doi.org:10.3389/fmed.2020.594495
105 Zhao, M. M. *et al.* Cathepsin L plays a key role in SARS-CoV-2 infection in humans and humanized mice and is a promising target for new drug development. *Signal Transduct Target Ther* **6**, 134 (2021). https://doi.org:10.1038/s41392-021-00558-8
106 Amraei, R. *et al.* CD209L/L-SIGN and CD209/DC-SIGN act as receptors for SARS-CoV-2. *bioRxiv : the preprint server for biology* (2021). https://doi.org:10.1101/2020.06.22.165803
107 Malone, B., Urakova, N., Snijder, E. J. & Campbell, E. A. Structures and functions of coronavirus replication–transcription complexes and their relevance for SARS-CoV-2 drug design. *Nature Reviews Molecular Cell Biology* **23**, 21-39 (2021). https://doi.org:10.1038/s41580-021-00432-z
108 Malone, B., Urakova, N., Snijder, E. J. & Campbell, E. A. Structures and functions of coronavirus replication-transcription complexes and their relevance for SARS-CoV-2 drug design. *Nat Rev Mol Cell Biol* **23**, 21-39 (2022). https://doi.org:10.1038/s41580-021-00432-z
109 V'Kovski, P., Kratzel, A., Steiner, S., Stalder, H. & Thiel, V. Coronavirus biology and replication: implications for SARS-CoV-2. *Nature reviews. Microbiology* **19**, 155-170 (2021). https://doi.org:10.1038/s41579-020-00468-6
110 Liu, J. *et al.* SARS-CoV-2 cell tropism and multiorgan infection. *Cell Discov* **7**, 17 (2021). https://doi.org:10.1038/s41421-021-00249-2
111 Li, M. Y., Li, L., Zhang, Y. & Wang, X. S. Expression of the SARS-CoV-2 cell receptor gene ACE2 in a wide variety of human tissues. *Infect Dis Poverty* **9**, 45 (2020). https://doi.org:10.1186/s40249-020-00662-x
112 Liu, J. *et al.* Infection of human sweat glands by SARS-CoV-2. *Cell Discov* **6**, 84 (2020). https://doi.org:10.1038/s41421-020-00229-y
113 Wang, W. *et al.* Detection of SARS-CoV-2 in different types of clinical specimens. *JAMA* **323**, 1843-1844 (2020). https://doi.org:10.1001/jama.2020.3786
114 Martinez, R. M. Clinical samples for SARS-CoV-2 detection: Review of the early literature. *Clin Microbiol Newsl* **42**, 121-127 (2020). https://doi.org:10.1016/j.clinmicnews.2020.07.001

115 Li, W. *et al.* Receptor and viral determinants of SARS-coronavirus adaptation to human ACE2. *EMBO J* **24**, 1634-1643 (2005). https://doi.org:10.1038/sj.emboj.7600640
116 Parolin, C. *et al.* Animal hosts and experimental models of SARS-CoV-2 Infection. *Chemotherapy* **66**, 8-16 (2021). https://doi.org:10.1159/000515341
117 Looi, L. M. & Chua, K. B. Lessons from the Nipah virus outbreak in Malaysia. *Malays J Pathol* **29**, 63-67 (2007). https://www.mjpath.org.my/2007.2/02Nipah_Virus_lessons.pdf
118 Abdullah Al Dulal, R. *One dies of Nipah virus in Rajshahi*, <https://www.dhakatribune.com/bangladesh/2023/03/02/one-dies-of-nipah-virus-in-rajshahi> (2023).
119 Goh, K. J. *et al.* Clinical features of Nipah virus encephalitis among pig farmers in Malaysia. *N Engl J Med* **342**, 1229-1235 (2000). https://doi.org:10.1056/NEJM200004273421701
120 Organization, W. H. *Ten threats to global health in 2019*, <https://www.who.int/news-room/spotlight/ten-threats-to-global-health-in-2019> (2019).
121 Chua, K. B. *et al.* Fatal encephalitis due to Nipah virus among pig-farmers in Malaysia. *Lancet* **354**, 1257-1259 (1999). https://doi.org:10.1016/S0140-6736(99)04299-3
122 Montini Maluda, M. C. *et al.* Nineteen years of Japanese Encephalitis surveillance in Sabah, Malaysian Borneo. *The American journal of tropical medicine and hygiene* **103**, 864-868 (2020). https://doi.org:10.4269/ajtmh.19-0928
123 Centers for Disease, C. & Prevention. Outbreak of Hendra-like virus--Malaysia and Singapore, 1998-1999. *MMWR. Morbidity and mortality weekly report* **48**, 265-269 (1999). https://www.cdc.gov/mmwr/preview/mmwrhtml/00056866.htm
124 Chua, K. B. Nipah virus outbreak in Malaysia. *Journal of clinical virology : the official publication of the Pan American Society for Clinical Virology* **26**, 265-275 (2003). https://doi.org:10.1016/s1386-6532(02)00268-8
125 Parashar, U. D. *et al.* Case-control study of risk factors for human infection with a new zoonotic paramyxovirus, Nipah virus, during a 1998-1999 outbreak of severe encephalitis in Malaysia. *The Journal of infectious diseases* **181**, 1755-1759 (2000). https://doi.org:10.1086/315457
126 Hyatt, A. D., Zaki, S. R., Goldsmith, C. S., Wise, T. G. & Hengstberger, S. G. Ultrastructure of Hendra virus and Nipah virus within cultured cells and host animals. *Microbes and infection* **3**, 297-306 (2001). https://doi.org:10.1016/s1286-4579(01)01383-1
127 Gurley, E. S. *et al.* Person-to-person transmission of Nipah virus in a Bangladeshi community. *Emerging infectious diseases* **13**, 1031-1037 (2007). https://doi.org:10.3201/eid1307.061128
128 Chadha, M. S. *et al.* Nipah virus-associated encephalitis outbreak, Siliguri, India. *Emerging infectious diseases* **12**, 235-240 (2006). https://doi.org:10.3201/eid1202.051247
129 Homaira, N. *et al.* Nipah virus outbreak with person-to-person transmission in a district of Bangladesh, 2007. *Epidemiol Infect* **138**, 1630-1636 (2010). https://doi.org:10.1017/S0950268810000695
130 Sazzad, H. M. *et al.* Nipah virus infection outbreak with nosocomial and corpse-to-human transmission, Bangladesh. *Emerging infectious diseases* **19**, 210-217 (2013). https://doi.org:10.3201/eid1902.120971
131 Nikolay, B. *et al.* Transmission of Nipah virus - 14 Years of investigations in Bangladesh. *N Engl J Med* **380**, 1804-1814 (2019). https://doi.org:10.1056/NEJMoa1805376

132 Luby, S. P., Gurley, E. S. & Hossain, M. J. Transmission of human infection with Nipah virus. *Clinical infectious diseases : an official publication of the Infectious Diseases Society of America* **49**, 1743-1748 (2009). https://doi.org:10.1086/647951
133 Harit, A. K. *et al.* Nipah/Hendra virus outbreak in Siliguri, West Bengal, India in 2001. *The Indian journal of medical research* **123**, 553-560 (2006). https://pubmed.ncbi.nlm.nih.gov/16783047/
134 Arunkumar, G. *et al.* Outbreak investigation of Nipah virus disease in Kerala, India, 2018. *The Journal of infectious diseases* **219**, 1867-1878 (2019). https://doi.org:10.1093/infdis/jiy612
135 Yadav, P. D. *et al.* Nipah virus outbreak in Kerala State, India amidst of COVID-19 pandemic. *Frontiers in public health* **10**, 818545 (2022). https://doi.org:10.3389/fpubh.2022.818545
136 Yadav, P. D. *et al.* Nipah virus sequences from humans and bats during Nipah outbreak, Kerala, India, 2018. *Emerging infectious diseases* **25**, 1003-1006 (2019). https://doi.org:10.3201/eid2505.181076
137 Ching, P. K. G. *et al.* Outbreak of Henipavirus infection, Philippines, 2014. *Emerging infectious diseases* **21**, 328-331 (2015). https://doi.org:10.3201/eid2102.141433
138 Olson, J. G. *et al.* Antibodies to Nipah-like virus in bats (Pteropus lylei), Cambodia. *Emerging infectious diseases* **8**, 987-988 (2002). https://doi.org:10.3201/eid0809.010515
139 Reynes, J.-M. *et al.* Nipah virus in Lyle's flying foxes, Cambodia. *Emerging infectious diseases* **11**, 1042-1047 (2005). https://doi.org:10.3201/eid1107.041350
140 Li, Y. *et al.* Antibodies to Nipah or Nipah-like viruses in bats, China. *Emerging infectious diseases* **14**, 1974-1976 (2008). https://doi.org:10.3201/eid1412.080359
141 Hasebe, F. *et al.* Serologic evidence of nipah virus infection in bats, Vietnam. *Emerging infectious diseases* **18**, 536-537 (2012). https://doi.org:10.3201/eid1803.111121
142 Wacharapluesadee, S. *et al.* Bat Nipah virus, Thailand. *Emerging infectious diseases* **11**, 1949-1951 (2005). https://doi.org:10.3201/eid1112.050613
143 Sendow, I. *et al.* Screening for Nipah virus infection in West Kalimantan province, Indonesia. *Zoonoses and public health* **57**, 499-503 (2010). https://doi.org:10.1111/j.1863-2378.2009.01252.x
144 Buden, D. W., Helgen, K. M. & Wiles, G. J. Taxonomy, distribution, and natural history of flying foxes (Chiroptera, Pteropodidae) in the Mortlock Islands and Chuuk State, Caroline Islands. *ZooKeys*, 97-135 (2013). https://doi.org:10.3897/zookeys.345.5840
145 Breed, A. C. *et al.* The distribution of henipaviruses in Southeast Asia and Australasia: is Wallace's line a barrier to Nipah virus? *PloS one* **8**, e61316 (2013). https://doi.org:10.1371/journal.pone.0061316
146 Halpin, K. *et al.* Pteropid bats are confirmed as the reservoir hosts of henipaviruses: a comprehensive experimental study of virus transmission. *The American journal of tropical medicine and hygiene* **85**, 946-951 (2011). https://doi.org:10.4269/ajtmh.2011.10-0567
147 Mohd Nor, M. N., Gan, C. H. & Ong, B. L. Nipah virus infection of pigs in peninsular Malaysia. *Rev Sci Tech* **19**, 160-165 (2000). https://doi.org:10.20506/rst.19.1.1202
148 Hsu, V. P. *et al.* Nipah virus encephalitis reemergence, Bangladesh. *Emerg Infect Dis* **10**, 2082-2087 (2004). https://doi.org:10.3201/eid1012.040701
149 Mills, J. N. *et al.* Nipah virus infection in dogs, Malaysia, 1999. *Emerg Infect Dis* **15**, 950-952 (2009). https://doi.org:10.3201/eid1506.080453

150 Luby, S. P. *et al.* Foodborne transmission of Nipah virus, Bangladesh. *Emerg Infect Dis* **12**, 1888-1894 (2006). https://doi.org:10.3201/eid1212.060732
151 Sahani, M. *et al.* Nipah virus infection among abattoir workers in Malaysia, 1998-1999. *Int J Epidemiol* **30**, 1017-1020 (2001). https://doi.org:10.1093/ije/30.5.1017
152 Epstein, J. H. *et al.* Feral cats and risk for Nipah virus transmission. *Emerg Infect Dis* **12**, 1178-1179 (2006). https://doi.org:10.3201/eid1207.050799
153 Tan, C. T. & Tan, K. S. Nosocomial transmissibility of Nipah virus. *J Infect Dis* **184**, 1367 (2001). https://doi.org:10.1086/323996
154 Escaffre, O. *et al.* Characterization of Nipah virus infection in a model of human airway epithelial cells cultured at an air-liquid interface. *J Gen Virol* **97**, 1077-1086 (2016). https://doi.org:10.1099/jgv.0.000441
155 Banerjee, S. *et al.* Nipah virus disease: A rare and intractable disease. *Intractable Rare Dis Res* **8**, 1-8 (2019). https://doi.org:10.5582/irdr.2018.01130
156 Tan, C. T. *et al.* Relapsed and late-onset Nipah encephalitis. *Annals of neurology* **51**, 703-708 (2002). https://doi.org:10.1002/ana.10212
157 Wong, S. C. *et al.* Late presentation of Nipah virus encephalitis and kinetics of the humoral immune response. *Journal of neurology, neurosurgery, and psychiatry* **71**, 552-554 (2001). https://doi.org:10.1136/jnnp.71.4.552
158 Chandni, R. *et al.* Clinical manifestations of Nipah virus-infected patients who presented to the emergency department during an outbreak in Kerala State in India, May 2018. *Clinical infectious diseases : an official publication of the Infectious Diseases Society of America* **71**, 152-157 (2020). https://doi.org:10.1093/cid/ciz789
159 Ng, B. Y., Lim, C. C., Yeoh, A. & Lee, W. L. Neuropsychiatric sequelae of Nipah virus encephalitis. *J Neuropsychiatry Clin Neurosci* **16**, 500-504 (2004). https://doi.org:10.1176/jnp.16.4.500
160 Farrar, J. J. Nipah-virus encephalitis--investigation of a new infection. *Lancet* **354**, 1222-1223 (1999). https://doi.org:10.1016/S0140-6736(99)90124-1
161 Guillaume, V. *et al.* Antibody prophylaxis and therapy against Nipah virus infection in hamsters. *Journal of virology* **80**, 1972-1978 (2006). https://doi.org:10.1128/JVI.80.4.1972-1978.2006
162 Jiang, J., Zenewicz, L. A., San Mateo, L. R., Lau, L. L. & Shen, H. Activation of antigen-specific CD8 T cells results in minimal killing of bystander bacteria. *Journal of immunology* **171**, 6032-6038 (2003). https://doi.org:10.4049/jimmunol.171.11.6032
163 Chong, H. T. *et al.* Treatment of acute Nipah encephalitis with ribavirin. *Ann Neurol* **49**, 810-813 (2001). https://doi.org:10.1002/ana.1062
164 Daniels, P., Ksiazek, T. & Eaton, B. T. Laboratory diagnosis of Nipah and Hendra virus infections. *Microbes and infection* **3**, 289-295 (2001). https://doi.org:10.1016/s1286-4579(01)01382-x
165 Shete, A. M. *et al.* Antibody response in symptomatic & asymptomatic Nipah virus cases from Kerala, India. *Indian J Med Res* **154**, 533-535 (2021). https://doi.org:10.4103/ijmr.IJMR_4388_20
166 Lo Presti, A. *et al.* Origin and evolution of Nipah virus. *J Med Virol* **88**, 380-388 (2016). https://doi.org:10.1002/jmv.24345
167 Sudeep, A. B. *et al.* Detection of Nipah virus in Pteropus medius in 2019 outbreak from Ernakulam district, Kerala, India. *BMC Infect Dis* **21**, 162 (2021). https://doi.org:10.1186/s12879-021-05865-7

168 Sun, B., Jia, L., Liang, B., Chen, Q. & Liu, D. Phylogeography, transmission, and viral proteins of Nipah virus. *Virologica Sinica* **33**, 385-393 (2018). https://doi.org:10.1007/s12250-018-0050-1
169 Gaudino, M. *et al.* High pathogenicity of Nipah virus from Pteropus lylei fruit bats, Cambodia. *Emerging infectious diseases* **26**, 104-113 (2020). https://doi.org:10.3201/eid2601.191284
170 Reynes, J. M. *et al.* Nipah virus in Lyle's flying foxes, Cambodia. *Emerging infectious diseases* **11**, 1042-1047 (2005). https://doi.org:10.3201/eid1107.041350
171 Cappelle, J. *et al.* Nipah virus circulation at human-bat interfaces, Cambodia. *Bull World Health Organ* **98**, 539-547 (2020). https://doi.org:10.2471/BLT.20.254227
172 Marsh, G. A. *et al.* Cedar virus: a novel Henipavirus isolated from Australian bats. *PLoS pathogens* **8**, e1002836 (2012). https://doi.org:10.1371/journal.ppat.1002836
173 Wu, Z. *et al.* Novel Henipa-like virus, Mojiang Paramyxovirus, in rats, China, 2012. *Emerg Infect Dis* **20**, 1064-1066 (2014). https://doi.org:10.3201/eid2006.131022
174 Hayman, D. T. *et al.* Evidence of henipavirus infection in West African fruit bats. *PLoS One* **3**, e2739 (2008). https://doi.org:10.1371/journal.pone.0002739
175 Madera, S. *et al.* Discovery and genomic characterization of a novel Henipavirus, Angavokely Virus, from fruit bats in Madagascar. *Journal of virology*, e0092122 (2022). https://doi.org:10.1128/jvi.00921-22
176 Lee, S. H. *et al.* Discovery and genetic characterization of novel paramyxoviruses related to the genus Henipavirus in Crocidura species in the Republic of Korea. *Viruses* **13** (2021). https://doi.org:10.3390/v13102020
177 Vanmechelen, B. *et al.* The characterization of multiple novel paramyxoviruses highlights the diverse nature of the subfamily Orthoparamyxovirinae. *Virus Evol* **8**, veac061 (2022). https://doi.org:10.1093/ve/veac061
178 Vanmechelen, B. *et al.* The characterization of multiple novel paramyxovirus species highlights the diverse nature of the subfamily Orthoparamyxovirinae. 2022.2003.2010.483612 (2022). https://doi.org:10.1101/2022.03.10.483612 %J bioRxiv
179 Zhang, X. A. *et al.* A zoonotic Henipavirus in febrile patients in China. *The New England journal of medicine* **387**, 470-472 (2022). https://doi.org:10.1056/NEJMc2202705
180 Drexler, J. F. *et al.* Bats host major mammalian paramyxoviruses. *Nat Commun* **3**, 796 (2012). https://doi.org:10.1038/ncomms1796
181 Drexler, J. F. *et al.* Henipavirus RNA in African bats. *PloS one* **4**, e6367 (2009). https://doi.org:10.1371/journal.pone.0006367
182 Baker, K. S. *et al.* Co-circulation of diverse paramyxoviruses in an urban African fruit bat population. *The Journal of general virology* **93**, 850-856 (2012). https://doi.org:10.1099/vir.0.039339-0
183 Chua, K. B. *et al.* Nipah virus: a recently emergent deadly paramyxovirus. *Science* **288**, 1432-1435 (2000). https://doi.org:10.1126/science.288.5470.1432
184 Eaton, B. T., Broder, C. C., Middleton, D. & Wang, L. F. Hendra and Nipah viruses: different and dangerous. *Nature reviews. Microbiology* **4**, 23-35 (2006). https://doi.org:10.1038/nrmicro1323
185 Wang, L. F. *et al.* The exceptionally large genome of Hendra virus: support for creation of a new genus within the family Paramyxoviridae. *Journal of virology* **74**, 9972-9979 (2000). https://doi.org:10.1128/jvi.74.21.9972-9979.2000

186 Harcourt, B. H. *et al.* Molecular characterization of the polymerase gene and genomic termini of Nipah virus. *Virology* **287**, 192-201 (2001). https://doi.org:10.1006/viro.2001.1026
187 Egelman, E. H., Wu, S. S., Amrein, M., Portner, A. & Murti, G. The Sendai virus nucleocapsid exists in at least four different helical states. *J Virol* **63**, 2233-2243 (1989). https://doi.org:10.1128/JVI.63.5.2233-2243.1989
188 Kolakofsky, D. *et al.* Paramyxovirus RNA synthesis and the requirement for hexamer genome length: the rule of six revisited. *Journal of virology* **72**, 891-899 (1998). https://doi.org:10.1128/JVI.72.2.891-899.1998
189 Jensen, K. S. *et al.* Development of a novel real-time polymerase chain reaction assay for the quantitative detection of Nipah virus replicative viral RNA. *PLoS One* **13**, e0199534 (2018). https://doi.org:10.1371/journal.pone.0199534
190 Bruno, L. *et al.* Nipah dirus disease: Epidemiological, clinical, diagnostic and legislative aspects of this unpredictable emerging zoonosis. *Animals (Basel)* **13** (2022). https://doi.org:10.3390/ani13010159
191 Levroney, E. L. *et al.* Novel innate immune functions for galectin-1: galectin-1 inhibits cell fusion by Nipah virus envelope glycoproteins and augments dendritic cell secretion of proinflammatory cytokines. *J Immunol* **175**, 413-420 (2005). https://doi.org:10.4049/jimmunol.175.1.413
192 Aguilar, H. C. *et al.* A novel receptor-induced activation site in the Nipah virus attachment glycoprotein (G) involved in triggering the fusion glycoprotein (F). *The Journal of biological chemistry* **284**, 1628-1635 (2009). https://doi.org:10.1074/jbc.M807469200
193 Diederich, S., Moll, M., Klenk, H. D. & Maisner, A. The nipah virus fusion protein is cleaved within the endosomal compartment. *The Journal of biological chemistry* **280**, 29899-29903 (2005). https://doi.org:10.1074/jbc.M504598200
194 Lamb, R. a. P., GD. in *Fields Virology* Vol. 1 (ed BN. Fields, Knipe, DM. and Howley, PM.) Ch. 957-995, (Lippincott, Williams, and Wilkins, 2013).
195 Earp, L. J., Delos, S. E., Park, H. E. & White, J. M. The many mechanisms of viral membrane fusion proteins. *Current topics in microbiology and immunology* **285**, 25-66 (2005). https://doi.org:10.1007/3-540-26764-6_2
196 Pernet, O., Pohl, C., Ainouze, M., Kweder, H. & Buckland, R. Nipah virus entry can occur by macropinocytosis. *Virology* **395**, 298-311 (2009). https://doi.org:10.1016/j.virol.2009.09.016
197 Wilkinson, D. G. How attraction turns to repulsion. *Nature cell biology* **5**, 851-853 (2003). https://doi.org:10.1038/ncb1003-851
198 Pitulescu, M. E. & Adams, R. H. Eph/ephrin molecules--a hub for signaling and endocytosis. *Genes & development* **24**, 2480-2492 (2010). https://doi.org:10.1101/gad.1973910
199 Cattaneo, R. *et al.* Altered transcription of a defective measles virus genome derived from a diseased human brain. *EMBO J* **6**, 681-688 (1987). https://doi.org:10.1002/j.1460-2075.1987.tb04808.x
200 Hausmann, S., Garcin, D., Delenda, C. & Kolakofsky, D. The versatility of paramyxovirus RNA polymerase stuttering. *Journal of virology* **73**, 5568-5576 (1999). https://doi.org:10.1128/JVI.73.7.5568-5576.1999

201 Fagotto, F., Winklbauer, R. & Rohani, N. Ephrin-Eph signaling in embryonic tissue separation. *Cell adhesion & migration* **8**, 308-326 (2014). https://doi.org:10.4161/19336918.2014.970028
202 Cayuso, J., Xu, Q. & Wilkinson, D. G. Mechanisms of boundary formation by Eph receptor and ephrin signaling. *Developmental biology* **401**, 122-131 (2015). https://doi.org:10.1016/j.ydbio.2014.11.013
203 Park, I. & Lee, H. S. EphB/ephrinB signaling in cell adhesion and migration. *Molecules and cells* **38**, 14-19 (2015). https://doi.org:10.14348/molcells.2015.2116
204 Hruska, M. & Dalva, M. B. Ephrin regulation of synapse formation, function and plasticity. *Molecular and cellular neurosciences* **50**, 35-44 (2012). https://doi.org:10.1016/j.mcn.2012.03.004
205 Gokhale, M. D. *et al.* Detection of possible Nipah virus infection in Rousettus leschenaultii and Pipistrellus Pipistrellus bats in Maharashtra, India. *Journal of infection and public health* **14**, 1010-1012 (2021). https://doi.org:10.1016/j.jiph.2021.05.001
206 Ching, P. K. *et al.* Outbreak of henipavirus infection, Philippines, 2014. *Emerging infectious diseases* **21**, 328-331 (2015). https://doi.org:10.3201/eid2102.141433
207 Mungall, B. A. *et al.* Vertical transmission and fetal replication of Nipah virus in an experimentally infected cat. *The Journal of infectious diseases* **196**, 812-816 (2007). https://doi.org:10.1086/520818
208 Middleton, D. J. *et al.* Experimental Nipah virus infection in pigs and cats. *Journal of comparative pathology* **126**, 124-136 (2002). https://doi.org:10.1053/jcpa.2001.0532
209 Bellini, W. J., Harcourt, B. H., Bowden, N. & Rota, P. A. Nipah virus: an emergent paramyxovirus causing severe encephalitis in humans. *J Neurovirol* **11**, 481-487 (2005). https://doi.org:10.1080/13550280500187435
210 Geisbert, T. *et al.* Serological evidence of Henipavirus exposure in cattle, goats and pigs in Bangladesh. *PLoS Neglected Tropical Diseases* **8** (2014). https://doi.org:10.1371/journal.pntd.0003302
211 Bossart, K. N. *et al.* A Hendra virus G glycoprotein subunit vaccine protects African green monkeys from Nipah virus challenge. *Science translational medicine* **4**, 146ra107 (2012). https://doi.org:10.1126/scitranslmed.3004241
212 Prasad, A. N. *et al.* A lethal aerosol exposure model of Nipah virus strain Bangladesh in african green monkeys. *The Journal of infectious diseases* **221**, S431-S435 (2020). https://doi.org:10.1093/infdis/jiz469
213 Marianneau, P. *et al.* Experimental infection of squirrel monkeys with nipah virus. *Emerging infectious diseases* **16**, 507-510 (2010). https://doi.org:10.3201/eid1603.091346
214 Dhondt, K. P. *et al.* Type I interferon signaling protects mice from lethal henipavirus infection. *The Journal of infectious diseases* **207**, 142-151 (2013). https://doi.org:10.1093/infdis/jis653
215 Leon, A. J. *et al.* Host gene expression profiles in ferrets infected with genetically distinct henipavirus strains. *PLoS Negl Trop Dis* **12**, e0006343 (2018). https://doi.org:10.1371/journal.pntd.0006343
216 Clayton, B. A. *et al.* Transmission routes for nipah virus from Malaysia and Bangladesh. *Emerging infectious diseases* **18**, 1983-1993 (2012). https://doi.org:10.3201/eid1812.120875

217 Escaffre, O. *et al.* Experimental infection of syrian hamsters with aerosolized Nipah virus. *The Journal of infectious diseases* **218**, 1602-1610 (2018). https://doi.org:10.1093/infdis/jiy357
218 Jinek, M. *et al.* A programmable dual-RNA-guided DNA endonuclease in adaptive bacterial immunity. *Science* **337**, 816-821 (2012). https://doi.org:10.1126/science.1225829
219 Makarova, K. S. & Koonin, E. V. Annotation and classification of CRISPR-Cas systems. *Methods in molecular biology* **1311**, 47-75 (2015). https://doi.org:10.1007/978-1-4939-2687-9_4
220 Makarova, K. S., Wolf, Y. I. & Koonin, E. V. Comparative genomics of defense systems in archaea and bacteria. *Nucleic acids research* **41**, 4360-4377 (2013). https://doi.org:10.1093/nar/gkt157
221 Swarts, D. C. & Jinek, M. Mechanistic insights into the cis- and trans-acting DNase activities of Cas12a. *Mol Cell* **73**, 589-600.e584 (2019). https://doi.org:10.1016/j.molcel.2018.11.021
222 Hiranniramol, K., Chen, Y. & Wang, X. CRISPR/Cas9 guide RNA design rules for predicting activity. *Methods Mol Biol* **2115**, 351-364 (2020). https://doi.org:10.1007/978-1-0716-0290-4_19
223 Koonin, E. V., Makarova, K. S. & Zhang, F. Diversity, classification and evolution of CRISPR-Cas systems. *Current opinion in microbiology* **37**, 67-78 (2017). https://doi.org:10.1016/j.mib.2017.05.008
224 Makarova, K. S. *et al.* Evolutionary classification of CRISPR-Cas systems: a burst of class 2 and derived variants. *Nat Rev Microbiol* **18**, 67-83 (2020). https://doi.org:10.1038/s41579-019-0299-x
225 Wu, X. *et al.* A warm-start digital CRISPR/Cas-based method for the quantitative detection of nucleic acids. *Anal Chim Acta* **1196**, 339494 (2022). https://doi.org:10.1016/j.aca.2022.339494
226 Chen, X. *et al.* A CRISPR-Cas12b-based platform for ultrasensitive, rapid, and highly specific detection of Hepatitis B Virus genotypes B and C in clinical application. *Front Bioeng Biotechnol* **9**, 743322 (2021). https://doi.org:10.3389/fbioe.2021.743322
227 Chen, J. S. *et al.* CRISPR-Cas12a target binding unleashes indiscriminate single-stranded DNase activity. *Science* **360**, 436-439 (2018). https://doi.org:10.1126/science.aar6245
228 Nguyen, L. T. *et al.* A thermostable Cas12b from Brevibacillus leverages one-pot discrimination of SARS-CoV-2 variants of concern. *EBioMedicine* **77**, 103926 (2022). https://doi.org:10.1016/j.ebiom.2022.103926
229 Tran, M. H. *et al.* A more efficient CRISPR-Cas12a variant derived from Lachnospiraceae bacterium MA2020. *Mol Ther Nucleic Acids* **24**, 40-53 (2021). https://doi.org:10.1016/j.omtn.2021.02.012
230 Son, H. *et al.* Mg(2+)-dependent conformational rearrangements of CRISPR-Cas12a R-loop complex are mandatory for complete double-stranded DNA cleavage. *Proc Natl Acad Sci U S A* **118** (2021). https://doi.org:10.1073/pnas.2113747118
231 Fozouni, P. *et al.* Amplification-free detection of SARS-CoV-2 with CRISPR-Cas13a and mobile phone microscopy. *Cell* **184**, 323-333 e329 (2021). https://doi.org:10.1016/j.cell.2020.12.001
232 Shinoda, H. *et al.* Amplification-free RNA detection with CRISPR-Cas13. *Commun Biol* **4**, 476 (2021). https://doi.org:10.1038/s42003-021-02001-8

233 Harrington, L. B. *et al.* Programmed DNA destruction by miniature CRISPR-Cas14 enzymes. *Science* **362**, 839-842 (2018). https://doi.org:10.1126/science.aav4294
234 Hu, Z. *et al.* Cas14a1-mediated nucleic acid diagnostics for spinal muscular atrophy. *Biosensors (Basel)* **12** (2022). https://doi.org:10.3390/bios12050268
235 Ge, X. *et al.* Cas14a1-mediated nucleic acid detectifon platform for pathogens. *Biosens Bioelectron* **189**, 113350 (2021). https://doi.org:10.1016/j.bios.2021.113350
236 Pausch, P. *et al.* CRISPR-CasPhi from huge phages is a hypercompact genome editor. *Science* **369**, 333-337 (2020). https://doi.org:10.1126/science.abb1400
237 Yang, H., Gao, P., Rajashankar, K. R. & Patel, D. J. PAM-dependent target DNA recognition and cleavage by C2c1 CRISPR-Cas endonuclease. *Cell* **167**, 1814-1828 e1812 (2016). https://doi.org:10.1016/j.cell.2016.11.053
238 Zuo, Z. & Liu, J. Structure and dynamics of Cas9 HNH domain catalytic state. *Scientific reports* **7**, 17271 (2017). https://doi.org:10.1038/s41598-017-17578-6
239 Shmakov, S. *et al.* Discovery and functional characterization of diverse Class 2 CRISPR-Cas Systems. *Molecular cell* **60**, 385-397 (2015). https://doi.org:10.1016/j.molcel.2015.10.008
240 Saiki, R. K. *et al.* Enzymatic amplification of beta-globin genomic sequences and restriction site analysis for diagnosis of sickle cell anemia. 1985. *Biotechnology* **24**, 476-480 (1992).
241 Nalla, A. K. *et al.* Comparative performance of SARS-CoV-2 detection assays using seven different primer-probe sets and one assay kit. *Journal of clinical microbiology* **58** (2020). https://doi.org:10.1128/JCM.00557-20
242 Notomi, T. *et al.* Loop-mediated isothermal amplification of DNA. *Nucleic Acids Res* **28**, E63 (2000). https://doi.org:10.1093/nar/28.12.e63
243 Kellner, M. J. *et al.* A rapid, highly sensitive and open-access SARS-CoV-2 detection assay for laboratory and home testing. *Front Mol Biosci* **9**, 801309 (2022). https://doi.org:10.3389/fmolb.2022.801309
244 Dong, Y. *et al.* Multiplex, real-time, point-of-care RT-LAMP for SARS-CoV-2 detection using the HFman probe. *ACS sensors* **7**, 730-739 (2022). https://doi.org:10.1021/acssensors.1c02079
245 Zhang, X. *et al.* An HFman probe-based reverse transcription loop-mediated isothermal amplification (RT-LAMP) assay for HIV-1 detection. *Molecular and cellular probes* **64**, 101834 (2022). https://doi.org:10.1016/j.mcp.2022.101834
246 Huang, J., Li, P., Shi, S. J., Li, Y. H. & Xie, X. B. [Digital loop-mediated isothermal amplification detection technology and its application progress]. *Zhonghua yu fang yi xue za zhi [Chinese journal of preventive medicine]* **55**, 1518-1523 (2021). https://doi.org:10.3760/cma.j.cn112150-20210831-00850
247 Inaba, M. *et al.* Diagnostic accuracy of LAMP versus PCR over the course of SARS-CoV-2 infection. *Int J Infect Dis* **107**, 195-200 (2021). https://doi.org:10.1016/j.ijid.2021.04.018
248 Kantake, N., Madiraju, M. V., Sugiyama, T. & Kowalczykowski, S. C. Escherichia coli RecO protein anneals ssDNA complexed with its cognate ssDNA-binding protein: A common step in genetic recombination. *Proc Natl Acad Sci U S A* **99**, 15327-15332 (2002). https://doi.org:10.1073/pnas.252633399
249 Lobato, I. M. & O'Sullivan, C. K. Recombinase polymerase amplification: Basics, applications and recent advances. *Trends Analyt Chem* **98**, 19-35 (2018). https://doi.org:10.1016/j.trac.2017.10.015

250 Piepenburg, O., Williams, C. H., Stemple, D. L. & Armes, N. A. DNA detection using recombination proteins. *PLoS Biol* **4**, e204 (2006). https://doi.org:10.1371/journal.pbio.0040204

251 New England Biolabs, I. *Recombinase Polymerase Amplification and SIBA*, <https://international.neb.com/applications/dna-amplification-pcr-and-qpcr/isothermal-amplification/recombinase-polymerase-amplification-and-strand-invasion-based-amplification>

252 Tavares, L., Alves, P. M., Ferreira, R. B. & Santos, C. N. Comparison of different methods for DNA-free RNA isolation from SK-N-MC neuroblastoma. *BMC research notes* **4**, 3 (2011). https://doi.org:10.1186/1756-0500-1-140

253 Schrader, C., Schielke, A., Ellerbroek, L. & Johne, R. PCR inhibitors - occurrence, properties and removal. *Journal of applied microbiology* **113**, 1014-1026 (2012). https://doi.org:10.1111/j.1365-2672.2012.05384.x

254 Esser, K.-H., Marx, W. H. & Lisowsky, T. maxXbond: first regeneration system for DNA binding silica matrices. *Nature Methods* **3**, i-ii (2006). https://doi.org:10.1038/nmeth845

255 Esser, K.-H., Marx, W. H. & Lisowsky, T. Nucleic acid-free matrix: Regeneration of DNA binding columns. *BioTechniques* **39**, 270-271 (2005). https://doi.org:10.2144/05392af01

256 Berensmeier, S. Magnetic particles for the separation and purification of nucleic acids. *Appl Microbiol Biotechnol* **73**, 495-504 (2006). https://doi.org:10.1007/s00253-006-0675-0

257 Shafagati, N. *et al.* The use of Nanotrap particles for biodefense and emerging infectious disease diagnostics. *Pathog Dis* **71**, 164-176 (2014). https://doi.org:10.1111/2049-632X.12136

258 Douglas, T. A. *et al.* The use of hydrogel microparticles to sequester and concentrate bacterial antigens in a urine test for Lyme disease. *Biomaterials* **32**, 1157-1166 (2011). https://doi.org:10.1016/j.biomaterials.2010.10.004

259 Barclay, R. A. *et al.* Hydrogel particles improve detection of SARS-CoV-2 RNA from multiple sample types. *Sci Rep* **10**, 22425 (2020). https://doi.org:10.1038/s41598-020-78771-8

260 Li, H. *et al.* Degenerate sequence-based CRISPR diagnostic for Crimean-Congo hemorrhagic fever virus. *PLoS Negl Trop Dis* **16**, e0010285 (2022). https://doi.org:10.1371/journal.pntd.0010285

261 Li, Z. *et al.* A chemical-enhanced system for CRISPR-Based nucleic acid detection. *Biosens Bioelectron* **192**, 113493 (2021). https://doi.org:10.1016/j.bios.2021.113493

262 Teng, F. *et al.* Repurposing CRISPR-Cas12b for mammalian genome engineering. *Cell Discov* **4**, 63 (2018). https://doi.org:10.1038/s41421-018-0069-3

263 Lamas, A., Azinheiro, S., Roumani, F., Prado, M. & Garrido-Maestu, A. Evaluation of the effect of outer primer structure, and inner primer linker sequences, in the performance of Loop-mediated isothermal amplification. *Talanta* **260**, 124642 (2023). https://doi.org:10.1016/j.talanta.2023.124642

264 Nagamine, K., Hase, T. & Notomi, T. Accelerated reaction by loop-mediated isothermal amplification using loop primers. *Mol Cell Probes* **16**, 223-229 (2002). https://doi.org:10.1006/mcpr.2002.0415

265 Natoli, M. E. *et al.* Improving performance of a SARS-CoV-2 RT-LAMP assay for use with a portable isothermal fluorimeter: Towards a point-of-care molecular testing strategy. *J Biomol Tech* **32**, 180-185 (2021). https://doi.org:10.7171/jbt.21-3203-013
266 Lee, S. *et al.* Highly efficient DNA reporter for CRISPR/Cas12a-based specific and sensitive biosensor. *Biochip J* **16**, 463-470 (2022). https://doi.org:10.1007/s13206-022-00081-0
267 Rossetti, M. *et al.* Enhancement of CRISPR/Cas12a trans-cleavage activity using hairpin DNA reporters. *Nucleic Acids Res* **50**, 8377-8391 (2022). https://doi.org:10.1093/nar/gkac578
268 Liu, T. Y. *et al.* Accelerated RNA detection using tandem CRISPR nucleases. *medRxiv* (2021). https://doi.org:10.1101/2021.03.19.21253328
269 Yang, L., Arora, K., Beard, W. A., Wilson, S. H. & Schlick, T. Critical role of magnesium ions in DNA polymerase beta's closing and active site assembly. *J Am Chem Soc* **126**, 8441-8453 (2004). https://doi.org:10.1021/ja049412o
270 Goldschmidt, V. *et al.* Mg2+ dependency of HIV-1 reverse transcription, inhibition by nucleoside analogues and resistance. *Nucleic Acids Res* **34**, 42-52 (2006). https://doi.org:10.1093/nar/gkj411
271 Ahmad, A. & Ghasemi, J. New buffers to improve the quantitative real-time polymerase chain reaction. *Biosci Biotechnol Biochem* **71**, 1970-1978 (2007). https://doi.org:10.1271/bbb.70164
272 Rungrueng, N. *et al.* Ammonium sulfate improves sensitivity and avoids false negatives of polymerase chain reaction (PCR) for scale drop disease virus (SDDV) detection. *Aquaculture International* **29**, 527-538 (2021). https://doi.org:10.1007/s10499-020-00639-5
273 Abbasi, I., Kirstein, O. D., Hailu, A. & Warburg, A. Optimization of loop-mediated isothermal amplification (LAMP) assays for the detection of Leishmania DNA in human blood samples. *Acta Trop* **162**, 20-26 (2016). https://doi.org:10.1016/j.actatropica.2016.06.009
274 Cheng, S., Chen, Y., Monforte, J. A., Higuchi, R. & Van Houten, B. Template integrity is essential for PCR amplification of 20- to 30-kb sequences from genomic DNA. *PCR Methods Appl* **4**, 294-298 (1995). https://doi.org:10.1101/gr.4.5.294
275 Farell, E. M. & Alexandre, G. Bovine serum albumin further enhances the effects of organic solvents on increased yield of polymerase chain reaction of GC-rich templates. *BMC Res Notes* **5**, 257 (2012). https://doi.org:10.1186/1756-0500-5-257
276 Rajendrakumar, C. S., Suryanarayana, T. & Reddy, A. R. DNA helix destabilization by proline and betaine: possible role in the salinity tolerance process. *FEBS Lett* **410**, 201-205 (1997). https://doi.org:10.1016/s0014-5793(97)00588-7
277 Liu, D. X., Liang, J. Q. & Fung, T. S. Human Coronavirus-229E, -OC43, -NL63, and -HKU1 (Coronaviridae). *Encyclopedia of Virology*, 428-440 (2021). https://doi.org:10.1016/B978-0-12-809633-8.21501-X
278 Teng, F. *et al.* CDetection: CRISPR-Cas12b-based DNA detection with sub-attomolar sensitivity and single-base specificity. *Genome Biol* **20**, 132 (2019). https://doi.org:10.1186/s13059-019-1742-z
279 Guillaume, V. *et al.* Specific detection of Nipah virus using real-time RT-PCR (TaqMan). *J Virol Methods* **120**, 229-237 (2004). https://doi.org:10.1016/j.jviromet.2004.05.018

280 Özay, B. & McCalla, S. E. A review of reaction enhancement strategies for isothermal nucleic acid amplification reactions. *Sensors and Actuators Reports* **3**, 100033 (2021). https://doi.org:https://doi.org/10.1016/j.snr.2021.100033

281 Ding, X., Clark, K. D., Varona, M., Emaus, M. N. & Anderson, J. L. Magnetic ionic liquid-enhanced isothermal nucleic acid amplification and its application to rapid visual DNA analysis. *Anal Chim Acta* **1045**, 132-140 (2019). https://doi.org:10.1016/j.aca.2018.09.014

282 Yeh, H. Y., Shoemaker, C. A. & Klesius, P. H. Evaluation of a loop-mediated isothermal amplification method for rapid detection of channel catfish Ictalurus punctatus important bacterial pathogen Edwardsiella ictaluri. *J Microbiol Methods* **63**, 36-44 (2005). https://doi.org:10.1016/j.mimet.2005.02.015

283 Lin, X., Huang, X., Urmann, K., Xie, X. & Hoffmann, M. R. Digital loop-mediated isothermal amplification on a commercial membrane. *ACS Sens* **4**, 242-249 (2019). https://doi.org:10.1021/acssensors.8b01419

284 Joung, J. *et al.* Point-of-care testing for COVID-19 using SHERLOCK diagnostics. *medRxiv* (2020). https://doi.org:10.1101/2020.05.04.20091231

285 Cai, S., Jung, C., Bhadra, S. & Ellington, A. D. Phosphorothioated primers lead to loop-mediated isothermal amplification at low temperatures. *Anal Chem* **90**, 8290-8294 (2018). https://doi.org:10.1021/acs.analchem.8b02062

286 Ma, L., Chen, Z., Guan, W., Chen, Q. & Liu, D. Rapid and specific detection of all known Nipah virus strains' sequences with reverse transcription-loop-mediated isothermal amplification. *Frontiers in Microbiology* **10,** (2019). https://doi.org:10.3389/fmicb.2019.00418

287 Li, Z. *et al.* A chemical-enhanced system for CRISPR-based Nucleic Acid Detection. *Biosensors and Bioelectronics* **192,** 113493 (2021). https://doi.org/10.1016/j.bios.2021.113493